

**Mechanistic Investigations into the Palladium-Catalyzed Decarboxylative Allylic
Alkylation of Ketone Enolates Using the PHOX Ligand Architecture**

Thesis by

Nathaniel Haynes Sherden

In Partial Fulfillment of the Requirements

for the Degree of

Doctor of Philosophy

CALIFORNIA INSTITUTE OF TECHNOLOGY

Pasadena, California

2011

(Defended March 2nd, 2011)

© 2010

Nathaniel Haynes Sherden

All Rights Reserved

*To my family
for their endless love and support.*

Acknowledgements

The number of people that I would need to thank to fully credit for assistance with the work and accomplishment that is represented in this document is extensive. It is effectively guaranteed that I will miss someone though I will try to be comprehensive. Needless to say, if I were alone in the world this document and the work detailed herein would not have come to fruition, not even close.

Foremost, I would like to thank my family, especially my parents. My mother and father lent endless hours of support to me when I needed it most. Everything from making sure I was eating and sleeping in an acceptable manner, to keeping me sane (or saner as the case may be.) They made sure to support me in any even remotely reasonable way and frequently went far above and beyond the call of duty as parents.

After my vacation days dwindled to nothing and it became apparent that I was anchored in Pasadena until my grad school career ended, one way or another, my parents came to visit me instead of the reverse. Not only did they schedule trips such that they could catch me for individual weekends in Pasadena (which still required me to expend a vacation day), but they would spend as much as a week in town on these visits just so they could catch me for lunch and dinner on the surrounding weekdays as well. We did many exciting speed trips during these weekends including a ridiculous, but fun, attempt at seeing Death Valley in a drive-by tour that started and finished at my door in Pasadena in about 48-hours total time. These visits of theirs were very necessary and revitalizing distractions from the frustrations of my work when progress was not going well.

Similarly, Thanksgiving has always been a core Sherden family tradition. During the second year of graduate school I missed my first Thanksgiving at home ever. Signs

indicated that this might become a recurring phenomenon for years to come. My wonderful parents responded by doing something completely unreasonable. They made sure to host a magnificent full Thanksgiving dinner in Pasadena in my tiny graduate student apartment with its woefully insufficient kitchen every year until I graduated. I can't even begin to say how moved I am by this. Even now as I write this it literally brings tears to my eyes that they did this just for me.

My younger brother Christian has been a fun support during graduate school. While my contact with him was probably limited to about one e-mail message and one phone call per month or less, I always had a grand old time interacting with him. Not only did Christian give me much needed support and cheer me up in my times of woe, but also his enthusiasm for tackling new challenges, and life in general, was infectious and inspirational. While Christian had few chances to visit me, due to his own busy life, he always was a constant source of enjoyment when he did. I hired him to be in charge of entertainment for my brief trip to Australia, and I doubt anyone could have done a better job. His vastly different perspectives and experiences relative to mine in all matters have helped me look at many things in my life and career in new ways as well. Given how differently we view the world I have never understood how we get along so well, but I cannot articulate how glad I am that we do.

Richard Donoho (a.k.a Uncle Dick, a.k.a. Battman) has been a much closer friend than he may know, and unfortunately, then I have had the courtesy to treat him as. I have always and will always count him as family. To most of my other friends Richard Donoho may be noted as the man who supplied me with countless elegant bottles of wine and other liquors, none of which I could have afforded myself. Richard Donoho is thus

the man primarily responsible for cultivating my pretentious taste in booze. But Uncle Dick has done so much more for me than that. Beyond the myriad things he did for me before graduate school, he has aided in every Pasadena based Thanksgiving, gone on many a ridiculous one weekend trips (including the Death Valley one), and wrote to me constantly while I was at graduate school.

This later bit is an important point. When averaged across my entire graduate student career, Richard Donoho wrote to me about once every other month. His letters were not simple and cheap e-mail or text messages either. No, Dick Donoho prefers classic forms of communication, not just because he is generally a neo-Ludite, but because he wants to show that he cares in the most personal way possible. He wrote me many multi-page, handwritten, and honest-to-god traditional letters of the form which require the time and effort to create that no one else these days seems to care to spare. Even counting my e-mail correspondence, it is likely that no other friend or family member may have written to me as much as Richard Donoho did while I was at graduate school. When feeling forgotten and unloved while working in the chemical “mines,” few things can revive oneself like a truly personal handwritten note from a dear friend. I find that his comically cynical and peculiarly witty take on life, the universe, and everything was, and is, always engaging. My greatest regret is that I didn’t call him as much as I should have and later promised him I would while in graduate school.

A number of more distant family members were also immensely supportive of me in this undertaking. Both the Thorns (Uncle Mike and Aunt Sue) as well as the Haynes (Aunt Cindy and ~~Uncle Richard Mr. Man~~ Reverend Uncle Amos) sent me a number of letters and care packages during my tenure at Caltech. These were all greatly appreciated

and much treasured. To this day I still use the rather fancy air filter that Uncle Mike and Aunt Sue sent me in one such package.

Few friends from prior to graduate school stuck with me throughout my time in graduate school. I can't blame them; I more or less disappeared from existence during this time. This just goes to show all the more how good those friends who did stick with me were.

Foremost among such true and resilient friends is Scott Montgomery Priz (e.e.e.). Not only did Scott maintain a close friendship with me even after it required active work to do so, but he was the only friend who came to visit me almost every year. Scott is also possibly the most moral and upstanding person I know.

Scott's enthusiasm for life and adventure has always been a necessary pick-me up when my chemistry projects were stalled and I felt exhausted and despondent, as was often the case early on. I have to admit I have always been jealous of Scott's life; he always manages to lead an interesting and exciting one, which is in stark contrast to my own. This is, of course, because Scott constantly chooses to live life to the fullest. I try to use his example to inspire myself to do the same, but obviously I have a long way to go in this matter.

Phillip Petri has actually been my friend since before either of us was old enough to talk. At least I think it was before we could talk; I could be wrong about that, but then he still has still been a friend for longer than I can remember apparently. Not only did he stay in touch, but also in my fourth year he provided me a much-needed distraction by inviting me to visit him in his new home, Australia. Once there he chauffeured me around on a crazy eight-day bonanza of non-stop entertainment that cleared my head and

left me refreshed and ready to get back to work. If he hadn't made me promise to see him, I probably wouldn't have left Pasadena for any period of time during my tenure at Caltech.

Sarah Helfinstein and Isaac Yonemoto also stayed in touch with me a bit even after I had disappeared into the depths of grad school. It was fun commiserating with both of them about the ups and downs of academia. Isaac even offered me the possibility of a job after graduating, which I am still grateful for. As with just about everyone else in my life, I should have called them both more often.

I also need to thank the Stoltz group at large. The Stoltz group has been a wonderfully intelligent and high-paced group in which to work, learn, and do research. Almost everyone in the Stoltz group during my tenure there was committed not just to his or her own work, but also to helping each other as well. Such comradely, plus the general enthusiasm for doing and discussing chemistry, are two of the key ingredients that make the high-level and high-pressure work environment of the Stoltz group an invigorating and enjoyable place to work at instead of exhausting or demoralizing one like so many others are or can be.

Among the group at large there are a number of key individuals whom I need to thank. First and foremost is Brian. Brian gave me unusually high levels of trust and independence. While I did frequently burn myself because of this (both metaphorically and literally) it was a very unique and valuable learning experience that I cannot imagine I could have gotten anywhere else in the world. Where else would a well intentioned, but naïve, fresh college graduate be told "figure this problem out" and then be allowed to do so however he felt with free reign over numerous top-of-the-line multimillion dollar

pieces of equipment and what effectively amounted to a limitless budget for expensive and dangerous chemicals and other resources? Brian has also really imparted a vast knowledge and love of synthetic chemistry to me during my time under his supervision. I treasure this highly and cannot thank him enough for it and so many other things as well.

Brian is also unshakably understanding and patient. In all honesty, given some of the things I did in my first two years when I didn't really understand anything, I probably would have fired me. So, thank you Brian for being more patient and understanding than I am. Brian, if you are reading this, I am really sorry about all the gray hairs and stress or frustration related brain aneurisms I probably caused over all the years. I honestly meant well. I am also sorry I spread myself so thin. I got so excited with the very open ended project you had given me, and the limitless resources to pursue it that I got too busy pursuing new aspects of it instead of polishing off areas where I was making headway. Only when I started running out of time at the end did I realized my error. Thank you for preventing me from making another when I tried to overcompensate for this by staying extra long to finish the myriad projects I had started. I will always lament the numerous projects I did not get to finish, but I will look back fondly and nostalgically to the research environment you provided me with that allowed me to continuously spawn the projects that I did have the pleasure of working on.

Doug Behenna provided me with just about everything in graduate school, which is why I referred to him only half jokingly as "the giving tree" at my thesis defense. As I mentioned then, none of my projects would have existed without Doug's pioneering work on the Stoltz group's palladium-catalyzed decarboxylative allylic alkylation of ketone enolates, the topic of thesis. Beyond that, Doug provided me with reagents, substrates,

materials, papers, preps, the occasional presentation slide, suggested corrections to my papers and reports, as well as important perspectives on anything and everything, ect.... Doug always knew exactly the right combination of encouragement, support, and savage criticism necessary to keep me working my hardest, and he doled out each in heaps exactly as situations required.

Hosea Nelson was probably one of my favorite people to talk chemistry with. He is knowledgeable, excitable about chemistry, and highly creative and innovative. This made theorizing with him about everything from big picture chemistry proposals to “why did my reaction fail” useful, interesting, and informative. More than once he flew into the lab to try something we had just talked about when mutual interest in the idea was high enough or it seemed like a slick enough idea that it might just be crazy enough to work. Hosea if you are reading this, I apologize if I lead you down any wild goose chases with any of my cockamamie ideas or distracted you too much from all the vital chemistry (and “biologist” babysitting) that you had to do. Hosea also made sure I experienced some of the LA culture and cuisine, something I would not have done and thus not enjoyed or appreciated, without the help of others like himself. Also very important, Hosea was a constant source of worldly wisdom and common sense, which is very important to people such as myself who severely lack both.

I cannot thank either Hosea Nelson or Dr. Kristy Tran enough for reading and laboriously making corrections to the one hundred page monstrosity that was Appendix 4A originally designed for this thesis. I felt awful when that appendix was subsequently discarded due to lack of PI interest given all the personal time these two invested in it

purely out of generosity. I will not forget their efforts involved in that document, and I will always owe them both in return.

Kevin Kuhn was a good Caltech friend for years along with Kevin Allen and John Enquist. While they are three separate entities, each of whom I owe thanks to individually, they are included here as one because I often ended up spending time with them only when we were all together. Kevin Kuhn organized the closest thing the rest of us had to a life on weekends. While I knew he was the ringleader of our little troupe that sought fun on Friday (and sometimes Saturday) getaways, I wasn't aware how much he was responsible for on our outings until he graduated before the rest of us. Upon his graduation, the remaining three of us ceased utterly to have regular Friday outings, and I ceased utterly to have any sort of life outside the lab. All three of us shared similar tastes in all things and I quickly came to severely miss Kevin, Kevin, and John when they graduated before me.

Kevin Allen and John Enquist were especially a near singular entity as far as my involvement with them was concerned. They shared a bay wherever they went, and eventually ended up sharing a hood. Getting any closer for those two would have required marriage, and frankly most married people aren't as close as they were. I did not really get to know John individually until after Kevin Allen left, which was a pity because it was almost eerie how much I found that he and I share in interests and perspective by the end of his tenure at Caltech. I will miss you Kevin, Kevin, and John for all the good times, your wonderful friendship, and interesting chemistry discussions. May everyone be so lucky to find such a great running crew wherever they may end up in life.

Matt Winston and Allen Hong were the people primarily responsible for occasionally getting me out of the lab and eating healthy food my last two years in graduate school. Beyond being friends, both of them are eager inspiring chemists who were a lot of fun to talk chemistry with and always full of good new ideas and fresh perspectives. Their energy in the lab was top notch as well, and when they didn't make me feel old and used up by comparison, their energy was quite motivating. I also owe Matt a personal debt of gratitude, as he was the person who took a night off to drive me to the emergency room after I accidentally injected myself with tetra-*n*-propyltin that one time.

Neal Mankad also requires an acknowledgment, and not just because he was one of only two normal roommates of the six I had during my entire graduate student career. In early X-ray work with my unstable intermediate, Neal worked tirelessly with me to try and obtain the crystal structure of actual effervescent crystals. Among many other things, he put in long hours with me in the X-ray lab hosing down surfaces with liquid nitrogen before use. I have never seen someone work so hard for someone else's project before or since especially given that my project was in a completely different research group that neither he nor anyone in his group had any collaboration with. Neil was one of the most charitable people I have ever met and did all this for me purely out of generosity.

The staff and facilities at Caltech are top notch and I cannot thank them all enough. Perhaps first and foremost are Larry Henling and Dr. Mike Day who ran Caltech's X-ray crystallography facility. These two spoil researchers rotten with their abilities to solve challenging crystal structures. Sure Larry almost always tells everyone how awful their crystals all are, but he almost always manages to solve them anyway. In

one record example I witnessed Larry Henling and Dr. Mike Day solved and publish a crystal structure from a set of crystals provided by a graduate student that were simultaneously twined and hollow. I have never heard of anyone achieving this before and may never hear of that again.

As many of my best results reported herein are based not just on X-ray crystallography results, but on the X-ray crystallography results of exotic unstable compounds, it must be acknowledged that both Larry and Mike worked tirelessly to make the full story told in this thesis possible. In essence they worked very hard to make me look good. Even though Larry has always been a stickler for good crystals, Larry was never frustrated by the increasingly worse and less crystalline materials I started bringing him as I began to run out of time in graduate school and I got more and more desperate to get crystal structures of certain complexes before I left. The bigger the challenge I brought Larry the more bemused he became. He was always willing to take new approaches to attaining difficult structures, and actively encouraged Neal and I to hose down his lab space with liquid nitrogen in the initial struggle to get a structure of some of my more exotic complexes.

Tom Dunn fixed everything but glassware. The sheer range of stuff that he put back together successfully, and often in record time, is shocking. Whenever a hotplate of any make or brand anywhere in the CCE division broke due to reasons ranging from being partially dissolved in acid to being dropped dozens of feet onto cement, Tom Dunn fixed it. When the 600 MHz pentanuclear NMR probe malfunctioned and Caltech was too cheep to shell out the money to buy a replacement for it or for a proper specialist to repair it, Tom Dunn and David Vander Veldt fixed it. When network printers and group

specific equipment of any shape or form broke anywhere in the CCE division, Tom Dunn fixed them. Any time I couldn't get a Coca-Cola and was looking for a soft drink of any form, Tom Don fixed this. When a certain graduate student, who shall remain nameless, tried to cleverly and covertly modify the electronics on his expensive new hood and instead destroyed the whole apparatus utterly, Tom Dunn fixed it. More importantly, Tom Dunn fixed this hood discretely.

One of the many bits of wisdom former Stoltz group Dr. Michael Krout imparted to me was, "If you are doing synthetic chemistry and you aren't breaking any glassware, you probably are not working hard enough." Rick Gerhart was the Tom Dunn of glassware. Given that the entire institute of Caltech seemed to be functioning by Dr. Krout's prescription, Rick had his work cut out for him. Yet the man could not be drowned in broken glassware in need of repair no matter how hard we all inadvertently tried. With skill and grace that was as fantastic to behold as it was fast, Rick would elegantly fuse what was essentially large pieces of glass shrapnel back into fully function lab equipment with surprising rapidity. There was never a task too big or too small and he loved challenges.

Rick was also always excited about making new exotic pieces of glassware to fill the whim of us researchers. He was eager when I had him make a custom trap for the glove box. He was annoyed when I decided not to have him make a far more elaborate custom trap for the glove box (trap version 2.0) that would have required an intense collaboration between him and the machine shop. I was surprised to find how badly Rick wanted that challenge and had been looking forward to it.

David Vander Veldt and Scott Ross ran a fantastic NMR lab. Frequently dealing in stride with the repercussions of graduate student abuse of the equipment, they consistently maintained a highly functional NMR lab on what was a shoestring budget by most NMR lab standards. Both were always eager and willing to help in any function. David Vander Veldt is the reason why all of the kinetics and other dynamic NMR studies reported herein were possible, as he was the primary support behind it, help with it, and error checker on it. David Vander Veldt also frequently came in on Saturdays and other inconvenient times just to swap NMR probes for me upon my request so I could run elaborate NMR experiments whenever I felt like it, such as a VT (CH)₂gHMBCAD{³¹P}, which was one of many experiments that Scott Ross showed me how to perform.

Agnes Tong and Dian Buchness worked hard to help successfully coral flaky graduate students such as myself through all the bureaucratic hurdles at Caltech. They have pulled this off with a high degree of success and tolerance for the people like me whom they are often forced to deal with. Anne Penny helped connect me with everything I needed that was not directly lab-work related, from laser pointers, to room bookings and my final paycheck and my forgotten mail. Joe Drew ran a tight ship on managing the stockroom. He personally delivered most of my orders and supplied me with just about every type of box or related container and the necessary attendant packing material that I required during the course of grad school for free.

Abstract

Palladium-catalyzed asymmetric allylic alkylation has become a large and important field for chemical synthesis. Many methodologies in this field offer mild conditions under which challenging and important molecular features can be reliably synthesized, including chiral all-carbon quaternary stereocenters. As a result, palladium-catalyzed asymmetric allylic alkylation has found significant use in total synthesis, and growing use in industry. While the general process of palladium-catalyzed asymmetric allylic alkylation has been studied for decades, there have been a number of recent modifications and developments, such as asymmetric versions of decarboxylative allylic alkylation procedures that are not yet well understood. The development of future implementations and improvements to palladium-catalyzed asymmetric allylic alkylation and related methodologies is expected to be facilitated by a better understanding of these more recent developments, and thus further mechanistic investigation is warranted.

Reported herein is a set of investigations into the palladium-catalyzed decarboxylative asymmetric allylic alkylation of ketone enolates using the PHOX ligand architecture. By monitoring the reaction via ^{31}P NMR, a series of previously unidentified key intermediates is discovered. Two representatives of these key intermediates are isolated and characterized. The solution behavior of these species under reaction-like conditions is studied along with a few novel and related complexes. The role of these intermediates and their impact on the behavior of the reaction and product formation is discussed. Previously confounding experimentally observed behavior for this methodology is rationalized via the properties elucidated for these discovered intermediates.

Table of Contents

Dedication	iii
Acknowledgements	iv
List of Figures	xix
List of Schemes	xxi
List of Tables	xxii
List of Abbreviations	xxiii
Chapter 1	1
The History and Previous Investigations of Palladium-Catalyzed Decarboxylative Asymmetric Allylic Alkylation of Ketone Enolates Using the PHOX Ligand Architecture	
1.1 INTRODUCTION AND BACKGROUND	1
1.1.1 General Background	1
1.1.2 Palladium-Catalyzed Decarboxylative Asymmetric Allylic Alkylation	5
1.2 A QUESTION OF MECHANISM	7
1.3 INITIAL MECHANISTIC INVESTIGATION	10
Chapter 2	23
Unusual Allylpalladium Carboxylate Complexes: Identification of the Resting State of Catalytic Enantioselective Decarboxylative Allylic Alkylation Reactions of Ketones	
2.1 INTRODUCTION	23
2.2 OBSERVING THE REACTION BY ³¹ P NMR	23
2.2.1 ³¹ P NMR Studies of Allyl Enol Carbonates and Allyl β-Keto Ester Reactions	23
2.2.2 ³¹ P NMR Studies of Silyl Enol Ether Reactions	25
2.3 ISOLATION AND CHARACTERIZATION OF INTERMEDIATES	28
2.3.1 Olefin Complex 30	28
2.3.2 Carboxylate 31	29
2.3.3 The Carbonate Complexes	33
2.4 ROLE AND SIGNIFICANCE OF THE INTERMEDIATES	34
2.4.1 Analogy to Putative Key Palladium Intermediate 27	34
2.4.2 The Function of Complexes 30 and 31 in the Catalytic Cycle	36
2.5 CONCLUSIONS	38
2.6 EXPERIMENTAL PROCEDURES	39
2.6.1 Materials and Methods	39
2.6.2 ³¹ P NMR Studies	42
2.6.3 Synthesis of [Pd ₂ (mtdba) ₃]	51
2.6.4 Synthesis, Handling, and Characterization Methods for Intermediate 1 :	56
2.6.5 Synthesis and Characterization of Other New Molecules	63
2.6.6 Controlled Thermal Decomposition of Intermediate 31	70
2.6.7 Rate Constant and Half-Life of Complex 31 at 24 °C in THF	77
2.6.8 Water Tolerance Experiments	79

Appendix 1	87
Spectra Relevant to Chapter 2	
Appendix 2	104
X-ray Crystallography Reports Relevant to Chapter 2	
Chapter 3	131
Solution Structure and Behavior of Palladium Allyl Carboxylates and Carbonates	
3.1 INTRODUCTION	131
3.2 ANALYZING SOLUTION STRUCTURE AND CHEMICAL BEHAVIOR VIA NMR.....	132
3.2.1 The Solution Structure of Carboxylates 31 and 32	132
3.2.2 The Chemical Behavior of Carboxylates 31 and 32 in Solution	134
3.3 ANALYZING THE SOLUTION BEHAVIOR OF π -ALLYL CATION 25 BY NMR.....	138
3.3.1 EXSY Spectra for π -Allyl Cation 25	138
3.3.2 Analyzing the Exo/Endo Isomerization Mechanism of 25	139
3.3.3 No Allyl Termini Scrambling Caused by π -Allyl Cation 25	142
3.4 ALLYL TERMINI SCRAMBLING VIA OXIDATIVE ADDITION AND REDUCTIVE ELIMINATION	144
3.4.1 The Oxidative Addition and Reductive Elimination Equilibrium	144
3.4.2 Possible Mechanisms for Allyl Termini Scrambling	147
3.5 EXAMINING SELECTIVITY IN REDUCTIVE ELIMINATION.....	149
3.5.1 Literature Precedent For the Reductive Elimination of Allyl Carboxylates	149
3.5.2 Mechanistic Possibilities with Selective Reductive Elimination	150
3.6 EFFECTS ON THE DECARBOXYLATIVE ALLYLIC ALKYLATION OF KETONE ENOLATES	152
3.7 EXPERIMENTAL PROCEDURES	155
3.7.1 Materials and Methods	155
3.7.2 Measuring the Kinetics and Activation Parameters for Exo/Endo Allyl Isomerization in π -Allyl Cation 25 via Saturation Transfer	155
Appendix 3	167
Comprehensive Bibliography	
About the Author	175

List of Figures

Figure 1.1. Nonlinear Effect Study of Palladium-Catalyzed Decarboxylative Allylic Alkylation.....	11
Figure 1.2. Kinetics Studies Show Zero-Order Dependence on Substrate.....	13
Figure 1.3. Results of DFT Simulation for Outer-Sphere Allylic Alkylation Starting with 24 and 25 ...	15
Figure 1.4 Results of DFT Simulation for Inner-Sphere Allylic Alkylation Starting with 24 and 25	17
Figure 2.1. ³¹ P NMR Studies of Allylic Alkylation With β-Ketoester and Enol Carbonate Substrates...	25
Figure 2.2. ³¹ P NMR Studies of Allylic Alkylation With Silyl Enol Ether Substrates.....	27
Figure 2.3. Estimated Structures for Carbonate Intermediates	34
Figure 2.4. Select Examples of Typical Palladium Allyl Carboxylate and Carbonate Species Found in the Literature	36
Figure A1.1. ¹ H NMR spectrum of 3-(triethylsilyl)benzaldehyde (37) in CDCl ₃	88
Figure A1.2. ¹³ C NMR spectrum of 3-(triethylsilyl)benzaldehyde (37) in CDCl ₃	89
Figure A1.3. IR spectrum of 3-(triethylsilyl)benzaldehyde (37).....	89
Figure A1.4. ¹ H NMR spectrum of 1,5-bis-[3-(triethylsilyl)phenyl]penta-1,4-dien-3-one, mtdba (38) in CDCl ₃	90
Figure A1.5. ¹³ C NMR spectrum of 1,5-bis-[3-(triethylsilyl)phenyl]penta-1,4-dien-3-one, mtdba (38) in CDCl ₃	91
Figure A1.6. IR spectrum of 1,5-bis-[3-(triethylsilyl)phenyl]penta-1,4-dien-3-one, mtdba (38) in CDCl ₃	91
Figure A1.7. ¹ H NMR spectrum of [Pd ₂ (mtdba) ₃] (39) in CDCl ₃	92
Figure A1.8. ¹³ C NMR spectrum of [Pd ₂ (mtdba) ₃] (39) in CDCl ₃	93
Figure A1.9. ¹ H NMR spectrum of intermediate 31 in THF _{d-8} at -28 °C.....	94
Figure A1.10. ¹³ C NMR spectrum of intermediate 31 in THF _{d-8} at -28 °C.....	95
Figure A1.11. IR spectrum of intermediate 31	95
Figure A1.12. ¹ H NMR spectrum of [(<i>S</i>)- <i>t</i> -BuPHOX]Pd(allyl)(OAc)•1/2THF (32) in THF _{d-8}	96
Figure A1.13. ¹³ C NMR spectrum of [(<i>S</i>)- <i>t</i> -BuPHOX]Pd(allyl)(OAc)•1/2THF (32) in THF _{d-8}	97
Figure A1.14. IR spectrum of [(<i>S</i>)- <i>t</i> -BuPHOX]Pd(allyl)(OAc)•1/2THF (32)	97
Figure A1.15. ¹ H NMR spectrum of [(<i>S</i>)- <i>t</i> -BuPHOX]Pd(dba) (30) in THF _{d-8}	98
Figure A1.16. ¹³ C NMR spectrum of [(<i>S</i>)- <i>t</i> -BuPHOX]Pd(dba) (30) in THF _{d-8}	99
Figure A1.17. IR spectrum of [(<i>S</i>)- <i>t</i> -BuPHOX]Pd(dba) (30)	99
Figure A1.18. ¹ H NMR spectrum of [(<i>S</i>)- <i>t</i> -BuPHOX]Pd(allyl)•PF ₆ Salt (25) in CDCl ₃	100
Figure A1.19. ¹³ C NMR of [(<i>S</i>)- <i>t</i> -BuPHOX]Pd(allyl)•PF ₆ Salt (25) in CDCl ₃	101
Figure A1.20. IR of [(<i>S</i>)- <i>t</i> -BuPHOX]Pd(allyl)•PF ₆ Salt (25).....	101
Figure A1.21. ¹ H NMR spectrum of (<i>S</i>)- <i>t</i> -BuPHOX oxide (i) in CDCl ₃	102
Figure A1.22. ¹³ C NMR spectrum of (<i>S</i>)- <i>t</i> -BuPHOX oxide (i) in CDCl ₃	103
Figure A1.23. IR NMR spectrum of (<i>S</i>)- <i>t</i> -BuPHOX oxide (i)	103
Figure A2.1. Representation of [(<i>S</i>)- <i>t</i> -BuPHOX]Pd(0)(dba) 30	105
Figure A2.2. Representation of Palladium Allyl Carboxylate 31	115
Figure A2.3. Representation of Palladium Allyl Acetate 32	123
Figure 3.1. Palladium η ¹ Allyl Species of Interest to the Study of Allylic Alkylation.....	132
Figure 3.2. Characteristic η ¹ and η ³ Allyl ¹³ C NMR Shifts (δ) Found for 31 , 32 , and 25 in THF _{d-8} ..	133
Figure 3.3. Characteristic η ¹ and η ³ Allyl ¹ H NMR Shifts (δ) Found for 31 , 32 , and 25 in THF _{d-8}	134
Figure 3.4. Allyl Termini Exchange Patterns for 31 and 32	135
Figure 3.5. Allyl Exchange Pattern Between Endo and Exo 25	139
Figure 3.6. The Only Allyl Isomerization Mode Observable for 25	139
Figure 3.7. ¹ H NMR Broadening Indicating THF _{d-8} Accelerated Allyl Isomerization Relative to CDCl ₃ 140	
Figure 3.8. Activation Parameters for Exo/Endo Allyl Isomerization of 25	141
Figure 3.9. Equatorial Associative Exo/Endo Allyl Isomerization Mechanism of 25 as Demonstrated for Carboxylate Nucleophiles by Complexes 31 and 32	142
Figure 3.10. Possible Apical Associative Exo/Endo Allyl Isomerization Mechanism of 25	142

Figure 3.11. Minimum Isomerization Modes Necessary for 25 to Facilitate Complete Allyl Termini Exchange as Observed for Carboxylates 31 and 32	143
Figure 3.12. Apparent Free Allyl Acetate and Second Palladium Species in Equilibrium with 32	146
Figure 3.13. Possible Means of Allyl Termini Scrambling via the Allyl Carboxylate Equilibrium.....	148
Figure 3.14. Reported Mechanisms for Palladium Allyl Carboxylate Reductive Elimination.....	150
Figure 3.15. Allyl Termini Scrambling Mechanisms Most Consistent with the Literature.....	151
Figure 3.16. Carbonate 30 , the Putative Allyl Enol Carbonate Derived Analogue to Carboxylate 31	152
Figure 3.17. Complete Solution Behavior for Complexes 31 , 32 , and 25	154

List of Schemes

Scheme 1.1. Asymmetric Allylic Alkylation Used for the Synthesis of Chiral Quaternary Carbons.....	2
Scheme 1.2. Branched Versus Linear Allylic Alkylation Products Are Favored By Palladium Impeding the Generation of Allylic Quaternary Carbon Stereocenters.	3
Scheme 1.3. Select Examples of Palladium Catalyzed Allylic Alkylation Product Distributions.....	3
Scheme 1.4. The Linear Product Preference Found for Palladium-Catalyzed Asymmetric Allylic Alkylation Does Not Limit the Formation of Chiral Quaternary Carbon Stereocenters from Prochiral Nucleophiles.....	4
Scheme 1.5. Trost's Initial Allylic Alkylation Methodologies for Prochiral Ketone Nucleophiles.....	5
Scheme 1.6. Base-Free Palladium-Catalyzed Decarboxylative Allylic Alkylation of Ketone Enolates...	6
Scheme 1.7. Regioselective Preference in Tsuji's Allylic Alkylation Substrate Classes	6
Scheme 1.8. Palladium-Catalyzed Allylic Alkylation and the PHOX Ligand Architecture	7
Scheme 1.9. General Outer-Sphere Mechanism for Palladium-Catalyzed Allylic Alkylation of Soft Nucleophiles	8
Scheme 1.10. An Outer-Sphere Allylic Alkylation of Ketone Enolates Implies a Free Enolate.	8
Scheme 1.11. The Success of Potentially Enolate Sensitive Substrates.....	9
Scheme 1.12. Consistent Product Yield and Enantioinduction Implies a Common Mechanism.	14
Scheme 1.13. Generalized Inner-Sphere Mechanism for Palladium-Catalyzed Allylic Alkylation.....	16
Scheme 1.14. Original Crossover Experiment	18
Scheme 2.1. Asymmetric and Bond-Forming Events Are Understood to be Common to All Three Substrate Classes.	24
Scheme 2.2. Isolation and X-Ray Structure of Initial Catalyst Complex 30	29
Scheme 2.3. Decarboxylative Asymmetric Allylic Alkylation Catalyzed by Isolated Complex 30	29
Scheme 2.4. Isolation and X-Ray Structure of Palladium Carboxylate 31	31
Scheme 2.5. Synthesis and X-Ray Structure of Canonical Palladium Allyl Acetate Complex 32	33
Scheme 2.6. Underlying Structural and Chemical Similarity between 31 , 32 , and 27	35
Scheme 2.7. Thermal Decomposition of 31 in the Presence of Free dba Ligand in THF.....	37
Scheme 2.8. Thermal Decomposition of 31 Without dba in THF and Neat	37
Scheme 3.1. Initial Observation of Palladium Allyl Carboxylate 31	132
Scheme 3.2. The Three Possible Mechanisms for Chemical Exchange Between (<i>R,S</i>) and (<i>S,S</i>) 31 ..	137
Scheme 3.3. Stereochemical Enrichment of The Quaternary Center in the Synthesis of 31	137
Scheme 3.4. Allyl Acetate Reductive Elimination and Oxidative Addition Observed for 32 in THF _{d-8}	145
Scheme 3.5. Implied Equilibrium for Carboxylate 31 by Analogy to 32	145
Scheme 3.6. Select Examples of Previously Reported Systems with Palladium Allyl Species in Equilibrium with Allyl Carboxylates	145
Scheme 3.7. The Same Allyl Terminus Selectivity is Expected for the Two Standard Mechanisms of Allyl Carboxylate Reductive Elimination in PHOX Palladium Allyl Carboxylates.	151
Scheme 3.8. Crossover Experiment Shows Complete Crossover and Allyl Termini Scrambling.....	153

List of Tables

Table 1.1. The Effects of Water on Decarboxylative Asymmetric Allylic Alkylation.....	9
Table 1.2. Consistent Results Across All Three Substrate Classes.....	12
Table A2.1. Crystal Data and Structure Refinement for NHS03 (CCDC 606912).	106
Table A2.2. Atomic Coordinates ($\times 10^4$) and Equivalent Isotropic Displacement Parameters ($\text{\AA}^2 \times 10^3$) for NHS03 (CCDC 606912). $U(\text{eq})$ is defined as the trace of the orthogonalized U^{ij} tensor.	108
Table A2.3. Selected Bond Lengths [\AA] and Angles [$^\circ$] for NHS03 (CCDC 606912)	110
Table A2.4. Bond lengths [\AA] and angles [$^\circ$] for NHS03 (CCDC 606912).	111
Table A2.5. Anisotropic Displacement Parameters ($\text{\AA}^2 \times 10^4$) for NHS03 (CCDC 606912). The anisotropic displacement factor exponent takes the form: $-2\pi^2 [h^2 a^{*2} U^{11} + \dots + 2 h k a^* b^* U^{12}]$.	114
Table A2.6. Crystal Data and Structure Refinement for NHS20 (CCDC 695531)	116
Table A2.7. Atomic Coordinates ($\times 10^4$) and Equivalent Isotropic Displacement Parameters ($\text{\AA}^2 \times 10^3$) for NHS20 (CCDC 695531). $U(\text{eq})$ is defined as the trace of the orthogonalized U^{ij} tensor.	118
Table A2.8. Selected Bond Lengths [\AA] and Angles [$^\circ$] for NHS20 (CCDC 695531).....	119
Table A2.9. Bond Lengths [\AA] and Angles [$^\circ$] for NHS20 (CCDC 695531).....	120
Table A2.10. Anisotropic Displacement Parameters ($\text{\AA}^2 \times 10^4$) for NHS20 (CCDC 695531). The anisotropic displacement factor exponent takes the form: $-2\pi^2 [h^2 a^{*2} U^{11} + \dots + 2 h k a^* b^* U^{12}]$.	122
Table A2.11. Crystal Data and Structure Refinement for NHS22 (CCDC 701671).	124
Table A2.12. Atomic Coordinates ($\times 10^4$) and Equivalent Isotropic Displacement Parameters ($\text{\AA}^2 \times 10^3$) for NHS22 (CCDC 701671). $U(\text{eq})$ is defined as the trace of the orthogonalized U^{ij} tensor.	126
Table A2.13. Selected Bond Lengths [\AA] and Angles [$^\circ$] for NHS22 (CCDC 701671).	127
Table A2.14. Bond Lengths [\AA] and Angles [$^\circ$] for NHS22 (CCDC 701671).....	128
Table A2.15. Anisotropic Displacement Parameters ($\text{\AA}^2 \times 10^4$) for NHS22 (CCDC 701671). The anisotropic displacement factor exponent takes the form: $-2\pi^2 [h^2 a^{*2} U^{11} + \dots + 2 h k a^* b^* U^{12}]$.	130
Table 3.1. Some Select Rates and the Effects of Water on the Exo/Endo Allyl Isomerization of 25 ...	142

List of Abbreviations

$[\alpha]_D$	angle of optical rotation of plane-polarized light
Å	angstrom(s)
APCI	atmospheric pressure chemical ionization
app	apparent
aq	aqueous
Ar	aryl group
atm	atmosphere(s)
BHT	2,6-di- <i>tert</i> -butyl-4-methylphenol (“ <u>b</u> utylated <u>h</u> ydroxy <u>t</u> oluene”)
Bn	benzyl
bp	boiling point
br	broad
Bu	butyl
<i>i</i> -Bu	<i>iso</i> -butyl
<i>n</i> -Bu	butyl or <i>norm</i> -butyl
<i>t</i> -Bu	<i>tert</i> -butyl
Bz	benzoyl
<i>c</i>	concentration of sample for measurement of optical rotation
^{13}C	carbon-13 isotope
°C	degrees Celsius
calc’d	calculated
CCDC	Cambridge Crystallographic Data Centre
cm^{-1}	wavenumber(s)

comp	complex
conc.	concentrated
d	doublet
<i>d</i>	dextrorotatory
D	deuterium
dba	<i>trans,trans</i> -dibenzylideneacetone
DBU	1,8-diazabicyclo[5.4.0]undec-7-ene
DCE	1,2-dichloroethane
<i>de</i>	diastereomeric excess
DME	1,2-dimethoxyethane
DMF	<i>N,N</i> -dimethylformamide
DMSO	dimethylsulfoxide
DPPA	diphenylphosphorylazide
dppp	1,3-bis(diphenylphosphino)propane
dr	diastereomeric ratio
<i>ee</i>	enantiomeric excess
<i>E</i>	<i>trans</i> (entgegen) olefin geometry
e.g.	for example (Latin: <i>exempli gratia</i>)
EI	electron impact
eq	equation
ESI	electrospray ionization
Et	ethyl
<i>et al.</i>	and others (Latin: <i>et alia</i>)

FAB	fast atom bombardment
g	gram(s)
h	hour(s)
^1H	proton
^2H	deuterium
HPLC	high performance liquid chromatography
HRMS	high resolution mass spectrometry
Hz	hertz
i.e.	that is (Latin: <i>id est</i>)
IR	infrared spectroscopy
J	coupling constant
k	rate constant
kcal	kilocalorie(s)
kg	kilogram(s)
L	liter or neutral ligand
l	levorotatory
m	multiplet or meter(s)
M	molar or molecular ion
m	meta
μ	micro
Me	methyl
mg	milligram(s)
MHz	megahertz

min	minute(s)
mL	milliliter(s)
MM	mixed method
mol	mole(s)
mp	melting point
Ms	methanesulfonyl (mesyl)
MS	molecular sieves
<i>m/z</i>	mass-to-charge ratio
N	normal or molar
nm	nanometer(s)
NMR	nuclear magnetic resonance
NOE	nuclear Overhauser effect
NOESY	nuclear Overhauser enhancement spectroscopy
Nu / Nu ⁻	nucleophile (neutral / anionic)
<i>o</i>	ortho
[O]	oxidation
<i>t</i> -Oct	<i>tert</i> -octyl (1,1,3,3-tetramethylbutyl)
<i>p</i>	para
Ph	phenyl
pH	hydrogen ion concentration in aqueous solution
p <i>K_a</i>	acid dissociation constant
ppm	parts per million
PPTS	pyridinium <i>para</i> -toluenesulfonate

Pr	propyl
<i>i</i> -Pr	isopropyl
<i>n</i> -Pr	propyl or <i>norm</i> -propyl
psi	pounds per square inch
py	pyridine
q	quartet
R	alkyl group
<i>R</i>	rectus
ref	reference
R_f	retention factor
s	singlet or seconds
<i>s</i>	selectivity factor = $k_{rel(fast/slow)} = \ln[(1 - C)(1 - ee)] / \ln[(1 - C)(1 + ee)]$, where <i>C</i> = conversion
<i>S</i>	sinister
sat.	saturated
t	triplet
TBAF	tetra- <i>n</i> -butylammonium fluoride
TBAT	tetra- <i>n</i> -butylammonium difluorotriphenylsilicate
TCA	trichloroacetic acid
temp	temperature
TES	triethylsilyl
TFA	trifluoroacetic acid
TFE	2,2,2-trifluoroethanol
THF	tetrahydrofuran

TLC	thin layer chromatography
TMEDA	<i>N,N,N',N'</i> -tetramethylethylenediamine
TMS	trimethylsilyl
TOF	time-of-flight
tol	tolyl
Ts	<i>para</i> -toluenesulfonyl (tosyl)
UV	ultraviolet
w/v	weight per volume
v/v	volume per volume
X	anionic ligand or halide
Z	cis (zusammen) olefin geometry

Chapter 1

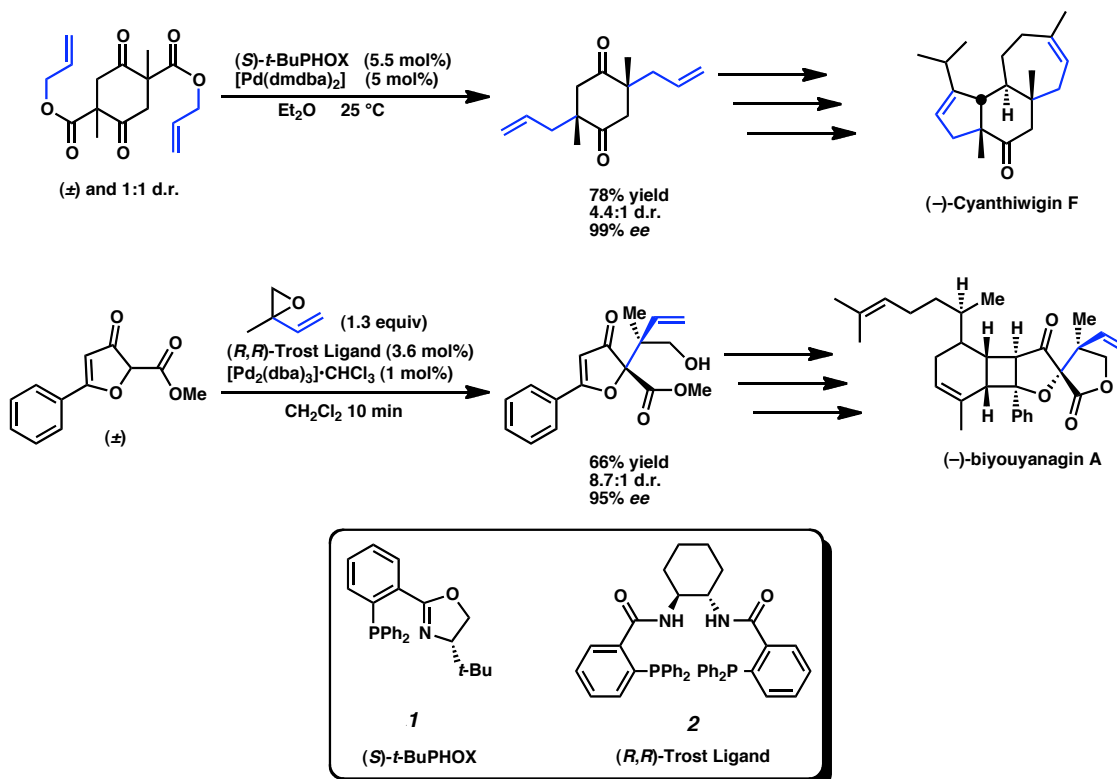
The History and Previous Investigations of Palladium-Catalyzed Decarboxylative Asymmetric Allylic Alkylation of Ketone Enolates Using the PHOX Ligand Architecture

1.1 Introduction and Background

1.1.1 General Background

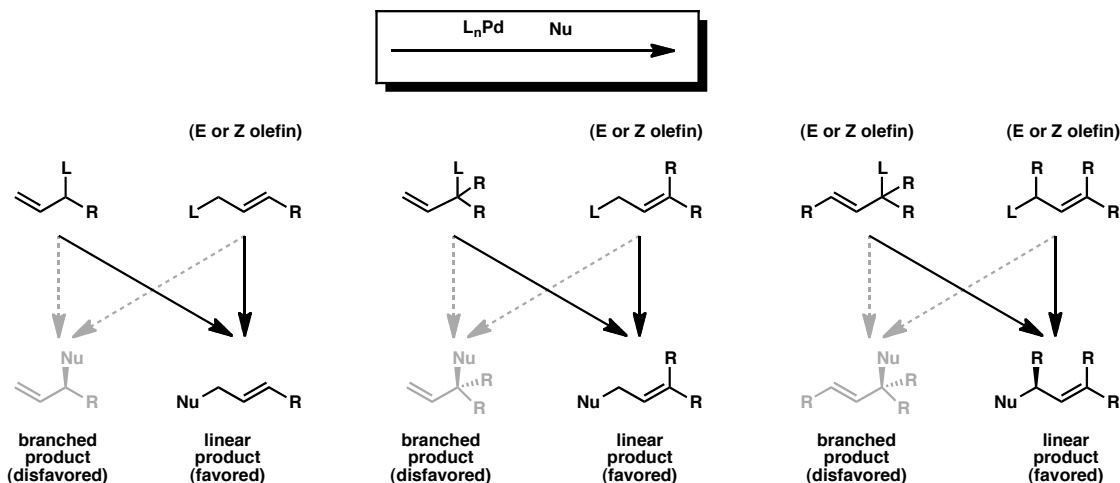
The asymmetric catalytic synthesis of all-carbon quaternary stereocenters remains an important challenge in chemical synthesis.¹ Continuous advancement in palladium-catalyzed asymmetric allylic alkylation chemistry has caused it to emerge as a particularly versatile solution among the few general classes of methodologies capable of rising to this challenge (Scheme 1.1 on page 2).² Initially, however, stereocontrol over carbon-carbon bond formation at highly substituted carbon centers in palladium-catalyzed asymmetric allylic alkylation was limited to the allyl fragment, and achiral nucleophiles were necessary in most implementations.^{3,4}

Scheme 1.1. Asymmetric Allylic Alkylation Used for the Synthesis of Chiral Quaternary Carbons⁵

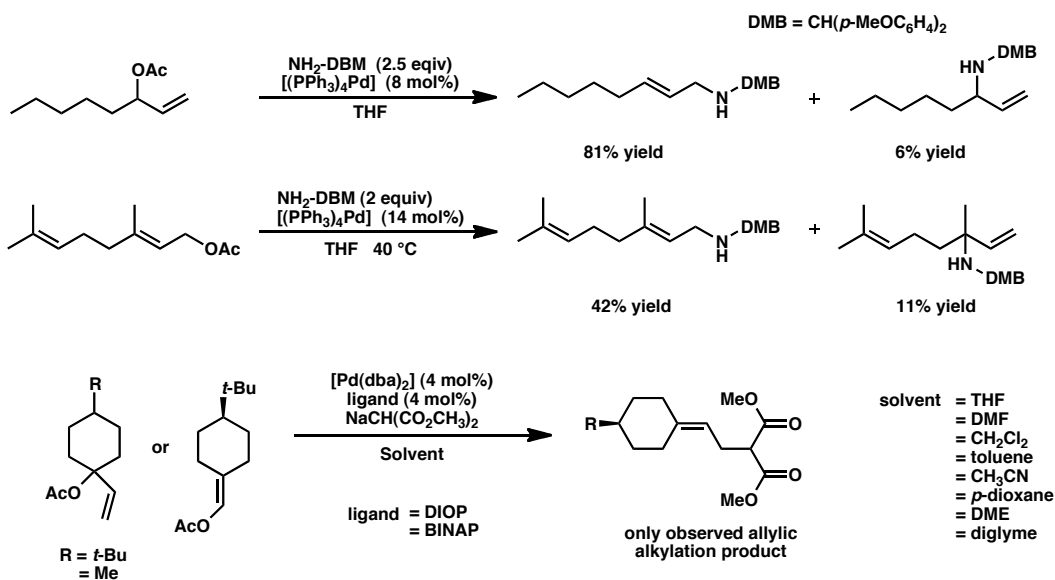


These early methodologies were generally limited to the formation of tertiary carbon stereocenters.⁶ This is because palladium-catalyzed allylic alkylation has a strong preference for alkylating with the least-hindered terminus of a differentially substituted allyl electrophile (Scheme 1.2 on page 3 and Scheme 1.3 on page 3).⁶ The preference of palladium for generating these linear instead of branched allylic alkylation products means that the formation of allylic quaternary centers is inherently disfavored whenever there is a less-substituted allyl terminus where alkylation can occur (Scheme 1.2, middle and right situations).

Scheme 1.2. Branched Versus Linear Allylic Alkylation Products Are Favored By Palladium Impeding the Generation of Allylic Quaternary Carbon Stereocenters.



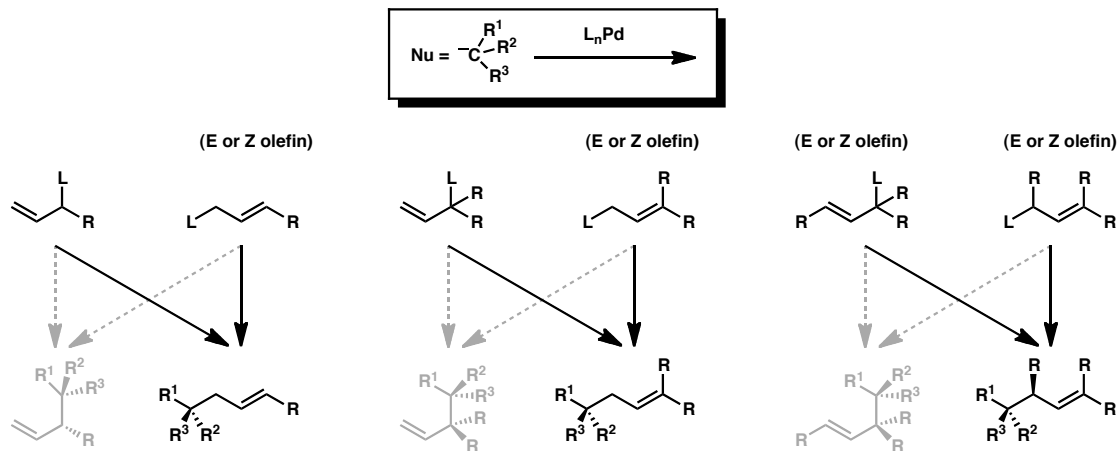
Scheme 1.3. Select Examples of Palladium Catalyzed Allylic Alkylation Product Distributions⁷



Subsequent developments in palladium-catalyzed asymmetric allylic alkylation by a number of groups allowed for the stereoselective generation of all-carbon quaternary stereocenters on the nucleophile for prochiral nucleophiles.^{8,9} These systems benefit from the fact that the linear over branched alkylation product preference of palladium, does not effect or limit the formation of quaternary stereocenters on prochiral nucleophiles (Scheme 1.4 on page 4). Thus by using nucleophiles that possess only a single reactive

site, the formation of chiral all-carbon quaternary stereocenters can reliably be made by these methodologies.

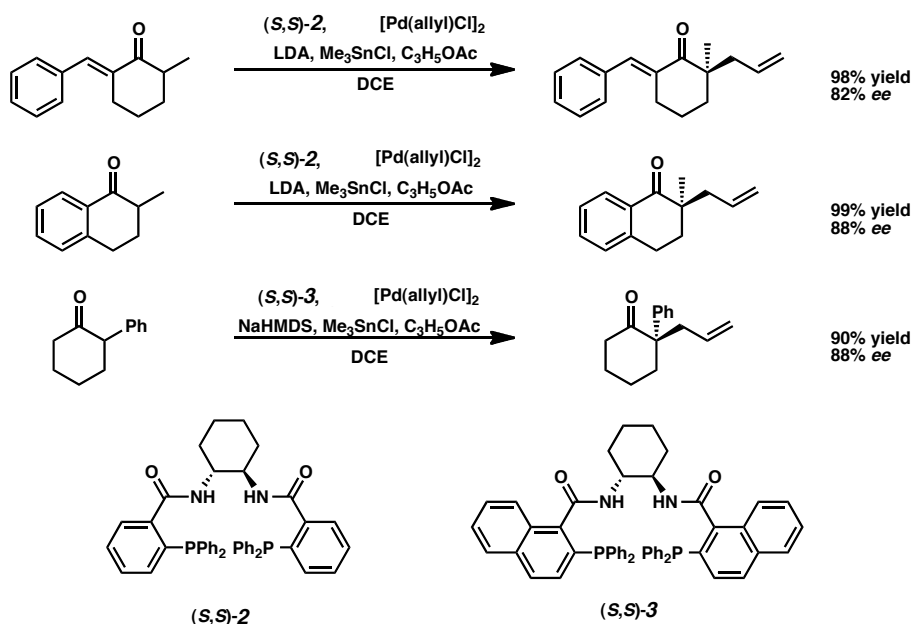
Scheme 1.4. The Linear Product Preference Found for Palladium-Catalyzed Asymmetric Allylic Alkylation Does Not Limit the Formation of Chiral Quaternary Carbon Stereocenters from Prochiral Nucleophiles.



While this development represents a key advancement in the synthesis of chiral all-carbon quaternary stereocenters, its early incarnations have some limitations. Most of these methodologies generate their carbon nucleophiles via stoichiometric deprotonation.^{8,9} For many carbon nucleophiles, such as ketone enolates, this requires the stoichiometric addition of strong base, such as LDA, to the reaction (Scheme 1.5 on page 5).⁹ Such harsh conditions can limit the functional group tolerance of these reactions. Successful substrates tend to be absent of functional groups that are sensitive to base, strong nucleophiles, or modest electrophiles. Also, because allylic alkylation occurs at any sufficiently nucleophilic site, it becomes necessary under such conditions to find means to prevent both ambiguous and multiple deprotonation events, as this would form alternate carbon nucleophiles prone to alkylation.^{1b} As a result, the scope of the nucleophiles used in these earlier methodologies is generally limited by the need for the

intended site of allylic alkylation to be the most acidic by a number of pK_a units (Scheme 1.5).^{1b}

Scheme 1.5. Trost's Initial Allylic Alkylation Methodologies for Prochiral Ketone Nucleophiles⁹

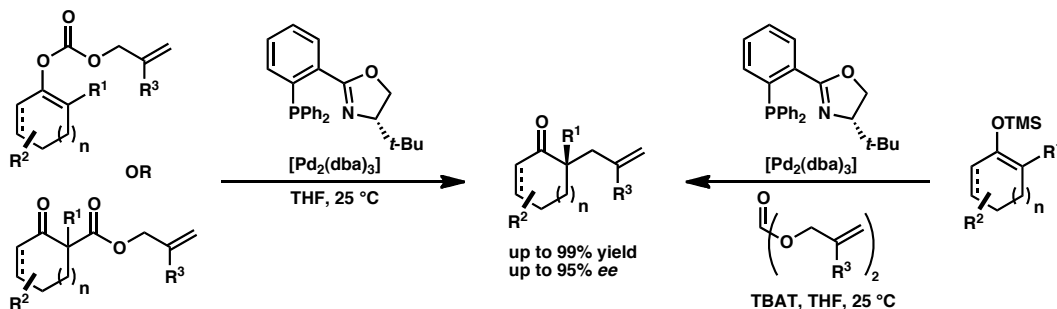


1.1.2 Palladium-Catalyzed Decarboxylative Asymmetric Allylic Alkylation

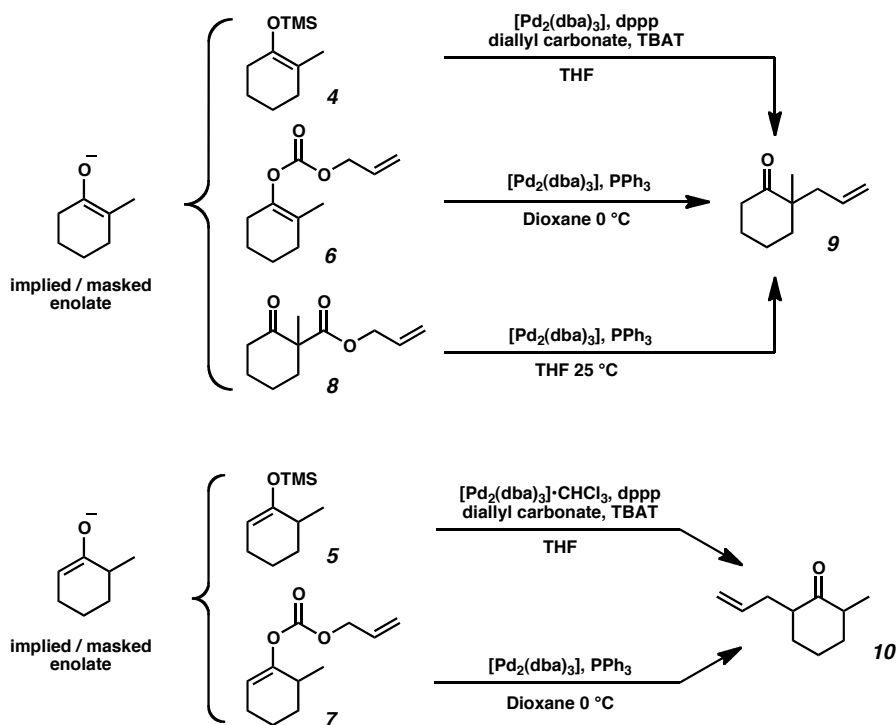
More recently, our group,¹⁰ and independently others,¹¹ reported a series of mild base-free palladium-catalyzed decarboxylative allylic alkylation conditions for ketone enolate nucleophiles (Scheme 1.6 on page 6). These methodologies are effective for generating chiral tetrasubstituted carbons, including all-carbon quaternary stereocenters, in high yield and good *ee*. The decarboxylative conditions employed by these methodologies are regioselective even for substrates possessing multiple sites of similar acidity to the one intended for alkylation. The success of these procedures relies on a few key enolate precursors as substrates: silyl enol ethers (**4** and **5**), allyl enol carbonates (**6** and **7**), and allyl β -ketoesters (**8**), which all function as masked ketone enolates and yield

the same allylic alkylation products (**9** and **10**) (Scheme 1.7 on page 6).^{10,11,12} The use of these masked enolate substrates in palladium catalyzed allylic alkylation was pioneered by Tsuji *et al.*, who demonstrated the strict regioselectivity for alkylation at the enolate geometry implied in the corresponding masked enolate.¹²

Scheme 1.6. Base-Free Palladium-Catalyzed Decarboxylative Allylic Alkylation of Ketone Enolates



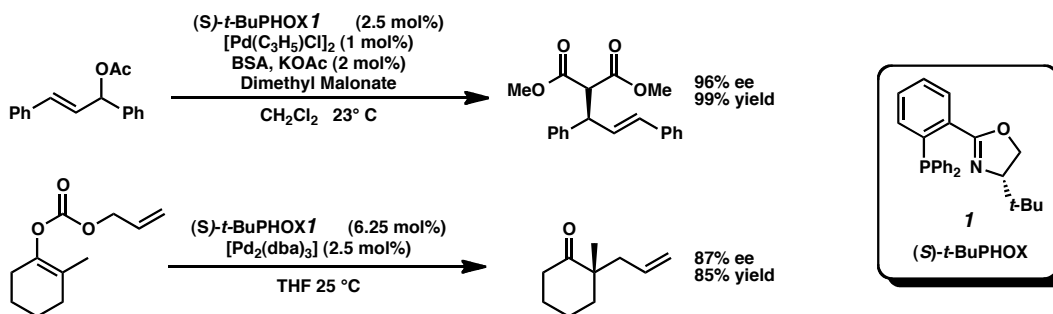
Scheme 1.7. Regioselective Preference in Tsuji's Allylic Alkylation Substrate Classes



Since its initial synthesis, the phophinoxazoline (PHOX) ligand architecture has proven highly effective for various palladium-catalyzed asymmetric allylic alkylation methodologies involving soft nucleophiles (Scheme 1.8, top reaction, on page 7).¹³ Our

initial system optimizations revealed that (*S*)-*t*-BuPHOX **1** was also an optimal ligand for effecting an asymmetric variant of the Tsuji alkylation while maintaining the mild conditions and regioselectivity found in Tsuji's original methodologies (Scheme 1.8, bottom reaction).^{10b} Subsequent to our initial reports, (*S*)-*t*-BuPHOX **1** has also found use in a few highly related decarboxylative asymmetric allylic alkylation systems.^{11a,f,14}

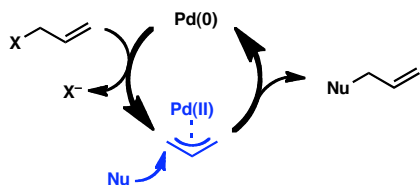
Scheme 1.8. Palladium-Catalyzed Allylic Alkylation and the PHOX Ligand Architecture



1.2 A Question of Mechanism

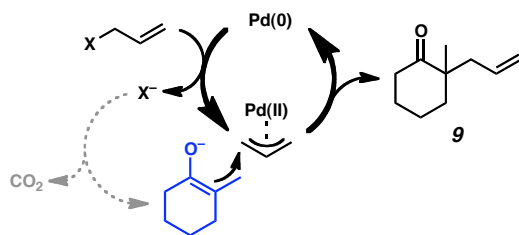
The mechanism of palladium-catalyzed asymmetric allylic alkylation of soft nucleophiles, defined as nucleophiles with a $pK_a < 20$,^{4,15} has been the subject of significant investigation, and is now well understood.^{4,15,16} The consensus of these studies is that bond forming occurs when soft nucleophiles attack directly at a π -allyl ligand of a palladium complex (Scheme 1.9 on page 8). This S_N2-like reaction is generally referred to as an outer-sphere allylic alkylation mechanism. Helmchen conducted some of the most pivotal of these seminal mechanistic studies on the PHOX ligand framework. It is thus accepted that outer-sphere allylic alkylation with soft nucleophiles is the standard allylic alkylation mechanism found for PHOX-ligand-based palladium catalysts.¹⁷

Scheme 1.9. General Outer-Sphere Mechanism for Palladium-Catalyzed Allylic Alkylation of Soft Nucleophiles



For the allylic alkylation of unstabilized ketone enolates, an outer-sphere mechanism would imply the formation of a free enolate species at least transiently during the course of the reaction (Scheme 1.10 on page 8). Mindful of the literature precedent concluding that palladium-catalyzed allylic alkylation functions by an outer-sphere mechanism, both in general and on the PHOX ligand framework, the initial supposition was that a free enolate was active in our allylic alkylation system. Subsequent to our initial publication, however, an increasingly large range of reaction conditions and substrate functional group diversity was explored.^{10a,18,19} In doing so it has become apparent that our methodology is surprisingly robust in light of a putative free enolate intermediate.

Scheme 1.10. An Outer-Sphere Allylic Alkylation of Ketone Enolates Implies a Free Enolate.



Substrates have been synthesized that present functionality with additional acidic sites or that serve as electrophiles potentially sensitive to free unstabilized ketone enolates, including: enones (**11** and **12**), nitriles (**13**), esters (**11** and **14**), and even unprotected aldehydes (**15**) (Scheme 1.11 on page 9).^{10b,19} Notably, all these substrates readily undergo palladium-catalyzed decarboxylative asymmetric allylic alkylation with

no more than the occasional trace of side products under our conditions. Even the addition of up to 33.3 equivalents of water to the reaction failed to quench the putative enolate intermediate and only modestly reduced the yield of allylic alkylation product (Table 1.1 on page 9).¹⁸ While some of the more challenging asymmetric allylic alkylation substrates we attempted produced alkylation products in modest or low *ee*, extremely few substrates were found to produce any side products or to significantly perturb allylic alkylation. Together these results raised serious questions about the possibility of a free enolate intermediate and thus the nature of the mechanism itself.

Scheme 1.11. The Success of Potentially Enolate Sensitive Substrates^{10b,19}

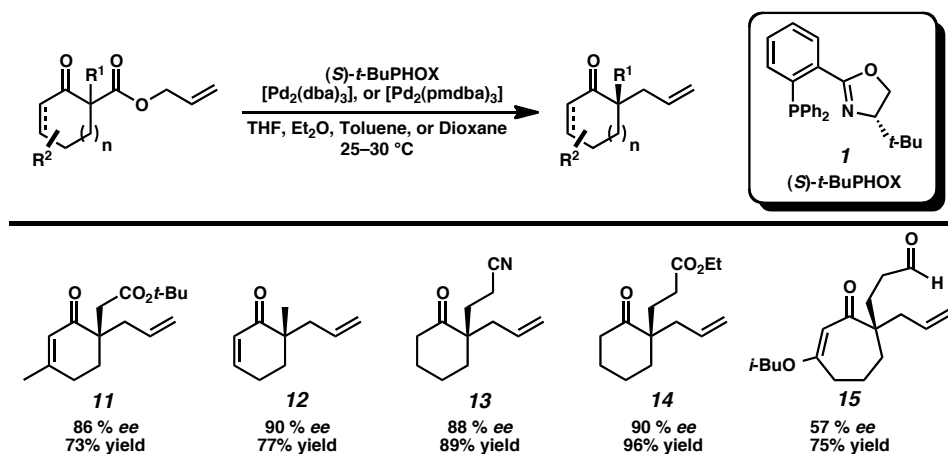
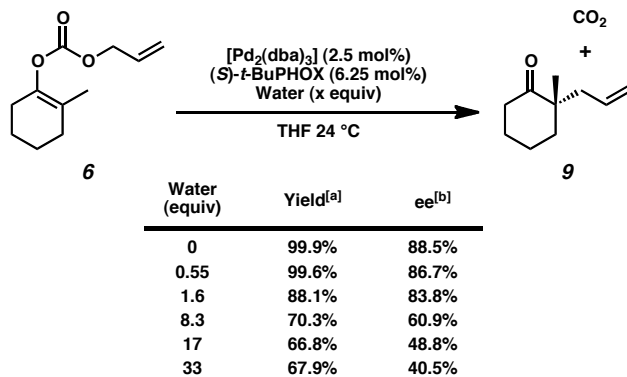


Table 1.1. The Effects of Water on Decarboxylative Asymmetric Allylic Alkylation



Data reported is the average of three trials. [a] GC yield relative to internal standard (tridecane), [b] Enantiomeric excess measured by chiral GC

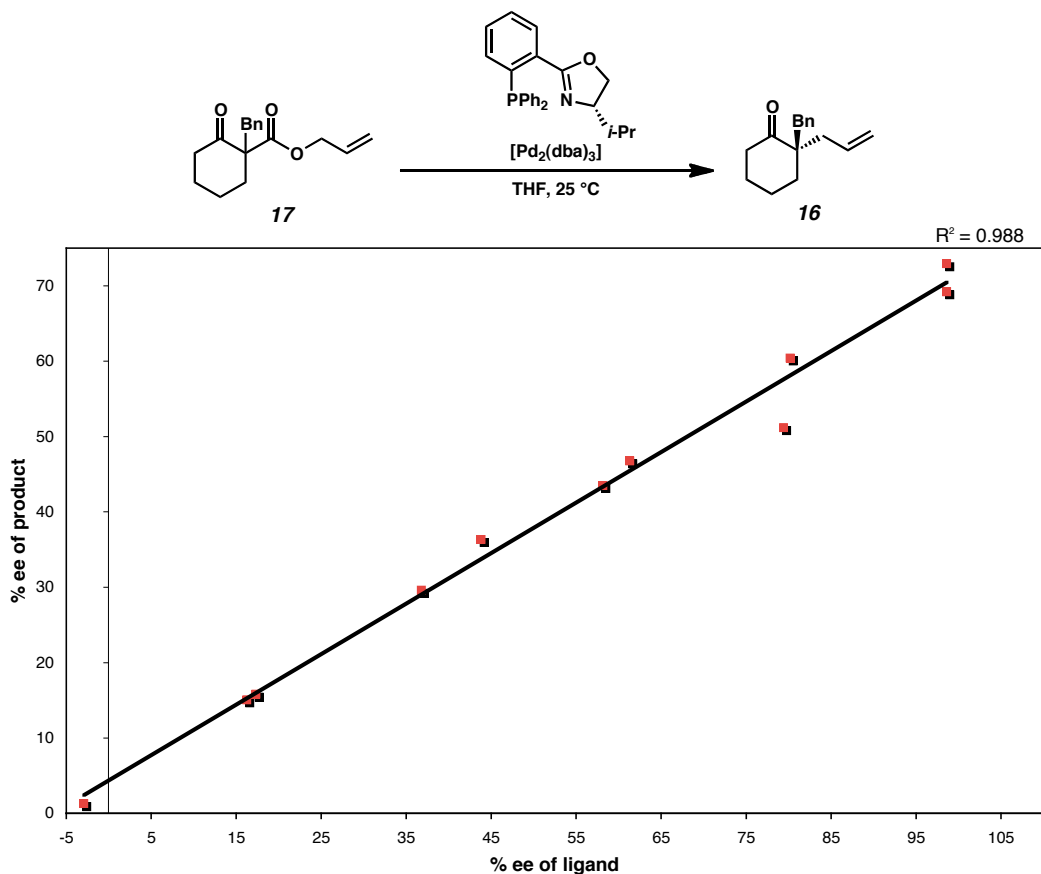
1.3 Initial Mechanistic Investigation

We began our mechanistic investigation by determining the molecularity of the active catalyst in the reaction as starting point from which to direct the design of subsequent experiments. The enantioinduction imparted by our catalyst system was high enough to make it a good candidate for performing a nonlinear effect study to determine active catalyst molecularity as pioneered by Kagan.²⁰ By plotting the *ee* of the alkylation product formed versus the *ee* of the source of enantioinduction used in the reaction, the linearity of the dependence between the two can be determined. A positive or negative nonlinear dependency requires that the source of enantioinduction must aggregate under reaction conditions while a linear correlation implies a reaction mechanism that is likely devoid of such aggregation.

To this end, the dependency of the *ee* of ketone **16**, produced via the palladium-catalyzed decarboxylative allylic alkylation of racemic allyl β -ketoester **17**, was plotted against the *ee* of isopropyl PHOX ligand used in the reaction (Figure 1.1 on page 11).²¹ The resulting linear dependency is strongly suggestive of no PHOX ligand aggregation under reaction conditions. This implies the exclusion of a number of mechanistic possibilities. First, it is likely that only one PHOX ligand binds to palladium under the reaction conditions as opposed to bis-PHOX-ligated palladium species, which have been reported.²² Second, the linear dependence suggests that there are no PHOX ligated palladium-catalyst aggregates in solution either as catalytically active species or as unproductive catalyst resting states. Third, the linear dependence suggests that the step

or steps related to enantioinduction and bond forming in the mechanism involve only a single palladium species.

Figure 1.1. Nonlinear Effect Study of Palladium-Catalyzed Decarboxylative Allylic Alkylation

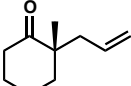
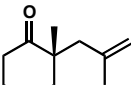
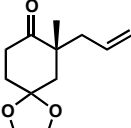
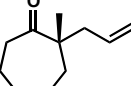


The *ee* of the *i*-PrPHOX ligand (X-axis) was varied by mixing freshly prepared stock solutions of enantiopure (*S*) and (*R*) *i*-PrPHOX ligand prior to each experiment and the mixture ratio confirmed by chiral HPLC. The product of each reaction was isolated and purified before obtaining *ee* (Y-axis) via HPLC.

The nonlinear effects studies were supported with traditional reaction kinetics studies. Kinetics studies of the decarboxylative allylic alkylation of allyl enol carbonate **XX** and allyl β -ketoester **XX** to form tetralone **23** determined that both the allyl enol carbonate and β -ketoester reactions were first order in catalyst and zero order in substrate (Figure 1.2 on page 13).²³ Notably all three substrate classes give allylic alkylation products in similar yields and practically identical *ee* (Table 1.2 on page 12).¹⁰ This is

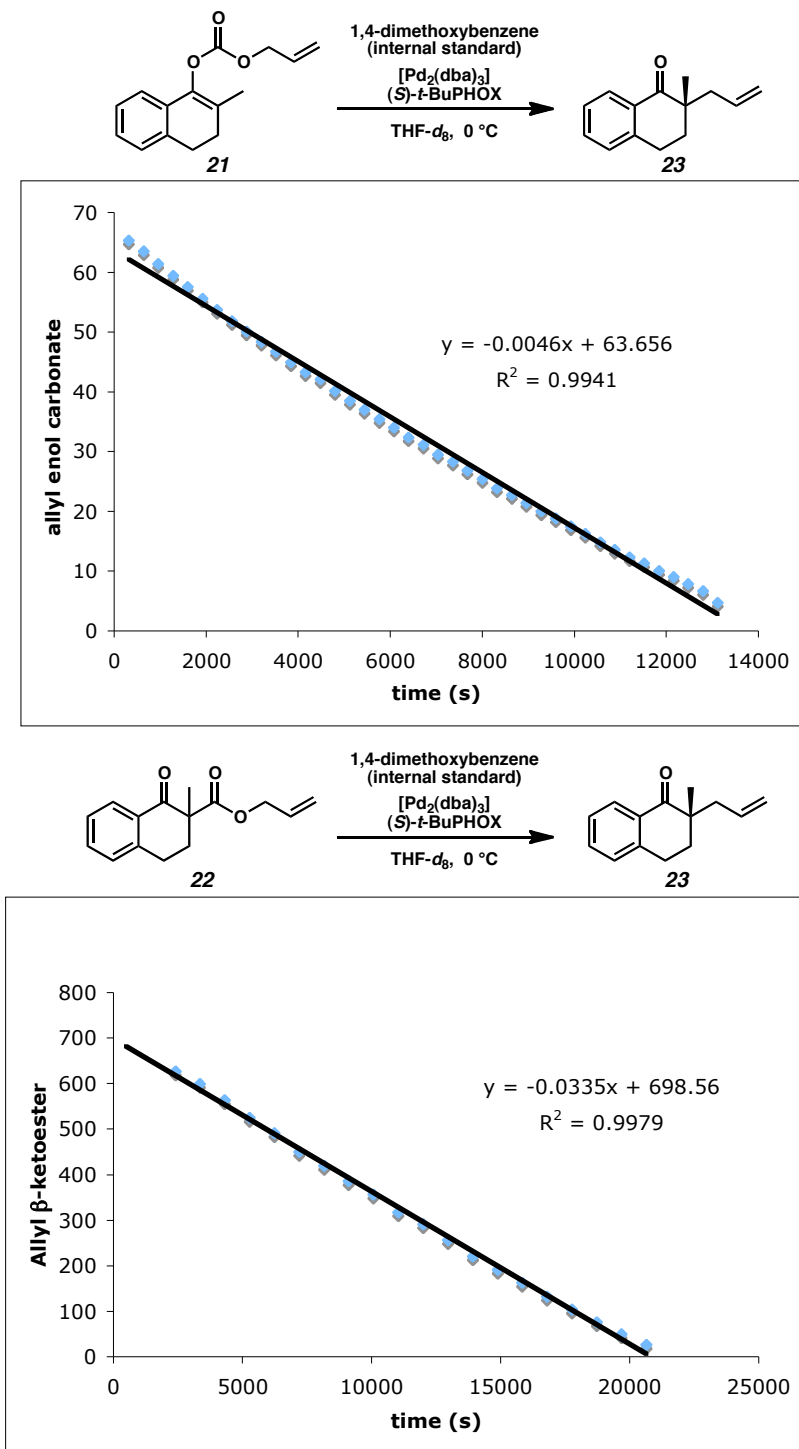
strongly suggestive of a single underlying mechanism that must converge at or before the formation of the ketone enolate intermediate (Scheme 1.12 on page 14). Together these results favor a universal mechanism involving a single monomeric PHOX palladium species for each step of both the productive catalytic cycle as well as any unproductive catalyst resting states that might exist.

Table 1.2. Consistent Results Across All Three Substrate Classes¹⁰

Product	allyl β -ketoester		allyl enol carbonate		silyl enol ether	
	yield ^a	ee ^b	yield ^a	ee ^b	yield ^a	ee ^b
 9	85	88	85	87	95	87
 18	87	92	89	92	79	91
 19	94	85	87	86	99	81
 20	83	87	81	87	94	86

[a] Isolated yield (%) from reactions with 1 mmol of substrate. [b] Measured by chiral GC or HPLC

Figure 1.2. Kinetics Studies Show Zero-Order Dependence on Substrate



Reactions were performed in an NMR tube on an 0.05 mm scale and monitored by ^1H NMR. Substrate concentration (Y-axis) is in arbitrary integration units relative to an internal standard consisting of 0.0175 mmol (35 mol%) 1,4-dimethoxybenzene.

With this knowledge in hand we turned to DFT to simulate the reaction of free enolate **24** with a single PHOX palladium π -allyl species **25**.^{23,24} Via DFT a traditional outer-sphere allylic alkylation path was identified favoring nucleophilic attack at the π -allyl terminus *trans* to phosphorous. This is in perfect accordance with previous mechanistic studies for palladium-catalyzed asymmetric allylic alkylation using the PHOX ligand architecture (Figure 1.3 on page 15).¹⁷ However, DFT simulation also predicted that this outer-sphere attack has practically no energy difference between the two facial approaches of the enolate nucleophile. If so, such an outer-sphere mechanism should result in near racemic allylic alkylation product.²⁴ The inconsistency of this simulated mechanism versus the experimentally observed results was highly unsatisfactory.

Scheme 1.12. Consistent Product Yield and Enantioinduction Implies a Common Mechanism.

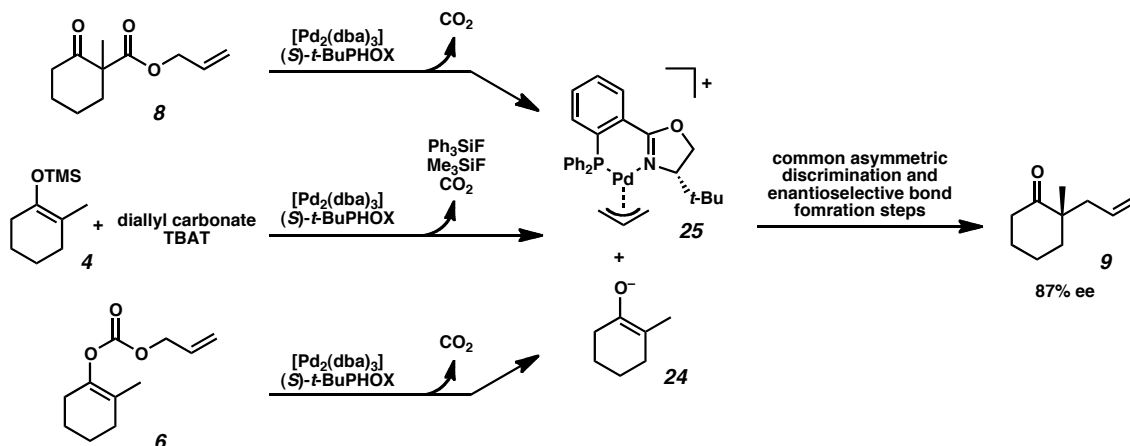
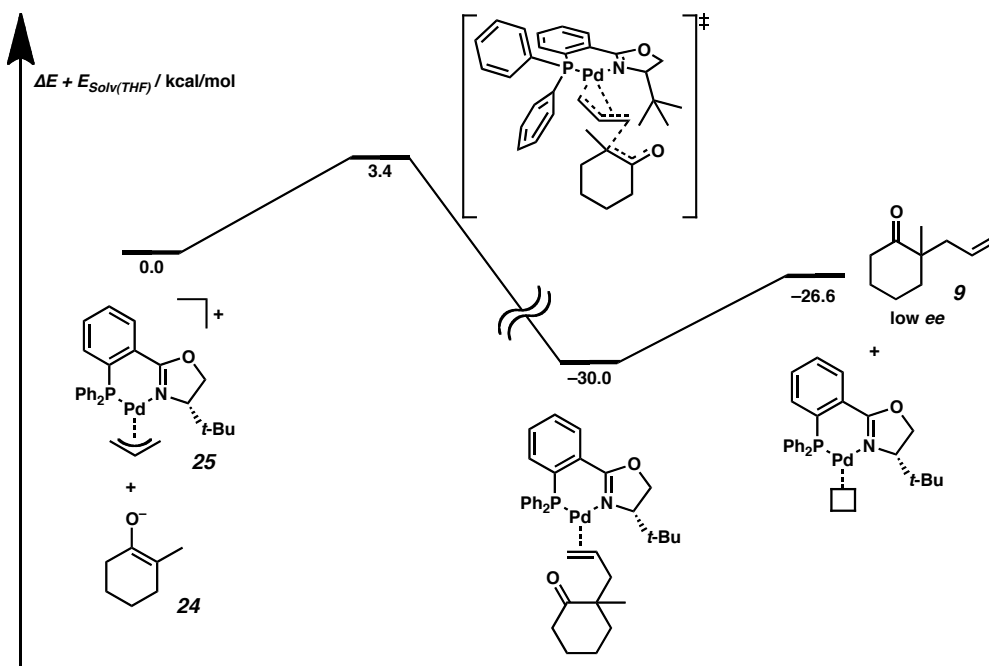
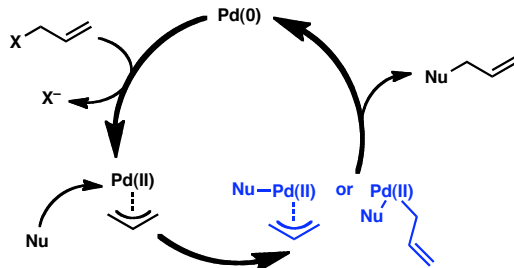


Figure 1.3. Results of DFT Simulation for Outer-Sphere Allylic Alkylation Starting with **24** and **25**

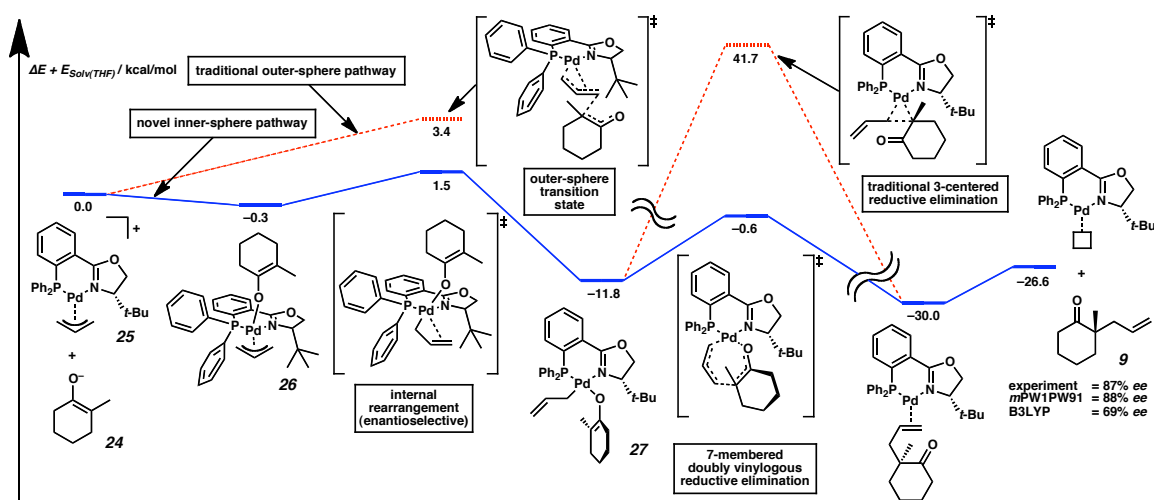
Literature precedent for the palladium-catalyzed allylic alkylation of hard nucleophiles suggests that they can proceed via an inner-sphere mechanism, whereby nucleophilic attack occurs at the metal center and subsequent bond forming occurs by a reductive elimination process (Scheme 1.13 on page 16).^{4,15} Noting this, we sought to use DFT to investigate an alternate inner-sphere alkylation pathway. DFT placed the energy of the ion-paired free enolate **24** and palladium π -allyl cation **25** as roughly isoenergetic to palladium π -allyl complex **26** with the enolate apically bound (Figure 1.4 on page 17). From complex **26** It was determined that an internal rearrangement involving the isomerization of the allyl ligand from an η -3 to an η -1 binding mode in conjunction with the collapse of the apical enolate ligand into the square plane could form palladium allyl enolate **27**. This internal rearrangement was computed to have a kinetic barrier 1.9 kcal/mole smaller than the outer-sphere allylic alkylation process

making the internal rearrangement the more kinetically favorable of the two processes.^{24,25}

Scheme 1.13. Generalized Inner-Sphere Mechanism for Palladium-Catalyzed Allylic Alkylation



O- to C-bond rearrangement of the enolate ligand from palladium allyl enolate **27** followed by a traditional 3-centered reductive elimination was calculated to have a prohibitively high kinetic barrier.^{23,24,26} However, a 7-centered doubly vinylogous reductive elimination directly from palladium allyl enolate **27** was determined to have a small kinetic barrier and thus be a viable mechanism for the production of ketone **9**. Previous calculation work²⁷ and subsequent experimentation²⁸ by others has demonstrated the feasibility and facile nature of highly related all-carbon 7-centered doubly vinylogous reductive eliminations from palladium to form carbon-carbon bonds. One particularly relevant example, the palladium-catalyzed allyl-allyl coupling of allylic carbonates and allylic boronic esters, has been achieved asymmetrically yielding products in high *ee*.^{28a} Subsequent calculations of orbital contribution and symmetry with all-carbon doubly vinylogous reductive eliminations from palladium have concluded that these are true pericyclic concerted reactions remarkably similar to the homo-Cope rearrangement but with a significantly smaller kinetic barrier.²⁹

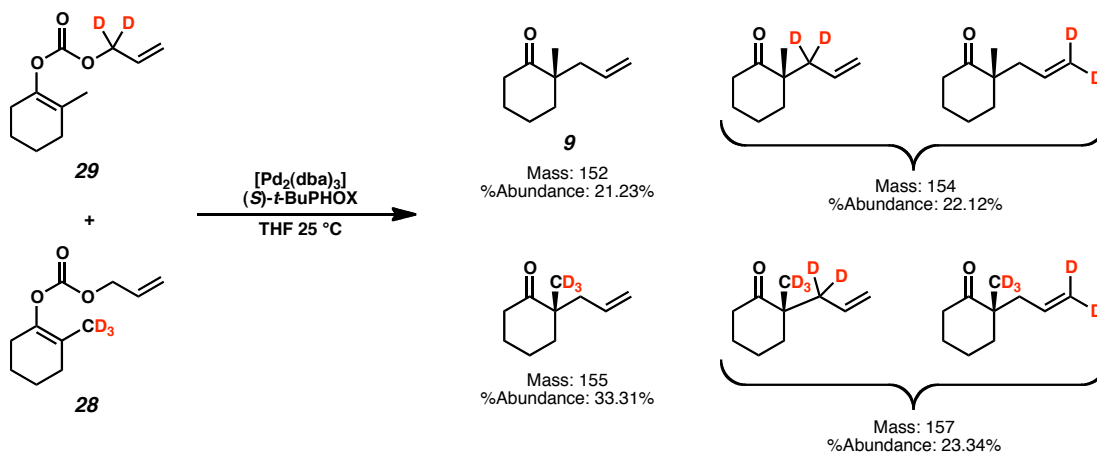
Figure 1.4 Results of DFT Simulation for Inner-Sphere Allylic Alkylation Starting with **24** and **25**

Notably DFT simulations found that the internal rearrangement from π -allyl palladium complex **26** to palladium allyl enolate **27** is enantioselective. The pro-*S* rearrangement that eventually gives rise to the experimentally observed enantiomer of product was calculated to be lower in energy than the pro-*R* rearrangement by 1.0 kcal/mol using the B3LYP basis set.²⁴ It was determined that most of the energy difference between the pro-*S* and pro-*R* rearrangements is due to the effects of chiral steric clashes manifested via intermolecular van der Waals interactions. To this effect, calculations on these internal rearrangements were also performed with the *mPW1PW91* functional, a hybrid DFT method considered better suited for accurately computing van der Waals interactions. The energy difference between the kinetic barriers for the pro-*S* and pro-*R* internal rearrangements arrived at by *mPW1PW91* was 1.6 kcal/mol, predicting product formation in roughly 88% *ee* at room temperature in excellent agreement with the experimentally observed results.

In search of experimental confirmation for an inner-sphere allylic alkylation mechanism we looked to a series of crossover experiments. Two different deuterium-

labeled forms of allyl enol carbonate **6** were synthesized, one with deuteration on the latent enolate fragment (**28**) and the other with deuteration on the allyl portion of the molecule (**29**) (Scheme 1.14 on page 18).^{10a} Performing a series of reactions with a one-to-one mixture of allyl enol carbonates **28** and **29** produced a statistical mixture of all six possible products, including those formed from allyl termini scrambling.^{10a} These results are a clear indication of complete crossover, seemingly indicating an outer-sphere mechanism.

Scheme 1.14. Original Crossover Experiment



Together these early mechanistic investigations painted a perplexing picture. The crossover experiments and literature precedence suggested an outer-sphere mechanism. However, DFT simulation, and the remarkable water and functional group tolerance of the reaction suggested an inner-sphere mechanism. A thorough follow-up study became necessary to reconcile these seemingly contradictory findings and to construct a complete and unifying mechanistic theory.

-
- (1) For reviews on the asymmetric catalytic synthesis of all-carbon quaternary stereocenters, see: (a) Trost, B. M.; Jiang, C.; *Synthesis* **2006**, *3*, 369–396. (b) Douglas, C. J.; Overman, L. E. *Proc. Natl. Acad. Sci. U.S.A.* **2004**, *101*, 5363–5367. (c) Christoffers, J.; Mann, A. *Angew. Chem., Int. Ed.* **2001**, *40*,

- 4591–4597. (d) Corey, E. J.; Guzman-Perez, A. *Angew. Chem., Int. Ed.* **1998**, *37*, 388–401.
- (2) For reviews of predominantly palladium-catalyzed asymmetric allylic alkylation with an emphasis on C-C bond forming including all-carbon quaternary stereocenters see: (a) Jensen, T.; Fristrup, P. *Dansk Kemi* **2009**, *90*, 32–34. (b) Braun, M.; Thorsten, M. *Angew. Chem., Int. Ed.* **2006**, *45*, 6952–6955. (c) Braun, M.; Meier, T. *Synlett* **2006**, 661–676. (d) You, S.-L.; Dai, L.-X. *Angew. Chem., Int. Ed.* **2006**, *45*, 5246–5248. (e) Trost, B. M. *J. Org. Chem.* **2004**, 532–539. (f) Helmchen, G.; Ernst, M.; Paradies, G. *Pure Appl. Chem.* **2004**, *76*, 494–506. (g) Trost, B. M.; Crawly, M. L. *Chem. Rev.* **2003**, *103*, 2921–2943. (h) Kazmaier, U. *Curr. Org. Chem.* **2003**, *7*, 317–328.
- (3) The contents of the most thorough reviews of palladium-catalyzed asymmetric allylic alkylation at the time demonstrate that the vast majority of methodologies were limited to systems that form tertiary carbon stereocenters on prochiral allyl fragments with achiral nucleophiles. For an example see reference 4.
- (4) Trost, B. M.; Van Vranken, D. L. *Chem. Rev.* **1996**, *96*, 395–422 and references therein.
- (5) (a) Du, C.; Li, L.; Li, Y.; Xie, Z. *Angew. Chem., Int. Ed.* **2009**, *48*, 7853–7856. (b) Enquist, J. A.; Stoltz, B. M. *Nature* **2008**, *453*, 1228–1231.
- (6) The well-known preference of palladium for nucleophilic substitution at the less hindered terminus of allyl electrophiles in π -allyl chemistry to afford the “linear” instead of “branched” alkylation products is actually in stark contrast to the chemical behavior seen in the π -allyl complexes of most other metals; see: (a) Graening, T.; Hartwig, J. F. *J. Am. Chem. Soc.* **2005**, *127*, 17192–17193. (b) Trost, B. M.; Hachiya, I. *J. Am. Chem. Soc.* **1998**, *120*, 1104–1105. (c) Glorius, F.; Pfaltz, A. *Org. Lett.* **1999**, *1*, 141–144. (d) Evans, P. A.; Nelson, J. D. *J. Am. Chem. Soc.* **1998**, *120*, 5581–5582. (e) Lloyd-Jones, G. C.; Pfaltz, A. *Angew. Chem., Int. Ed.* **1995**, *34*, 462–464.
- (7) (a) Fiaud, J.-C.; Legros, J.-Y. *J. Org. Chem.* **1990**, *55*, 4840–4849. (b) Trost, B. M.; Keinan, E. *J. Org. Chem.* **1979**, *44*, 3451–3457.
- (8) (a) Kuwano, R.; Uchida, K.; Ito, Y. *Org. Lett.* **2003**, *5*, 2177–2179. (b) Kuwano, R.; Ito, Y. *J. Am. Chem. Soc.* **1999**, *121*, 3236–3237. (c) Sawamura, M.; Nagata, H.; Sakamoto, H.; Ito, Y. *J. Am. Chem. Soc.* **1992**, *114*, 2586–2592. (d) Hayashi, T.; Kanehira, K.; Hagihara, T.; Kumada, M. *J. Org. Chem.* **1988**, *53*, 113–120.
- (9) (a) Trost, B. M.; Schroeder, G. M.; Kristensen, J. *Angew. Chem., Int. Ed.* **2002**, *41*, 3492–3495. (b) Trost, B. M.; Schroeder, G. M. *J. Am. Chem. Soc.* **1999**, *121*,

- 6759–6760. (c) Trost, B. M.; Radinov, R.; Grenzer, E. M. *J. Am. Chem. Soc.* **1997**, *119*, 7879–7880.
- (10) (a) Mohr, J. T.; Behenna, D. C.; Harned, A. M.; Stoltz, B. M. *Angew. Chem., Int. Ed.* **2005**, *44*, 6924–6927. (b) Behenna, D. C.; Stoltz, B. M. *J. Am. Chem. Soc.* **2004**, *126*, 15044–15045.
- (11) (a) Bélanger, É.; Cantin, K.; Messe, O.; Tremblay, M.; Paquin, J.-F. *J. Am. Chem. Soc.* **2007**, *129*, 1034–1035. (b) Trost, B. M.; Xu, J.; Reichle, M. *J. Am. Chem. Soc.* **2007**, *129*, 282–283. (c) Trost, B. M.; Xu, J. *J. Am. Chem. Soc.* **2005**, *127*, 2846–2847. (d) Burger, E. C.; Barron, B. R.; Tunge, J. A. *Synlett* **2006**, 2824–2826. (e) Trost, B. M.; Bream, R. N.; Xu, J. *Angew. Chem., Int. Ed.* **2006**, *45*, 3109–3112. (f) Nakamura, M.; Hajra, A.; Endo, K.; Nakamura, E. *Angew. Chem., Int. Ed.* **2005**, *44*, 7248–7251. (g) Trost, B. M.; Xu, J. *J. Am. Chem. Soc.* **2005**, *127*, 17180–17181.
- (12) (a) Tsuji, J.; Minami, I.; Shimizu, I. *Tetrahedron Lett.* **1983**, *24*, 1793–1796. (b) Tsuji, J.; Minami, I.; Shimizu, I. *Chem. Lett.* **1983**, 1325–1326. (c) Shimizu, I.; Yamada, T.; Tsuji, J. *Tetrahedron Lett.* **1980**, *21*, 3199–3202.
- (13) (a) Helmchen, G.; Pfaltz, A. *Acc. Chem. Res.* **2000**, *33*, 336–345. (b) von Matt, P.; Pfaltz, A. *Angew. Chem., Int. Ed. Engl.* **1993**, *32*, 566–568. (c) Sprinz, J.; Helmchen, G. *Tetrahedron Lett.* **1993**, *34*, 1769–1772. (d) Dawson, G. J.; Frost, C. G.; Williams, J. M. J.; Coote, S. J. *Tetrahedron Lett.* **1993**, *34*, 3149–3150.
- (14) Schulz, S. R.; Blechert, S. *Angew. Chem., Int. Ed.* **2007**, *46*, 3966–3970.
- (15) (a) Kuhn, O.; Mayr, Herbert. *Angew. Chem., Int. Ed.* **1999**, *38*, 343–346. (b) Åkermark, B.; Jutand, A. *J. Organomet. Chem.* **1981**, *217*, C41–C43.
- (16) For reviews of mechanistic studies for palladium-catalyzed asymmetric allylic alkylation, see: (a) Trost, B. M.; Lee, C. in *Catalytic Asymmetric Synthesis*, 2nd ed. (Ed.: Ojima, I.), Wiley-VCH, New York, **2000**, 593–649. (b) A. Pfaltz, M. Lautens, in *Comprehensive Asymmetric Catalysis* (Eds: Jacobsen, E. N.; Pfaltz, A.; Yamamoto, H.), Springer, Heidelberg, **1999**, 833–886.
- (17) (a) Vázquez, J.; Goldfuss, B.; Helmchen, G.; *J. Organomet. Chem.* **2002**, *641*, 67–70. (b) Kollmar, M.; Steinhagen, H.; Janssen, J. P.; Goldfuss, B.; Malinovskaya, S. A.; Vázquez, Rominger, F.; Helmchen, G. *Chem.—Eur. J.* **2002**, *8*, 3103–3114. (c) Kollmar, M.; Goldfuss, B.; Reggelin, M.; Rominger, F.; Helmchen, G. *Chem.—Eur. J.* **2001**, *7*, 4913–4927. (d) Helmchen, G.; Steinhagen, H.; Reggelin, M.; Kudis, S. in *Selective Reactions of Metal-Activated Molecules*, (Eds.: Werner, H.; Schreier, P.) Vieweg Verlag: Wiesbaden, 1998; 205–215. (e) Helmchen, G. *J. Organomet. Chem.* **1999**, *576*, 203–214. (f) Steinhagen, H.; Reggelin, M.; Helmchen, G.; *Angew. Chem., Int. Ed.* **1997**,

-
- 2108–2110. (g) Helmchen, G.; Kudis, S.; Sennhenn, P. Steinhagen, H. *Pure Appl. Chem.* **1997**, *69*, 513–518. (h) Sprintz, J.; Kiefer, M.; Helmchen, G.; Reggelin, M.; Huttner, G.; Walter, O.; Zsolnal, L. *Tetrahedron Lett.* **1994**, *35*, 1523–1526.
- (18) Behenna, D. C. *Progress Toward the Synthesis of (+)-Zoanthenol and The Development of an Asymmetric Tsuji Allylation Reaction*, Ph.D. Thesis, California Institute of Technology, Pasadena, CA, **2007**.
- (19) Hong, A. Y.; Krout, M. R.; Jensen, T.; Bennet, N. B.; Harned, A. M.; Stoltz, B. M. *Angew. Chem., Int. Ed.* **2011**, *in press*.
- (20) (a) Satyanarayana, T.; Abraham, S.; Kagan, H. B. *Angew. Chem., Int. Ed.* **2009**, *48*, 456–494. (b) Kagan, H. B.; Girard, C. *Angew. Chem., Int. Ed.* **1998**, *37*, 2922–2959.
- (21) The *R* and *S* *iso*-propyl PHOX ligands were used in place of the standard *R* and *S* *tert*-butyl PHOX ligands for this study due to the prohibitive cost of (*R*)-*tert*-butyl PHOX ligand. In general, *iso*-propyl and *tert*-butyl PHOX ligands give practically identical results when used with most standard substrates in palladium-catalyzed decarboxylative allylic alkylation of ketone enolates (see reference 10b). Similarly the *iso*-propyl and *tert*-Butyl variants of the PHOX ligand are known to demonstrate comparable results in other palladium catalyzed allylic alkylation systems as well (see reference 13). The *tert*-butyl variant of the ligand is only preferred over the *iso*-propyl variant in the palladium-catalyzed decarboxylative allylic alkylation of ketone enolates due to its slightly superior enantioinduction as revealed in the initial ligand screen (see reference 10b and the corresponding supporting information.)
- (22) While never isolated, bis-PHOX-ligated palladium species have been previously observed by NMR (see reference 17d). It may be possible that bis-PHOX-ligated palladium species can serve as active allylic alkylation catalysts in light of published evidence that bis-PHOX-ligated platinum species do serve as active catalysts in other allylic alkylation systems. Notably the bis-PHOX-ligated platinum species are reported to have the opposite sense of enantioinduction as the corresponding mono-PHOX-ligated platinum catalysts in allylic alkylation, see: John Blacker, A.; Clark, M. L.; Loft, M. S.; Williams, J. M. J. *Chem. Commun.* **1999**, 913–914.
- (23) Keith, J. A.; Behenna, D. C.; Mohr, J. T.; Ma, S.; Marinescu, S. C. Oxgaard, J.; Stoltz, B. M. Goddard, W. A. , III. *J. Am. Chem. Soc.* **2007**, *129*, 11876–11877.
- (24) Keith, J. A. *Computational Insight into Homogeneous Organopalladium Catalysis*, Ph.D. Thesis, California Institute of Technology, Pasadena, CA, **2008**.

- (25) In the initial publication (reference 23) the energy difference between the transition states for the pro-*S* internal rearrangement and the outer-sphere nucleophilic attack were determined to be 1.6 kcal/mol. Subsequent refinement in computing the energy of these transition states (reference 24) arrived at the 1.9 kcal/mol value.
- (26) Traditional 3-centered reductive elimination from palladium to form carbon-carbon bonds frequently has fairly high kinetic barriers relative to those found in palladium-catalyzed allylic alkylation. For an in depth discussion of the topic see: (a) Low, J. J.; Goddard, W. A., III. *J. Am. Chem. Soc.* **1986**, *108*, 6115–6128. (b) Low, J. J.; Goddard, W. A., III. *Organometallics* **1986**, *5*, 609–622.
- (27) (a) Cardenas, D. J.; Echavarren, A. M. *New J. Chem.* **2004**, *28*, 338–347. (b) Méndez, M.; Cuerva, J. M.; Gómez-Bengoa, E., Cárdenas, D. J.; Echavarren, A. M. *Chem.—Eur. J.* **2002**, *8*, 3620–3628.
- (28) (a) Zhang, P.; Brozek, L. A.; Morken, J. P. *J. Am. Chem. Soc.* **2010**, *132*, 10686–10688. (b) Flegeau, E. F.; Schneider, W.; Kobayashi S. *Chem.—Eur. J.* **2009**, 12247–12254.
- (29) Pérez-Rodríguez, M.; Braga, A. A. C.; de Lera, A. R.; Maseras, F.; Álvarez R. *Organometallics*, **2010**, *29*, 4983–4991.

Chapter 2

Unusual Allylpalladium Carboxylate Complexes: Identification of the Resting State of Catalytic Enantioselective Decarboxylative Allylic Alkylation Reactions of Ketones

2.1 Introduction

Our previous mechanistic investigations into the palladium-catalyzed decarboxylative asymmetric allylic alkylation of ketones enolates focused primarily on DFT simulation and product analysis under various conditions.¹ While these studies proved to be significantly informative, they did not create a complete mechanistic picture that could explain all of the experimentally observed results.² To this effect we sought to gain further experimental insight into this chemistry by studying the active catalytic reactions by NMR.

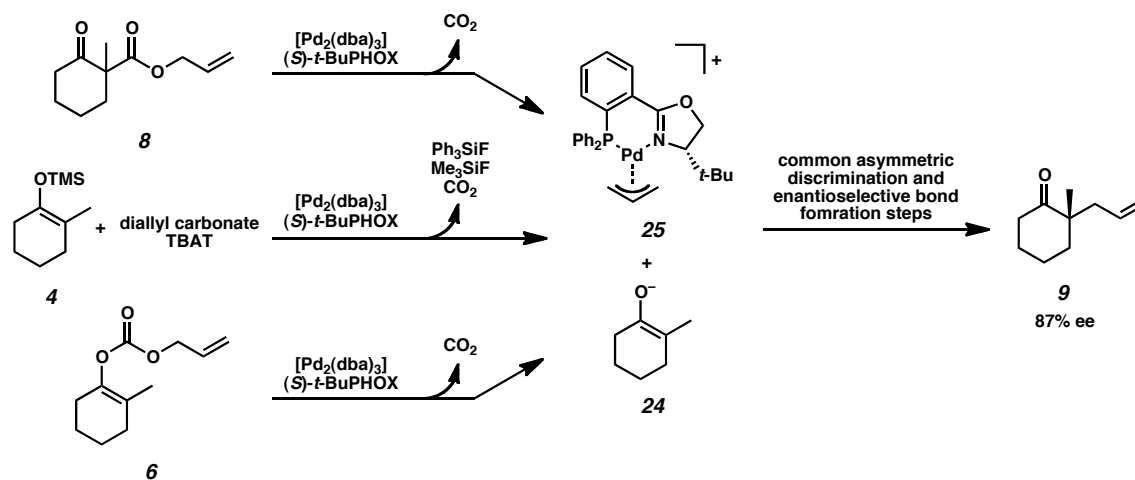
2.2 Observing the Reaction by ³¹P NMR

2.2.1 ³¹P NMR Studies of Allyl Enol Carbonates and Allyl β -Keto Ester Reactions

The phosphorous atom found in the PHOX ligand makes the allylic alkylation reaction a natural candidate for monitoring by ³¹P NMR. As all three substrate classes are understood to have a common underlying mechanism,² species visible by ³¹P NMR across

all three variants of the reaction represent potential key intermediates for this transformation (Scheme 2.1 on page 24). To this effect, the reactions of allyl enol carbonate **6**, allyl β -ketoester **8**, and silyl enol ether **4** were monitored and compared by ^{31}P NMR.

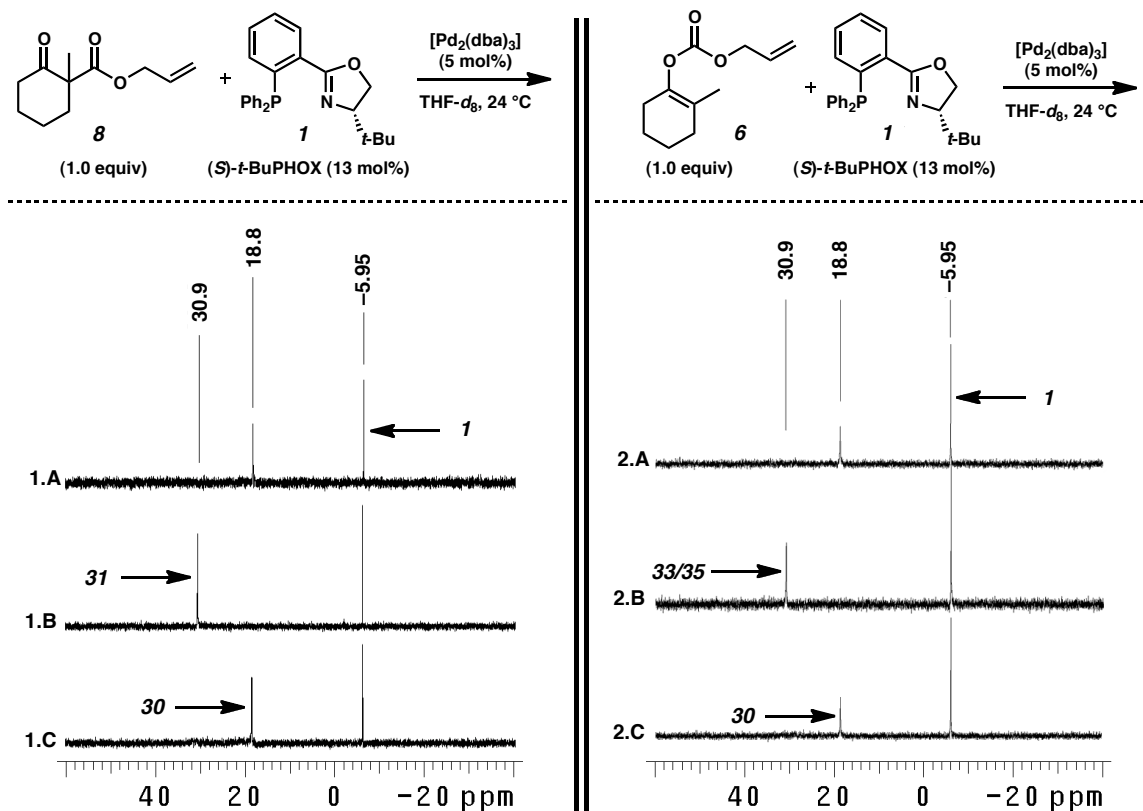
Scheme 2.1. Asymmetric and Bond-Forming Events Are Understood to be Common to All Three Substrate Classes.



Reactions of allyl enol carbonate **6** and allyl β -ketoester **8** appear nearly identical by ^{31}P NMR. The combination of $(S)\text{-}t\text{-BuPHOX}$ ligand **1** ($\delta = -5.95$ ppm) with $[\text{Pd}_2(\text{dba})_3]$ in a 2.6:1 ratio at room temperature for 30 minutes, as specified in our standard alkylation procedure,³ led to a single new phosphorous resonance at $\delta = 18.8$ ppm (Spectra **1.A** and **2.A**, in Figure 2.1 on page 25). The addition of β -ketoester **8** or allyl enol carbonate **6** resulted in the complete disappearance of the resonance at $\delta = 18.8$ ppm and produced a single long-lived resonance at $\delta = 30.9$ ppm (Spectra **1.B** and **2.B**, in Figure 2.1). As these reactions neared completion, the long-lived intermediates seen at $\delta = 30.9$ ppm slowly reverted to the initial resonance at $\delta = 18.8$ ppm (Spectra **1.C** and **2.C**, in Figure 2.1). Complete consumption of β -ketoester **8** and allyl enol carbonate **6** was

observed by TLC for these reactions approximately at the time when the resonance at $\delta = 18.8$ ppm began to reappear.

Figure 2.1. ^{31}P NMR Studies of Allylic Alkylation With β -Ketoester and Enol Carbonate Substrates



NMR tube reactions were run on a 63–66 μmol scale. Spectra **1.A** and **2.A** were obtained after mixing $[\text{Pd}_2(\text{dba})_3]$ and $(S)\text{-}t\text{-BuPHOX}$ in solution for 30 minutes. Spectrum **1.B** was obtained immediately after adding allyl β -ketoester **8** to the solution pictured in spectrum **1.A**. Spectrum **2.B** was obtained immediately after adding allyl enol carbonate **6** to the solution pictured in Spectrum **2.A**. Spectra **1.C** and **2.C** were obtained 30 minutes after substrates **8** and **6** could no longer be observed by TLC in their respective reactions.

2.2.2 ^{31}P NMR Studies of Silyl Enol Ether Reactions

The allylic alkylation reaction of silyl enol ether **4** by ^{31}P NMR bore many similarities to the NMR reactions of allyl β -ketoester **8** and allyl enol carbonate **6**. Starting from the resonance at $\delta = 18.8$ ppm formed during precomplexation (Spectrum

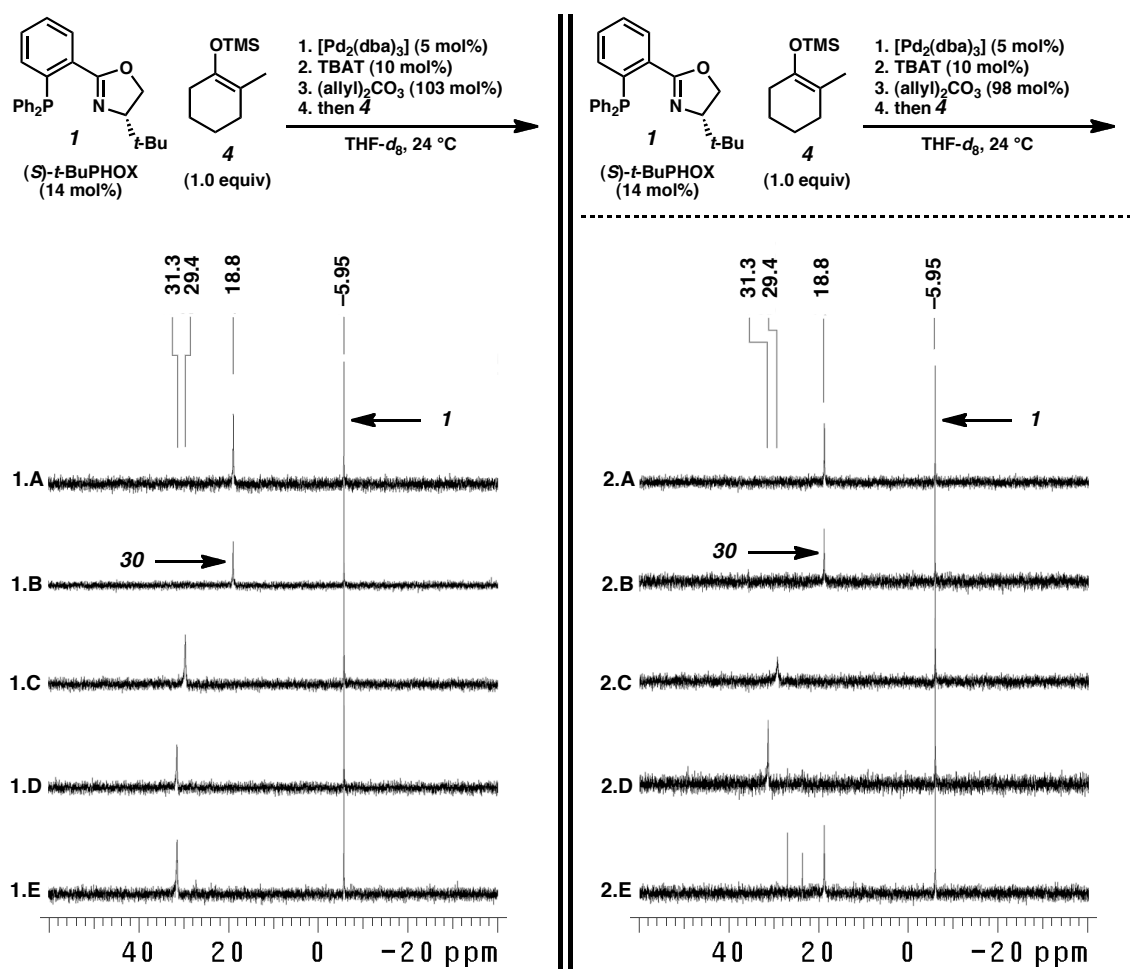
1.A, in Figure 2.2 on page 27), addition of 1 equivalent of TBAT⁴ produced no new resonances (Spectrum **1.B**, in Figure 2.2). This suggests that TBAT does not appreciably interact with the palladium catalyst. Subsequent addition of 10.6 equivalents of diallyl carbonate, an allyl electrophile, resulted in the complete disappearance of the resonance at $\delta = 18.8$ ppm and produced a new shift at $\delta = 29.4$ ppm (Spectrum **1.C**, in Figure 2.2). Addition of 10.3 equivalents of silyl enol ether **4** appeared to shift the resonance at $\delta = 29.4$ ppm to $\delta = 31.3$ ppm (Spectrum **1.D**, in Figure 2.2). The resonance at $\delta = 31.3$ ppm remained even after the reaction completed, as determined by the disappearance of silyl enol ether **4** via TLC (Spectrum **1.E**, in Figure 2.2).⁵

One of the most notable differences between the silyl enol ether and both the allyl enol carbonate and allyl β -ketoester reactions, is that the catalyst does not revert to the species responsible for the resonance at $\delta = 18.8$ ppm when the reaction is completed. As per the original conditions,^{3a} the NMR experiment with silyl enol ether **4** was performed with a slight excess of diallyl carbonate relative to silyl enol ether **4** (103 and 100 mol% respectively). This means that the silyl enol ether variant of the reaction differs from the other two by the presence of excess allyl electrophile relative to enolate nucleophile. This suggested that this persistent resonance at $\delta = 31.3$ ppm may be a palladium(II) allyl species derived from allyl acetate.

To confirm this hypothesis, the NMR experiment with silyl enol ether **4** was performed again but with less diallyl carbonate than enol ether **4** (98 and 100 mol%, respectively). For the main course of this reaction (Spectra **2.A** to **2.D**, in Figure 2.2) the spectra obtained were effectively identical to the other reaction with silyl enol ether **4** under the standard conditions (Spectra **1.A** to **1.D** left, in Figure 2.2) Gratifyingly,

however, this reaction did show reversion to the resonance at $\delta = 18.8$ ppm upon completion (Spectra **2.E**, in Figure 2.2) as observed for the allyl enol carbonate and allyl β -ketoester variants of the reaction (Spectra **1.C** and **2.C**, in Figure 2.1 on page 25). Some oxidative decomposition was observed for this reaction (resonances at $\delta = 27.2$ and 23.6 ppm, representing 11% and 10% of total phosphorus integration, respectively, in Spectra **2.E**, in Figure 2.2).⁶

Figure 2.2. ³¹P NMR Studies of Allylic Alkylation With Silyl Enol Ether Substrates



NMR tube reactions were run on a 67–68 μmol scale. Spectra **1.A** and **2.A** were obtained after mixing $[\text{Pd}_2(\text{dba})_3]$ and (S) -*t*-BuPHOX in solution for 30 minutes. Spectra **1.B** and **2.B** were obtained after adding TBAT to the solutions pictured in **1.A** and **2.A**, respectively. Spectra **1.C** and **2.C** were obtained after adding diallyl carbonate to the solutions pictured in **1.B** and **2.B**, respectively. Spectra **1.D** and **2.D** were obtained after adding silyl enol ether **4** to the solutions pictured in **1.C** and **2.C**, respectively. Spectra

1.E and **2.E** were obtained 30 minutes after silyl enol ether **4** could no longer be observed by TLC for the reactions initiated in **1.D** and **2.D**, respectively. In spectrum **2.E** the two extra resonances found downfield of $\delta = 20$ ppm are most likely oxidative decomposition products.⁶

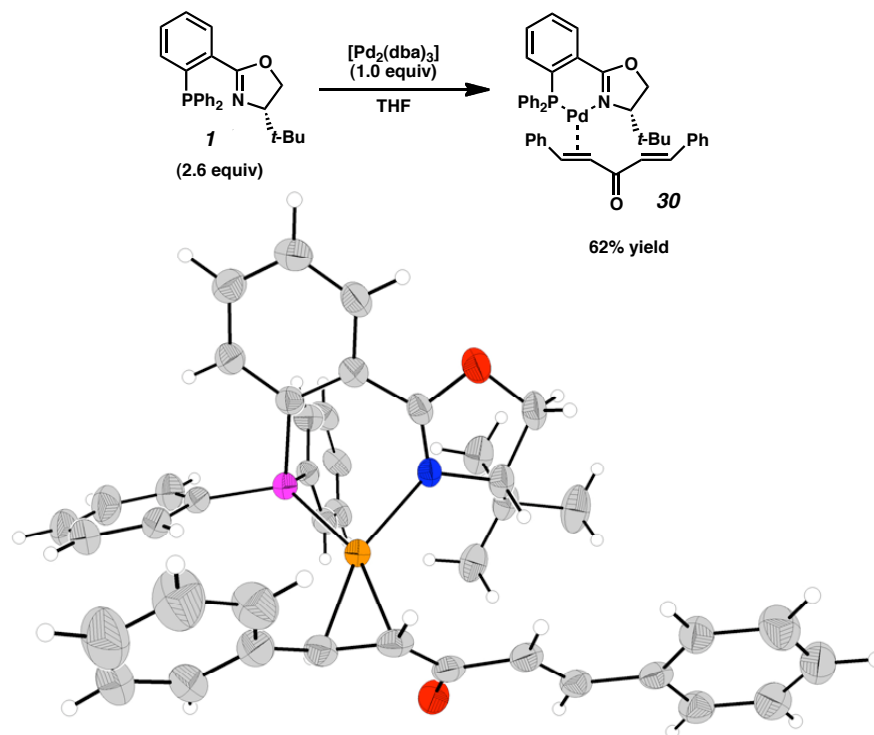
Integrating relative to the free PHOX ligand at $\delta = -5.95$ ppm suggests that the sum of the species represented at $\delta = 18.8, 29.4,$ and 31.3 ppm for the silyl enol ether variant and $\delta = 18.8$ and 30.9 ppm for the allyl enol carbonate and allyl β -ketoester variants are constant throughout the course of their respective reactions. As a result, any other PHOX-ligand-containing species that might form during the course of these reactions must be present in quantities too small to be observed by ³¹P NMR. The yield and *ee* of the allylic alkylation product **9** was obtained for each of the NMR reactions and gave results consistent with the standard conditions when run on a similar scale.

2.3 Isolation and Characterization of Intermediates

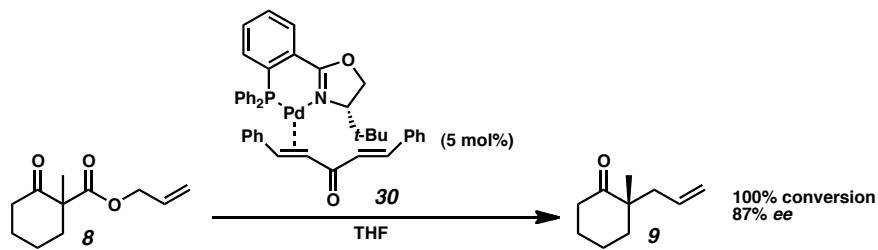
2.3.1 Olefin Complex **30**

Olefin complex **30** was synthesized and isolated using reaction-like conditions to combine (*S*)-*t*-BuPHOX ligand **1** and [Pd₂(dba)₃] in THF (Scheme 2.2 on page 29). [{(*S*)-*t*-BuPHOX}Pd(dba)] **30** was fully characterized including single-crystal X-ray diffraction, and in solution was found to have a ³¹P resonance of $\delta = 18.8$ ppm, matching the resonance found at the start of the reaction. Isolated samples of **30** were found to be competent for catalyzing the asymmetric allylic alkylation reaction, and gave results analogous to those observed for the standard reaction procedure (Scheme 2.3 on page 29). Based on these properties [{(*S*)-*t*-BuPHOX}Pd(dba)] **30** appears to be the initial catalytic species formed in our, and other related, allylic alkylation systems.^{3,7a,f}

Scheme 2.2. Isolation and X-Ray Structure of Initial Catalyst Complex **30**



Scheme 2.3. Decarboxylative Asymmetric Allylic Alkylation Catalyzed by Isolated Complex **30**



2.3.2 Carboxylate **31**

As the few apparent intermediates observed by NMR during the course of these reactions were long-lived singular species, the possibility was explored for the isolation of these species directly from the reaction. Initial efforts revealed that the apparent stability of these intermediates was largely illusory, and their seeming robustness under reaction conditions is the result of a steady-state equilibrium. Under reaction conditions, these intermediates decompose at a rate equivalent to their regeneration from the

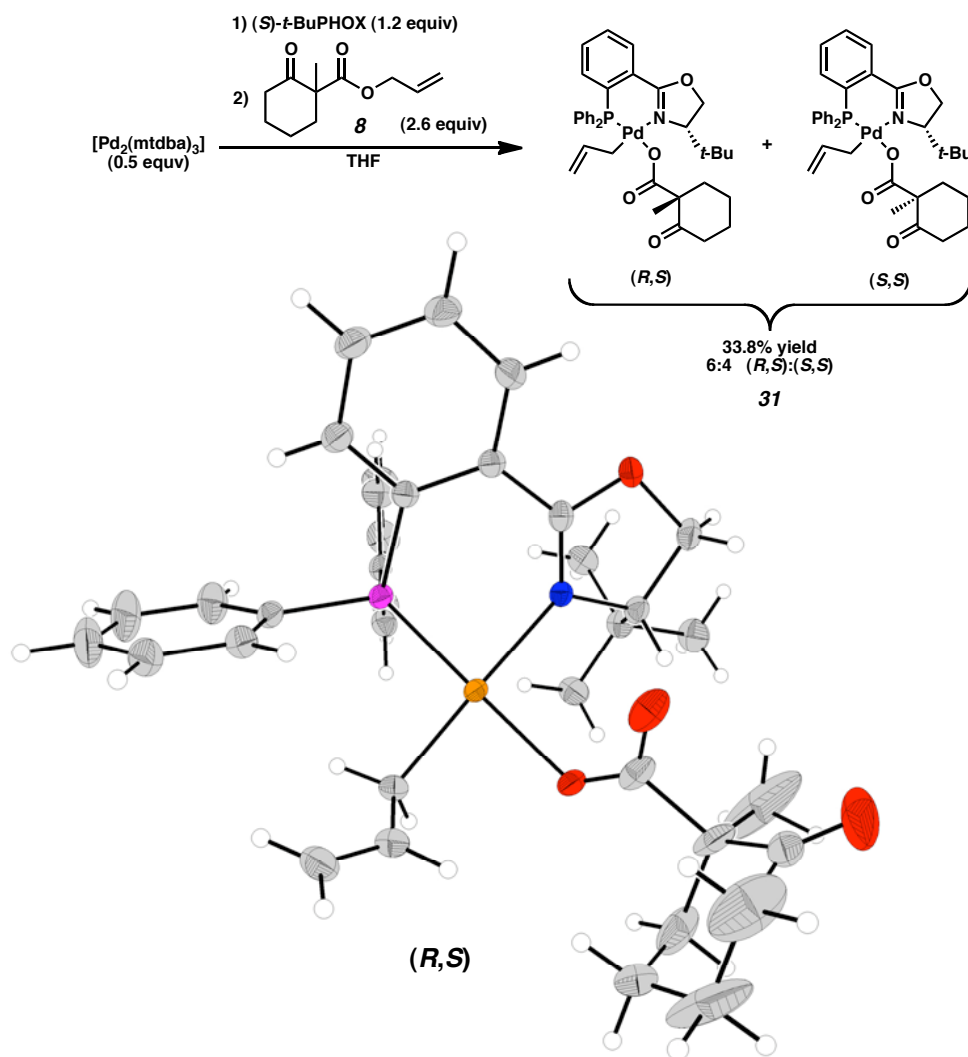
remaining reservoir of substrate. In the absence of excess substrate all of these species were found to be thermally unstable and short lived at room temperature, both in solution and as solvent-free solids. Even at reduced temperatures these species were also found to be sensitive to air and moisture.

However, at $-36\text{ }^{\circ}\text{C}$ in a nitrogen glove box, palladium allyl carboxylate **31** could be isolated from reaction-like conditions following the addition of allyl β -ketoester **8** as a substrate (Scheme 2.4 on page 31). This species was identified as the important intermediate corresponding to the ^{31}P NMR resonance at $\delta = 30.9$ ppm (Figure 2.1 on page 25). Interestingly, initial isolates of carboxylate **31**, which were impure, visibly expelled a gas (presumably CO_2) in the solid state and effervesced when submerged in a liquid. By using $[\text{Pd}_2(\text{mtdba})_3]$, a version of $[\text{Pd}_2(\text{dba})_3]$ modified to be more amenable toward use in organometallic synthesis,⁸ crystals of superior stability that contained carboxylate **31** in high purity were obtained. This allowed for the complete characterization of carboxylate **31** as a mixture of diastereomers resulting from the use of racemic β -ketoester **8** in its synthesis (Scheme 2.4 on page 31).

The structure of complex **31**, as determined in solution by NMR techniques⁹ and in the solid state by single-crystal X-ray diffraction, is rather uncommon. Complex **31** is a square-planar 16-electron species with a β -ketocarboxylate ligand *trans* to the phosphorus atom of the PHOX ligand and a σ -bound monohapto η^1 -allyl ligand *trans* to the nitrogen atom. Not only is the crystal structure of palladium carboxylate **31** the first example in the Cambridge Structural Database (CCDC) of a palladium species with a β -ketocarboxylate ligand, but it is also the first X-ray crystal structure of a transition-metal complex with a non-chelating carboxylate ligand *cis* to a σ -bound allyl group.^{10,11,12} By

contrast, the analogous PF_6 salt of $[\{(S)\text{-}t\text{-BuPHOX}\}\text{Pd}(\eta^3\text{-allyl})]$ (**25**) displays an $\eta^3\text{-}\pi$ -allyl bonding mode in both the solid state^{1c,13} and solution,¹³ as do related compounds.¹⁴

Scheme 2.4. Isolation and X-Ray Structure of Palladium Carboxylate **31**¹⁵

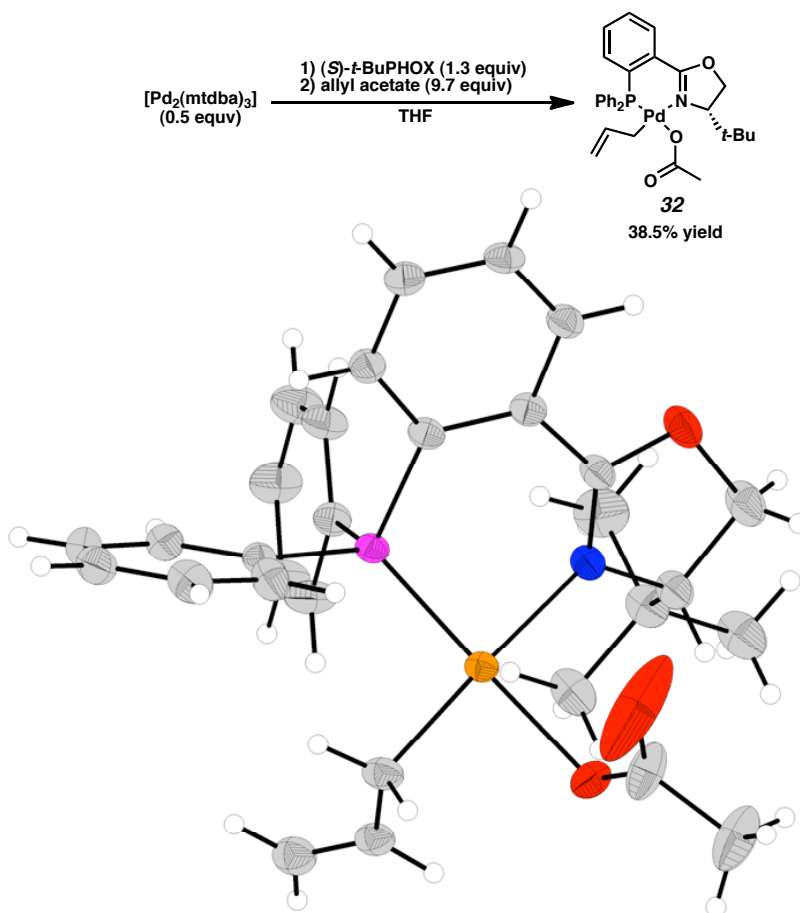


The presence of the β -ketocarboxylate ligand derived directly from deallylation of allyl β -ketoester **8** reveals that this complex must form after oxidative addition of the substrate, but prior to decarboxylation. Because **31** is the only observable species during the course of the catalytic reaction, we concluded that **31** is the catalyst's resting state and thus the rate-determining step for the allylic alkylation of allyl β -ketoester substrates is decarboxylation. This conclusion is consistent with the kinetics data for the overall

reaction, which shows a first-order dependence on catalyst and a zero-order dependence on the substrate concentration.^{2,1c} Decarboxylation has also been proposed as the rate-determining step for related palladium-catalyzed decarboxylative alkylation reactions.¹⁶

Despite the enormous number of transition-metal-catalyzed reactions involving allylic acetates and carbonates, a simple square planer transition metal species representing the canonical oxidative-addition adduct of allyl acetate and $L_nM(0)$ had not been reported prior to our work. With this in mind, and noting that intermediate **31** is basically an elaborated derivative of such a fundamental species, we synthesized the parent neutral $[(S)\text{-}t\text{-BuPHOX}]\text{Pd}(\eta\text{-1})(\text{OAc})$ complex **32** by the same means (Scheme 2.5 on page 33). The structure of complex **32**, a four-coordinate Pd(II) square-planar species in which the phosphorus atom and the acetate group have a *trans* relationship, is similar to that of carboxylate **31**. Together the structure and properties of palladium allyl carboxylates **32** and **31** may have implications not only for immediately related decarboxylative allylic alkylation reactions,^{7,17} but also for palladium-catalyzed allylic oxidation,^{18,19} palladium-catalyzed 1,4-diacetoxylation,^{18,20} and late-transition-metal-catalyzed decarboxylative reactions in general.

Scheme 2.5. Synthesis and X-Ray Structure of Canonical Palladium Allyl Acetate Complex **32**²¹

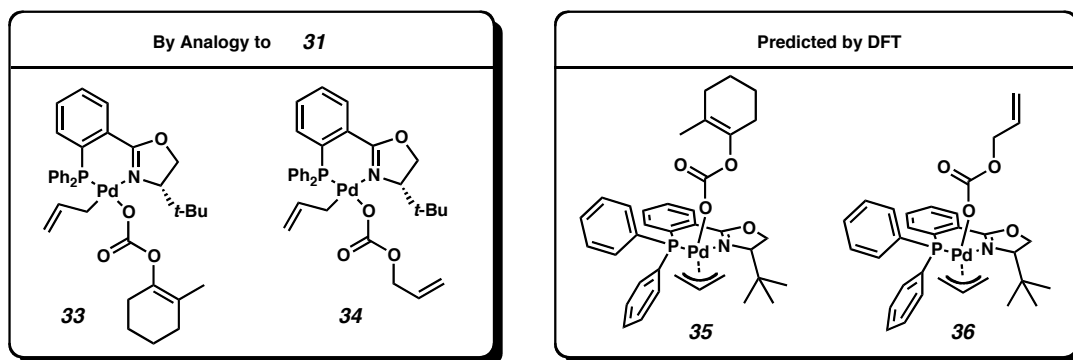


2.3.3 The Carbonate Complexes

This still leaves questions about the structures of the equivalent intermediates seen by ³¹P NMR at $\delta = 30.9$ ppm for the decarboxylative allylic alkylation of allyl enol carbonate **6** and at 29.4 and 31.3 ppm for silyl enol ether **4**. None of these species exhibits a ³¹P NMR spectrum similar to that of the corresponding π -allyl cation **25** ($\delta = 23.5$ and 22.5 ppm for the *exo* and *endo* η -3 allyl conformers of **25**, respectively). Instead, the phosphorous resonances and means of formation for these intermediates is closer to palladium carboxylates **31** and **32**.

By analogy to carboxylates **31** and **32**, the uncharacterized intermediates of the carbonate-based reactions are postulated to be palladium (II) allyl carbonate species with associated carbonate ligands. While the similarity of these intermediates to palladium allyl carboxylate **31** suggests that they may be palladium carbonates **33** and **34** (Figure 2.3 left, on page 34), DFT calculation predicts a tetragonal pyramidal structure with an η^3 allyl ligand and an apically coordinated carbonate ligand (carbonates **35** and **36** in Figure 2.3 right).^{1a} Similar neutral palladium η^3 allyl complexes with tetragonal pyramidal structures are known in the literature.²²

Figure 2.3. Estimated Structures for Carbonate Intermediates



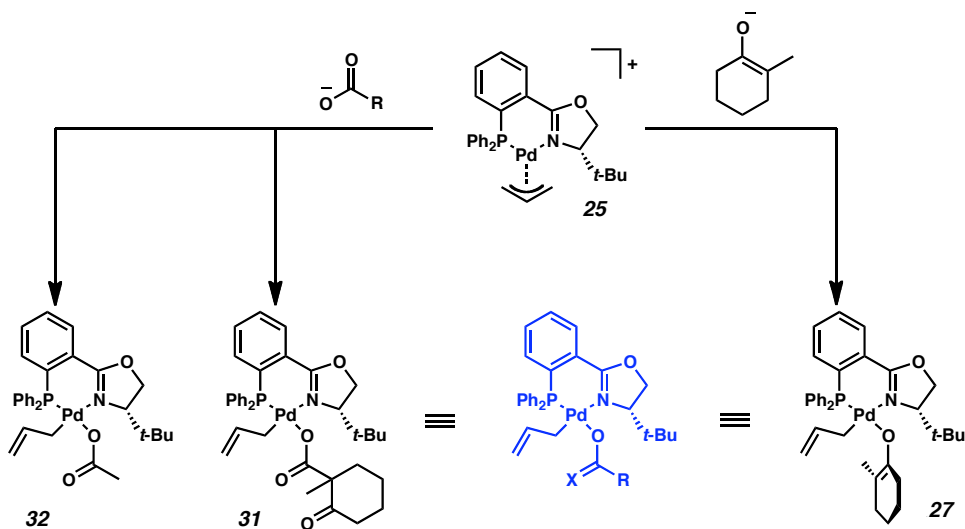
2.4 Role and Significance of the Intermediates

2.4.1 Analogy to Putative Key Palladium Intermediate **27**

Notably the arrangement and hybridization of the allyl and carboxylate ligands in palladium carboxylates **31** and **32** are similar to that of the palladium allyl enolate intermediate **27** (Scheme 2.6 on page 35). This is significant as enolate **27** is believed to be the key intermediate preceding the doubly vinylogous reductive elimination that represents the key bond-forming step for this reaction. While the reality of palladium carboxylate species **31** and **32** does not assure the existence of palladium enolate **27** or its

role as a key reaction intermediate, they do lend credence to the proposed structure for enolate **27** by setting structural precedents in this system. Furthermore, the solution behavior of complexes **31** and **32** demonstrates that even fairly weak nucleophiles are capable of displacing one end of the η^3 -allyl ligand in this system and binding to the palladium center.^{2,13}

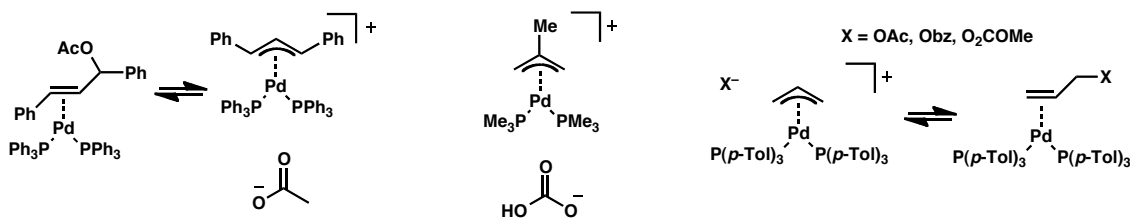
Scheme 2.6. Underlying Structural and Chemical Similarity between **31**, **32**, and **27**



This is significant, as almost all the palladium-catalyzed asymmetric allylic alkylation systems that are understood to function by an outer-sphere mechanism remain unable to demonstrate compounds isolable from reaction-like conditions that possess structures similar to carboxylates **31** and **32**. Instead, palladium-catalyzed allylic alkylation systems that function by an outer-sphere mechanism tend to produce allylic esters and allyl-carbonate-derived species that exist as either apparent η^2 olefin complexes,²³ or as palladium π -allyl cations (Figure 2.4 on page 36).²⁴ As a result, the high degree of similarity between palladium enolate **27** and palladium carboxylates **31** and **32** does lend credence to the key calculated palladium allyl enol structure **27** and its mechanistic role. It is possible that palladium allyl carboxylate complexes like **31** and **32**

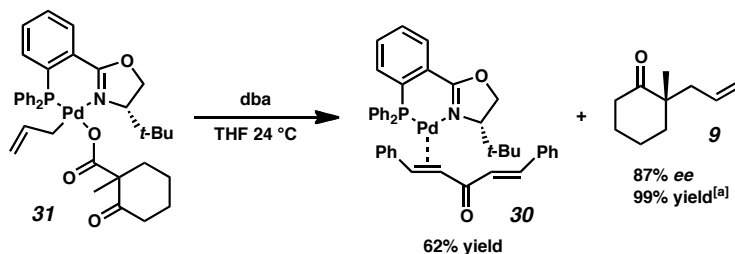
represent the best isolable model systems by which the key intermediate **27** may be experimentally studied.

Figure 2.4. Select Examples of Typical Palladium Allyl Carboxylate and Carbonate Species Found in the Literature^{23a,e,24e}



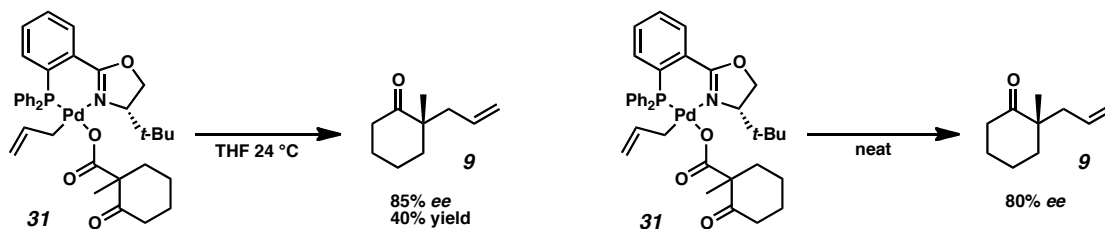
2.4.2 The Function of Complexes **30** and **31** in the Catalytic Cycle

To examine the role of carboxylate **31** in the catalytic cycle, it was subjected to reaction-like conditions in THF at 24 °C in the presence of free dba ligand, and the reaction was followed by ³¹P NMR. The half-life of carboxylate **31** was measured to be 7.3 min under these conditions, and after 40 minutes **31** could no longer be detected by NMR. During this time, the resonance at $\delta = 18.8$ ppm in the ³¹P NMR, seen at the end of the catalytic reaction, appeared, and after 40 minutes, became the only observable ³¹P resonance. Both allylic alkylation product **9** (99% yield, 87% *ee*) and [(*S*)-*t*-BuPHOX}Pd(dba)] **30** (62% yield), were obtained from this reaction (Scheme 2.7 on page 37). This reaction demonstrates that complex **30** is regenerated at the end of an allylic alkylation reaction, making it the catalyst's resting state in the absence of allyl electrophiles.

Scheme 2.7. Thermal Decomposition of **31** in the Presence of Free dba Ligand in THF

The yield of **30** and **9** are from two different runs. In the first run, only **30** was isolated, and in the second run only the yield and *ee* of **9** was assayed. [a] GC yield relative to internal standard (tridecane)

To determine if carboxylate **31** was part of the catalytic cycle or just an unproductive resting state, its decomposition was monitored in the absence of the dba ligand both in THF and neat. In THF solution at 24 °C in the absence of dba, allyl carboxylate **31** decomposes to give an increasingly complex mixture of phosphorous containing species by ³¹P NMR, none of which can be observed during the course of the catalytic reaction. Under these conditions, allylic alkylation product **9** appears to be the only metal or phosphine-free product formed in the reaction, and **9** can be isolated with 85% *ee* from solution (Scheme 2.8 on page 37). Most telling is that the neat thermal decomposition of crystalline carboxylate **31** in a nitrogen glove box at ambient temperature still yielded ketone **9** as the major organic product, albeit with slightly reduced enantioinduction (80% *ee*).

Scheme 2.8. Thermal Decomposition of **31** Without dba in THF and Neat

2.5 Conclusions

The ^{31}P NMR investigations of the palladium-catalyzed decarboxylative allylic alkylation reaction reveal long-lived singular intermediates for all three substrate variants of the methodology. The only two NMR detectable intermediates from the allyl β -ketoester variant of the methodology, dba complex **30** and carboxylate complex **31**, have been isolated and fully characterized. Carboxylate complex **31** represents the resting state of the catalyst for the allyl β -ketoester variant of the reaction while it is running and proves that decarboxylation is rate limiting. The dba complex **30**, is the initial catalytic species generated in the precomplexation of PHOX ligand **1** and $[\text{Pd}_2(\text{dba})_3]$. The dba complex **30** is also the catalyst's resting state in the absence of allyl electrophiles like allyl enol carbonates, allyl β -ketoesters, and diallyl carbonate. As a result, dba complex **30** will regenerate under reaction conditions when these species become fully consumed.

Carboxylate complex **31** and its parent **32** represent exceptionally rare examples of isolated transition metal complexes with a non-chelating carboxylate ligand *cis* to an η^1 -allyl ligand. However, many such species may actually play a prevalent role in an array of catalytic processes. Similar intermediates to carboxylate **31**, such as carbonates **34/36** and **33/35**, are expected for the allyl enol carbonate and silyl enol ether variants of the reaction, respectively. Finally, carboxylate complexes **31** and **32** lend credence to the existence and proposed structure of putative palladium enolate **27**, which is believed to be the key intermediate for this allylic alkylation system. All the intermediates observable by ^{31}P NMR appear to be part of the pre-decarboxylation phase of the mechanism, and thus not part of the universal underlying allylic alkylation mechanism that is expected to be common for all three reaction variants as previously simulated by DFT.^{1,2}

2.6 Experimental Procedures

2.6.1 Materials and Methods

Unless otherwise stated, reactions were performed in flame-dried glassware under an argon atmosphere using dry, deoxygenated solvents. Unless otherwise stated, solvents were purchased from Fisher Scientific, dried by passage through an activated alumina column under ultra high purity (UHP) argon, and either stored under UHP argon or stored over 4Å molecular sieves in a nitrogen glove-box after drying. Solvents stored over molecular sieves were filtered under a nitrogen atmosphere immediately before use to remove sieve dust. Petroleum ether was obtained from Fisher Scientific and is defined here as petroleum fractions that boil from 36–60 °C. The NMR solvents CDCl₃ and THF_{d-8} were purchased from Cambridge Isotope Laboratories and used as received. THF_{d-8} was purchased as 1 or 0.75 mL ampoules, which were only used in a nitrogen glove box to exclude water. All filtrations performed in a glove box or otherwise associated directly or indirectly with inorganic or organometallic complexes were performed exclusively with scintillated glass Buchner funnels or using 2.4 mm GF/A Whatman glass microfiber filter paper. Unless otherwise stated, all starting materials were purchased from Sigma-Aldrich or Alfa Aesar, and used as received. Tetrabutylammonium difluorotriphenylsilicate (TBAT) was purchased from Sigma-Aldrich and azeotropically dried five times from acetonitrile, backfilled with argon and then stored in a nitrogen glove box until immediately prior to use. Tris(dibenzylideneacetone)dipalladium(0) [Pd₂(dba)₃] and PdCl₂ were purchased from

Strem and stored in either a desiccator or a nitrogen glove box until immediately before use. 1-Methyl-2-oxo-cyclohexanecarboxylic acid allyl ester (β -ketoester **8**),²⁵ trimethyl(2-methylcyclohex-1-enyloxy)silane (**4**),^{3b} allyl 2-methylcyclohex-1-enyl carbonate (**6**),^{3b} and (*S*)-*t*-BuPHOX ligand (**1**)^{3b,26} were prepared by known methods. Reaction temperatures were controlled by an IKAmag temperature modulator. Thin-layer chromatography (TLC) was performed using E. Merck silica gel 60 F254 precoated plates (0.25 mm). SiliCycle® SiliaFlash® P60 Academic Silica Gel (particle size 40–63 μm ; pore diameter 60 Å), was used for flash chromatography. ¹H, ¹³C, ³¹P, and ¹⁹F NMR spectra were recorded on a Varian Inova 600 (at 600 MHz and 150 MHz for ¹H and ¹³C, respectively), a Varian Inova 500 (at 500 MHz and 125 MHz for ¹H and ¹³C, respectively), or a Varian Mercury 300 (at 300 MHz, 75 MHz, 121.4 MHz, and 282 MHz for ¹H, ¹³C, ³¹P, and ¹⁹F, respectively). ¹H NMR spectra are reported relative to residual CHCl₃ (δ 7.26)²⁷ or to the downfield proton in residual THF_{d,7} (δ 3.58).²⁷ Data for ¹H NMR spectra are reported as follows: chemical shift (δ ppm) (multiplicity,¹ coupling constant (Hz),² integration). Multiplicities are reported as follows: s = singlet, d = doublet, t = triplet, q = quartet, p = pentet, m = multiplet, comp. m = complex multiplet, app. = apparent, br. = broad. ¹³C NMR spectra are reported relative to CDCl₃ (δ 77.16)²⁷ or to the downfield carbon in THF_{d,8} (δ 67.21).²⁷ ³¹P NMR spectra are reported relative to

¹ In many cases hyperfine coupling could be observed but was not resolved enough that its splitting pattern could be determined. In such cases the larger coupling is calculated and the relevant multiplicities are indicated but terminated with m (multiplet) to signify the unresolved hyperfine coupling. For example (tm, $J = 7.2$ Hz, 1H) indicates a triplet of 7.2 Hz, with irresolvable hyperfine coupling. This is done in place of reporting the entire resonance as a multiplet for the purpose of reproducibility on lower field strength NMR spectrometers where only the larger calculable splitting(s) will be observed.

² When a lower case subscript is shown with the coupling constant, it indicates what type of splitting the constant is associated with in splitting patterns that consist of different multiplicities of coupling. For example (td, $J_t = 5.0$ Hz, $J_d = 3.3$ Hz, 1H) indicates that the triplet splitting has a 5.0 Hz coupling constant and the doublet has a 3.3 Hz coupling constant.

H₃PO₄ (δ 0.00) as an external standard consisting of 85% neat phosphoric acid or to free (*S*)-*t*-BuPHOX ligand (δ -5.95) as either an internal or external standard in THF_{d-8}. ¹⁹F NMR spectra are reported relative to CFCl₃ (δ 0.00) as an external standard. Analytical achiral gas chromatography (GC) was performed with an Agilent 6850 GC utilizing a DB-WAX (30 m x 0.25 mm) column (1.0 mL/min carrier gas flow). Analytical chiral GC was performed with an Agilent 6850 GC utilizing a G-TA (30 m x 0.25 mm) column (1.0 mL/min carrier gas flow). Optical rotations were measured with a Jasco P-1010 polarimeter at 589 nm. IR spectra were recorded on a Perkin Elmer Paragon 1000 spectrometer and are reported in frequency of absorption (cm⁻¹). High-resolution mass spectra were obtained from the Caltech Mass Spectral Facility or on an Agilent 6200 Series Time-of-Flight LC/MS/TOF system. Melting points were determined on a Thomas-Hoover melting point apparatus and are uncorrected. Boiling points are measured directly during distillation and are uncorrected. Crystallographic analyses were performed at the California Institute of Technology Beckman Institute X-Ray Crystallography Laboratory. Crystallographic data have been deposited at the CCDC, 12 Union Road, Cambridge CB2 1EZ, UK, and copies can be obtained upon request, free of charge, by quoting the publication citation and the deposition numbers provided with the structures below.

2.6.2 ³¹P NMR Studies

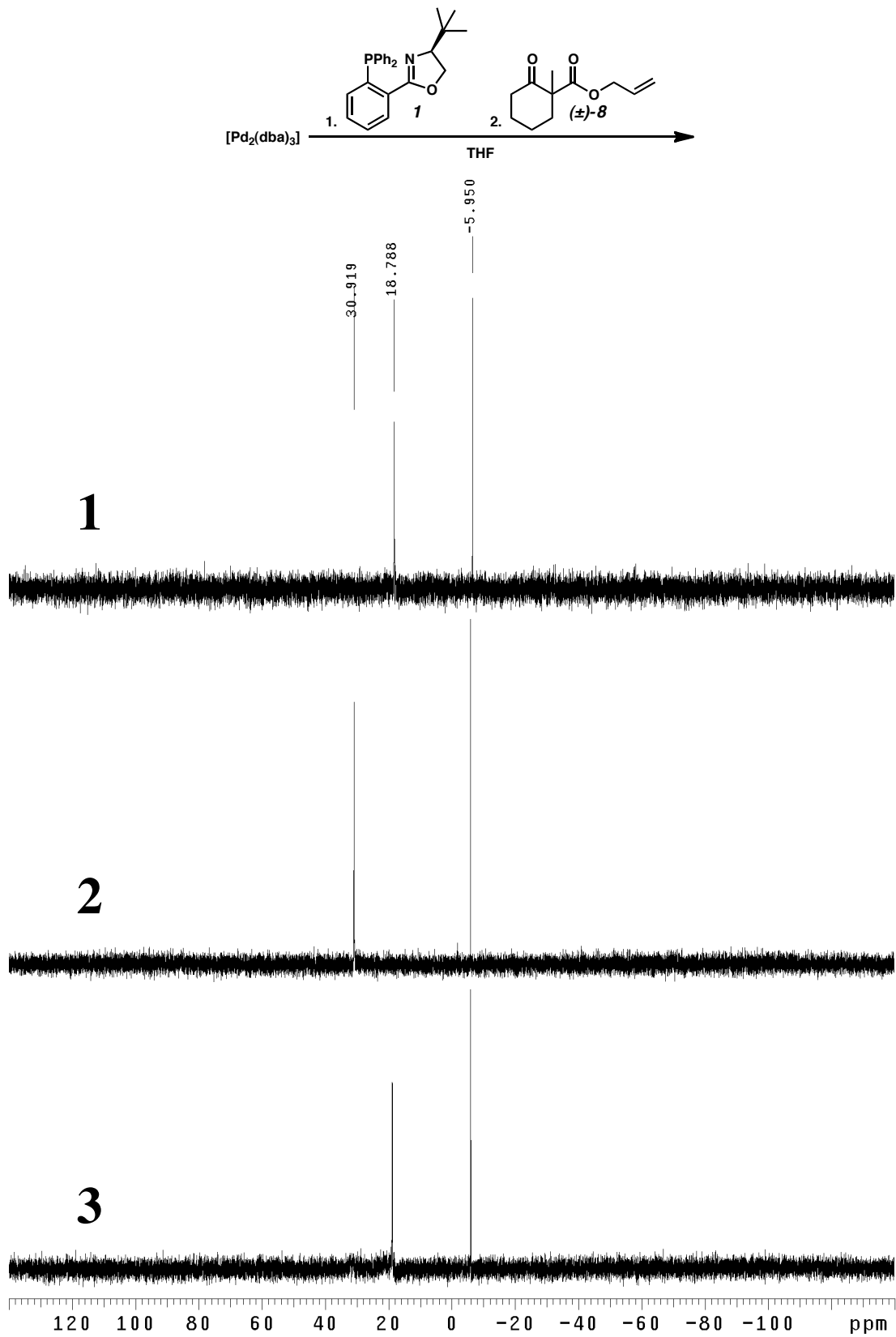
2.6.2.1 General Notes and Procedures

For NMR studies of the various allylic alkylation procedures, the reaction was followed by TLC. Due to air sensitivity, TLCs were taken either by cycling the NMR tube into a nitrogen glove box and taking an aliquot, or by connecting the NMR tube through its septum to an argon line with a needle while sampling the solution with a second needle and TLC spotter under slight argon overpressure. The most common product of air exposure was the phosphine oxide of (*S*)-*t*-BuPHOX ligand (the experimental procedure section contains characterization data for (*S*)-*t*-BuPHOX oxide for reference.)

2.6.2.2 The Decarboxylative Allylic Alkylation of β -Ketoester **8** Monitored by ³¹P NMR

In a nitrogen atmosphere glove box [Pd₂(dba)₃] (3.0 mg, 3.3 μ mol, 1 equiv) was placed in a 1 dram vial. (*S*)-*t*-Bu-PHOX ligand (**1**) (3.3 mg, 8.5 μ mol, 2.6 equiv) was weighed in a second 1 dram vial. THF (1 mL) was filtered through a pipette with glass filter paper directly into the vial containing the (*S*)-*t*-Bu-PHOX ligand (**1**). The solution was mixed manually by pipette until all the material had dissolved, forming a clear colorless solution. The solution was then moved by pipette to the vial containing [Pd₂(dba)₃]. This solution was mixed manually by pipette for 1 min during which time a dark red-purple solution formed that then lightened to a dark but richly orange color. This solution was then filtered through a pipette filter with glass filter paper directly into an NMR tube, separating a bright, richly orange filtrate from a black amorphous precipitate presumed to be colloidal Pd(0) particles. The NMR tube was then sealed with

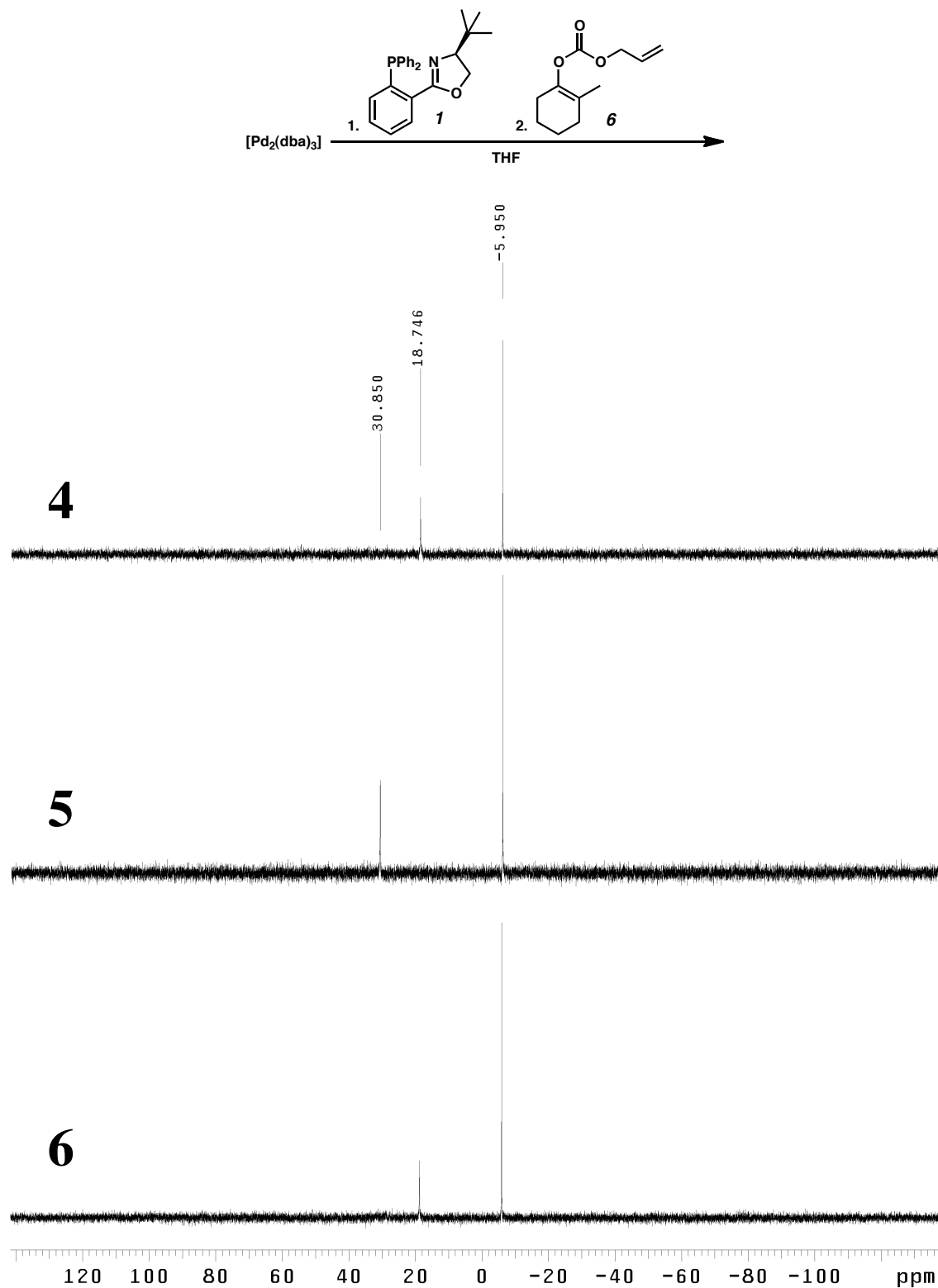
a septum and removed from the glove box. NMR spectrum #1 was taken at this time. Neat 1-methyl-2-oxo-cyclohexanecarboxylic acid allyl ester (β -ketoester **8**) (12.3 mg, 62.8 μ mol, 19.1 equiv) was added to the NMR tube via a 25 μ L Hamilton syringe in a single portion. The NMR tube was shaken vigorously for 30 s, and the solution quickly changed color from a rich orange to a lighter yellow-green. NMR spectrum #2 was taken at this time. The NMR tube was then placed in an oil bath regulated at 24 °C and warmed for 3 h, which was 20 min longer than it took for the solution's color to change from a light yellow-green to a rich orange and 30 minutes after allyl β -ketoester **8** could no longer be observed by TLC. NMR spectrum #3 was taken at this time.



2.6.2.3 The Decarboxylative Allylic Alkylation of Allyl 2-methylcyclohex-1-enyl carbonate (**6**) Monitored by ^{31}P NMR

In a nitrogen glove box (S)-t-BuPHOX ligand (3.3 mg, 8.5 μmol , 1.3 equiv) was weighed into a half-dram vial. $[\text{Pd}_2(\text{dba})_3]$ (2.9 mg, 3.2 μmol , 0.5 equiv) was weighed into a second half-dram vial. Anhydrous THF (1 mL) was filtered through a pipette filter with glass filter paper into the half-dram vial containing the PHOX ligand. The solution was mixed manually via pipette for a little less than 1 min until all material had dissolved. The resulting solution was transferred via pipette and added as a single portion to the half-dram vial containing the $[\text{Pd}_2(\text{dba})_3]$. The resulting solution was mixed manually via pipette for 2 min during which time it turned a dark purple-brown. The solution was left to stand and mix via diffusion for 30 min during which time it turned an orange color. The solution was filtered through a pipette with glass filter paper to separate a bright orange solution from a small amount of black precipitate presumed to be aggregated palladium(0) metal. The NMR tube was sealed with a septum and removed from the glove box. NMR spectrum #4 was taken at this time. Allyl 2-methylcyclohex-1-enyl carbonate (**6**) (12.9 mg, 65.7 μmol , 10.3 equiv) was added in a single portion via a syringe. The tube was fully inverted and righted causing an abrupt color change from a rich orange color to a light yellow-green solution. NMR spectrum #5 was taken at this time. The NMR tube was left to stand for 3 h at 24 °C during which time the solution turned orange, and 30 minutes after allyl enol carbonate **6** could no longer be observed by TLC. NMR spectrum #6 was taken at this time. The solution was concentrated under a jet of nitrogen to a small amount of yellow solution. Chromatography was performed in a pipette column on silica eluting with 5→10% Et_2O in petroleum ether affording 2-allyl-2-methylcyclohexanone (87.4% *ee* [assay: GC, G-TA

column {100 °C isothermal for 30 min}, major enantiomer (S) Ret. Time = 14.897 min, minor enantiomer (R) Ret. Time = 17.313 min], clear colorless oil).



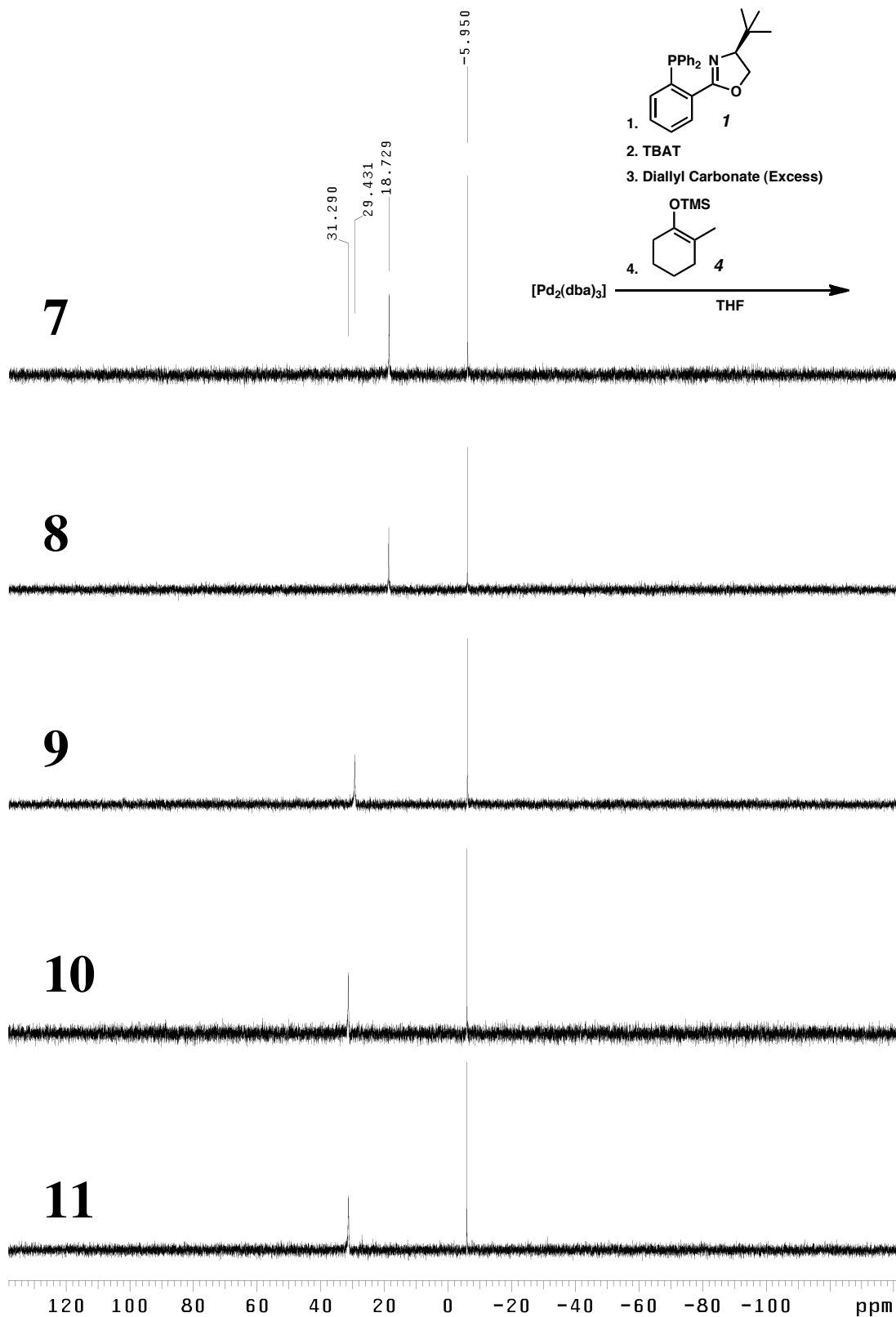
2.6.2.4 The Decarboxylative Allylic Alkylation of Trimethyl(2-methylcyclohex-1-enyloxy)silane (**4**) Monitored by ^{31}P NMR (standard alkylation procedure)

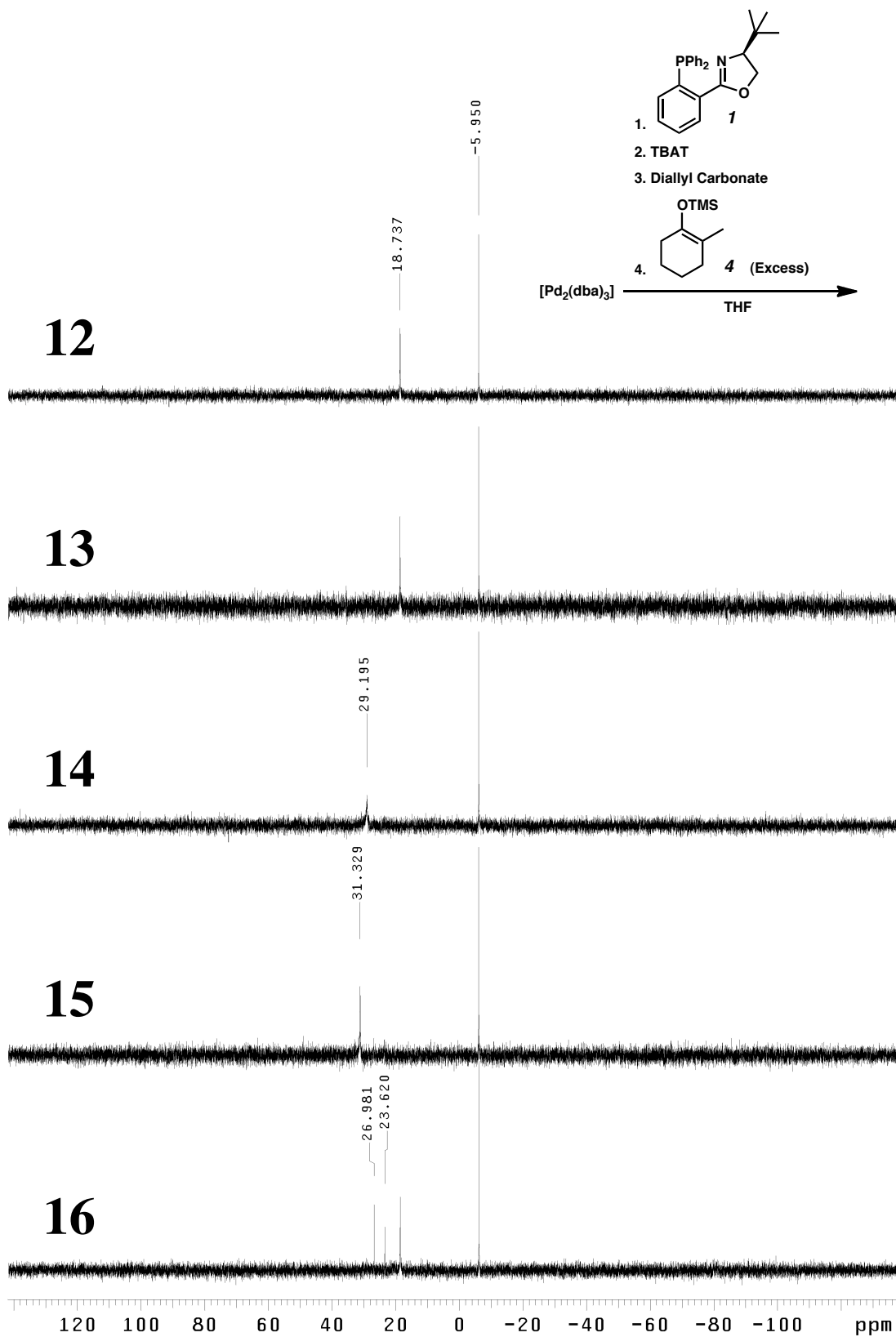
In a nitrogen glove box (S)-t-BuPHOX ligand (3.5 mg, 9.0 μmol , 1.4 equiv) was weighed into a half-dram vial. $[\text{Pd}_2(\text{dba})_3]$ (3.0 mg, 3.3 μmol , 0.5 equiv) was weighed into a second half-dram vial. Anhydrous THF (1 mL) was added into the half-dram vial containing the PHOX ligand. The solution was mixed manually via pipette for 1 min until all of the solids had dissolved. The resulting solution was added to the half-dram vial containing the $[\text{Pd}_2(\text{dba})_3]$ via pipette in a single portion. The resulting solution was mixed manually via pipette for 2 min during which time it turned a dark purple-brown. The solution was left to stand and mix via diffusion for 30 min during which time it turned an orange color. The solution was filtered through a pipette with glass filter paper to separate a bright orange solution from a small amount of black precipitate presumed to be aggregated palladium(0) metal. The NMR tube was sealed with a septum and removed from the glove box. NMR spectrum #7 was taken at this time. The NMR tube was cycled back into the glove box. TBAT (3.6 mg, 6.7 μmol , 1 equiv) was weighed into a half-dram vial in the glove box. The contents of the NMR tube were emptied into the half-dram vial. The solution was mixed manually by pipette for 1 min until all the material had dissolved. The resulting solution was returned to the NMR tube, which was resealed with a septum and removed from the glove box. NMR spectrum #8 was taken at this time. Diallyl carbonate (10 μL , 9.9 mg, 69.7 μmol , 10.6 equiv) was added via a syringe in one portion. The NMR tube was inverted once resulting in a rapid color change from a rich orange to a light yellow-green. NMR spectrum #9 was taken at this time. Trimethyl(2-methylcyclohex-1-enyloxy)silane (**4**) (12.5 mg, 67.8 μmol , 10.3 equiv) was added via a syringe in one portion. NMR spectrum #10 was taken at this

time. The NMR tube was left to stand for 10 h at 24 °C during which time the solution turned orange. NMR spectrum #11 was taken at this time. The solution was then concentrated under a jet of nitrogen to a small amount of yellow oil. Chromatography was performed on a pipette column on silica eluting with 5→10% Et₂O in petroleum ether affording 2-allyl-2-methylcyclohexanone (84.5% *ee* [assay: GC, G-TA column {100 °C isothermal for 30 min}], major enantiomer (S) Ret. Time = 14.897 min, minor enantiomer (R) Ret. Time = 17.313 min], clear colorless oil).

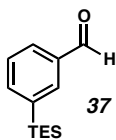
2.6.2.5 The Decarboxylative Allylic Alkylation of Trimethyl(2-methylcyclohex-1-enyloxy)silane (**4**) Monitored by ³¹P NMR (excess nucleophile)

The procedure above was repeated with the following changes: Diallyl carbonate (9.0 μL, 8.9 mg, 62.7 μmol, 9.8 equiv), Trimethyl(2-methylcyclohex-1-enyloxy)silane (**4**) (12.4 mg, 67.2 μmol, 10.5 equiv). NMR spectra 12 to 16 were taken at the equivalent intervals to NMR spectra 7 to 11. The *ee* was 84.9% as measured by GC.



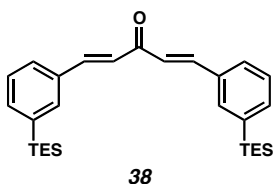


2.6.3 Synthesis of $[Pd_2(mtdba)_3]$



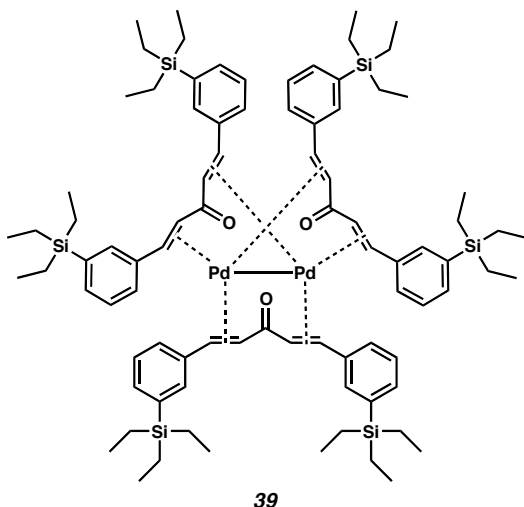
3-(Triethylsilyl)benzaldehyde (37): Anhydrous THF (160 mL) was added to a 250 mL 14/20 round-bottom flask with a stir bar. To this solution was added 3-bromobenzaldehyde diethylacetal (8.0 mL, 10 g, 39 mmol) via syringe. The solution was cooled to $-78\text{ }^{\circ}\text{C}$ and *n*-BuLi (2.5 M solution in hexanes, 36 mL, 90 mmol, 2.3 equiv) was added dropwise to the cooled stirring solution via syringe over 45 min. The solution was left to stir at $-78\text{ }^{\circ}\text{C}$ for 2 h. Triethylsilylchloride (7.6 mL, 6.8 g, 45 mmol, 1.2 equiv) was added via syringe over 15 min. The solution was stirred for 3 h at $-78\text{ }^{\circ}\text{C}$, and allowed to warm to and maintain room temperature over 8 h. The solution was quenched with aq HCl (2 N, 90 mL) and diluted with diethyl ether (45 mL). The phases were separated. The aq phase was extracted with diethyl ether (2 x 25 mL). The organic phases were merged, washed with aq saturated sodium chloride (1 x 100 mL), dried over magnesium sulfate, filtered with dichloromethane, and concentrated in vacuo. The resulting liquid was diluted with THF (6 mL), acetic acid (15 mL), and water (4 mL), and stirred for 3 h. The solution was slowly and carefully quenched with saturated aq sodium bicarbonate (100 mL) causing the rapid evolution of gas. The solution was diluted with diethyl ether (30 mL), and the phases were separated. The aq phase was extracted with diethyl ether (2 x 25 mL). The organic phases were washed with saturated aq sodium chloride (1 x 50 mL), dried over sodium sulfate, filtered with ethyl acetate, and concentrated in vacuo. The resulting yellow oil was bulb-to-bulb distilled on a kugelrohr at 0.3 torr and $130\text{--}180\text{ }^{\circ}\text{C}$ using a 25 mL bulb before the final collection bulb to help

fractionate the distillate. Volatile impurities were removed from the distillate in a kugelrohr distillation at 0.2 torr and 15–85 °C affording 3-(triethylsilyl)benzaldehyde (**37**) (4.86 g, 56.5% yield, faintly colored clear oil). TLC (R_f 0.65, 5% diethyl ether in petroleum ether, observed by UV). ^1H NMR (500 MHz, CDCl_3) δ 10.03 (s, 1H), 7.98 (s, 1H), 7.85 (ddd, $J = 7.6, 1.5, 1.5$ Hz, 1H), 7.75 (ddd, $J = 7.3, 1.2, 1.2$ Hz, 1H), 7.52 (dd, $J = 7.6, 7.3$ Hz, 1H), 0.97 (t, $J = 7.8$ Hz, 9H), 0.85 (qm, $J = 7.8$ Hz, 6H); ^{13}C NMR (125 MHz, CDCl_3) δ 193.1, 140.4, 139.1, 135.73, 135.70, 130.2, 128.5, 7.5 (br. s), 3.3; IR (neat film, NaCl) 2955, 2910, 2876, 2808, 2716, 1700, 1586, 1572, 1458, 1415, 1370, 1263, 1238, 1205, 1170, 1123, 1106, 1010, 891, 864, 790, 734, 720, 696 cm^{-1} ; HRMS (LC/MS TOF, Multi Mode: APCI/ESI) m/z calc'd for $\text{C}_{13}\text{H}_{21}\text{OSi}$ $[\text{M} + \text{H}]^+$: 221.1356, found: 221.1361.



1,5-Bis-[3-(triethylsilyl)phenyl]penta-1,4-dien-3-one, (mtdba) (38): To a 250 mL Erlenmeyer flask with a stir bar were added sodium hydroxide (1.92 g, 48.0 mmol, 5.4 equiv) and water (20 mL). Stirring was started, and once all the sodium hydroxide had dissolved, ethanol (200 proof, 34 mL) was added. The solution was cooled to 0 °C, and 3-(triethylsilyl)benzaldehyde (**37**) (4.08 g, 18.5 mmol, 2.04 equiv) was added dropwise over 5 min. Acetone (650 μL , 514 mg, 8.85 mmol) was added dropwise to the cooled stirring solution over 2 min. The solution was stirred for 5 min at 0 °C, and the cold bath was removed and the solution was stirred at room temperature for 9 h. The solution was diluted with water (25 mL) and hexanes (50 mL). The aq phase was

extracted with hexanes (2 x 25 mL) and 1:1 hexanes:diethyl ether (2 x 25 mL). The organic phases were washed with water (2 x 25 mL) and saturated aq sodium chloride (50 mL). The organic phases were then dried with magnesium sulfate, filtered with dichloromethane, and concentrated in vacuo. Chromatography was performed with 0.5% → 5% Et₂O in petroleum ether on silica gel to afford 1,5-bis-[3-(triethylsilyl)phenyl]penta-1,4-dien-3-one (**38**) (54.4% yield, bright yellow-green waxy solid). TLC (*R_f* 0.41, 5% ether in petroleum ether, observed by UV and stained with anisaldehyde [orange]); mp 72.5–74.5 °C;²⁸ ¹H NMR (500 MHz, CDCl₃) δ 7.75 (d, *J* = 16.0 Hz, 2H), 7.70 (s, 2H), 7.65 (d, *J* = 7.7 Hz, 2H), 7.53 (d, *J* = 7.3 Hz, 2H), 7.41 (dd, *J* = 7.7, 7.3 Hz, 2H), 7.10 (d, *J* = 16.0 Hz, 2H), 0.98 (t, *J* = 7.8 Hz, 18H), 0.83 (qm, *J* = 7.9 Hz, 12H); ¹³C NMR (125 MHz, CDCl₃) δ 189.2, 144.0, 138.8, 136.6, 134.9, 134.1, 128.39, 128.35, 125.4, 7.6, 3.4; IR (neat film, NaCl) 3047, 2954, 2909, 2874, 1652, 1619, 1456, 1415, 1394, 1323, 1237, 1187, 1096, 1010, 875, 793, 769, 735, 720 cm⁻¹; HRMS (LC/MS TOF, Multi Mode: APCI/ESI) *m/z* calc'd for C₂₉H₄₃OSi₂ [M + H]⁺: 463.28524, found: 463.28502.

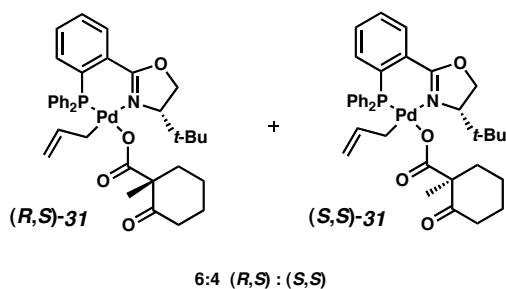


Tris{1,5-bis-[3-(triethylsilyl)phenyl]penta-1,4-dien-3-one}dipalladium(0), [Pd₂(mtdba)₃] (39):²⁹ 1,5-Bis-[3-(triethylsilyl)phenyl]penta-1,4-dien-3-one (**38**) (1.70 g, 3.67 mmol, 3.4 equiv) and sodium acetate (1.48 g, 18.0 mmol, 16.7 equiv) were added neat to a flame-dried 100 mL round-bottom flask with a stirbar. The flask was sparged with argon. Dry methanol (44 mL) was added via syringe. Stirring was started, and the solution was heated to 58 °C in an oil bath. Palladium(II) dichloride (382.6 mg, 2.158 mmol, 2 equiv) was added to the heated stirring solution in one portion. The solution was left to stir for about 5 min until it turned a dark purple-brown color. The temperature was reduced to 40 °C, and the solution was left to stir for 2 h. The solution was filtered on a 60 mL frit, and the solid was rinsed with methanol (2 x 15 mL) and then water (2 x 25 mL). The dark purple powder was collected, dissolved in hexanes (15 mL) and was filtered on a frit rinsing with hexanes (25 mL). The filtrate was diluted with ethanol (100 mL, 200 proof), methanol (100 mL), and cooled to -20 °C in a freezer for 36 h forming crystals.³⁰ Crystals were recovered by filtration on a 30 mL frit and were rinsed with methanol (30 mL) yielding a first crop of tris{1,5-bis-[3-(triethylsilyl)phenyl]penta-1,4-dien-3-one}dipalladium(0) [Pd₂(mtdba)₃] (**39**) (62.9% yield, dark purple crystalline

flakes). The filtrate was concentrated in vacuo, redissolved in hexanes (2 mL), diluted with ethanol (5 mL, 200 proof), then methanol (5 mL) and left to crystallize in a $-20\text{ }^{\circ}\text{C}$ freezer. After 36 h, crystals formed. The second crop of crystals were recovered by filtration on a 15 mL frit, then were washed with methanol (4 x 5 mL) and then ethanol³¹ (10 x 8 mL) yielding a second crop of tris{1,5-bis-[3-(triethylsilyl)phenyl]penta-1,4-dien-3-one}dipalladium(0) [$\text{Pd}_2(\text{mtdba})_3$] (**39**) (9.7% yield, 72.6% yield total, dark-purple crystalline flakes). mp $194\text{ }^{\circ}\text{C}$ (decomposition); ^1H NMR (600 MHz, CDCl_3 , $25\text{ }^{\circ}\text{C}$) δ 7.68–7.79 (comp. m, 3H), 7.76 (d, $J = 15.8\text{ Hz}$, 0.3H), 7.69 (br. s, 0.35H), 7.63 (dm, $J = 7.9\text{ Hz}$, 0.18H), 7.58 (d, $J = 7.3\text{ Hz}$, 0.2H), 7.51–7.37 (comp. m, 3.73H), 7.34–7.12 (comp. m, 4.56H), 7.11–7.00 (comp. m, 1.54H), 6.88 (br. s, 1H), 6.79–6.61 (m, 5.34H), 6.61–6.48 (m, 2H), 6.15 (d, $J = 14.0\text{ Hz}$ 1H), 6.07 (br. s, 0.67H), 5.95 (d, $J = 9.7\text{ Hz}$, 2H), 5.67 (br. s, 1H), 5.52–5.38 (comp. m, 1.77H), 5.38–5.20 (comp. m, 2.25H), 5.09 (d, $J = 12.6\text{ Hz}$, 1H), 4.94 (app. t, $J = 12.8\text{ Hz}$, 1.42), 4.88 (br. s, 0.91 H),³² 1.15–0.94 (m, 54H), 0.94–0.70 (m, 36H); ^{13}C NMR (150 MHz, CDCl_3 , $-10\text{ }^{\circ}\text{C}$) δ 188.9, 184.6, 182.6, 181.6, 180.8, 144.0, 142.0, 138.96, 138.92, 138.7, 138.6, 138.5, 138.4, 138.1, 138.0, 137.6, 137.4, 137.1, 137.0, 136.7 136.1, 135.8, 135.2, 135.0, 134.7 134.5, 134.4, 134.05, 133.95, 133.71, 133.70, 133.35, 133.34, 133.31, 133.0, 128.5, 128.3, 128.1, 112.4 (br. s), 110.8, 110.2 (br. s), 97.7 (br. s), 96.8 (br. s), 94.3 (br. s), 91.4 (br. s), 89.2 (br. s), 85.7 (br. s), 84.4 (br. s), 84.1 (br. s), 7.71, 7.68, 7.67, 7.654, 7.647, 7.5, 3.4, 3.32, 3.28, 3.26, 3.24, 3.23, 3.1; IR (neat film, NaCl) 3080, 3045, 3023, 2954, 2909, 2875, 1621, 1585, 1570, 1544, 1464, 1416, 1386, 1323, 1297, 1239, 1186, 1120, 1082, 1010, 975, 911, 877, 861, 791, 736, 720, 686, 611 cm^{-1} ; IR (Fluorolube® mull, CaF_2) 3076, 3041, 3020, 2950, 2906, 2872, 1620, 1586, 1568, 1544, 1455, 1415, 1385 cm^{-1} ; HRMS (high field FAB, 2-

nitrophenyl octyl ether) m/z calc'd for $C_{87}H_{126}O_3Pd_2Si_6$ $[M]^+$: 1601.6505, found: 1601.6477.

2.6.4 Synthesis, Handling, and Characterization Methods for Intermediate 1:



2.6.4.1 Synthesis

Complexes (R,S)-31 and (S,S)-31: In a glove box with a nitrogen atmosphere, (*S*)-*t*-BuPHOX ligand (**1**) (148.8 mg, 384.0 μ mol, 1.24 equiv) was added to a 20 mL scintillation vial. $[Pd_2(mtdba)_3]$ (**39**) (248.9 mg, 155.4 μ mol, 0.5 equiv) was weighed into a 1 dram vial.⁸ Anhydrous THF (1 mL) was added to the 20 mL vial containing (*S*)-*t*-BuPHOX ligand (**1**). The 20 mL scintillation vial was swirled manually until all the (*S*)-*t*-BuPHOX ligand (**1**) had dissolved. Anhydrous THF (3 x 1 mL) was added into the 1 dram vial containing $[Pd_2(mtdba)_3]$ (**39**), each portion was mixed manually by pipette and then added dropwise to the solution of (*S*)-*t*-BuPHOX ligand (**1**) in the 20 mL scintillation vial. The solution was swirled manually by hand for 1 min, and then left to stand and mix by diffusion for 1.5 h. The solution was cooled to -36 °C in a freezer in the glove box. Once cooled, the solution was then moved to a precooled aluminum block at -36 °C in the glove box. Then, 1-methyl-2-oxo-cyclohexanecarboxylic acid allyl ester (β -ketoester **2**) (157 mg, 800 μ mol, 2.57 equiv) was added via a syringe in a single portion. The solution was stirred manually for 1 min while cold, and moved to a -36 °C

freezer in the glove box. The reaction was left to stand for 10 min in the freezer. The solution was then diluted with hexanes (12 mL) that had been precooled to $-20\text{ }^{\circ}\text{C}$, and then the mixture was concentrated in vacuo in a $-20\text{ }^{\circ}\text{C}$ freezer in the glove box to roughly 10 mL. The solution was moved in 2 mL portions to another 20 mL scintillation vial in a precooled aluminum block at $-36\text{ }^{\circ}\text{C}$ where each portion was individually triturated with hexanes (5 mL) that had been precooled to $-20\text{ }^{\circ}\text{C}$, then the supernatant was decanted via pipette. Solvent was removed from the precipitated material in vacuo at $-20\text{ }^{\circ}\text{C}$ in a freezer in the glove box to afford a mixture of complexes (*S,S*)- **31** and (*R,S*)- **31** (72.4 mg, 33.8% yield, bright yellow powder). ^1H NMR (600 MHz, $\text{THF}_{d,8}$, $-28\text{ }^{\circ}\text{C}$) δ 8.19 (app. br. t, $J = 3.5\text{ Hz}$, 1H), 7.69 (app. t, $J = 7.5\text{ Hz}$, 1H), 7.62 (app. t, $J = 7.2\text{ Hz}$, 1H), 7.59–7.46 (comp. m, 8H), 7.25 (app. t, $J = 9.0\text{ Hz}$, 2H), 7.03 (app. t, $J = 8.8\text{ Hz}$, 1H), 6.23 (br. s, 1H), 5.11 (s, 1H), 4.57 (d, $J = 9.7\text{ Hz}$, 1H), 4.55–4.47 (m, 1H), 4.47 (br. s, 1H), 4.40–4.23 (comp. m, 2H), 3.06 (br. s, 0.35H), 2.94–2.85 (br. m, 1H), 2.86–2.77 (m, 0.65H), 2.48 (dd, $J = 14.0, 13.8\text{ Hz}$, 1H), 2.17 (d, $J = 13.2\text{ Hz}$, 0.35H), 2.11 (d, $J = 12.9\text{ Hz}$, 0.65H), 1.97–1.85 (m, 1H), 1.84–1.70 (m, 1H), 1.63–1.38 (m, 1H), 1.38–1.45 (m, 1H), 1.33–1.18 (m, 1.3H), 1.14 (s, 1.95H), 1.11 (s, 1.05H), 0.92–0.87 (m, 0.35H), 0.69 (s, 9H); ^{13}C NMR (150 MHz, $\text{THF}_{d,8}$, $-28\text{ }^{\circ}\text{C}$) δ 210.3, 210.2, 176.7, 176.6, 163.6, 143.8 (app. br. s), 135.8, 134.9 (d, $J_{\text{CP}} = 11.0\text{ Hz}$), 134.7 (d, $J_{\text{CP}} = 12.2\text{ Hz}$), 133.7 (d, $J_{\text{CP}} = 6.6\text{ Hz}$), 133.4 (d, $J_{\text{CP}} = 7.7\text{ Hz}$), 132.4 (d, $J_{\text{CP}} = 9.4\text{ Hz}$), 132.1, 131.4, 131.08, 131.02, 130.7, 130.45, 130.37, 130.04, 129.97, 129.9, 129.8, 129.3, 129.0, 106.3 (app. br. s), 70.3, 68.1, 67.9, 67.8, 59.4, 41.85, 41.81, 40.6, 40.5, 35.1, 29.2 (app. br. s), 28.9, 28.7, 25.9, 25.8, 25.7, 24.55, 24.48, 23.0, 22.9; ^{31}P NMR (121.4 MHz, $\text{THF}_{d,8}$, $24\text{ }^{\circ}\text{C}$) δ 30.9; ^{31}P NMR (121.4 MHz, $\text{THF}_{d,8}$, $-20\text{ }^{\circ}\text{C}$) δ 30.8; IR (neat film, NaCl) 3065, 2956, 2930,

2858, 1708, 1662, 1623, 1613, 1571, 1483, 1465, 1437, 1372, 1346, 1313, 1243, 1166, 1142, 1117, 1099, 1062, 1029, 959, 900, 876, 848, 814, 781, 696, 675 cm^{-1} ; IR (Fluorolube® mull, CaF_2) 3076, 3055, 3016, 2959, 2934, 2924, 2874, 2853, 1711, 1634, 1616, 1604, 1568, 1480, 1465, 1448, 1433, 1373 cm^{-1} ; HRMS (FAB, 2-nitrophenyl octyl ether) m/z calc'd for $\text{C}_{28}\text{H}_{31}\text{NOPPd}$ [$\text{M} - \text{C}_8\text{H}_{11}\text{O}_3$] $^+$: 534.1178, found: 534.1187; X-ray quality crystals were grown by partially dissolving freshly synthesized intermediate **31** in cold (-20 °C) THF using the undissolved material to act as a nucleation site for crystals, and then the solution was layered with cold hexanes (-20 °C). Diethyl ether was added dropwise until most of the finer precipitation on the boundary between the layers had redissolved and layer diffusion was allowed to progress at -36 °C in a glove box freezer.

2.6.4.2 Handling and Characterization Methods for Complexes (*S,S*)-**31** and (*R,S*)-**31**

Due to the instability of complexes (*S,S*)-**31** and (*R,S*)-**31**, basic handling and the acquisition of characterization data often required special procedures to achieve good reproducible results. These procedures are outlined here.

General Handling Notes: All glassware and metalware were precooled to -36 °C in a freezer for 1 h before being allowed to come into contact with complexes (*S,S*)-**31** and (*R,S*)-**31**. If during operation, glassware or metalware warmed to the point that it was just barely perceptibly cool through triple gloves, it was returned to the -36 °C freezer for at least 20 min before being used again. All solvents that came in contact with complexes (*S,S*)-**31** and (*R,S*)-**31** were precooled to either -36 °C or -20 °C in a freezer as indicated. Complexes (*S,S*)-**31** and (*R,S*)-**31** were only ever exposed to argon or nitrogen atmospheres; even as a solvent-free crystalline solid at subzero temperatures

these complexes appear to react with air and possibly moisture. Decomposition of these complexes by poor handling could be readily determined by indicative color change. Healthy samples of the complexes are a bright yellow, reminiscent of a classic highlighter pen. Air exposure leads to an orange color change while minimal thermal decomposition leads to a more subtle color change resulting in a yellow-beige hue. In cases where some decomposition had occurred, samples could be partially recovered with tolerable, but not analytical, purity by manually excising incorrectly colored regions using precooled implements. Such recovered samples are unfit for NMR or IR characterization, but give consistent results when used in reactions. Samples of complexes (*S,S*)-**31** and (*R,S*)-**31** store well as a desolvated solid at $-36\text{ }^{\circ}\text{C}$ in a glove box freezer for months, but do eventually show signs of decomposition by ^1H NMR.

Thin-Film IR on NaCl plates: In a glove box, a few milligrams of the diastereomeric mixture of complexes (*S,S*)-**31** and (*R,S*)-**31** were added to a half-dram vial in an aluminum block that had been precooled to $-36\text{ }^{\circ}\text{C}$ in a freezer. The sample was dissolved in minimal anhydrous THF that had been precooled to $-36\text{ }^{\circ}\text{C}$ in a freezer, and then the solution was carefully deposited via a pipette on a NaCl IR plate that had been precooled to $-36\text{ }^{\circ}\text{C}$ in a freezer. The IR plate was quickly moved into a small desiccator inside the glove box, and the desiccator was inserted into a $-20\text{ }^{\circ}\text{C}$ freezer in the glove box. A vacuum hose was connected to the desiccator inside the glove box in the $-20\text{ }^{\circ}\text{C}$ freezer, and a gentle vacuum was applied reducing the solution on the IR plate to a thin yellow-green film over 5 h. The thin film was then sandwiched between a second NaCl IR plate that had been precooled to $-36\text{ }^{\circ}\text{C}$. The fine gap between the two plates was sealed over with Parafilm®, and the sealed plates were returned to the

desiccator in a $-20\text{ }^{\circ}\text{C}$ freezer for 20 min. The desiccator was sealed, quickly removed from the glove box, and then partially submerged in a bucket of powdered dry ice that was carried to the spectrometer. The sealed plates were removed from the desiccator whereupon they quickly frosted over. A Kimwipe® was used to vigorously polish both exterior faces of the two-plate sandwich until they were just barely warm enough that they did not readily frost over (roughly 1 min), but that the sample in between the two plates was still cold. The two-plate sandwich was then inserted into the spectrometer just above a fresh dish full of anhydrous CaCl_2 and a rushing stream of nitrogen. It is recommended that new or otherwise valuable NaCl plates not be used for this procedure as they are left opaque and lightly pitted by the unavoidable quick frosting and polishing.

Fluorolube® mull IR on CaF_2 plates: In a glove box, a small amount of partially frozen Fluorolube® was spread thinly with a spatula across the center of a CaF_2 IR plate that had been precooled to $-36\text{ }^{\circ}\text{C}$ in a freezer. A few milligrams of the mixture of complexes (*S,S*)-**1** and (*R,S*)-**1** were added on top of the Fluorolube® film as a powder. The powder and Fluorolube® film were then sandwiched between a second CaF_2 IR plate that had been precooled to $-36\text{ }^{\circ}\text{C}$ in a freezer, and the materials were mulled briskly between the two cold IR plates for 1 min. The plates were sealed, moved cold to the spectrometer and spectra were taken as per the procedure for the thin film IR on NaCl plates above. Unlike NaCl plates, CaF_2 plates seem unblemished by their unavoidable exposure to frost and polishing in this procedure.

NMR Spectra (^1H , ^{13}C , ^{31}P): In a glove box with a nitrogen atmosphere, roughly 20 mg of the mixture of complexes (*S,S*)-**31** and (*R,S*)-**31** were added to a half-dram vial in an aluminum block, both of which had been precooled to $-36\text{ }^{\circ}\text{C}$. A fresh ampule of

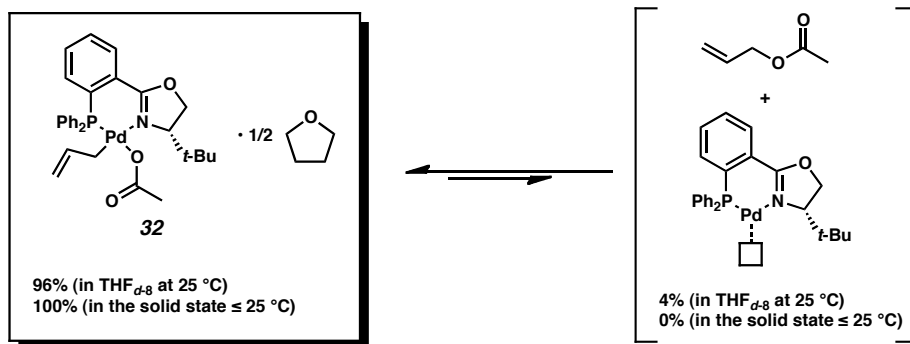
THF_{d,8} that had been precooled to -36 °C was opened, and 0.75 mL of THF_{d,8} was used portion-wise to dissolve the material and move it into an NMR tube that had been precooled to -36 °C. The tube was quickly sealed with a plastic cap and removed from the glove box, where it was immediately submerged to within a few centimeters of its top in powdered dry ice in a dewar. The dewar was carried to the spectrometer, which was then cooled to the desired temperature before quickly removing the NMR tube from the dry ice and inserting it into the instrument. Phosphorus spectra obtained at reduced temperatures could not be directly referenced to phosphoric acid as outlined in the Materials and Methods section due to the relatively high freezing point of the phosphoric acid standard. Instead, subzero ³¹P NMR spectra were referenced to free (*S*)-*t*-BuPHOX ligand (δ -5.95) used as either an internal or external standard in THF_{d,8}. The reported 24 °C ³¹P NMR spectrum was recorded by generating the mixture of intermediates (*S,S*)-**31** and (*R,S*)-**31** in situ as outlined in the section on NMR experiments in this supporting information (Page 5).

2.6.4.3 Effervescent Crystals

Synthesis: In a nitrogen glove box (*S*)-*t*-BuPHOX ligand (**1**) (96.7 mg, 250 μ mol, 1.3 equiv) followed by [Pd₂(dba)₃] (86.2 mg, 94.1 μ mol, 0.5 equiv) were added, neat, into a 20 mL scintillation vial. Anhydrous THF (8 mL) was filtered through a pipette with glass filter paper directly into the 20 mL scintillation vial. The solution was mixed manually by pipette for two minutes, and then left to stand and mix by diffusion for 20 min. During this time an initially dark red-purple solution formed, which then lightened to a dark, rich, orange color. The solution was filtered through a pipette with glass filter paper into five separate 1 dram vials evenly (1.6 mL each). This filtration

separated a rich orange filtrate from a black precipitate presumed to be aggregated palladium(0) metal. The vials were sealed with plastic screw caps and removed from the box. On the bench, the vials were individually opened, and β -ketoester **8** (210 mg, 1.07 mmol, 28.5 equiv), was added by syringe to each vial, after which they were resealed. The vials were then swirled manually for 5 seconds, during which time the solution underwent a rapid color change from a rich orange to a lighter yellow green. The vials were left to stand and mix by diffusion for an additional 10 min. Each vial was then opened and inserted into a 20 mL scintillation vial containing 5 mL of hexanes for vapor diffusion. The atmosphere of each two-vial apparatus was gently displaced with a flow of argon from a hose, and then the 20 mL vial was sealed tightly with a plastic screw cap. These self-contained vapor diffusion apparatus were left to slowly crystallize at $-20\text{ }^{\circ}\text{C}$ in a freezer for a week. During this time the inner vials begin to grow one of two crystal forms, clear colorless fine feathery needles or clear colorless large glassy blocks. The formation of colored crystals results from impurities or improper handling. The type of crystal form often varies from vial to vial, but is usually homogeneous within a given vial. Only the clear colorless large glassy blocks show visible signs of effervescence, though various characterization methods (HRMS and partial crystal structure) suggest that both crystal forms are predominantly composed of intermediate **31**, and both can be thermally decomposed to yield 2-allyl-2-methylcyclohexanone with reproducible and reasonably high enantioinduction.

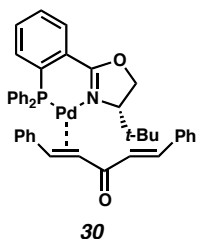
2.6.5 Synthesis and Characterization of Other New Molecules



Allyl Acetate Complex 32, half THF adduct:³³ In a nitrogen glove box (*S*)-*t*-BuPHOX ligand (**3**) (75.6 mg, 195 μ mol, 1.3 equiv) was weighed into a 20 mL scintillation vial. [Pd₂(mtdba)₃] (**39**) (120.2 mg, 75.06 μ mol, 0.5 equiv) was weighed into a 1 dram vial. Anhydrous THF (0.5 mL) was added to the 20 mL scintillation vial, which was swirled manually for 30 s until all of the (*S*)-*t*-BuPHOX ligand (**1**) had dissolved. Anhydrous THF (3 x 0.5 mL) was added to the 1 dram vial containing [Pd₂(mtdba)₃] (**39**). The solution in the 1 dram vial was mixed manually by pipette resulting in the formation of a dark purple solution, which was added dropwise to the solution in the 20 mL scintillation vial containing (*S*)-*t*-BuPHOX ligand (**1**). The resulting solution in the 20 mL scintillation vial was swirled manually for 1 min, and then left to stand and mix by diffusion for 1.5 h, during which time the solution turned from a dark purple to a rich orange color. Allyl acetate (146 mg, 1.46 mmol, 9.7 equiv) was added in one portion via syringe. The solution was swirled manually for 1 min then left to stand for 20 min, during which time its color lightened slightly to a yellow-orange. The solution was then carefully layered with hexanes (18 mL) and allyl acetate (200 μ L) and left to crystallize via layer diffusion in a -20 °C freezer in the glove box resulting in

the formation of small yellow-green crystal clusters and powder. This mixture of crystals and powder was redissolved in THF (3 x 0.5 mL) and filtered through a pipette filter with glass filter paper into a 1 dram vial to separate a yellow-orange solution from a small amount of gray material. The solution was then layered with hexanes (0.5 mL) causing the solution to become cloudy with precipitate. Diethyl ether (1 mL) was added to the solution carefully, so as not to disturb the interface between the two layers, and was added until most of the finer suspended precipitate had dissolved, leaving two distinct homogenous layers. The vial was then left in a $-36\text{ }^{\circ}\text{C}$ freezer to crystallize via layer diffusion. The mother liquor was decanted, the crystals were powdered, washed with hexanes (1 x 5 mL), and azeotroped with hexanes (1 x 5 mL), before being dried in vacuo affording complex **32** as a half THF adduct (34.3 mg, 38.5% yield, yellow green powder). mp 128–131 $^{\circ}\text{C}$ (decomp); ^1H NMR (500 MHz, THF_{d-8}) δ 8.18 (ddd, $J_{\text{HP}} = 4.0$ Hz, $J = 7.9$ Hz, 1.1 Hz, 1H), 7.64 (app. tt, $J = 7.7$, 1.3 Hz, 1H) 7.56–7.40 (comp. m, 9H), 7.32–7.26 (m, 2H), 7.04 (ddd, $J_{\text{HP}} = 1.2$ Hz, $J = 10.0$, 7.8, 1H), 6.19 (dddd, $J_{\text{HP}} = 1.7$ Hz, $J = 11.6$, 11.1, 10.8, 10.2 Hz, 1H), 4.56–4.39 (comp. m, 3.7H), 4.39–4.31 (m, 1H), 3.64–3.59 (m, 2H), 2.75 (br. s, 1H), 1.99–1.84 (comp. m, 1.3 H), 1.80 (s, 3H), 1.79–1.75 (m, 2H), 0.72 (s, 9H); ^{13}C NMR (125 MHz, THF_{d-8}) δ 174.8, 163.5 (d, $J_{\text{CP}} = 2.7$ Hz), 144.1 (app. br. s), 135.9 (d, $J_{\text{CP}} = 1.8$ Hz), 134.96 (d, $J_{\text{CP}} = 10.1$ Hz), 134.86 (d, $J_{\text{CP}} = 11.5$ Hz), 133.2 (d, $J_{\text{CP}} = 10.1$ Hz), 133.1 (d, $J_{\text{CP}} = 8.3$ Hz), 132.2 (d, $J_{\text{CP}} = 1.5$ Hz), 132.1 (d, $J_{\text{CP}} = 2.3$ Hz), 131.9 (d, $J_{\text{CP}} = 35.9$ Hz), 131.7 (d, $J_{\text{CP}} = 2.8$ Hz), 131.5 (d, $J_{\text{CP}} = 30.4$ Hz), 130.9 (d, $J_{\text{CP}} = 12.4$ Hz), 130.3 (d, $J_{\text{CP}} = 50.6$ Hz), 129.8 (d, $J_{\text{CP}} = 11.0$ Hz), 129.6 (d, $J_{\text{CP}} = 11.0$ Hz), 106.0 (app. br. s), 75.4, 70.3, 68.4, 35.1, 30.1 (app. br. s.), 26.5, 26.1, 24.9; ^{31}P NMR (121.4 MHz, THF_{d-8}) δ 31.1; IR (neat film, NaCl) 3059, 2962, 2869, 1632, 1606,

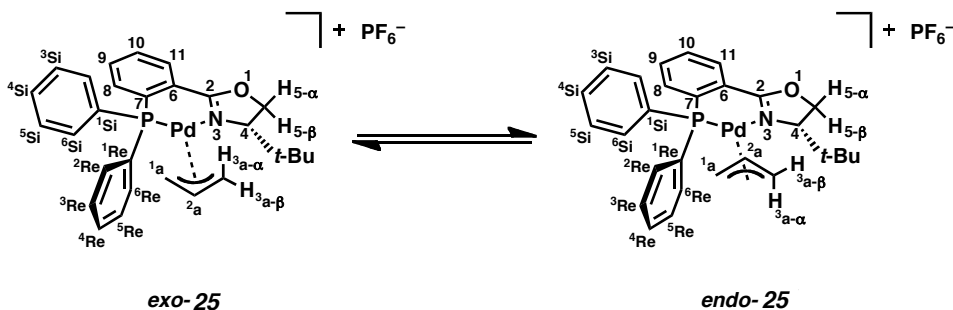
1581, 1482, 1436, 1372, 1321, 1244, 1213, 1192, 1144, 1115, 1099, 1063, 1058, 1028, 958, 928, 876, 781, 747, 730, 708; IR (Fluorolube® mull, CaF₂) 3066, 2958, 2909, 2867, 1637, 1609, 1580, 1565, 1481, 1436, 1372; HRMS (FAB, 2-nitrophenyl octyl ether) *m/z* calc'd for C₃₀H₃₅O₃NPPd [M + H]⁺: 594.1390, found: 594.1393. X-ray quality crystals were obtained by layering a concentrated THF solution of complex **7** with hexanes. Diethyl ether was added dropwise until most of the finer precipitation on the boundary between the layers had redissolved. Allyl acetate (≈ 10 μL per 30 mg of **32**) was added for stability, and layer diffusion was allowed to progress at – 36 °C in a freezer in a nitrogen glove box.



[(*S*)-*t*-BuPHOX]Pd(dba)] pre-catalyst **30:³⁴ In a nitrogen glove box (*S*)-*t*-BuPHOX ligand (**1**) (323.4 mg, 830.4 μmol, 2.5 equiv) and [Pd₂(dba)₃] (302.4 mg, 330 μmol, 1 equiv) were weighed directly into a 100 mL round bottom flask with a stirbar, neat, in the order specified. Anhydrous THF (70 mL) was filtered through a pipette filter with glass filter paper and added to the flask. Stirring was started and the solution quickly became a dark red-purple color. The solution was left to stir for 8 h, turning a dark orange color with a small amount of black precipitate. The solution was filtered through a 15 mL frit separating an intensely orange-red solution from a thick silting of insoluble black powder presumed to be particulate Pd(0). The solution was concentrated in vacuo to a thin foamy red film. Minimal diethyl ether (pipette filtered, 5 x 1.2 mL) was used to**

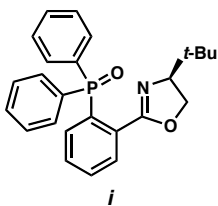
dissolve the film and transfer it to a 50 mL round-bottom flask. An orange-red powder started to precipitate from the ethereal solution in the new flask. The ether solution was layered with 20 mL of hexanes, and then cooled to $-36\text{ }^{\circ}\text{C}$ in a glove box freezer. The solution was filtered on a 30 mL frit, separating a bright orange fluffy solid from a bright orange filtrate. The orange solid was rinsed with hexanes until the filtrate was almost clear (20 x 5 mL). The material was subsequently recrystallized from diethyl ether layered with hexanes, followed by a second recrystallization using toluene layered with hexanes. The solids were rinsed with 1:1 toluene/hexanes, diethyl ether, and then 1:1 Et_2O /hexanes. The material was dissolved in THF and layered with hexanes and left to precipitate at $-36\text{ }^{\circ}\text{C}$ in a glove box freezer. The resulting light yellow solution was decanted, and the solids rinsed with hexanes (2 x 3 mL). This THF/hexanes precipitation and hexanes wash was repeated four times. The material was then azeotroped in hexanes (4 x 5 mL) and dried in vacuo for 16 h to afford precatalyst **30** (300 mg, 62.2%, yellow powder). mp $144.5\text{--}147\text{ }^{\circ}\text{C}$; ^1H NMR (500 MHz, THF_{d_8}) δ 8.18 (br. s, 0.07H), 8.12–8.01 (m, 0.89H), 7.76–7.66 (comp. m, 0.19H), 7.61 (br. s, 0.23H), 7.53 (d, $J = 7.3\text{ Hz}$, 1.43H), 7.51–6.95 (m, 17.57H) 6.87 (br. s, 4H), 6.68 (br. s, 0.15H), 6.53 (app. t, $J = 8.7\text{ Hz}$, 1.48H), 5.04 (br. s, 0.09H), 4.89 (m, 0.73H), 4.76 (s, 0.08H), 4.63 (app. dd, $J = 9.3, 9.0\text{ Hz}$, 0.75H), 4.53 (br. s, 0.14H), 4.30 (m, 1.07H), 4.23–4.13 (m, 0.77H), 4.05 (app. dd, $J = 9.5, 9.3\text{ Hz}$, 0.75H), 4.01 (br. s, 0.2 Hz, 0.2H), 2.49 (s, 0.02H), 2.48–2.44 (comp. m, 0.04H), 2.04 (s, 0.1H), 1.37–1.26 (m, 0.24H), 0.82 (br. s, 8H), 0.42 (br. s, 1H); ^{13}C NMR (125 MHz, THF_{d_8}) δ 184.2, 164.6, 146.4, 143.2, 138.2, 137.4 (br. s), 136.1, 135.8, 135.6, 135.3, 135.1, 134.83, 134.75, 134.5, 134.2, 134.1, 133.4, 133.3, 132.7, 131.3, 131.2, 131.1, 130.78, 130.77, 130.6, 130.3, 129.8, 129.6, 129.5, 129.4, 129.3, 129.2, 129.1,

128.8, 128.3, 127.4 (br. s), 126.8, 125.9, 124.2, 80.2 (br. s), 79.9 (br. s), 69.5 (br. s), 68.9, 68.1, 58.3 (br. s), 35.5, 30.5; ^{31}P NMR (121.4 MHz, $\text{THF}_{d,8}$) δ 21.26 (0.1P), 18.97 (0.9P); IR (neat film, NaCl) 3055, 2958, 2867, 1638, 1622, 1581, 1568, 1496, 1472, 1435, 1359, 1332, 1310, 1280, 1239, 1202, 1141, 1108, 1095, 1068, 1054, 1028, 998, 967, 920, 862, 761, 747 cm^{-1} ; IR (Fluorolube® mull, CaF_2) 3055, 3009, 2953, 2867, 1638, 1618, 1597, 1568, 1578, 1493, 1466, 1448, 1433, 1359 cm^{-1} ; HRMS (FAB, 2-nitrophenyl octyl ether) m/z calc'd for $\text{C}_{42}\text{H}_{41}\text{PPdO}_2\text{N}$ $[\text{M} + \text{H}]^+$: 728.1910, found: 728.1925. X-ray quality crystals were grown from THF via successive layer diffusion in a glove box with Et_2O at -20°C to form seed crystals, and then hexanes at -20°C .



$[(\{S\}\text{-}t\text{-BuPHOX})\text{Pd}(\text{allyl})]\text{PF}_6$ Salt and 1/2 EtOH adduct (25** PF_6^-):** The hexafluorophosphate salt of complex **25** was prepared using Zehnder's method³⁵ with (*S*)-*t*-BuPHOX ligand (**1**) to afford a quantitative yield of rapidly interconverting *exo* and *endo* allyl isomers (ca. 60/40 in CDCl_3 , 67/33 in $\text{THF}_{d,8}$ as the 1/2 EtOH adduct, and 44/56 in the solid state crystallized from EtOH as a 1/2 EtOH adduct) as a light yellow powder; mp (1/2 EtOH adduct) 152–154 $^\circ\text{C}$ (decomp.); ^1H NMR (300 MHz, CDCl_3) δ 8.30 (app. ddd, $J = 7.7, 4.1, 1.1$ Hz, 0.6H), 8.24 (app. ddd, $J = 7.7, 4.4, 1.1$ Hz, 0.4H), 7.74–7.42 (comp. m, 8H), 7.39–7.11 (comp. m, 4H), 7.04–6.87 (comp. m, 1H), 5.96–5.82 (m, 0.4H), 5.82–5.67 (m, 0.6H), 4.96–4.86 (comp. m, 1H), 4.68 (app. q, $J = 9.9$ Hz, 1H),

4.49 (app. dt, $J_d = 11.3$ Hz, $J_t = 3.9$ Hz, 1H), 4.19 (app. dt, $J_d = 11.3$ Hz, $J_t = 4.4$ Hz, 1H), 4.03 (app. dd, $J = 14.3, 9.4$ Hz, 0.6H), 3.63–3.48 (comp. m, 1H), 3.32 (app. d, $J = 6.6$ Hz, 0.4H), 3.16 (app. d, $J = 12.7$ Hz, 0.4H), 2.77 (app. d, $J = 12.1$ Hz, 0.6H), 0.64 (s, 3.5 H), 0.56 (s, 5.5 H); ^{13}C NMR (75 MHz, CDCl_3) δ 164.9–164.8 (3 peaks), 134.9, 134.8, 134.0–133.3 (7 peaks), 132.9–132.6 (4 peaks), 132.2–132.1 (3 peaks), 131.8 (app. d, $J = 2.3$ Hz), 130.2–128.8 (13 peaks), 128.5–127.8 (5 peaks), 127.3, 122.4 (app. d, $J = 6.0$ Hz), 122.4, 83.3–79.4 (6 peaks), 69.8, 69.7, 58.6, 54.1, 54.0, 34.3, 25.2; ^{31}P NMR (121.4 MHz, CDCl_3) δ 23.2 (s, 0.6P), 22.2 (s, 0.4P), –143.4 (septet, $J_{\text{PF}} = 711.0$ Hz, 1P); ^{31}P NMR (121.4 MHz, $\text{THF}_{d,8}$) δ 23.5 (s, 0.67P), 22.5 (s, 0.33P), –143.8 (septet, $J_{\text{PF}} = 710.4$ Hz, 1P); ^{19}F NMR (242 MHz, CDCl_3) δ –73.7 (d, $J_{\text{FP}} = 712.6$ Hz); IR (Neat Film from CDCl_3 , NaCl) 3062, 2964, 2872, 2271, 1971, 1899, 1826, 1621, 1584, 1568, 1482, 1437, 1372, 1315, 1249, 1211, 1145, 1121, 1100, 1060, 1028, 958, 913, 836, 778, 732, 697, 678 cm^{-1} ; HRMS (FAB, 3-nitrobenzyl alcohol) m/z calc'd for $\text{C}_{28}\text{H}_{31}\text{ONPPd} [\text{M-PF}_6]^+$: 534.1178, found 534.1182; Anal. calcd for $\text{C}_{29}\text{H}_{34}\text{F}_6\text{NO}_{1.5}\text{P}_2\text{Pd}$ (1/2 EtOH adduct): C, 49.55; H, 4.88; N, 1.99; O, 3.41. Found: C, 49.48; H, 4.82; N, 1.97; O, 3.67. $[\alpha]_{\text{D}}^{27.1} +256.6$ (c 3.72, CH_2Cl_2). X-ray quality crystals were grown from the slow cooling of a hot and concentrated EtOH solution. See CCDC deposition number: 245187 or Appendix 2 for X-ray structural data of this compound.



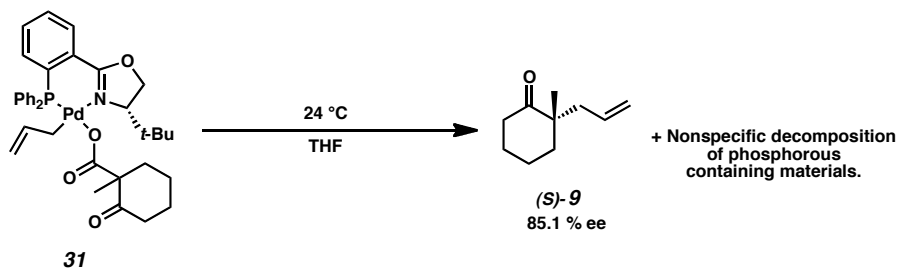
(S)-*t*-BuPHOX Oxide (i): To a solution of (*S*)-*t*-BuPHOX ligand (**1**) (150 mg, 0.387 mmol, 1 equiv) in THF (2.5 mL) was added a 5% aqueous H₂O₂ solution (1.94 mL). After 15 min the reaction mixture was diluted with EtOAc (5 mL) and brine (5 mL), washed with 10% aqueous Na₂CO₃ (5 mL) and brine (5 mL), dried with magnesium sulfate, and filtered. Chromatography was performed with 5% methanol in dichloromethane on silica gel to afford (*S*)-*t*-BuPHOX oxide (**i**) (149.3 mg, 96% yield, white foam). TLC (*R_f* 0.20, 3% methanol in dichloromethane); ¹H, NMR (300 MHz, CDCl₃) δ 7.95 (ddd, *J* = 7.5, 3.9, 1.2 Hz, 1H), 7.81–7.33 (comp. m, 7H), 7.52–7.31 (comp. m, 7H), 3.84 (dd, *J* = 8.1, 8.1 Hz, 1H), 3.57, (dd, *J* = 9.9 Hz, *J* = 9.9 Hz, 1H), 3.41 (dd, *J* = 9.9 Hz, 8.4 Hz, 1H), 0.77 (s, 9H); ¹³C NMR (75 MHz, CDCl₃) δ 163.1, 135.0 (d, *J*_{CP} = 10.1 Hz), 133.7 (d, *J*_{CP} = 107.1 Hz), 133.3 (d, *J*_{CP} = 11.7 Hz), 138.2 (app. dd, *J*_{CP} = 12.3, 1.4 Hz), 75.9, 68.8, 33.6, 25.8; ³¹P NMR (121.4 MHz, CDCl₃) δ 30.3; ³¹P NMR (121.4 MHz, THF_{d,8}) δ 27.2;^[36] IR (Neat Film, NaCl) 3057, 2957, 2903, 2868, 2217, 1664, 1589, 1565, 1477, 1438, 1356, 1337, 1307, 1248, 1201, 1119, 1108, 1067, 1028, 963, 930, 905 cm⁻¹; HRMS (FAB) *m/z* calc'd for C₂₅H₂₇O₂NP [M]⁺: 404.1779, found 404.1799; [α]_D^{27.6} –69.3 (*c* 1.96, CH₂Cl₂).

2.6.6 Controlled Thermal Decomposition of Intermediate **31**

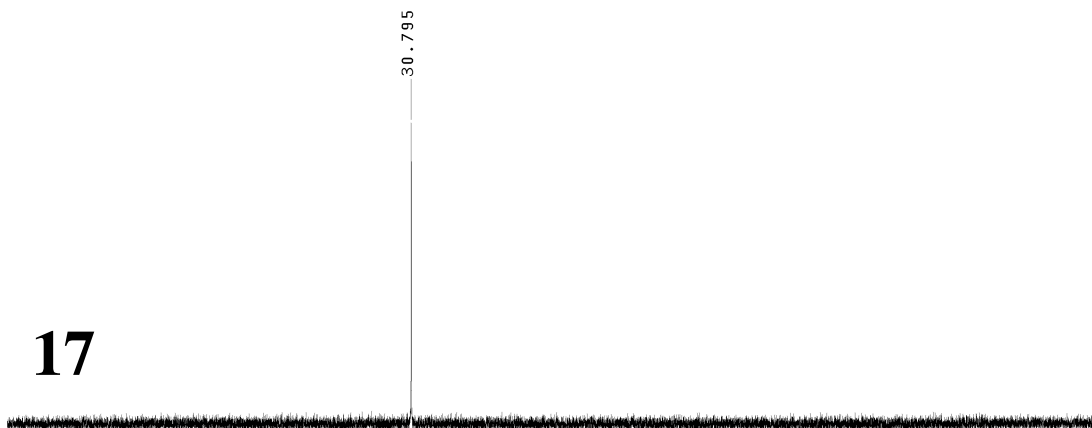
2.6.6.1 Controlled Thermal Decomposition of Intermediate **31** in the Absence of dba Ligand in Solution (THF)

Until the sample left the glove box, all of the following operations were performed in a cold aluminum block with implements and containers [such as the half-dram vial and NMR tube] that had been precooled to -36°C in a glove box freezer. In a nitrogen glove box, intermediate **31** (22.8 mg, $33.0\ \mu\text{mol}$, 1 equiv) was weighed into a half-dram vial. A 1 mL ampule of $\text{THF}_{\text{d},8}$ that had been precooled to -36°C in a glove box freezer was opened, and its contents were used to dissolve the sample of intermediate **31** and transfer it to an NMR tube. The NMR tube was tightly sealed with a plastic cap, and was then cooled again to -36°C in a glove box freezer for 20 min. The NMR tube was then quickly removed from the glove box and immediately submerged in powdered dry ice. The NMR probe was precooled to -20°C while the NMR tube was still submerged in dry ice. The NMR tube was removed from the dry ice, quickly inserted into the precooled spectrometer, and NMR spectrum #17 was taken at -20°C . The NMR tube was then allowed to sit at 24°C outside the spectrometer for 30 minutes, during which time the solution turned from light yellow-green to a light orange color. After the 30 min spent outside the spectrometer, the NMR tube was resubmerged in dry ice until NMR spectrum #18 was taken with the probe regulated at 24°C , showing trace amounts of intermediate **31** left. The NMR tube was left to sit outside the spectrometer at 24°C for 2 h during which time the solution began to turn from light orange to dark red-purple. NMR spectrum #19 was taken at 24°C at this time revealing complete consumption of intermediate **31**. The NMR tube was cycled into a nitrogen glove box and the solution

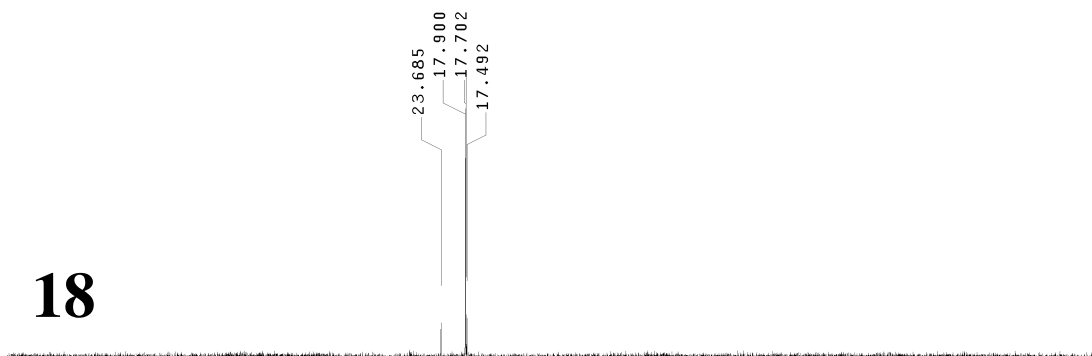
was concentrated in vacuo to a dark purple semisolid. The semisolid was rinsed with hexanes, and this wash was saved. Attempts to separate the semisolid into its constituent compounds were unsuccessful. The hexane wash was removed from the box and concentrated in vacuo to a dark brown semisolid. Chromatography was performed with 5% ether in petroleum ether to afford (*S*)-2-allyl-2-methylcyclohexanone **9** (2.0 mg, 40% yield, 85.1% *ee* [assay: GC, G-TA column {100 °C isothermal for 30 min}, major enantiomer (*S*) ret. time = 14.897 min, minor enantiomer (*R*) ret. time = 17.313 min], clear colorless oil).



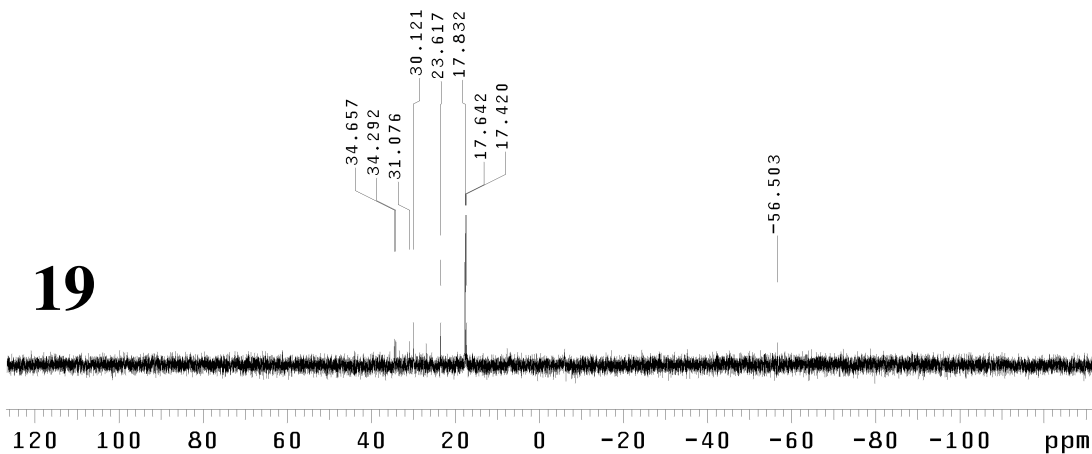
17



18



19



2.6.6.2 Controlled Thermal Decomposition of Intermediate **31** in the Presence of dba Ligand in Solution (THF) (Isolation of Complex **30** Only)

Until the sample left the glove box, all of the following operations were performed in a cold aluminum block with implements and containers, such as the half-dram vial and NMR tube, that had been precooled to -36°C in a glove box freezer. Intermediate **31** (11.3 mg, 16.4 μmol , 1 equiv) was weighed into a half-dram vial. Dibenzylideneacetone (9.6 mg, 46 μmol , 2.8 equiv) was added to the half-dram vial. A 1 mL ampule of THF_{d_8} that had been precooled to -36°C in a glove box freezer was opened and the contents were added to the half-dram vial. The resulting solution was mixed manually by pipette for 1 min until all the solids had dissolved forming a yellow solution. The solution was transferred to an NMR tube via pipette. The NMR tube was sealed with an appropriately sized septum, quickly removed from the glove box, and submerged in dry ice to within two inches of its cap. An initial NMR was taken at -20°C revealing intermediate **31** as the only detectable phosphorous-containing compound.³ The tube was left to sit at 24°C for 40 min, after which time a ^{31}P NMR spectrum indicated complete conversion to precatalyst complex **30** as the only detectable phosphorous-containing compound. The NMR tube was cycled back into a nitrogen glove box, where its contents were moved to a 1 dram vial and concentrated in vacuo to roughly 50 μL of thick red-orange oil. The oil was triturated with hexanes (1 mL) and the resulting mixture was filtered in a pipette with glass filter paper. The solids were rinsed with hexanes (12 x 0.5 mL) and these washes were merged and saved. The solids were rinsed with additional hexanes (10 x 1 mL) and these washes were not saved. The saved hexane washes were left to stand for 20 min, during which time yellow-orange

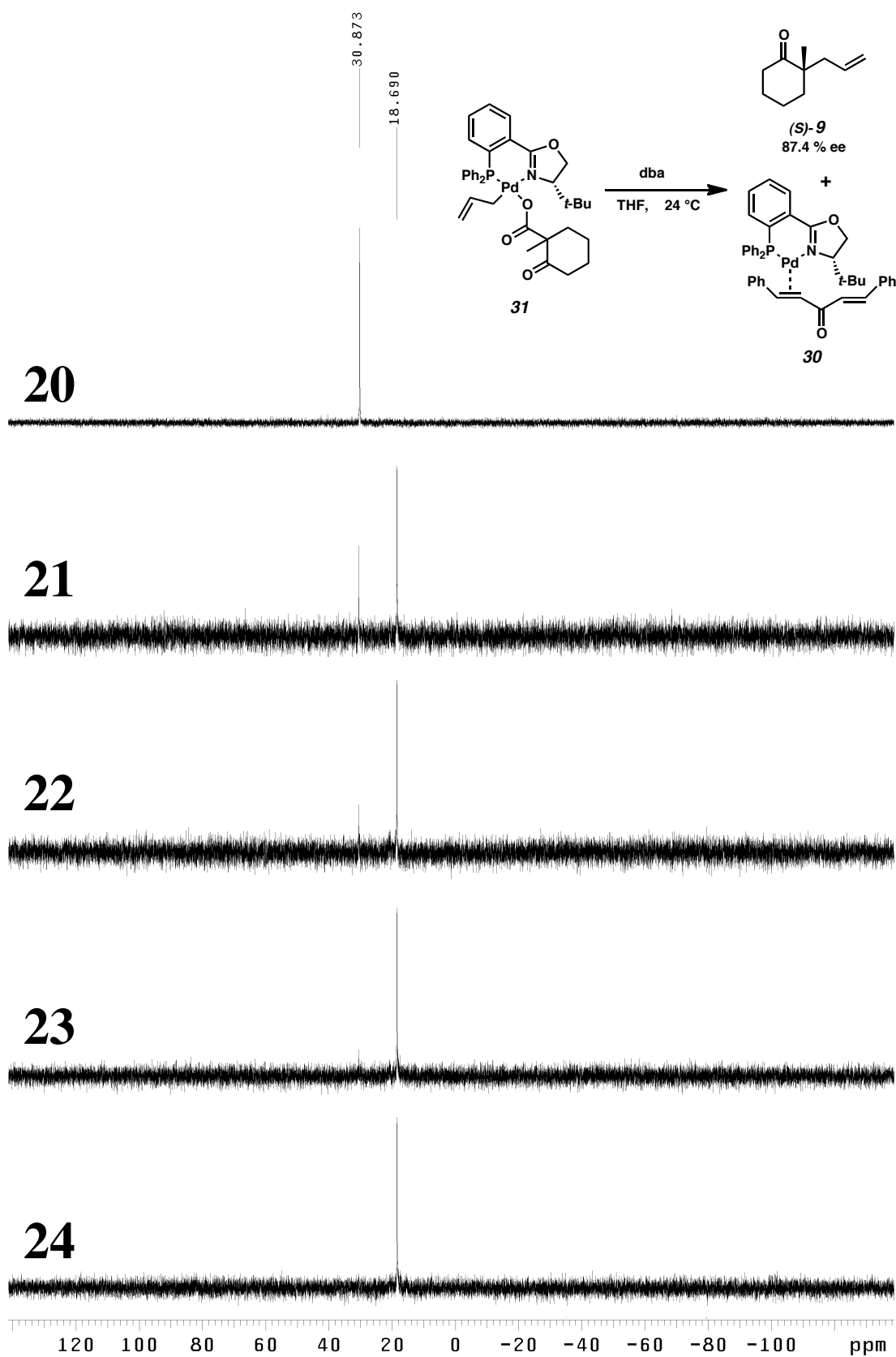
³ See the following procedure for representative spectra.

material began to crystallize and precipitate. These precipitated solids were then filtered in a pipette with glass filter paper. All of the samples of the precipitated red-orange material were dissolved in minimal THF, merged, and filtered through a pipette with glass filter paper into a 20 mL scintillation vial. The solution was concentrated in vacuo to a thin red film. This film was washed with diethyl ether (1 mL) and hexanes (2 x 1 mL). The remaining solids were azeotroped once from diethyl ether and twice from hexanes to afford precatalyst complex **5** (7.1 mg, 62% yield, yellow powder).

2.6.6.3 Controlled Thermal Decomposition of Intermediate **31** in the Presence of dba Ligand in Solution (THF) (Isolation of 2-allyl-2-methylcyclohexanone **9** Only)

Until the sample left the glove box, all of the following operations were performed in cold aluminum block with implements and containers, such as a half-dram vial and NMR tube, that had been precooled to -36°C in a glove box freezer before use. Dibenzylideneacetone (3.3 mg, $16\ \mu\text{mol}$, 1.5 equiv) was weighed into a 1 dram vial. Intermediate **31** (7.3 mg, $11\ \mu\text{mol}$, 1 equiv) was weighed into a separate half-dram vial. Anhydrous THF that had been precooled to $-36\ ^{\circ}\text{C}$ in the glove box freezer was added into the 1 dram vial containing the dibenzylideneacetone. The solution was mixed manually via pipette for roughly 10 s until all the material had dissolved resulting in the formation of a yellow solution. The solution was transferred via pipette to the half-dram vial containing intermediate **31**, where it was mixed manually via pipette for 10 s until all the material had dissolved, resulting in the formation of a yellow-green solution. The NMR tube was sealed with a septum, quickly removed from the glove box, and submerged in dry ice to within two inches of its top. NMR spectrum # 20 was taken at this time with the probe precooled to $-20\ ^{\circ}\text{C}$. The NMR tube was then left to stand at 24

°C. After 17 min at 24 °C NMR spectrum #21 was taken. After 22 min, NMR spectrum #22 was taken. After 30.5 min, NMR spectrum #23 was taken. After 40 min, NMR spectrum #24 was taken indicating complete conversion to precatalyst **30** as the only detectable phosphorous-containing compound. Tridecane (4.0 μL , 3.0 mg, 16 μmol , 1.5 equiv) was added via a 10 μL Hamilton syringe. The solution was concentrated under a jet of nitrogen to roughly 100 μL of viscous orange oil. The oil was triturated with 0.5 mL of diethyl ether and the resulting mixture was filtered through a pipette filter with a 3 cm plug of dry silica gel. The materials were eluted with diethyl ether separating a faintly pink solution from red/orange insoluble solids. The filtrate afforded 2-allyl-2-methyl-cyclohexanone (**9**) (99% GC yield [DB-WAX column {60 °C initial temp for 10 min, then ramp 5 °C/min for 36 min to 240 °C, hold at 240 °C for 12 min}, ret. time of tridecane = 13.243 min, ret. time 2-allyl-2-methylcyclohexanone = 18.399 min], 87.4% *ee* [assay: GC, G-TA column {100 °C isothermal for 30 min}, major enantiomer (*S*) ret. time = 14.897 min, minor enantiomer (*R*) ret. time = 17.313 min]).



2.6.7 Rate Constant and Half-Life of Complex **31** at 24 °C in THF

Data were extracted from spectra 21 to 23 of the above reaction. Data point one at 18 min (spectrum #21) was set to time = 0 min for the sake of the regression plot. Data from NMR spectrum #20 were omitted as the spectrum was taken at a different temperature.

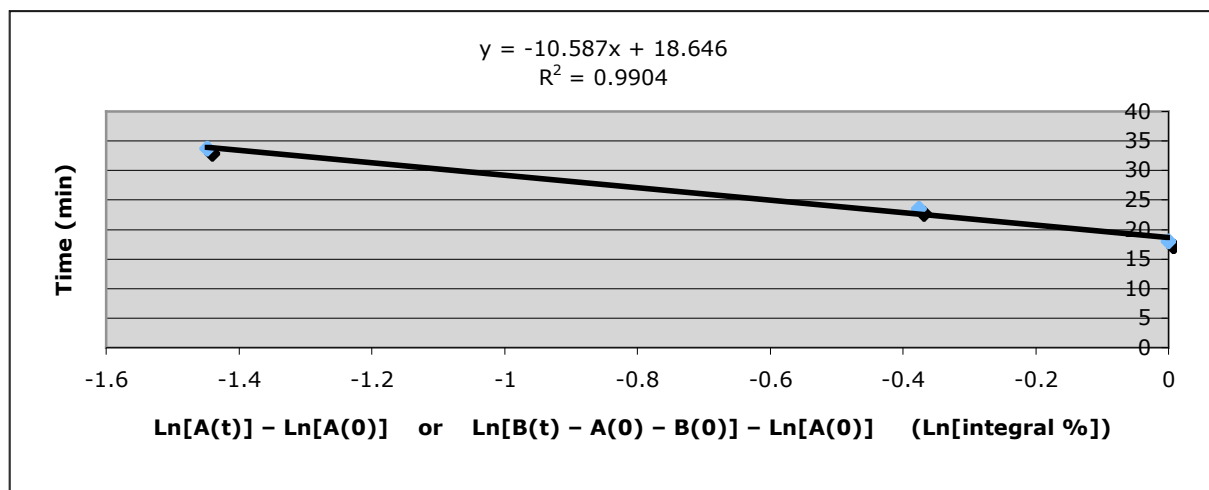
Raw Data:

Data Point	Intermediate 31 (integral)	Complex 30 (integral)	Time (min)	Complex 30 Adjusted* (integral)
1 (spectrum 21)	0.37	1	17-19 (18)	1.1111
2 (spectrum 22)	0.23	1	22-25 (23.5)	1.1111
3 (spectrum 23)	0.07	1.01	30.5-37 (33.75)	1.1222

[*] The adjusted value of the major resonance for complex **30** is used instead of attempting to integrate both the major and minor resonances for complex **30**, as the minor resonance's contribution is so small that its integration is highly affected by baseline noise giving a poor plot fit. The adjusted integral value for complex **30** is determined by taking the integral value of the major ³¹P resonance for complex **30** and dividing it by its relative fraction to the total integral, 0.9. See the ³¹P NMR characterization data for complex **30** in this experimental section or its ³¹P NMR spectrum reproduced in Appendix 1 for more data on the multiple ³¹P resonances for complex **30**.

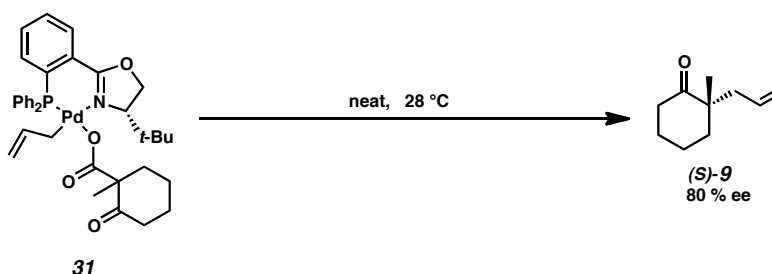
Derived Data:

Data Point	Intermediate 31 (% ³¹ P) = A(t)	Complex 30 (% ³¹ P) = B(t)	Ln[A(t)] – Ln[A(0)]	Ln[B(t) – A(0) – B(0)] – Ln[A(0)]
1	0.249812	0.75019	0	0
2	0.171499	0.82850	-0.37612	-0.37612
3	0.058714	0.94129	-1.44803	-1.44803

Linear Regression Plot:

=> Rate constant, $k = 1/x = -9.45 \times 10^{-2} \text{ min}^{-1}$ or $-1.58 \times 10^{-4} \text{ s}^{-1}$ at $24 \text{ }^\circ\text{C}$

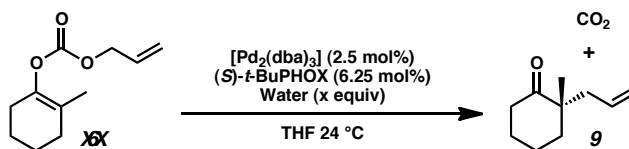
=> Half-life = $[\ln(0.5) / k] = 7.34 \text{ min}$ at $24 \text{ }^\circ\text{C}$

**2.6.7.1 Controlled Thermal Decomposition of Intermediate 31 in the Solid State**

In a nitrogen glove box, intermediate **31** (15 mg, 22 μmol , 1 equiv) was added to a 20 mL scintillation vial. The vial was tightly sealed, and then left to stand at ambient glove box temperature ($28 \text{ }^\circ\text{C}$). After 36 h the decomposed material, now black in color, was moved to the bench where it was partially dissolved by pulverization under diethyl ether (5 x 1 mL) with manual grinding by a stainless steel spatula. The resulting heterogeneous mixture was filtered through a pipette filter with a 2 inch plug of silica gel that had been prewetted/packed with diethyl ether, separating a dark maroon filtrate from a black insoluble solid. The filtrate was concentrated under a jet of nitrogen to a dark maroon oil with some small darkly colored crystalline masses. Chromatography was

performed on a pipette column eluting with 5% diethyl ether in petroleum ether affording 2-allyl-2-methylcyclohexanone (**9**) (80% *ee* [assay: GC, G-TA column {100 °C isothermal for 30 minutes}], major enantiomer (*S*) ret. time = 14.897 min, minor enantiomer (*R*) ret. time = 17.313 min], clear colorless oil).

2.6.8 Water Tolerance Experiments



Water (equiv)	Yield ^[a]	ee ^[b]
0	99.9%	88.5%
0.55	99.6%	86.7%
1.6	88.1%	83.8%
8.3	70.3%	60.9%
17	66.8%	48.8%
33	67.9%	40.5%

Data reported is the average of three trials. [a] GC yield relative to internal standard (tridecane). [b] Enantiomeric excess measured by chiral GC.

Complete Table of Runs:

Water (L, equiv)	Time (h)	GC Conversion (%)	GC Yield (%)	ee (%)
0.0 μL = 0 equiv	1.5	100 %	100.5 %	88.5 %
“”	1.0	100 %	101.6 %	88.4 %
“”	1.0	100 %	97.2 %	88.7 %
<i>Averaged =</i>	<i>1.2</i>	<i>100 %</i>	<i>99.9 %</i>	<i>88.5 %</i>
1.0 μL = 0.55 equiv	1.5	100 %	100.6 %	86.6 %
“”	0.5	100 %	103.0 %	87.0 %
“”	0.5	100 %	95.4 %	86.6 %
<i>Averaged =</i>	<i>0.8</i>	<i>100 %</i>	<i>99.6 %</i>	<i>86.7 %</i>
3.0 μL = 1.6 equiv	0.75	100 %	88.5 %	83.6 %
“”	0.5	100 %	87.4 %	83.9 %
“”	0.5	100 %	88.3 %	84.0 %
<i>Averaged =</i>	<i>0.6</i>	<i>100 %</i>	<i>88.1 %</i>	<i>83.8 %</i>

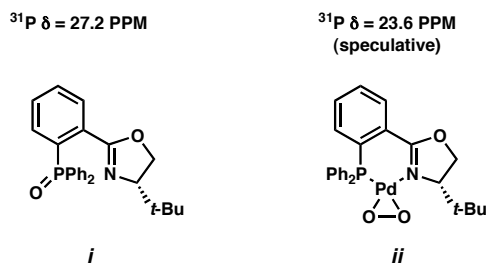
15 μL = 8.3 equiv	0.75	100 %	75.3 %	60.3 %
“”	0.5	100 %	70.8 %	62.4 %
“”	0.5	100 %	70.3 %	59.9 %
<i>Averaged</i> =	<i>0.6</i>	<i>100 %</i>	<i>70.3 %</i>	<i>60.9%</i>
30 μL = 17 equiv	0.75	100 %	67.8 %	50.4 %
“”	0.75	100 %	65.6 %	48.7 %
“”	0.75	100 %	66.9 %	47.4 %
<i>Averaged</i> =	<i>0.75</i>	<i>100 %</i>	<i>66.8 %</i>	<i>48.4 %</i>
60 μL = 33 equiv	1.5	100 %	64.3 %	40.4 %
“”	1.0	100 %	73.5 %	40.0 %
“”	6.0	78.2 %	(66.0 %)*	41.0 %
<i>Averaged</i> =	<i>2.8</i>	<i>92.7 %</i>	<i>67.9 %</i>	<i>40.5 %</i>

[*] Based on conversion. The uncorrected yield was 51.6%.

General Procedure: A 1 dram vial equipped with a magnetic stir bar was flame dried under vacuum. After cooling under dry argon, $[\text{Pd}_2(\text{dba})_3]$ (4.6 mg, 0.005 mmol, 0.05 equiv) and (*S*)-*t*-BuPHOX ligand (**31**) (0.0125 mmol, 0.125 equiv) were added. After the flask was flushed with argon, THF (3.0 mL) was added and the contents were stirred at 25 °C for 30 min. Tridecane (12.25 μL), water, and then carbonic acid allyl ester 2-methyl-cyclohex-1-enylmethyl ester (**6**) (19.6 mg, 0.1 mmol, 1.0 equiv) were added by syringe in the given order. When the reaction was complete by TLC, the reaction mixture was diluted with hexanes (5 mL), filtered through a small plug of silica gel and analyzed by GC. A GC yield was determined on DB-WAX column (70 °C initial temp, 5 °C/min ramp to 180 °C), tridecane ret. time = 7.000 min, ketone **9** ret. time = 12.309 min, carbonate **6** ret. Time = 17.771 min. Enantiopurity was determined by GC on a GT-A column (100°C isothermal for 30 min) major enantiomer (*S*) ret. time = 14.897 min, minor enantiomer (*R*) ret. time = 17.313 min.

- (1) (a) Keith, J. A. *Computational Insight into Homogeneous Organopalladium Catalysis*, Ph.D. Thesis, California Institute of Technology, Pasadena, CA, **2008**. (b) Behenna, D. C. *Progress Toward the Synthesis of (+)-Zoanthenol and The Development of an Asymmetric Tsuji Allylation Reaction*, Ph.D. Thesis, California Institute of Technology, Pasadena, CA, **2007**. (c) Keith, J. A.; Behenna, D. C.; Mohr, J. T.; Ma, S.; Marinescu, S. C.; Oxgaard, J.; Stoltz, B. M. Goddard, W. A., III. *J. Am. Chem. Soc.* **2007**, *129*, 11876–11877.
- (2) For a thorough discussion, see: Chapter 1.
- (3) (a) Mohr, J. T.; Behenna, D. C.; Harned, A. M.; Stoltz, B. M. *Angew. Chem., Int. Ed.* **2005**, *44*, 6924–6927. (b) Behenna, D. C.; Stoltz, B. M. *J. Am. Chem. Soc.* **2004**, *126*, 15044–15045.
- (4) TBAT (Tetrabutylammonium difluorotriphenylsilicate) is a dry fluoride source used to activate silyl enol ether **4** for allylic alkylation, as specified in the original allylic alkylation conditions, see reference 3b.
- (5) It is possible that the resonances at $\delta = 31.3$ and 29.4 ppm correspond to the same carbonate complex (such as **34** or **36**). The carboxylate species **31** and **32** and the π -allyl cation **25** are all extremely fluxional in solution (see Chapter 3), and are thus strongly effected by solution conditions. If this is also true of the carbonate complex initially observed at $\delta = 29.4$ ppm, then the sudden change in solution upon the addition of silyl enol ether **4** and its reaction with TBAT might be more than enough to shift the carboxylate complex 2 ppm to the resonance found at $\delta = 31.3$ ppm. Consistent with this hypothesis is that the resonance at $\delta = 31.3$ ppm lasts beyond the end of the reaction when there is excess diallyl carbonate, but this species reverts to the dba complex **30** at the end of the reaction when there is excess silyl enol ether. This is consistent with both resonances $\delta = 29.4$ and 31.3 ppm being some form of palladium carbonate complex, and is strongly suggestive that neither resonance corresponds to a palladium enolate complex like **27**.
- (6) The decarboxylative asymmetric allylic alkylation reaction is very sensitive to oxygen, and many NMR experiment runs show some oxidative decomposition by their completion in spite of precautions to exclude air. The resonance at $\delta \approx 27$ ppm (see reference 36) is the phosphine oxide of the PHOX ligand **i**, and a common oxidative decomposition product (see the experimental procedures section of this chapter for complete characterization of **i**). The resonance at $\delta \approx 23.6$ ppm is as of yet unidentified, but it seems to appear before the formation of PHOX oxide **i** when oxidation begins to occur and then slowly disappear over time. It is tentatively postulated that $\delta = 23.6$ ppm may correspond to μ -peroxy palladium species **ii**. This highly speculative assignment is based off of analogy to other palladium systems that react directly with O₂ to form oxidizing species,

see: Konnick, M. M.; Guzei, L. A.; Stahl, S. S. *J. Am. Chem. Soc.* **2004**, *126*, 10212–10213 and references therein.



- (7) (a) Bélanger, É.; Houzé C.; Guimond, N.; Cantin, K.; Paquin, J.-F. *Chem. Commun. (Cambridge, U. K.)* **2008**, 3251–3253. (b) Bélanger, É.; Cantin, K.; Messe, O.; Tremblay, M.; Paquin, J.-F. *J. Am. Chem. Soc.* **2007**, *129*, 1034–1035. (c) Nakamura, M.; Hajra, A.; Endo, K.; Nakamura, E. *Angew. Chem., Int. Ed.* **2005**, *44*, 7248–7251.
- (8) It should be noted that the use of this custom $[\text{Pd}_x(\text{dba})_y]$ derivative in this reaction was not arbitrarily decided upon. Most common $[\text{Pd}_x(\text{dba})_y]$ derivatives were tried in this reaction first, including: $[\text{Pd}_2(\text{dba})_3]$, “[Pd(dba)₂], $[\text{Pd}(\text{pmdba})_2]$, and $[\text{Pd}_2(\text{dmdba})_3]$. The problem with most other dba ligands is that they are comparably crystalline and have similar solubility to palladium complexes **31** and **32**. As complexes **31**, and **32** need to be purified by recrystallization, this results in prohibitive purification issues. The mtdba ligand, however was designed for use in organometallic synthesis by being completely non-crystalline (it does not crystallize but can be congealed into a waxy amorphous solid), and by having enhanced solubility in strongly apolar solvents like hexanes and pentanes, which do not appreciably dissolve most palladium(II) complexes such as **31**, and **32**. Not only do these properties make mtdba easy to separate from complexes **31**, and **32**, but palladium(0) byproducts and unreacted palladium(0) species, such as $[\{(S)\text{-}t\text{-BuPHOX}\}\text{Pd}(\text{mtdba})]$, have a tendency to bind with mtdba, which enhances the solubility of these species in organic solvents and makes them easier to separate from the intended palladium(II) products as well.
- (9) For a thorough analysis of the solution structures and behavior of complexes **25**, **31**, and **32**, see: chapter 3.
- (10) Chelating ligands with a carboxylate functionality bound to a metal *cis* to an η -1 allyl group behave very differently from non-chelating carboxylate ligands in the same arrangement. Notably, chelated carboxylate complexes tend to be relatively stable and inert compared to the corresponding monodentate species. Generally the chelated complexes exhibit practically none of the fluxion solution behavior found for complexes like **25**, **31**, and **32**, as discussed in Chapter 3. For a recent and highly relevant example of a chelating carboxylate ligand *cis* to an η -1 allyl,

- and a short discussion of its solution behavior and relative stability, see reference 11.
- (11) Wencel, J.; Laurent, I.; Toupet, L.; Crévisy, C.; Mauduit, M. *Organometallics*, **2010**, *29*, 1530–1533.
- (12) Transition metal complexes with a carboxylate ligand *trans* to a σ -bound allyl group typically are relatively simple to synthesize and are generally more stable due to the *trans* arrangement of these two ligands, which prevents various potential mechanisms of decarboxylation such as doubly vinylogous reductive elimination. This is also true for metal complexes that adopt geometries that do not put these two ligands roughly within 90° of one another, such as linear complexes. Such allyl acetate transition metal complexes are noticeably less rare. In contrast, reported examples of transition-metal complexes with a non-chelating carboxylate ligand *cis* to a σ -bound allyl group are limited to a single ruthenium complex and a single rhodium complex, neither of which have a crystal structure among their other characterization data; see: (b) Planas, J. G.; Marumo, T.; Ichikawa, Y.; Hirano, M.; Komiya, S. *J. Mol. Catal. A* **1999**, *147*, 137–154. (c) M. J. Payne, D. J. Cole-Hamilton, *J. Chem. Soc. Dalton Trans.* **1997**, 3167–3176.
- (13) See Chapter 3 for a through discussion.
- (14) For comprehensive discussions of highly related complexes, see: (a) Kollmar, M.; Goldfuss, B.; Reggelin, M.; Rominger, F.; Helmchen, G. *Chem.–Eur. J.* **2001**, *7*, 4913–4927. (b) Liu, S.; Müller, J. F. K.; Neuburger, M.; Schaffner, S.; Zehnder, M. *J. Organomet. Chem.* **1997**, *549*, 283–293.
- (15) The crystal structure of palladium carboxylate **31** exists as a superposition of the two diastereomers resulting from the use of racemic β -ketoester **31** (\approx 6:4 d.r. found in the crystal structure). The structure depicted in Scheme 2.4 corresponds to the (*R,S*) major diastereomer only.
- (16) (a) Chattopadhyay, K.; Jana, R.; Day, V. W.; Douglas, J. T.; Tunge, J. A. *Org. Lett.* **2010**, *12*, 3042–3045. (b) Trost, B. M.; Xu, J.; Schmidt, T. *J. Am. Chem. Soc.* **2009**, *131*, 18343–18357. (c) Recio, A. III.; Tunge, J. A. *Org. Lett.* **2009**, *24*, 5630–5633.
- (17) (a) Burger, E. C.; Barron, B. R.; Tunge, J. A. *Synlett* **2006**, 2824–2826. (b) Mohr, J. T.; Stoltz, B. M. *Chem. Asian J.* **2007**, *2*, 1476–1491, and references therein.
- (18) (a) Grennber, H.; Langer, V.; Bäckvall, J.-E. *J. Chem. Soc. Chem. Commun.* **1991**, 1190–1192. (b) Bäckvall, J.-E.; Hopkins, R. B.; Grennberg, H.; Mader, M. M.; Awasthi, A. K. *J. Am. Chem. Soc.* **1990**, *112*, 5160–5166.

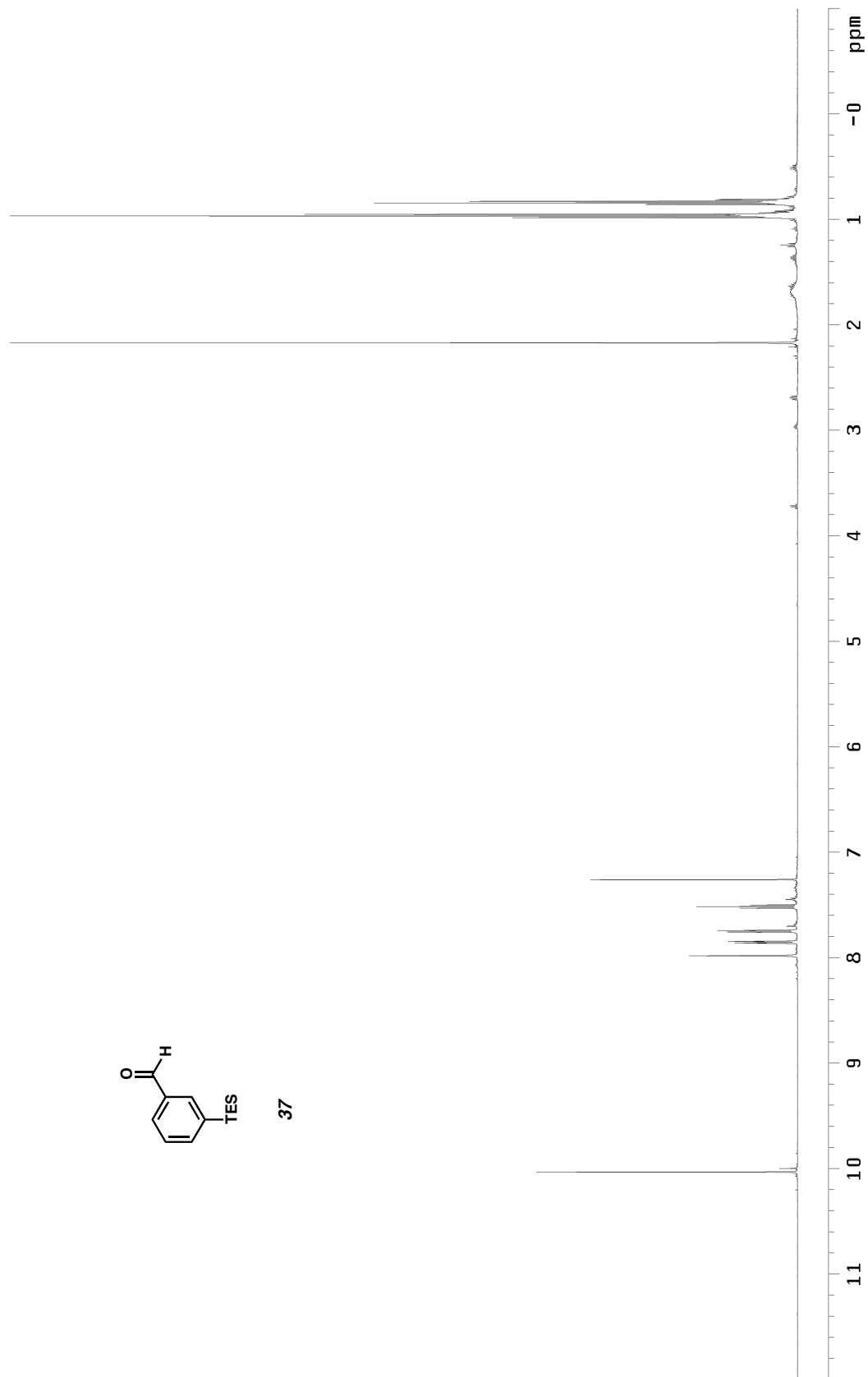
- (19) (a) Moiseev, I. I.; Vargaftik, M. N. *Coord. Chem. Rev.* **2004**, *248*, 2381–2391. (b) Hansson, S.; Heumann, A.; Rein, T.; Åkermark, B. *J. Org. Chem.* **1990**, *55*, 975–984. (c) Byström, S. E.; Larsson, E. M.; Åkermark, B. *J. Org. Chem.* **1990**, *55*, 5674–5675. (d) Åkermark, B.; Hansson, S.; Rein, T.; Vågberg, J.; Heumann, A.; Bäckvall, J.-E. *J. Organomet. Chem.* **1989**, *369*, 433–444.
- (20) Bäckvall, J.-E.; Byström, S. E.; Nordberg, R. E. *J. Org. Chem.* **1984**, *49*, 4619–4631.
- (21) The crystal structure of **32** contains 4 discrete rotamers of the complex per unit cell. Scheme 2.5 depicts only one of the rotamers found in the unit cell.
- (22) For some fully characterized examples of tetragonal pyramidal palladium(II) η^3 -allyl complexes with a halide associated as a fifth ligand, apically or otherwise, see: (a) Johns, A. M.; Utsunomiya, M.; Incarvito, C. D.; Hartwig, J. F. *J. Am. Chem. Soc.* **2006**, *128*, 1828–1839. (b) Hansson, S.; Norrby, P.-O.; Sjögren, M. P. T.; Åkermark, B.; Cucciolito, M. E.; Giordano, F.; Vitagliano, A. *Organometallics* **1993**, *12*, 4940–4948.
- (23) For studies of palladium-catalyzed allylic alkylation in which putative neutral palladium(0) η^2 -olefin complexes of allylic esters and carbonates as are reported as intermediates, see: (a) Evans, L.; A.; Fey, N.; Harvey, J. N.; Hose, D.; Lloyd-Jones, G. C.; Murray, P.; Orpen, A. G.; Osborne, R.; Owen-Smith, G. J. J.; Purdie, M. *J. Am. Chem. Soc.* **2008**, *130*, 14471–14473. (b) Fristrup, P.; Ahlquist, M.; Tanner, D.; Norrby, P.-O. *J. Phys. Chem. A* **2008**, *112*, 12862–12867. (c) Zalubovskis, R.; Bouet, A.; Fjellander, E.; Constant, S.; Linder, D.; Fischer, A.; Lacour, J.; Privalov, T.; Moberg, C. *J. Am. Chem. Soc.* **2008**, *130*, 1845–1855. (d) Amatore, C.; Jutand, A.; Mensah, L.; Ricard, L. *J. Organomet. Chem.* **2007**, *692*, 1457–1464. (e) Amatore, C.; Bahsoun, A. A.; Jutand, A.; Mensah, L.; Meyer, G.; Ricard, L. *Organometallics* **2005**, *24*, 1569–1577. (f) Tang, D.; Luo, X.; Shen, W.; Li, M. *J. Mol. Struct.* **2005**, *716*, 79–87. (g) Amatore, C.; Gamez, S.; Jutand, A. *Chem.—Eur. J.* **2001**, *7*, 1273–1280. (h) Hagelin, H.; Svensson, M.; Åkermark, B.; Norrby, P.-O. *Organometallics*, **1999**, *18*, 4574–4583. (i) Suzuki, T.; Fujimoto, H. *Inorg. Chem. (Washington, DC, U. S.)* **1999**, *38*, 370–382.
- (24) For structures and other studies of η^3 -allyl Pd, Pt, and Ni complexes with non-coordinating carboxylate and bicarbonate counterions formed from the reaction of allylic esters and carbonates with $L_nM(0)$ complexes for use as models for group 10 metal catalyzed allylic alkylation, see: (a) Böttcher, L.; Scholz, A.; Walther, D.; Weisbach, N.; Görls, H. *Z. Anorg. Allg. Chem.* **2003**, *629*, 2103–2112. (b) Jacob, V.; Weakley, T. J. R.; Haley, M. M. *Organometallics* **2002**, *21*, 5394–5400. (c) Pawlas, J.; Nakao, Y.; Kawatsura, M.; Hartwig, J. F. *J. Am. Chem. Soc.* **2002**, *124*, 3669–3679. (d) Dervisi, A.; Edwards, P. G.; Newman, P. D.; Tooze, R. P.; Coles, S. J.; Hursthouse, M. B.; *J. Chem. Soc. Dalton Trans.*

-
- 1999**, 1113–1120. (e) Ozawa, F.; Son, T.-i.; Ebina, S.; Osakada, K.; Yamamoto, A. *Organometallics*, **1992**, *11*, 171–176.
- (25) Mohr, J. T.; Krout, M. R.; Stoltz, B. M. *Org. Synth.* **2009**, *86*, 194–211.
- (26) (a) Krout, M. R.; Mohr, J. T.; Stoltz, B. M.; *Org. Synth.* **2009**, *86*, 181–193; (b) Tani, K.; Behenna, D. C.; McFadden, R. M.; Stoltz, B. M.; *Org. Lett.* **2007**, *9*, 2529–2531; (c) Peer, M.; de Jong, J. C.; Kiefer, M.; Langer, T.; Rieck, H.; Schell, H.; Sennhenn, P.; Sprinz, J.; Steinhagen, H.; Wiese, B.; Helmchen, G. *Tetrahedron* **1996**, *52*, 7547–7583.
- (27) Fulmer, G. R.; Miller, A. J. M.; Sherden, N. H.; Gottlieb, H. E.; Nudelman, A.; Stoltz, B. M.; Bercaw, J. E.; Goldberg, K. I. *Organometallics* **2010**, *29*, 2176–2179.
- (28) The material becomes soft and relaxes noticeably above 68 °C but does not actually change states until the given range.
- (29) [Pd₂(mtdba)₃] is highly dynamic in solution giving the observed intricate NMR spectra with fractional resonance integrations. This dynamic nature has been reported for all published [Pd_x(dba)_y] derivatives as of this writing. For some select examples see: Fairlamb, I. J. S.; Kapdi, A. R.; Lee, A. F. *Org. Lett.* **2004**, *6*, 4435–4438.
- (30) The solution of the crude complex in hexanes is immiscible with methanol and no crystallization or precipitation occurs even on the interface between the two phases. By adding ethanol first, the methanol becomes miscible and the resulting ternary solvent system becomes ideal for crystallization at lower temperatures.
- (31) The second crop of crystals often formed with an amorphous white or off-white solid. This amorphous solid is weakly soluble in ethanol and is the reason for the recommended ethanol washes of the second crystal crop.
- (32) This resonance overlaps significantly with the triplet immediately down field of it. The reported integrations were estimated from the combined integration of these two resonances of 2.33H.
- (33) It should be noted that while palladium allyl acetate **32** does not appear prone to the thermal decarboxylation mechanism that causes palladium carboxylate **31** to decompose near and above room temperature, **32** is still thermally unstable in roughly the same temperature range. The rate of thermal decomposition for **32**, however is considerably slower than **31**. Unlike **31**, **32** can be worked with at room temperature for hours at a time without any noticeable decomposition, but **32** must still be stored cold (≈ –36 °C or lower) if it is to be kept for more than a day or so without beginning to decompose. Thermal decomposition for **32** was

-
- found to be slower in the solid state than in solution. Decomposition of **32** is visibly obvious as the complex undergoes a color change from a light yellow green to a darker orange and then brown as it decays. While the thermal decomposition pathway for **32** is unknown and unstudied, it is hypothesized to start with loss of allyl acetate from the complex via reductive elimination. The resulting 14 electron [$\{(S)\text{-}t\text{-BuPHOX}\}\text{Pd}(0)$] species then presumably has many options for farther chemical transformations by which it can undergo non-specific decomposition.
- (34) Complex **30** exists as a mixture of dba rotomers in solution. For a study of relevant palladium dba complexes, see: Herrmann, W. A.; Thiel, W. R.; Broßmer, C.; Öfele, K.; Priermeier, T.; Scherer, W. *J. Organomet. Chem.* **1993**, *461*, 51-61.
- (35) Liu, S.; Müller, J. F. K.; Beuburger, M.; Shaffner, S.; Zehnder, M. *J. Organomet. Chem.* **1997**, *549*, 283–293.
- (36) Experimentally this resonance appears to be highly sensitive to solution conditions and has been seen to drift significantly (often up to half a ppm) during the course of a reaction.

Appendix 1

Spectra of Compounds Relevant to Chapter 2

Figure A1.1. ¹H NMR spectrum of 3-(triethylsilyl)benzaldehyde (**37**) in CDCl₃

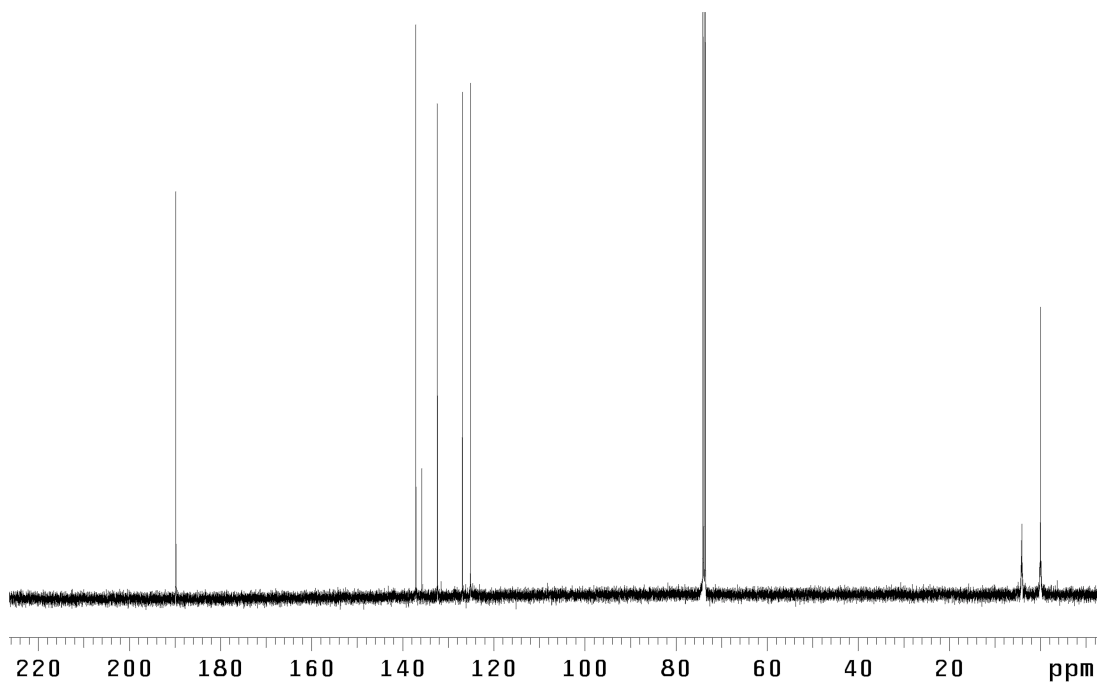


Figure A1.2. ^{13}C NMR spectrum of 3-(triethylsilyl)benzaldehyde (**37**) in CDCl_3

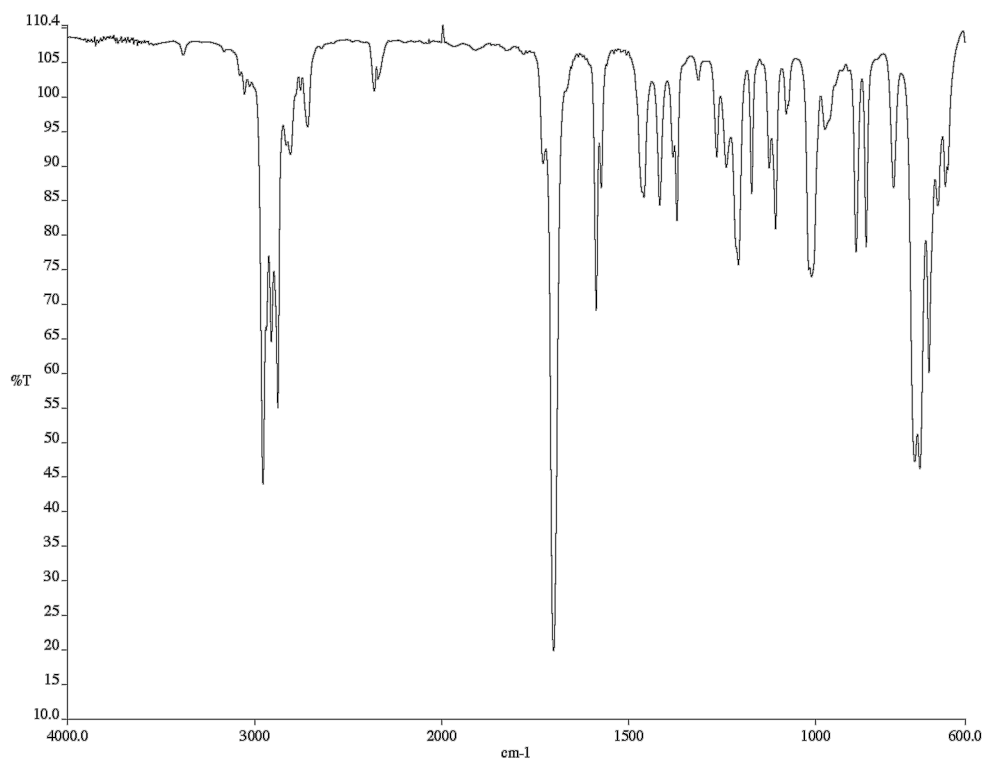
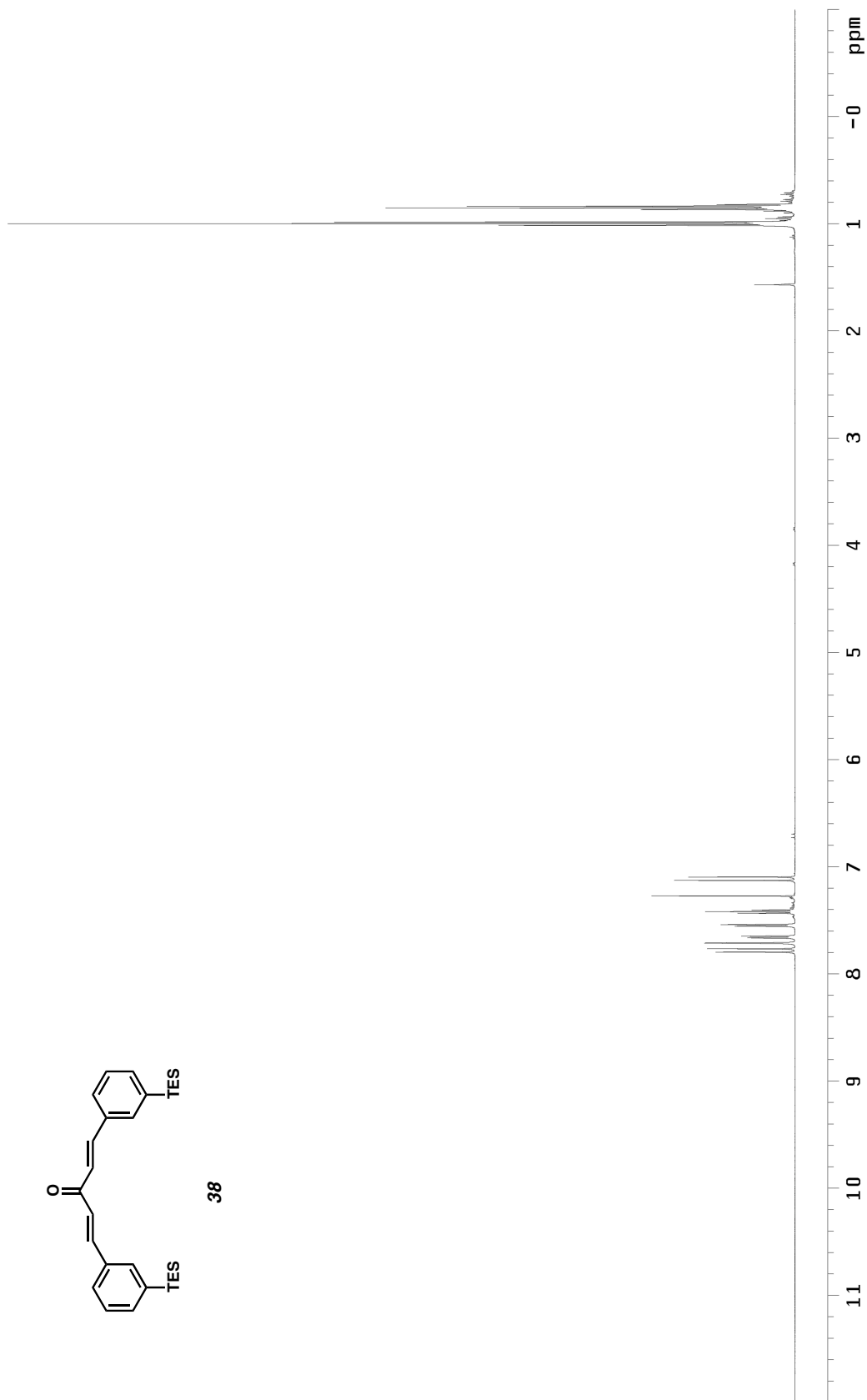


Figure A1.3. IR spectrum of 3-(triethylsilyl)benzaldehyde

Figure A1.4. ¹H NMR spectrum of 1,5-bis-[3-(triethylsilyl)phenyl]penta-1,4-dien-3-one, **38** in CDCl₃

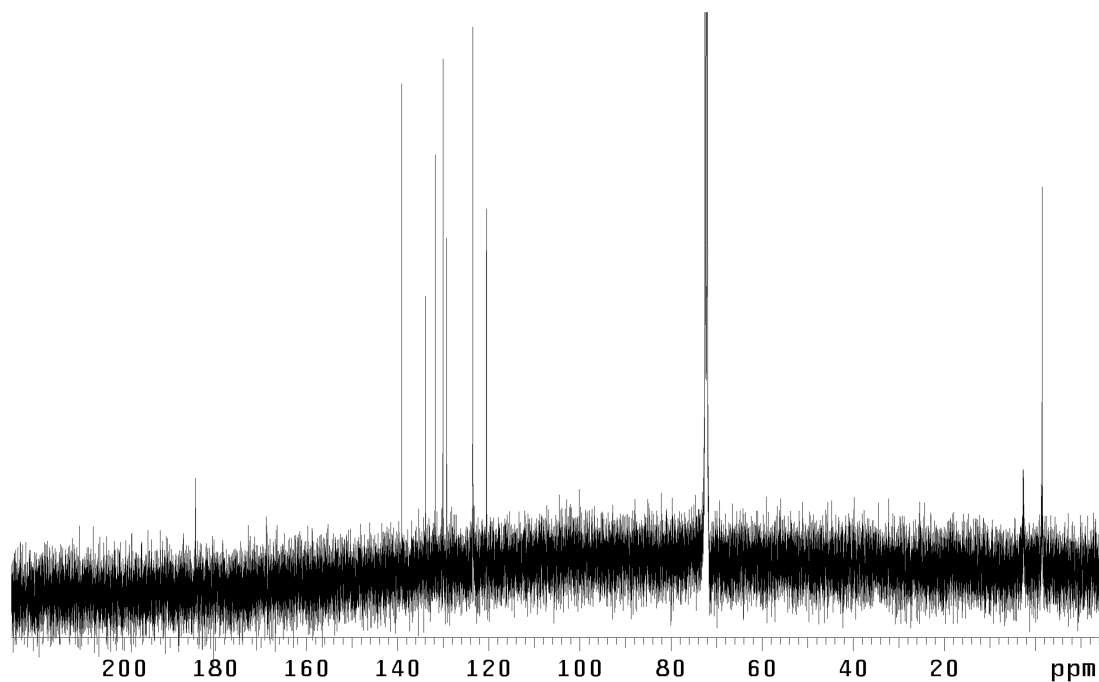


Figure A1.5. ^{13}C NMR spectrum of 1,5-bis-[3-(triethylsilyl)phenyl]penta-1,4-dien-3-one, mtdba (**38**) in CDCl_3

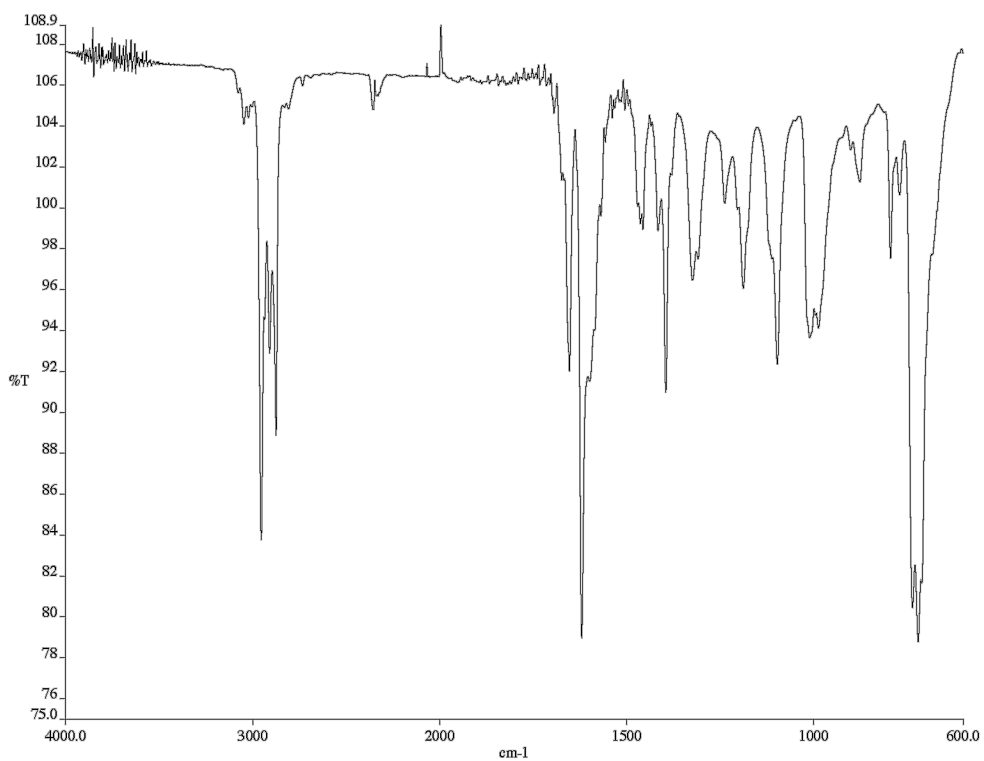
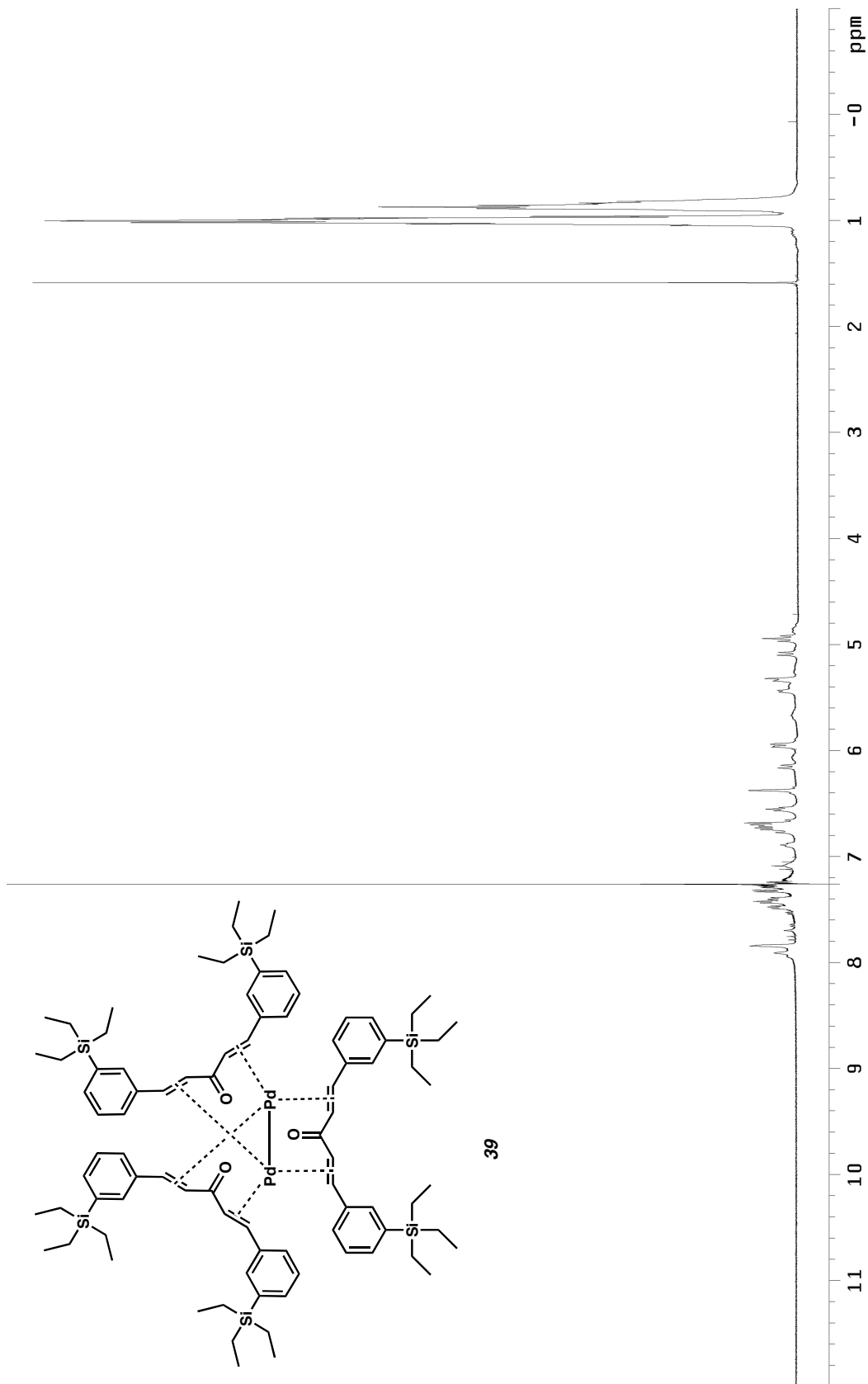


Figure A1.6. IR spectrum of 1,5-bis-[3-(triethylsilyl)phenyl]penta-1,4-dien-3-one, mtdba (**38**) in CDCl_3

Figure A1.7. 1H NMR spectrum of $[Pd_2(mtdba)_3]$ (39) in $CDCl_3$

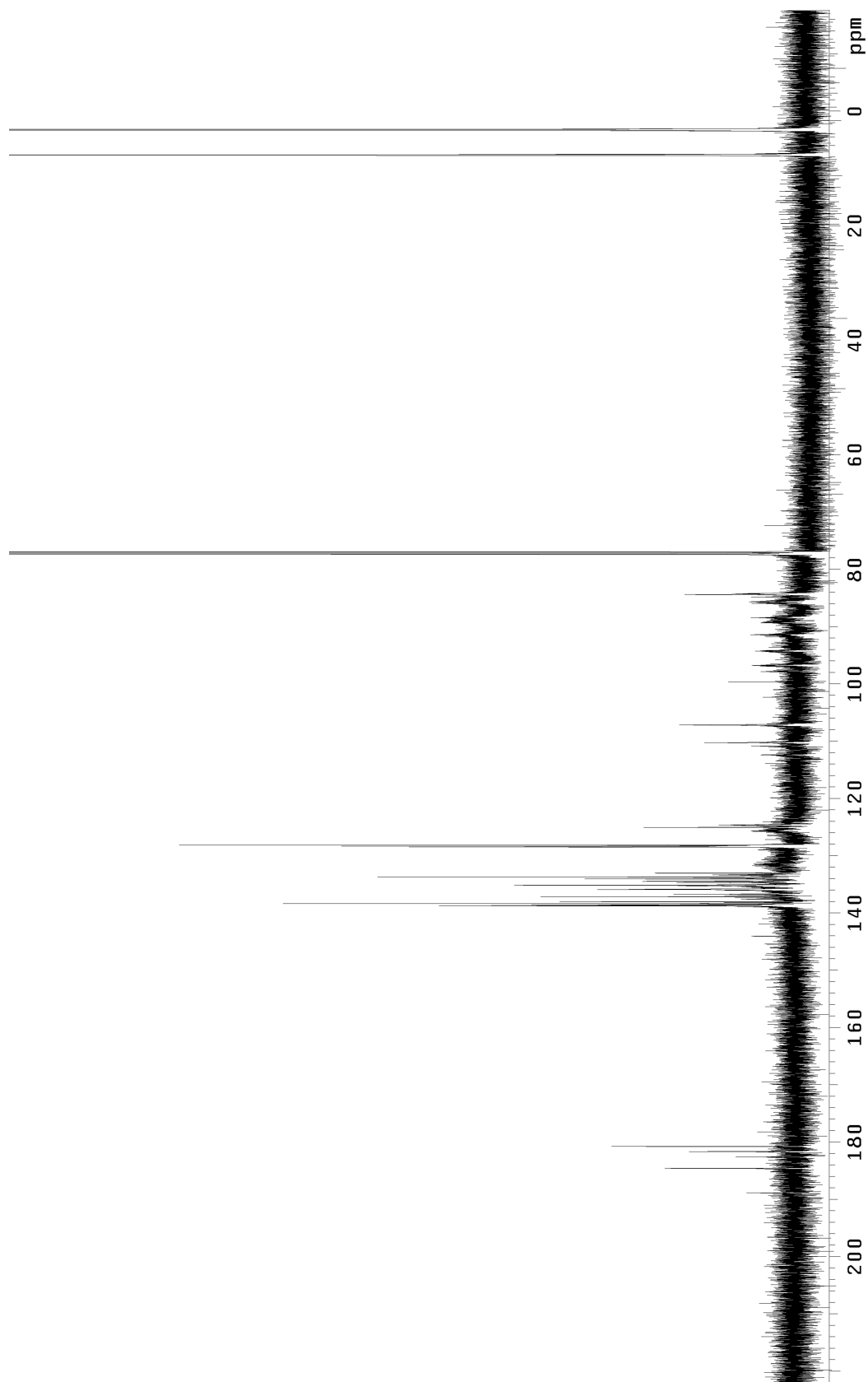
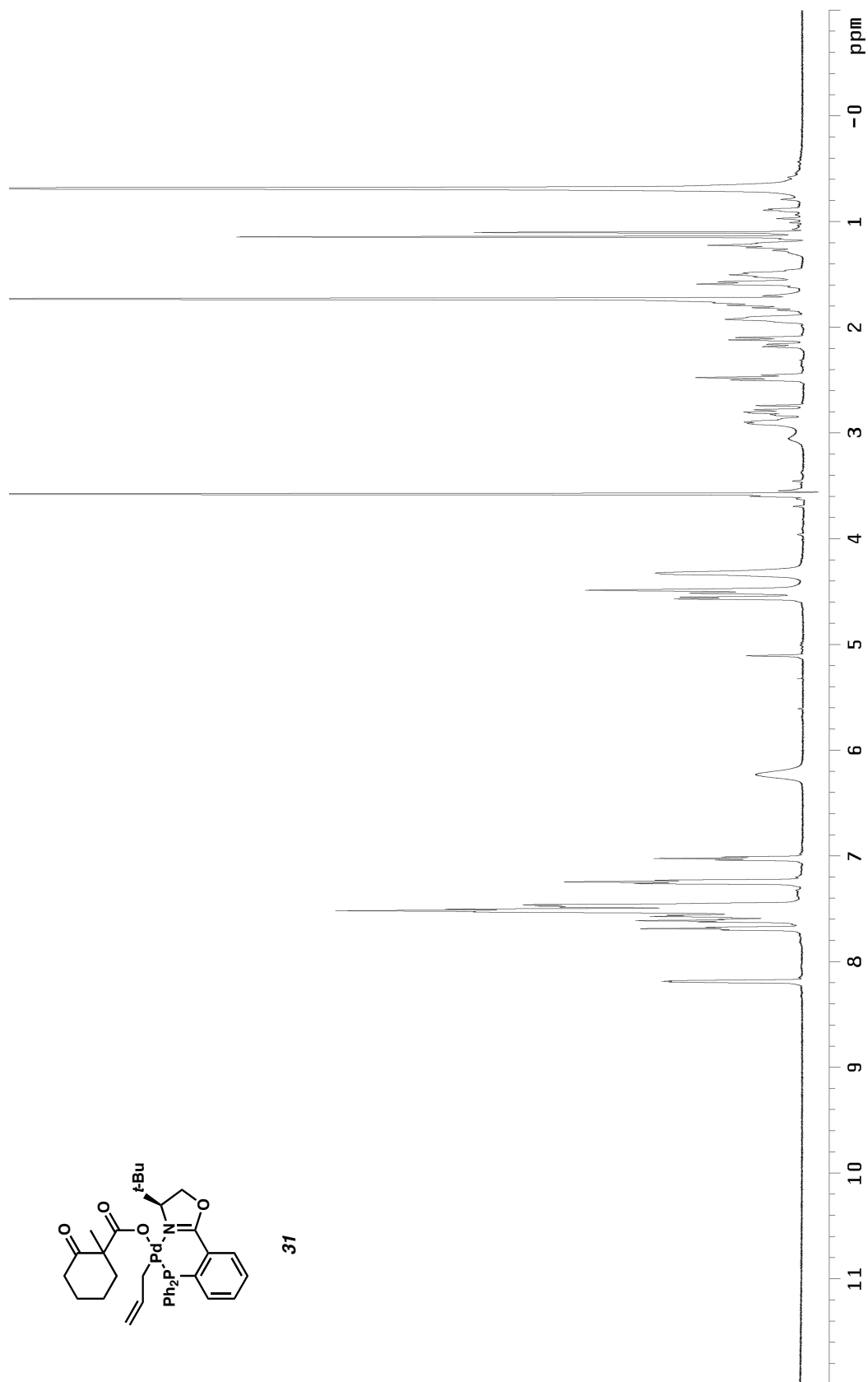


Figure A1.8. ^{13}C NMR spectrum of $[\text{Pd}_2(\text{mtdba})_3]$ (**39**) in CDCl_3

Figure A1.9. ^1H NMR spectrum of intermediate **31** in THF-d_8 at $-28\text{ }^\circ\text{C}$

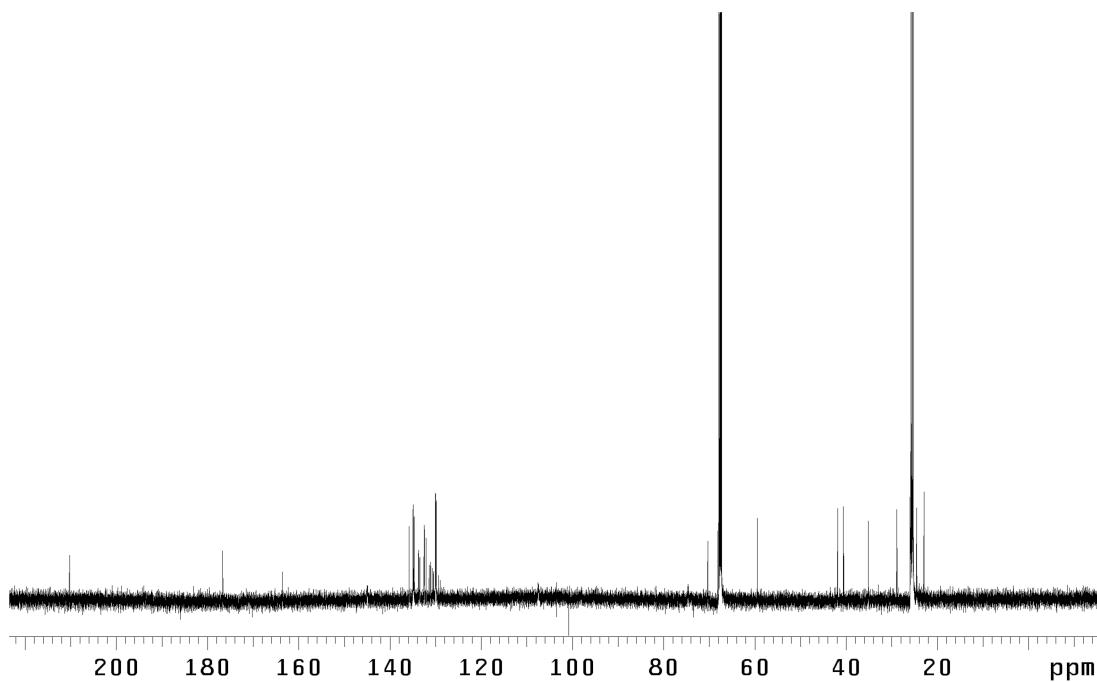


Figure A1.10. ^{13}C NMR spectrum of intermediate **31** in THF_{d-8} at $-28\text{ }^\circ\text{C}$

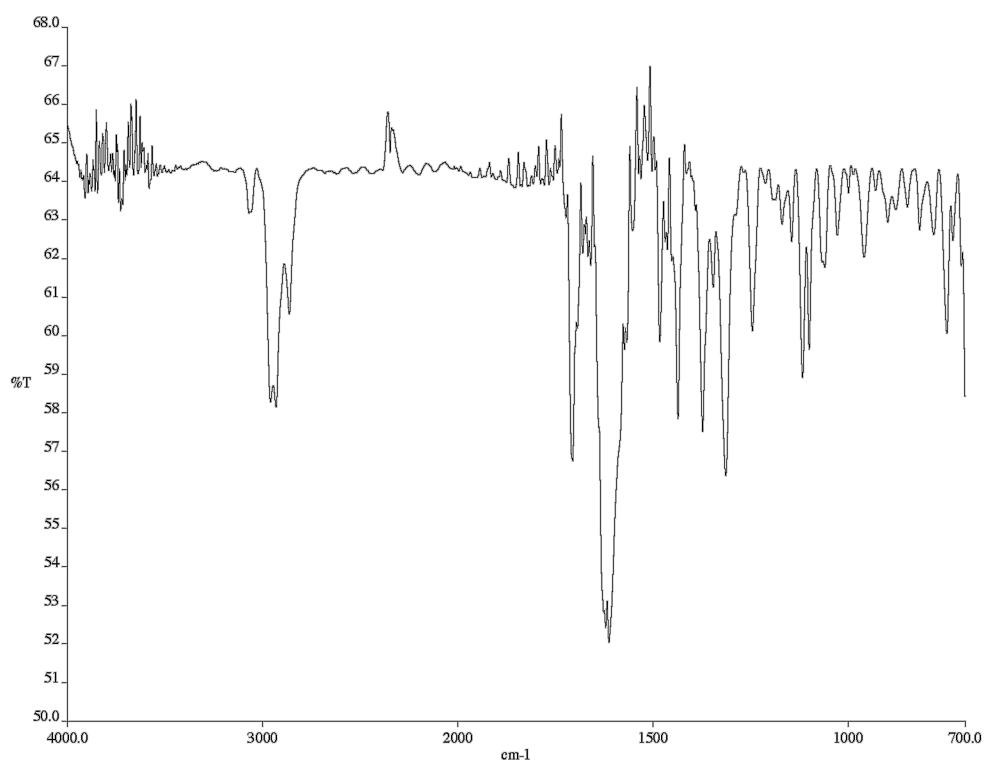
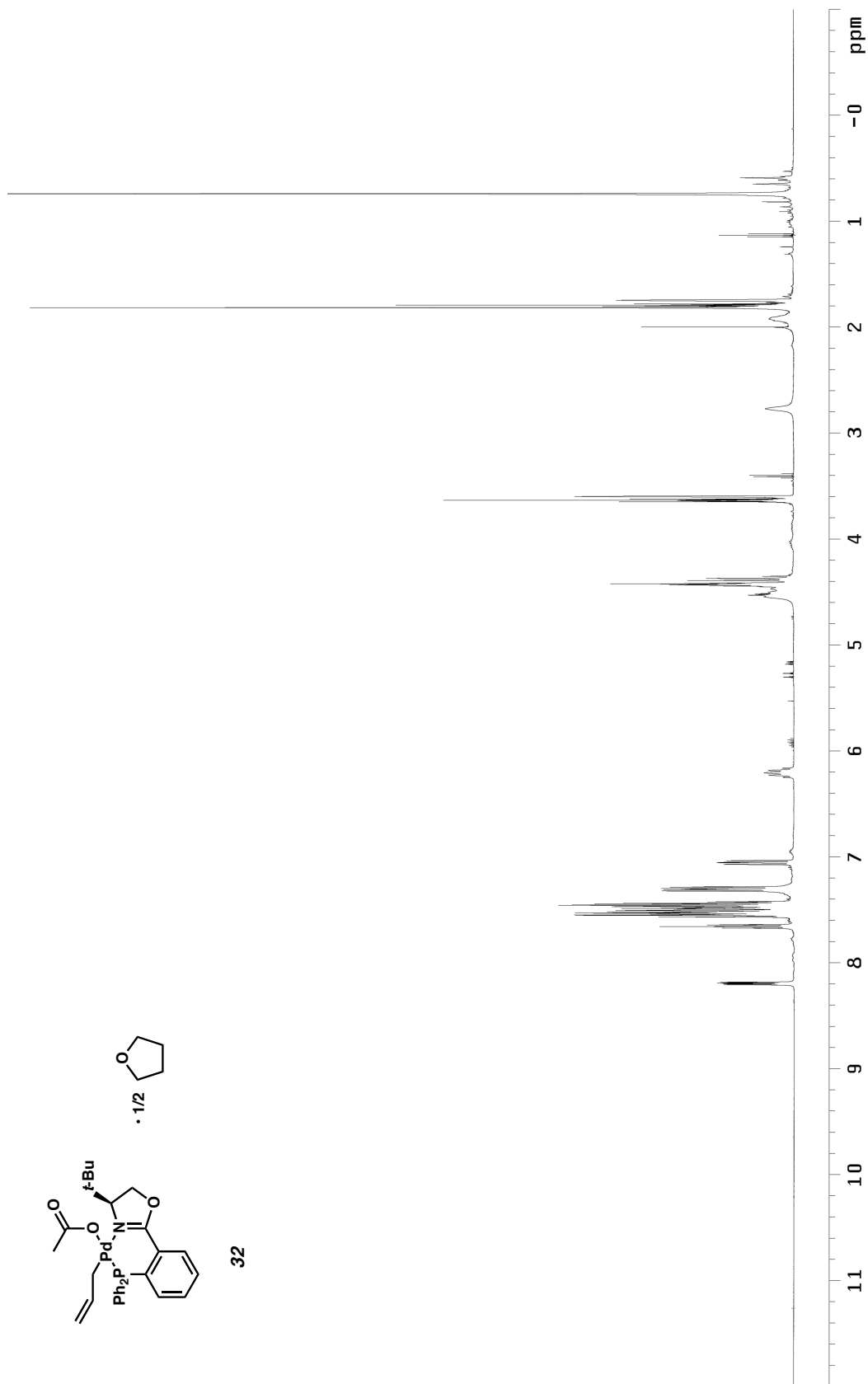


Figure A1.11. IR spectrum of intermediate **31**

Figure A1.12. ^1H NMR spectrum of [(S)-t-BuPHOX]Pd(allyl)(OAc)•1/2THF (**32**) in THF- d_8

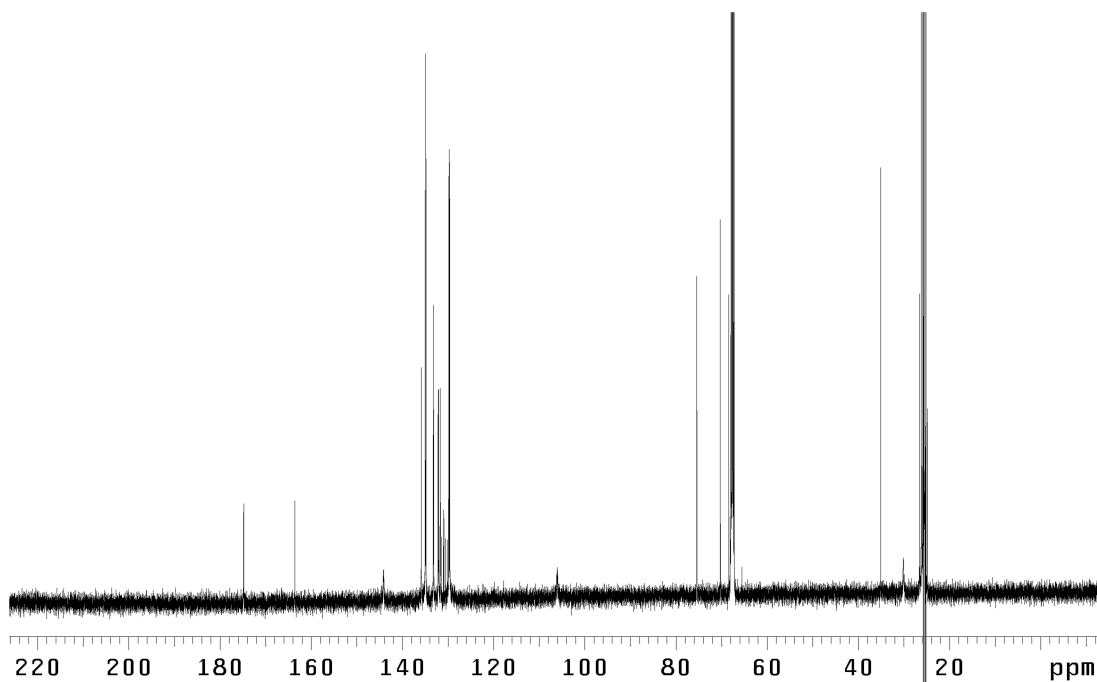


Figure A1.13. ^{13}C NMR spectrum of $[(\text{S})\text{-t-BuPHOX}]\text{Pd}(\text{allyl})(\text{OAc})\cdot 1/2\text{THF}$ (**32**) in THF_{d-8}

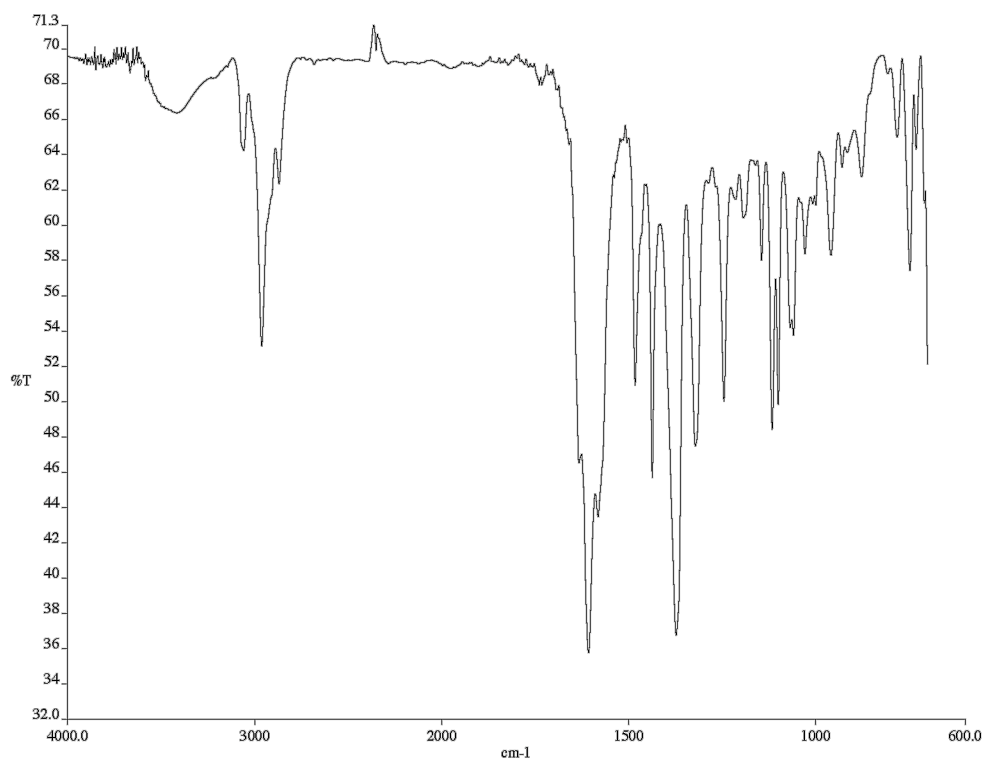


Figure A1.14. IR spectrum of $[(\text{S})\text{-t-BuPHOX}]\text{Pd}(\text{allyl})(\text{OAc})\cdot 1/2\text{THF}$ (**32**)

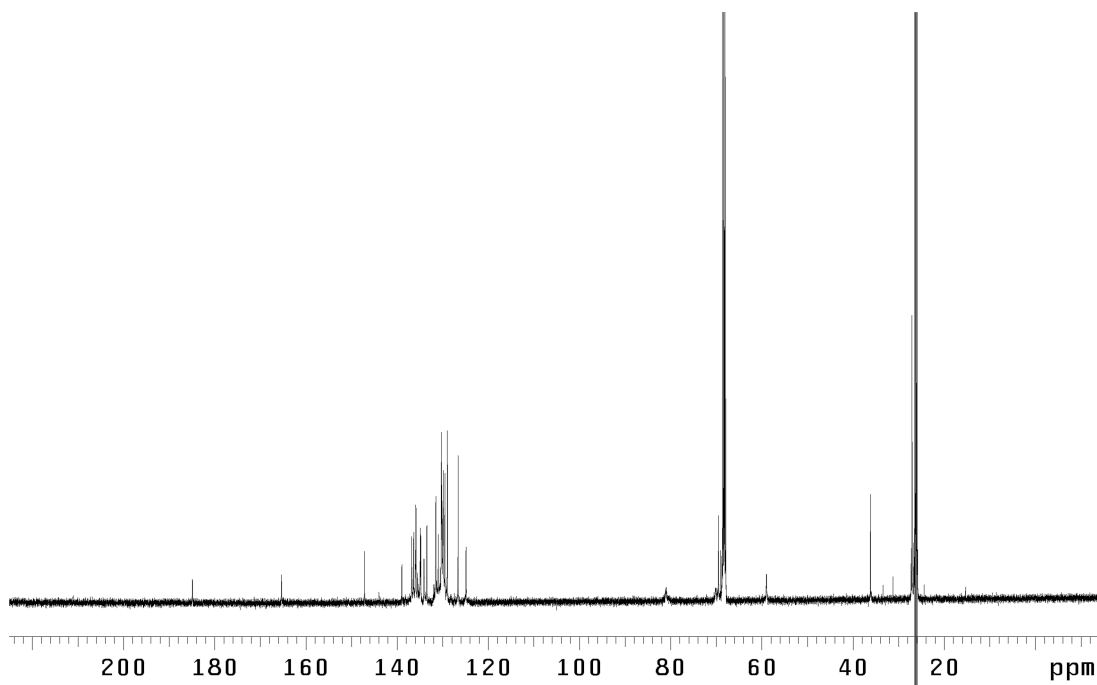


Figure A1.16. ^{13}C NMR spectrum of $[(S)\text{-}t\text{-BuPHOX}]\text{Pd}(\text{dba})$ (**30**) in THF_{d-8}

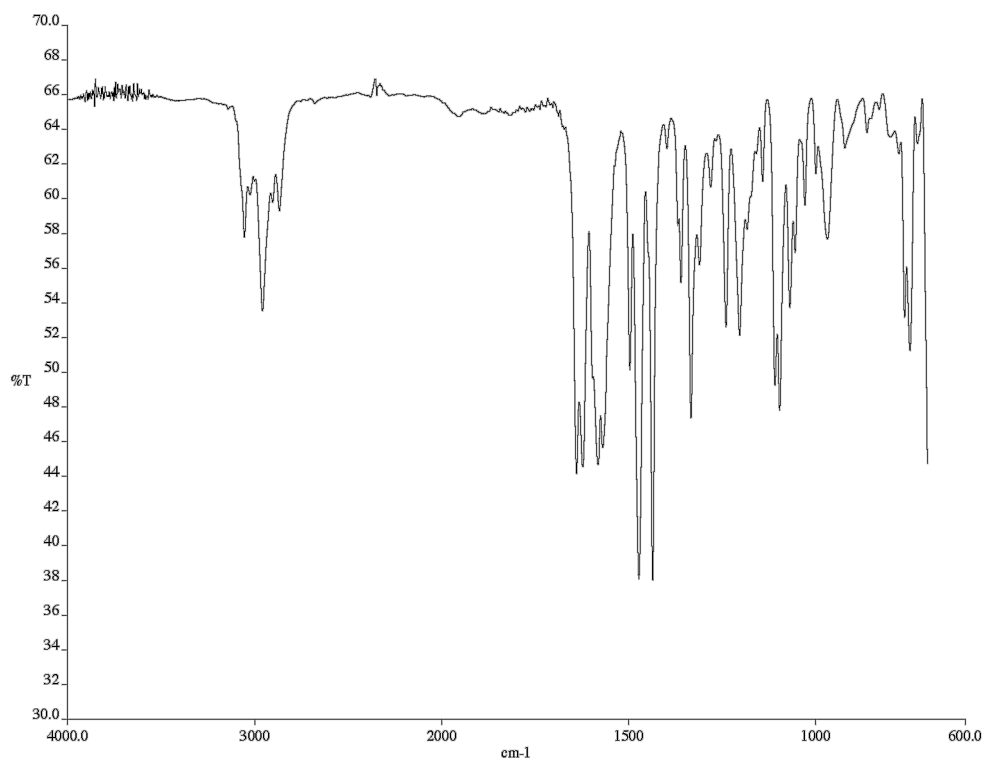


Figure A1.17. IR spectrum of $[(S)\text{-}t\text{-BuPHOX}]\text{Pd}(\text{dba})$ (**30**)

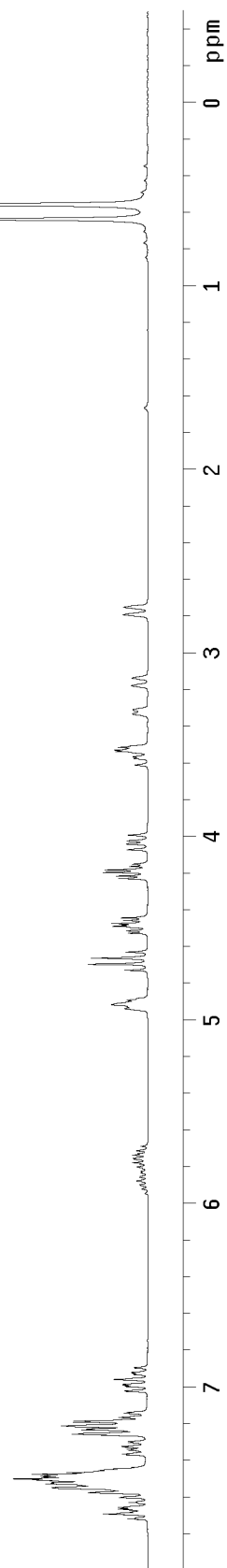
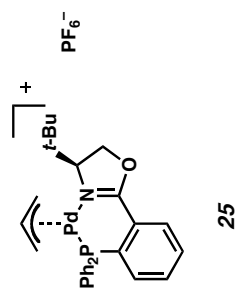


Figure A1.18. ^1H NMR spectrum of $[(S)\text{-}t\text{-BuPHOX}]\text{Pd}(\text{allyl})\text{PF}_6$ Salt (**25**) in CDCl_3

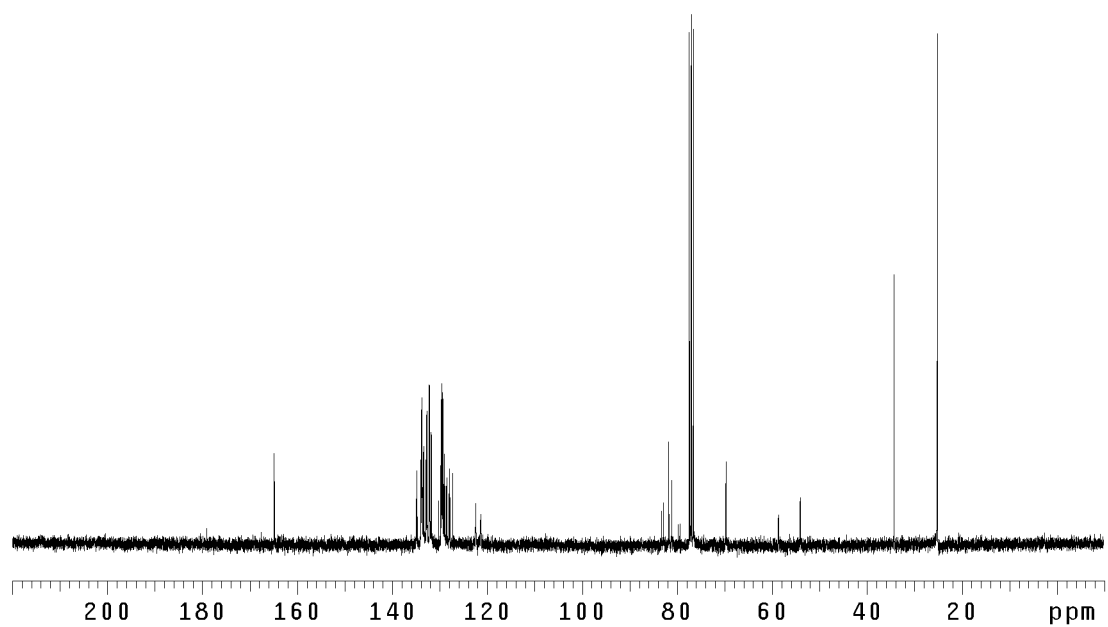


Figure A1.19. ^{13}C NMR of $[(\text{S})\text{-t-BuPHOX}]\text{Pd}(\text{allyl})\cdot\text{PF}_6$ Salt (**25**) in CDCl_3

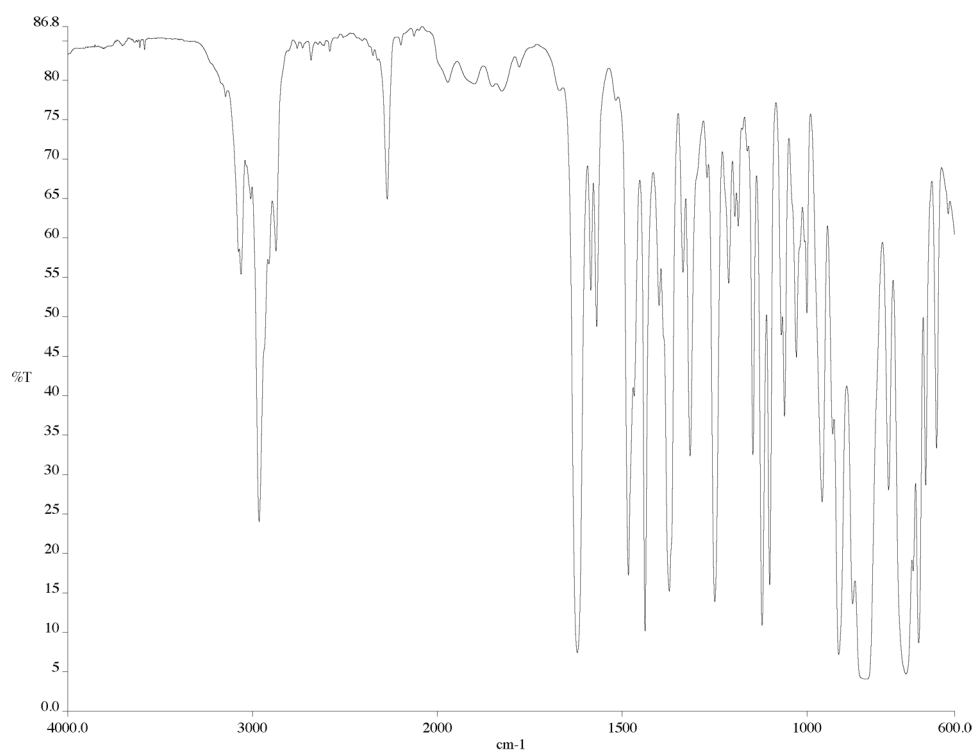
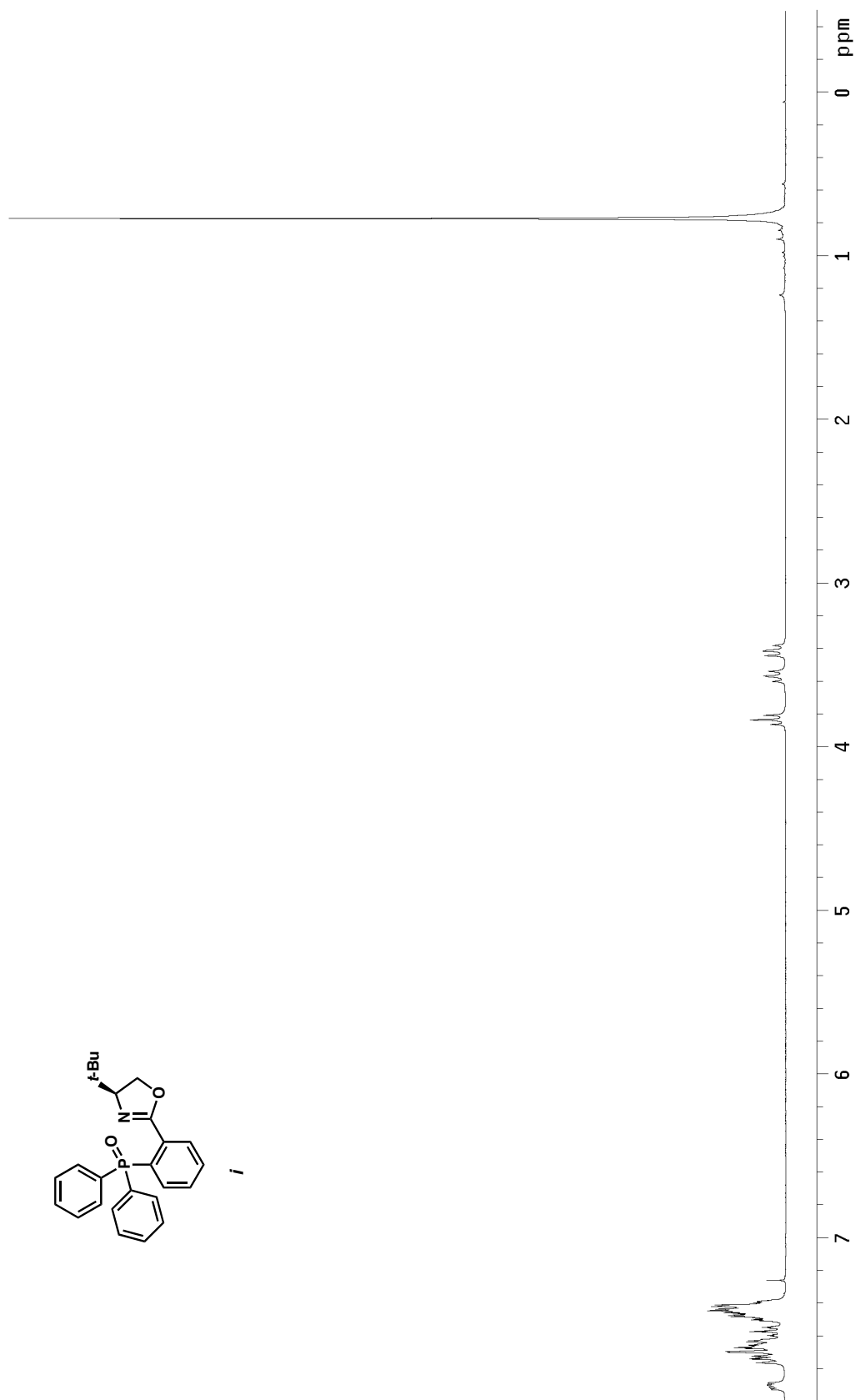


Figure A1.20. IR of $[(\text{S})\text{-t-BuPHOX}]\text{Pd}(\text{allyl})\cdot\text{PF}_6$ Salt (**25**)

Figure A1.21. ^1H NMR spectrum of (S)-t-BuPHOX oxide (I) in CDCl_3

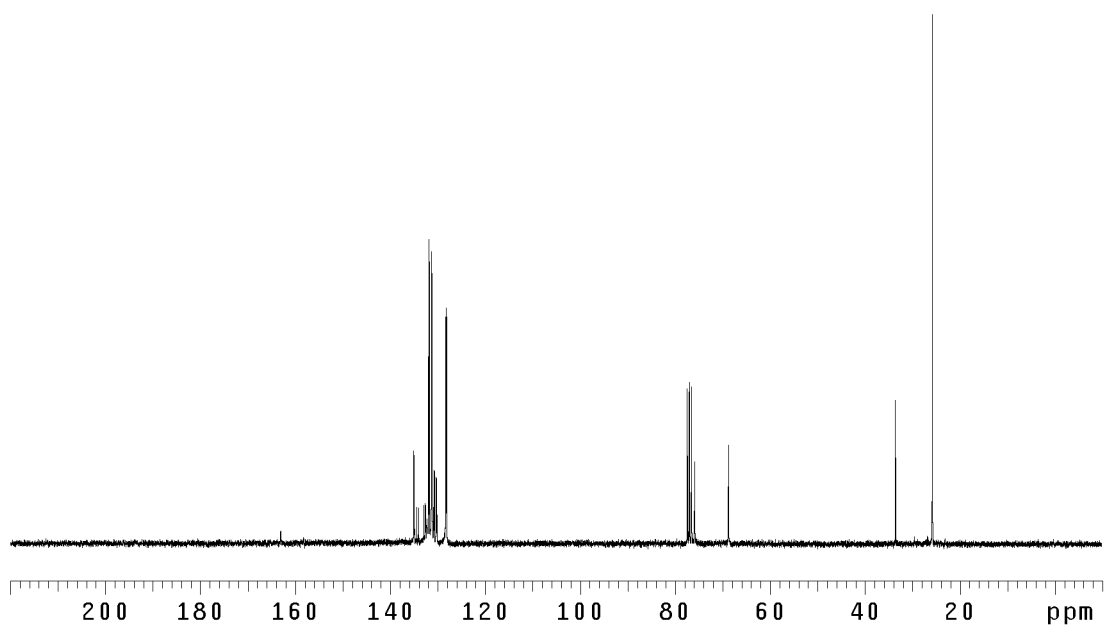


Figure A1.22. ^{13}C NMR spectrum of (S)-t-BuPHOX oxide (i) in CDCl_3

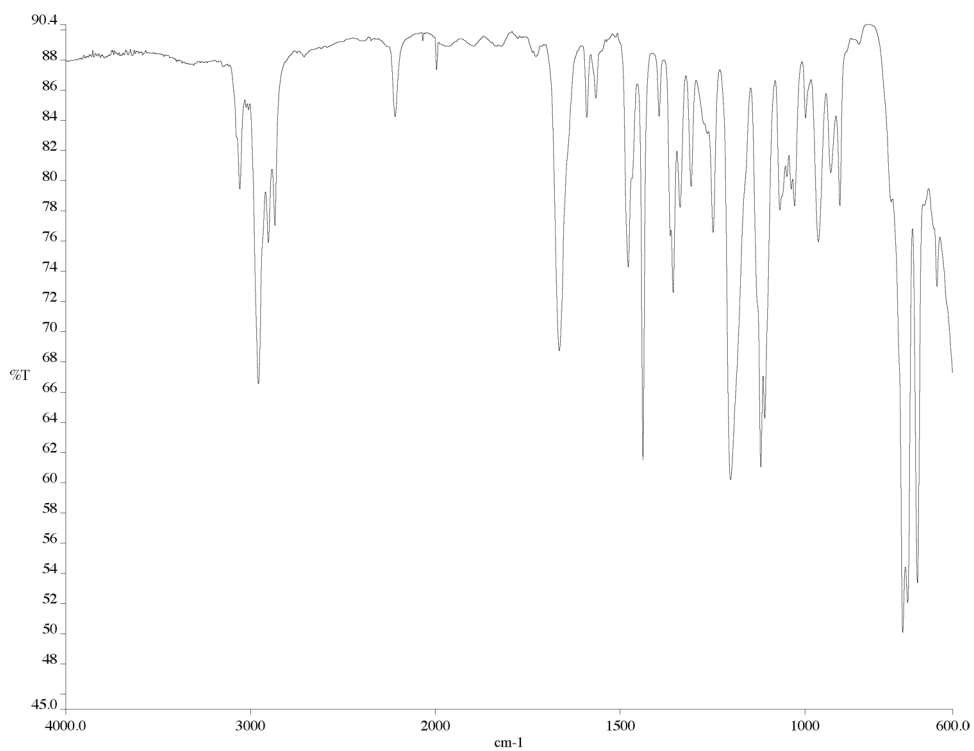


Figure A1.23. IR NMR spectrum of (S)-t-BuPHOX oxide (i)

Appendix 2

X-Ray Crystallographic Data Relevant to Chapter 2

CALIFORNIA INSTITUTE OF TECHNOLOGY
BECKMAN INSTITUTE
X-RAY CRYSTALLOGRAPHY LABORATORY



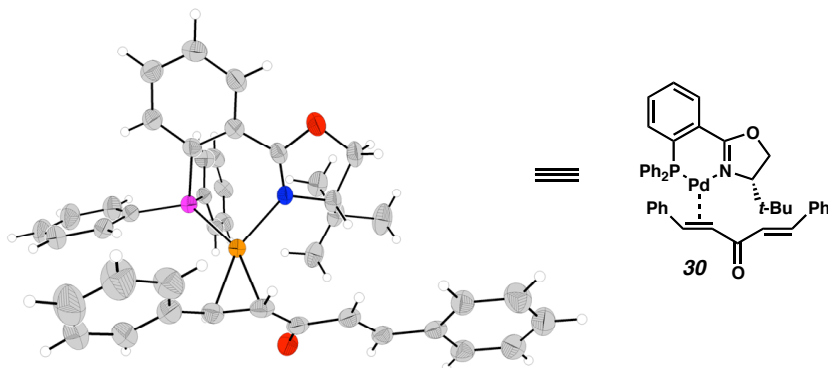
Date 09 May 2006

Crystal Structure Analysis of:
[(*S*)-*t*-BuPHOX}Pd(0)(dba)] 30
(NHS03, 606912)

Contents

Table A2.1. Crystal Data 106
Figures Minimum Overlap, Unit Cell Contents, Stereo View of Unit Cell Contents
Table A2.2. Atomic Coordinates 108
Table A2.3. Selected Bond Distances and Angles 110
Table A2.4. Full Bond Distances and Angles 111
Table A2.5. Anisotropic Displacement Parameters 114
Observed and calculated structure factors are available upon request.

Figure A2.1. Representation of [(*S*)-*t*-BuPHOX}Pd(0)(dba)] **30**



Note: Crystallographic data have been deposited at the CCDC, 12 Union Road, Cambridge CB2 1EZ, UK, and copies can be obtained on request, free of charge, by quoting the publication citation and the deposition number 606912.

Table A2.1. Crystal Data and Structure Refinement for NHS03 (CCDC 606912).

Empirical formula	C ₄₂ H ₄₀ NO ₂ PPd • C ₄ H ₈ O
Formula weight	800.22
Crystallization solvent	THF
Crystal habit	Block
Crystal size	0.26 x 0.25 x 0.25 mm ³
Crystal color	Orange

Data Collection

Type of diffractometer	Bruker SMART 1000
Wavelength	0.71073 Å MoK α
Data collection temperature	100(2) K
θ range for 25286 reflections used in lattice determination	2.45 to 29.83°
Unit cell dimensions	a = 10.3986(4) Å b = 13.8720(5) Å c = 27.4970(10) Å
Volume	3966.4(3) Å ³
Z	4
Crystal system	Orthorhombic
Space group	P2 ₁ 2 ₁ 2 ₁
Density (calculated)	1.340 Mg/m ³
F(000)	1664
θ range for data collection	2.09 to 32.87°
Completeness to $\theta = 32.87^\circ$	94.5 %
Index ranges	-15 ≤ h ≤ 15, -19 ≤ k ≤ 20, -35 ≤ l ≤ 41
Data collection scan type	ω scans at 5 ϕ settings
Reflections collected	66411
Independent reflections	13693 [R _{int} = 0.0693]
Absorption coefficient	0.549 mm ⁻¹
Absorption correction	None
Max. and min. transmission	0.8749 and 0.8704

Table A2.1. (cont.)**Structure Solution and Refinement**

Structure solution program	Bruker XS v6.12
Primary solution method	Direct methods
Secondary solution method	Difference Fourier map
Hydrogen placement	Geometric positions
Structure refinement program	Bruker XL v6.12
Refinement method	Full matrix least-squares on F^2
Data / restraints / parameters	13693 / 39 / 468
Treatment of hydrogen atoms	Riding
Goodness-of-fit on F^2	1.482
Final R indices [$I > 2\sigma(I)$, 10165 reflections]	$R_1 = 0.0400$, $wR_2 = 0.0643$
R indices (all data)	$R_1 = 0.0642$, $wR_2 = 0.0672$
Type of weighting scheme used	Sigma
Weighting scheme used	$w = 1/\sigma^2(F_o^2)$
Max shift/error	0.005
Average shift/error	0.000
Absolute structure parameter	-0.048(16)
Largest diff. peak and hole	0.710 and -0.467 e. \AA^{-3}

Special Refinement Details

The crystal contains solvent of crystallization, disordered at one site in the unit cell. The solvent was modeled as THF and included in least-squares refinement with geometric restraints on all of the THF atoms. The temperature factors were allowed to refine and the values reflect the diffuse nature of the electron density in the area.

Refinement of F^2 against ALL reflections. The weighted R-factor (wR) and goodness of fit (S) are based on F^2 , conventional R-factors (R) are based on F , with F set to zero for negative F^2 . The threshold expression of $F^2 > 2\sigma(F^2)$ is used only for calculating R-factors(gt), etc., and is not relevant to the choice of reflections for refinement. R-factors based on F^2 are statistically about twice as large as those based on F , and R-factors based on ALL data will be even larger.

All esds (except the esd in the dihedral angle between two l.s. planes) are estimated using the full covariance matrix. The cell esds are taken into account individually in the estimation of esds in distances, angles, and torsion angles; correlations between esds in cell parameters are only used when they are defined by crystal symmetry. An approximate (isotropic) treatment of cell esds is used for estimating esds involving l.s. planes.

Table A2.2. Atomic Coordinates ($\times 10^4$) and Equivalent Isotropic Displacement Parameters ($\text{\AA}^2 \times 10^3$) for NHSO3 (CCDC 606912). $U(\text{eq})$ is defined as the trace of the orthogonalized U^{ij} tensor.

	x	y	z	U_{eq}	Occ
Pd(1)	9271(1)	8680(1)	9206(1)	30(1)	1
P(1)	9236(1)	9154(1)	8415(1)	32(1)	1
O(1)	11984(2)	6645(1)	8627(1)	46(1)	1
O(2)	7180(2)	7972(1)	10054(1)	45(1)	1
N(1)	10248(2)	7406(1)	8929(1)	31(1)	1
C(1)	10164(2)	6412(2)	9132(1)	37(1)	1
C(2)	11452(3)	5964(2)	8971(1)	44(1)	1
C(3)	11234(2)	7448(2)	8658(1)	32(1)	1
C(4)	11688(2)	8257(2)	8353(1)	31(1)	1
C(5)	12979(3)	8238(2)	8210(1)	39(1)	1
C(6)	13476(3)	8930(2)	7908(1)	42(1)	1
C(7)	12700(3)	9663(2)	7737(1)	41(1)	1
C(8)	11424(2)	9710(2)	7883(1)	38(1)	1
C(9)	10896(2)	9024(2)	8197(1)	33(1)	1
C(10)	8947(3)	5866(2)	8963(1)	44(1)	1
C(11)	7739(2)	6394(2)	9129(1)	51(1)	1
C(12)	8987(3)	4861(2)	9206(1)	66(1)	1
C(13)	8935(3)	5739(2)	8411(1)	55(1)	1
C(14)	8547(3)	11428(2)	9696(1)	58(1)	1
C(15)	9116(4)	12335(2)	9681(1)	70(1)	1
C(16)	10441(4)	12418(3)	9713(2)	84(1)	1
C(17)	11151(3)	11607(3)	9776(1)	77(1)	1
C(18)	10594(3)	10699(2)	9795(1)	58(1)	1
C(19)	9275(3)	10595(2)	9753(1)	43(1)	1
C(20)	8641(3)	9643(2)	9754(1)	38(1)	1
C(21)	9157(2)	8812(2)	9977(1)	37(1)	1
C(22)	8364(2)	8002(2)	10116(1)	37(1)	1
C(23)	9048(2)	7173(2)	10344(1)	36(1)	1
C(24)	8433(2)	6431(2)	10532(1)	36(1)	1
C(25)	9022(2)	5584(2)	10767(1)	35(1)	1
C(26)	8230(3)	4863(2)	10959(1)	45(1)	1
C(27)	8749(3)	4058(2)	11181(1)	51(1)	1
C(28)	10073(3)	3972(2)	11229(1)	53(1)	1
C(29)	10846(3)	4680(2)	11039(1)	53(1)	1
C(30)	10341(2)	5470(2)	10816(1)	41(1)	1
C(31)	8793(2)	10365(2)	8215(1)	37(1)	1
C(32)	8054(3)	10537(2)	7810(1)	52(1)	1
C(33)	7702(3)	11478(2)	7685(1)	62(1)	1
C(34)	8095(3)	12226(2)	7969(1)	59(1)	1
C(35)	8856(3)	12077(2)	8372(1)	58(1)	1
C(36)	9188(3)	11135(2)	8495(1)	43(1)	1
C(37)	8328(2)	8378(2)	8005(1)	32(1)	1
C(38)	8799(2)	8048(2)	7558(1)	40(1)	1
C(39)	8057(3)	7464(2)	7268(1)	50(1)	1
C(40)	6833(3)	7191(2)	7407(1)	46(1)	1
C(41)	6351(3)	7505(2)	7850(1)	46(1)	1
C(42)	7095(3)	8090(2)	8145(1)	39(1)	1

C11	3074(4)	3874(4)	8577(2)	72(2)	0.661(5)
C21	3790(5)	3787(5)	8994(2)	103(2)	0.661(5)
C31	5064(6)	3878(11)	8871(3)	355(12)	0.661(5)
C41	5137(8)	4356(9)	8435(3)	192(5)	0.661(5)
O11	3826(6)	4525(5)	8282(2)	163(3)	0.661(5)
C12	5073(7)	3895(5)	8910(2)	43(2)	0.339(5)
C22	4005(9)	4464(7)	8849(4)	148(7)	0.339(5)
C32	4284(11)	5145(7)	8502(3)	95(4)	0.339(5)
C42	5277(10)	4803(6)	8223(4)	79(4)	0.339(5)
O12	5633(8)	3881(5)	8428(3)	109(3)	0.339(5)

Table A2.3. Selected Bond Lengths [\AA] and Angles [$^\circ$] for NHS03 (CCDC 606912)

Pd(1)-C(20)	2.118(2)
Pd(1)-C(21)	2.131(2)
Pd(1)-N(1)	2.1753(19)
Pd(1)-P(1)	2.2730(6)
C(20)-Pd(1)-C(21)	38.81(9)
C(20)-Pd(1)-N(1)	154.96(9)
C(21)-Pd(1)-N(1)	116.38(9)
C(20)-Pd(1)-P(1)	119.55(7)
C(21)-Pd(1)-P(1)	157.84(7)
N(1)-Pd(1)-P(1)	84.69(5)

Table A2.4. Bond lengths [\AA] and angles [$^\circ$] for NHS03 (CCDC 606912).

Pd(1)-C(20)	2.118(2)
Pd(1)-C(21)	2.131(2)
Pd(1)-N(1)	2.1753(19)
Pd(1)-P(1)	2.2730(6)
P(1)-C(37)	1.822(3)
P(1)-C(31)	1.826(2)
P(1)-C(9)	1.836(3)
O(1)-C(3)	1.362(3)
O(1)-C(2)	1.447(3)
O(2)-C(22)	1.243(3)
N(1)-C(3)	1.269(3)
N(1)-C(1)	1.491(3)
C(1)-C(2)	1.542(4)
C(1)-C(10)	1.546(3)
C(3)-C(4)	1.479(3)
C(4)-C(5)	1.399(3)
C(4)-C(9)	1.413(3)
C(5)-C(6)	1.371(4)
C(6)-C(7)	1.380(4)
C(7)-C(8)	1.388(4)
C(8)-C(9)	1.398(3)
C(10)-C(11)	1.524(4)
C(10)-C(13)	1.528(4)
C(10)-C(12)	1.547(3)
C(14)-C(15)	1.391(4)
C(14)-C(19)	1.390(4)
C(15)-C(16)	1.386(5)
C(16)-C(17)	1.356(5)
C(17)-C(18)	1.387(4)
C(18)-C(19)	1.384(5)
C(19)-C(20)	1.476(4)
C(20)-C(21)	1.412(3)
C(21)-C(22)	1.446(3)
C(22)-C(23)	1.490(3)
C(23)-C(24)	1.317(3)
C(24)-C(25)	1.475(3)
C(25)-C(26)	1.399(3)
C(25)-C(30)	1.388(3)
C(26)-C(27)	1.382(4)
C(27)-C(28)	1.388(4)
C(28)-C(29)	1.371(4)
C(29)-C(30)	1.361(4)
C(31)-C(36)	1.378(3)
C(31)-C(32)	1.374(4)
C(32)-C(33)	1.399(4)
C(33)-C(34)	1.362(4)
C(34)-C(35)	1.376(4)
C(35)-C(36)	1.393(4)
C(37)-C(42)	1.396(3)
C(37)-C(38)	1.400(3)

C(38)-C(39)	1.374(4)
C(39)-C(40)	1.381(4)
C(40)-C(41)	1.390(4)
C(41)-C(42)	1.383(4)
C11-O11	1.445(6)
C11-C21	1.371(4)
C21-C31	1.373(5)
C31-C41	1.373(5)
C41-O11	1.446(6)
C12-C22	1.373(5)
C12-O12	1.446(6)
C22-C32	1.373(5)
C32-C42	1.372(5)
C42-O12	1.446(6)
C(20)-Pd(1)-C(21)	38.81(9)
C(20)-Pd(1)-N(1)	154.96(9)
C(21)-Pd(1)-N(1)	116.38(9)
C(20)-Pd(1)-P(1)	119.55(7)
C(21)-Pd(1)-P(1)	157.84(7)
N(1)-Pd(1)-P(1)	84.69(5)
C(37)-P(1)-C(31)	103.10(12)
C(37)-P(1)-C(9)	103.12(11)
C(31)-P(1)-C(9)	103.22(11)
C(37)-P(1)-Pd(1)	115.45(8)
C(31)-P(1)-Pd(1)	123.91(9)
C(9)-P(1)-Pd(1)	105.63(8)
C(3)-O(1)-C(2)	105.89(19)
C(3)-N(1)-C(1)	108.0(2)
C(3)-N(1)-Pd(1)	123.10(17)
C(1)-N(1)-Pd(1)	126.36(15)
N(1)-C(1)-C(2)	102.37(19)
N(1)-C(1)-C(10)	112.85(19)
C(2)-C(1)-C(10)	115.3(2)
O(1)-C(2)-C(1)	104.91(19)
N(1)-C(3)-O(1)	117.5(2)
N(1)-C(3)-C(4)	128.7(2)
O(1)-C(3)-C(4)	113.7(2)
C(5)-C(4)-C(9)	119.2(2)
C(5)-C(4)-C(3)	116.8(2)
C(9)-C(4)-C(3)	123.9(2)
C(6)-C(5)-C(4)	121.3(2)
C(7)-C(6)-C(5)	120.1(2)
C(6)-C(7)-C(8)	119.7(3)
C(7)-C(8)-C(9)	121.5(2)
C(8)-C(9)-C(4)	118.1(2)
C(8)-C(9)-P(1)	120.33(18)
C(4)-C(9)-P(1)	121.50(18)
C(11)-C(10)-C(13)	110.3(2)
C(11)-C(10)-C(1)	110.4(2)
C(13)-C(10)-C(1)	111.2(2)
C(11)-C(10)-C(12)	109.0(2)
C(13)-C(10)-C(12)	109.0(2)
C(1)-C(10)-C(12)	106.8(2)

C(15)-C(14)-C(19)	121.6(3)
C(14)-C(15)-C(16)	119.7(3)
C(17)-C(16)-C(15)	118.7(3)
C(16)-C(17)-C(18)	122.1(3)
C(19)-C(18)-C(17)	120.4(3)
C(18)-C(19)-C(14)	117.5(3)
C(18)-C(19)-C(20)	122.4(3)
C(14)-C(19)-C(20)	120.1(3)
C(21)-C(20)-C(19)	124.2(2)
C(21)-C(20)-Pd(1)	71.09(13)
C(19)-C(20)-Pd(1)	115.13(18)
C(20)-C(21)-C(22)	122.2(2)
C(20)-C(21)-Pd(1)	70.10(14)
C(22)-C(21)-Pd(1)	103.12(16)
O(2)-C(22)-C(21)	123.6(2)
O(2)-C(22)-C(23)	120.3(2)
C(21)-C(22)-C(23)	116.1(2)
C(24)-C(23)-C(22)	122.4(2)
C(23)-C(24)-C(25)	126.4(2)
C(26)-C(25)-C(30)	117.7(2)
C(26)-C(25)-C(24)	119.3(2)
C(30)-C(25)-C(24)	123.0(2)
C(27)-C(26)-C(25)	120.9(3)
C(26)-C(27)-C(28)	119.9(3)
C(29)-C(28)-C(27)	118.9(3)
C(30)-C(29)-C(28)	121.5(3)
C(29)-C(30)-C(25)	121.1(3)
C(36)-C(31)-C(32)	118.9(2)
C(36)-C(31)-P(1)	118.1(2)
C(32)-C(31)-P(1)	123.0(2)
C(31)-C(32)-C(33)	120.6(3)
C(34)-C(33)-C(32)	119.4(3)
C(33)-C(34)-C(35)	121.3(3)
C(34)-C(35)-C(36)	118.6(3)
C(31)-C(36)-C(35)	121.2(3)
C(42)-C(37)-C(38)	118.0(2)
C(42)-C(37)-P(1)	118.3(2)
C(38)-C(37)-P(1)	123.69(19)
C(39)-C(38)-C(37)	120.4(2)
C(40)-C(39)-C(38)	121.3(3)
C(39)-C(40)-C(41)	119.2(3)
C(42)-C(41)-C(40)	119.8(3)
C(41)-C(42)-C(37)	121.4(3)
O11-C11-C21	103.3(4)
C31-C21-C11	108.1(3)
C21-C31-C41	108.2(3)
O11-C41-C31	106.3(4)
C41-O11-C11	104.2(6)
C22-C12-O12	102.9(4)
C12-C22-C32	108.0(3)
C42-C32-C22	108.0(3)
C32-C42-O12	106.3(4)

Table A2.5. Anisotropic Displacement Parameters ($\text{\AA}^2 \times 10^4$) for NHS03 (CCDC 606912). The anisotropic displacement factor exponent takes the form: $-2\pi^2 [h^2 a^{*2} U^{11} + \dots + 2 h k a^* b^* U^{12}]$.

	U ¹¹	U ²²	U ³³	U ²³	U ¹³	U ¹²
Pd(1)	313(1)	282(1)	309(1)	15(1)	6(1)	5(1)
P(1)	328(3)	294(3)	330(3)	38(2)	14(3)	24(3)
O(1)	536(11)	376(11)	468(11)	33(8)	14(9)	137(9)
O(2)	299(10)	538(12)	527(12)	145(10)	34(9)	35(9)
N(1)	388(11)	244(10)	299(11)	13(9)	-22(9)	15(9)
C(1)	531(14)	261(12)	320(14)	2(12)	-76(11)	11(12)
C(2)	659(18)	255(13)	409(16)	33(12)	-69(14)	101(13)
C(3)	408(14)	259(13)	304(14)	-33(11)	-52(12)	70(11)
C(4)	333(13)	333(13)	276(13)	-34(11)	-32(11)	21(11)
C(5)	403(16)	349(14)	424(16)	-12(13)	4(13)	94(12)
C(6)	347(14)	457(17)	458(16)	-68(13)	41(12)	3(12)
C(7)	430(16)	423(15)	372(16)	10(12)	59(12)	-36(13)
C(8)	350(14)	380(15)	394(16)	48(12)	-12(12)	32(12)
C(9)	359(14)	319(11)	301(12)	-13(9)	5(11)	17(11)
C(10)	650(20)	307(13)	364(14)	39(11)	-98(13)	-81(13)
C(11)	540(16)	459(15)	518(18)	112(16)	-143(14)	-145(15)
C(12)	920(30)	358(14)	710(20)	117(16)	-260(20)	-181(15)
C(13)	800(30)	424(16)	409(16)	-31(13)	-168(16)	-81(15)
C(14)	620(18)	459(18)	670(20)	-15(17)	148(16)	101(16)
C(15)	860(30)	366(17)	860(30)	-44(16)	170(20)	13(19)
C(16)	990(30)	470(20)	1060(30)	-150(20)	10(30)	-160(20)
C(17)	630(20)	600(20)	1080(30)	-60(20)	-90(20)	-197(18)
C(18)	513(19)	516(18)	720(20)	-100(15)	-23(18)	-52(17)
C(19)	471(15)	405(14)	411(15)	-59(11)	-15(16)	-64(16)
C(20)	393(14)	406(15)	351(15)	-40(12)	3(12)	40(12)
C(21)	275(12)	529(15)	297(12)	-18(11)	26(11)	39(14)
C(22)	325(15)	495(16)	286(14)	13(12)	43(11)	35(12)
C(23)	319(15)	479(14)	288(13)	14(11)	15(11)	32(12)
C(24)	318(12)	475(16)	280(12)	1(12)	-1(10)	47(13)
C(25)	360(15)	423(13)	268(12)	-19(12)	29(12)	-4(10)
C(26)	356(15)	571(18)	412(17)	51(13)	42(12)	7(13)
C(27)	579(18)	479(18)	483(18)	93(14)	56(15)	2(15)
C(28)	630(20)	484(19)	479(18)	95(14)	-82(16)	66(16)
C(29)	395(16)	591(18)	608(18)	58(15)	-99(16)	24(16)
C(30)	382(14)	438(14)	410(15)	67(14)	-19(13)	1(11)
C(31)	346(14)	337(14)	421(16)	86(12)	101(12)	44(11)
C(32)	590(20)	433(17)	521(19)	82(14)	-87(15)	31(15)
C(33)	594(19)	490(20)	790(20)	235(18)	-49(17)	65(17)
C(34)	570(20)	404(18)	790(30)	231(17)	96(19)	106(15)
C(35)	690(20)	340(16)	700(20)	42(15)	180(18)	32(15)
C(36)	424(14)	361(15)	502(15)	97(11)	94(14)	10(14)
C(37)	297(13)	312(14)	362(15)	55(11)	-27(11)	63(10)
C(38)	359(14)	493(16)	357(15)	-11(13)	-25(11)	20(12)
C(39)	517(19)	541(18)	443(18)	-121(14)	-56(14)	100(15)
C(40)	394(16)	473(17)	522(19)	-108(14)	-126(14)	47(13)
C(41)	310(14)	421(16)	640(20)	-35(15)	-64(14)	36(12)
C(42)	409(16)	348(14)	421(16)	-4(12)	6(13)	71(12)

CALIFORNIA INSTITUTE OF TECHNOLOGY
BECKMAN INSTITUTE
X-RAY CRYSTALLOGRAPHY LABORATORY



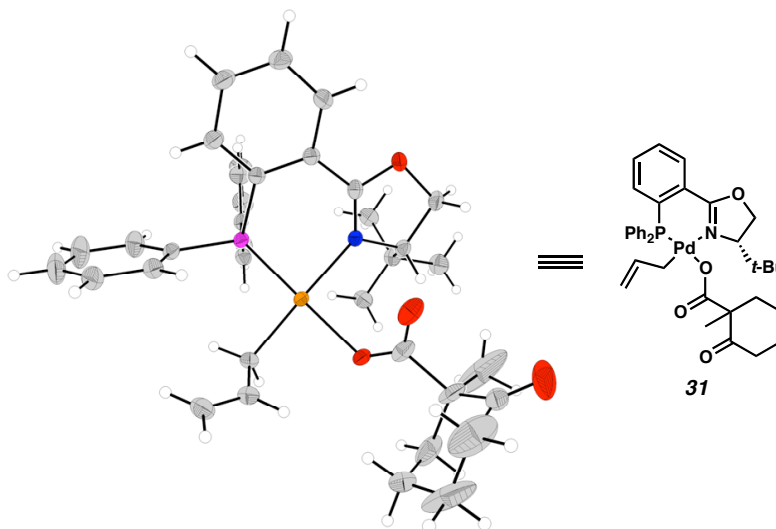
Date 18 July 2008

Crystal Structure Analysis of:
Palladium Allyl Carbonate 31
(NHS20, 695531)

Contents

Table A2.6. Crystal Data 116
Figures Minimum Overlap, A and B
Table A2.7. Atomic Coordinates 118
Table A2.8. Selected Bond Distances and Angles 119
Table A2.9. Full Bond Distances and Angles 120
Table A2.10. Anisotropic Displacement Parameters 122
Observed and calculated structure factors are available upon request.

Figure A2.2. Representation of Palladium Allyl Carboxylate **31**



Note: Crystallographic data have been deposited at the CCDC, 12 Union Road, Cambridge CB2 1EZ, UK, and copies can be obtained on request, free of charge, by quoting the publication citation and the deposition number 695531.

Table A2.6. Crystal Data and Structure Refinement for NHS20 (CCDC 695531)

Empirical formula	C ₃₆ H ₄₂ NO ₄ PPd
Formula weight	690.08
Crystallization solvent	Ether/THF/hexanes
Crystal habit	Blade
Crystal size	0.17 x 0.10 x 0.06 mm ³
Crystal color	Pale yellow



Data Collection

Type of diffractometer	Bruker KAPPA APEX II
Wavelength	0.71073 Å MoK α
Data collection temperature	100(2) K
θ range for 9986 reflections used in lattice determination	2.50 to 33.63°
Unit cell dimensions	a = 10.7719(4) Å b = 12.4117(4) Å c = 24.7631(8) Å
Volume	3310.77(19) Å ³
Z	4
Crystal system	Orthorhombic
Space group	P2 ₁ 2 ₁ 2 ₁
Density (calculated)	1.384 Mg/m ³
F(000)	1432
θ range for data collection	2.06 to 34.15°
Completeness to $\theta = 34.15^\circ$	94.0 %
Index ranges	-16 \leq h \leq 9, -18 \leq k \leq 17, -39 \leq l \leq 35
Data collection scan type	ω scans; 11 settings
Reflections collected	62894
Independent reflections	12522 [R _{int} = 0.0472]
Absorption coefficient	0.648 mm ⁻¹
Absorption correction	None
Max. and min. transmission	0.9622 and 0.8979

Table A2.6. (cont.)**Structure Solution and Refinement**

Structure solution program	SHELXS-97 (Sheldrick, 2008)
Primary solution method	Direct methods
Secondary solution method	Difference Fourier map
Hydrogen placement	Geometric positions
Structure refinement program	SHELXL-97 (Sheldrick, 2008)
Refinement method	Full matrix least-squares on F^2
Data / restraints / parameters	12522 / 0 / 402
Treatment of hydrogen atoms	Riding
Goodness-of-fit on F^2	1.778
Final R indices [$I > 2\sigma(I)$, 10824 reflections]	$R_1 = 0.0347$, $wR_2 = 0.0482$
R indices (all data)	$R_1 = 0.0454$, $wR_2 = 0.0488$
Type of weighting scheme used	Sigma
Weighting scheme used	$w = 1/\sigma^2(F_o^2)$
Max shift/error	0.002
Average shift/error	0.000
Absolute structure parameter	-0.023(12)
Largest diff. peak and hole	1.696 and -1.113 e.Å ⁻³

Special Refinement Details

Crystals were mounted on a glass fiber using Paratone oil then placed on the diffractometer under a nitrogen stream at 100K.

The ketone oxygen (O4) is disordered over two positions, bonded to C28 (39.8%) or C32 (60.2%). The thermal ellipsoids and the difference Fourier in this area suggest there is some small rotational component to this disorder as well. The rotational component was not included in the model.

Refinement of F^2 against ALL reflections. The weighted R-factor (wR) and goodness of fit (S) are based on F^2 , conventional R-factors (R) are based on F , with F set to zero for negative F^2 . The threshold expression of $F^2 > 2\sigma(F^2)$ is used only for calculating R-factors(gt), etc., and is not relevant to the choice of reflections for refinement. R-factors based on F^2 are statistically about twice as large as those based on F , and R-factors based on ALL data will be even larger.

All esds (except the esd in the dihedral angle between two l.s. planes) are estimated using the full covariance matrix. The cell esds are taken into account individually in the estimation of esds in distances, angles, and torsion angles; correlations between esds in cell parameters are only used when they are defined by crystal symmetry. An approximate (isotropic) treatment of cell esds is used for estimating esds involving l.s. planes.

Table A2.7. Atomic Coordinates ($\times 10^4$) and Equivalent Isotropic Displacement Parameters ($\text{\AA}^2 \times 10^3$) for NHS20 (CCDC 695531). $U(\text{eq})$ is defined as the trace of the orthogonalized U^{ij} tensor.

	x	y	z	U_{eq}	Occ
Pd(1)	3632(1)	7917(1)	8446(1)	17(1)	1
P(1)	5054(1)	7679(1)	9067(1)	18(1)	1
O(1)	6459(1)	10035(1)	7822(1)	25(1)	1
O(2)	2273(1)	8140(1)	7828(1)	27(1)	1
O(3)	3711(1)	7986(1)	7181(1)	34(1)	1
O(4A)	2329(3)	8627(6)	6044(2)	206(5)	0.602(4)
O(4B)	-327(4)	8506(5)	7173(2)	73(2)	0.398(4)
N(1)	4786(1)	9182(1)	8149(1)	17(1)	1
C(1)	6611(2)	7734(2)	8768(1)	18(1)	1
C(2)	7547(2)	7083(2)	8966(1)	25(1)	1
C(3)	8770(2)	7172(2)	8776(1)	28(1)	1
C(4)	9051(2)	7913(2)	8384(1)	28(1)	1
C(5)	8125(2)	8571(2)	8179(1)	24(1)	1
C(6)	6898(2)	8498(2)	8358(1)	18(1)	1
C(7)	5979(2)	9225(2)	8117(1)	19(1)	1
C(8)	5407(2)	10555(2)	7558(1)	25(1)	1
C(9)	4276(2)	10150(2)	7871(1)	21(1)	1
C(10)	3687(2)	10973(2)	8264(1)	25(1)	1
C(11)	4604(2)	11384(2)	8687(1)	29(1)	1
C(12)	3221(2)	11928(2)	7921(1)	35(1)	1
C(13)	2575(2)	10459(2)	8548(1)	30(1)	1
C(14)	5105(2)	8772(2)	9554(1)	20(1)	1
C(15)	6212(2)	9262(2)	9713(1)	29(1)	1
C(16)	6191(2)	10115(2)	10076(1)	40(1)	1
C(17)	5077(2)	10470(2)	10288(1)	38(1)	1
C(18)	3976(2)	9991(2)	10138(1)	33(1)	1
C(19)	3981(2)	9144(2)	9769(1)	25(1)	1
C(20)	5098(2)	6447(2)	9464(1)	21(1)	1
C(21)	5154(2)	6451(2)	10023(1)	34(1)	1
C(22)	5217(3)	5480(2)	10303(1)	48(1)	1
C(23)	5212(2)	4513(2)	10025(1)	45(1)	1
C(24)	5147(2)	4506(2)	9471(1)	34(1)	1
C(25)	5085(2)	5473(2)	9192(1)	27(1)	1
C(26)	2636(2)	8148(2)	7339(1)	29(1)	1
C(27)	1653(2)	8437(2)	6908(1)	36(1)	1
C(28)	427(2)	7910(3)	7042(1)	54(1)	1
C(29)	418(3)	6739(3)	7002(1)	88(1)	1
C(30)	720(3)	6405(3)	6448(2)	85(1)	1
C(31)	1946(3)	6768(3)	6299(1)	81(1)	1
C(32)	2059(2)	7979(3)	6346(1)	65(1)	1
C(33)	1563(4)	9651(2)	6886(2)	147(2)	1
C(34)	2405(2)	6836(2)	8778(1)	25(1)	1
C(35)	2163(2)	5939(2)	8413(1)	30(1)	1
C(36)	2358(2)	4904(2)	8503(1)	33(1)	1

Table A2.8. Selected Bond Lengths [\AA] and angles [$^\circ$] for NHS20 (CCDC 695531)

Pd(1)-C(34)	2.0552(19)	C(34)-Pd(1)-N(1)	173.26(7)
Pd(1)-N(1)	2.1331(16)	C(34)-Pd(1)-O(2)	86.02(7)
Pd(1)-O(2)	2.1361(12)	N(1)-Pd(1)-O(2)	93.27(5)
Pd(1)-P(1)	2.1895(5)	C(34)-Pd(1)-P(1)	94.65(6)
		N(1)-Pd(1)-P(1)	86.19(4)
		O(2)-Pd(1)-P(1)	178.84(4)

Table A2.9. Bond Lengths [Å] and Angles [°] for NHS20 (CCDC 695531)

Pd(1)-C(34)	2.0552(19)	C(34)-Pd(1)-N(1)	173.26(7)
Pd(1)-N(1)	2.1331(16)	C(34)-Pd(1)-O(2)	86.02(7)
Pd(1)-O(2)	2.1361(12)	N(1)-Pd(1)-O(2)	93.27(5)
Pd(1)-P(1)	2.1895(5)	C(34)-Pd(1)-P(1)	94.65(6)
P(1)-C(14)	1.817(2)	N(1)-Pd(1)-P(1)	86.19(4)
P(1)-C(20)	1.819(2)	O(2)-Pd(1)-P(1)	178.84(4)
P(1)-C(1)	1.8348(17)	C(14)-P(1)-C(20)	105.51(9)
O(1)-C(7)	1.346(2)	C(14)-P(1)-C(1)	102.26(9)
O(1)-C(8)	1.458(2)	C(20)-P(1)-C(1)	103.02(9)
O(2)-C(26)	1.273(3)	C(14)-P(1)-Pd(1)	112.79(7)
O(3)-C(26)	1.238(3)	C(20)-P(1)-Pd(1)	120.74(7)
O(4A)-C(32)	1.136(5)	C(1)-P(1)-Pd(1)	110.57(5)
O(4B)-C(28)	1.144(5)	C(7)-O(1)-C(8)	105.99(14)
N(1)-C(7)	1.288(2)	C(26)-O(2)-Pd(1)	118.15(13)
N(1)-C(9)	1.490(2)	C(7)-N(1)-C(9)	107.74(16)
C(1)-C(2)	1.382(3)	C(7)-N(1)-Pd(1)	129.28(13)
C(1)-C(6)	1.424(2)	C(9)-N(1)-Pd(1)	122.58(12)
C(2)-C(3)	1.403(3)	C(2)-C(1)-C(6)	118.95(16)
C(3)-C(4)	1.372(3)	C(2)-C(1)-P(1)	120.17(13)
C(4)-C(5)	1.384(3)	C(6)-C(1)-P(1)	120.72(13)
C(5)-C(6)	1.397(2)	C(1)-C(2)-C(3)	121.31(19)
C(6)-C(7)	1.467(2)	C(4)-C(3)-C(2)	119.87(19)
C(8)-C(9)	1.529(3)	C(3)-C(4)-C(5)	119.68(17)
C(9)-C(10)	1.546(3)	C(4)-C(5)-C(6)	121.86(18)
C(10)-C(13)	1.528(3)	C(5)-C(6)-C(1)	118.32(17)
C(10)-C(11)	1.528(3)	C(5)-C(6)-C(7)	118.06(17)
C(10)-C(12)	1.542(3)	C(1)-C(6)-C(7)	123.61(16)
C(14)-C(15)	1.396(3)	N(1)-C(7)-O(1)	116.63(17)
C(14)-C(19)	1.400(3)	N(1)-C(7)-C(6)	128.47(17)
C(15)-C(16)	1.389(3)	O(1)-C(7)-C(6)	114.89(16)
C(16)-C(17)	1.382(3)	O(1)-C(8)-C(9)	104.24(14)
C(17)-C(18)	1.377(3)	N(1)-C(9)-C(8)	101.89(14)
C(18)-C(19)	1.395(3)	N(1)-C(9)-C(10)	113.19(15)
C(20)-C(25)	1.384(3)	C(8)-C(9)-C(10)	115.42(16)
C(20)-C(21)	1.386(3)	C(13)-C(10)-C(11)	109.33(16)
C(21)-C(22)	1.391(3)	C(13)-C(10)-C(12)	108.63(17)
C(22)-C(23)	1.384(3)	C(11)-C(10)-C(12)	109.32(16)
C(23)-C(24)	1.373(3)	C(13)-C(10)-C(9)	109.59(16)
C(24)-C(25)	1.387(3)	C(11)-C(10)-C(9)	112.69(18)
C(26)-C(27)	1.547(3)	C(12)-C(10)-C(9)	107.19(16)
C(27)-C(28)	1.511(4)	C(15)-C(14)-C(19)	119.26(18)
C(27)-C(33)	1.511(3)	C(15)-C(14)-P(1)	122.58(15)
C(27)-C(32)	1.564(4)	C(19)-C(14)-P(1)	118.15(15)
C(28)-C(29)	1.457(5)	C(16)-C(15)-C(14)	120.0(2)
C(29)-C(30)	1.469(5)	C(17)-C(16)-C(15)	120.2(2)
C(30)-C(31)	1.443(4)	C(18)-C(17)-C(16)	120.6(2)
C(31)-C(32)	1.513(5)	C(17)-C(18)-C(19)	119.9(2)
C(34)-C(35)	1.458(3)	C(18)-C(19)-C(14)	120.1(2)
C(35)-C(36)	1.320(3)	C(25)-C(20)-C(21)	119.36(19)
		C(25)-C(20)-P(1)	118.08(15)

C(21)-C(20)-P(1)	122.56(17)
C(20)-C(21)-C(22)	119.7(2)
C(23)-C(22)-C(21)	120.3(2)
C(24)-C(23)-C(22)	120.2(2)
C(23)-C(24)-C(25)	119.6(2)
C(20)-C(25)-C(24)	120.8(2)
O(3)-C(26)-O(2)	125.94(18)
O(3)-C(26)-C(27)	117.4(2)
O(2)-C(26)-C(27)	116.7(2)
C(28)-C(27)-C(33)	112.5(3)
C(28)-C(27)-C(26)	110.2(2)
C(33)-C(27)-C(26)	107.42(19)
C(28)-C(27)-C(32)	106.5(2)
C(33)-C(27)-C(32)	110.4(3)
C(26)-C(27)-C(32)	109.76(18)
O(4B)-C(28)-C(29)	131.2(4)
O(4B)-C(28)-C(27)	113.8(4)
C(29)-C(28)-C(27)	115.0(3)
C(28)-C(29)-C(30)	110.2(3)
C(31)-C(30)-C(29)	110.7(3)
C(30)-C(31)-C(32)	111.3(3)
O(4A)-C(32)-C(31)	132.3(6)
O(4A)-C(32)-C(27)	113.5(5)
C(31)-C(32)-C(27)	114.1(2)
C(35)-C(34)-Pd(1)	111.39(14)
C(36)-C(35)-C(34)	127.6(2)

Table A2.10. Anisotropic Displacement Parameters ($\text{\AA}^2 \times 10^4$) for NHS20 (CCDC 695531). The anisotropic displacement factor exponent takes the form: $-2\pi^2[h^2 a^{*2} U^{11} + \dots + 2 h k a^* b^* U^{12}]$.

	U ¹¹	U ²²	U ³³	U ²³	U ¹³	U ¹²
Pd(1)	157(1)	174(1)	177(1)	5(1)	-26(1)	-1(1)
P(1)	156(2)	228(3)	144(2)	12(2)	3(2)	11(2)
O(1)	236(7)	281(7)	229(6)	92(6)	16(7)	15(7)
O(2)	232(7)	256(9)	312(8)	69(6)	-117(6)	-41(6)
O(3)	400(8)	326(8)	296(7)	-101(7)	-108(7)	112(9)
O(4A)	410(20)	4600(120)	1160(40)	2010(60)	-380(20)	-650(40)
O(4B)	340(30)	1510(60)	340(30)	-90(30)	20(20)	350(30)
N(1)	176(9)	157(9)	182(8)	17(6)	-10(6)	12(7)
C(1)	174(10)	214(11)	147(7)	-14(7)	-1(6)	-11(8)
C(2)	212(10)	292(11)	245(9)	21(10)	-13(7)	32(11)
C(3)	194(10)	357(11)	277(9)	11(9)	-22(8)	58(11)
C(4)	184(9)	371(11)	278(10)	3(12)	35(8)	59(11)
C(5)	214(10)	253(12)	244(10)	28(9)	35(8)	-1(9)
C(6)	184(9)	230(10)	140(9)	-18(7)	1(7)	-2(8)
C(7)	248(11)	217(11)	113(8)	-20(7)	5(7)	6(8)
C(8)	286(12)	240(11)	213(10)	63(8)	-19(9)	28(9)
C(9)	224(10)	179(10)	221(10)	29(8)	-34(8)	6(8)
C(10)	266(10)	181(10)	294(9)	13(7)	-5(10)	34(10)
C(11)	327(12)	225(12)	322(12)	-51(9)	35(9)	-21(10)
C(12)	406(13)	206(13)	436(13)	46(10)	-7(10)	45(10)
C(13)	241(11)	243(11)	419(15)	43(10)	44(10)	47(9)
C(14)	211(11)	245(11)	135(8)	16(7)	1(8)	3(9)
C(15)	276(12)	369(12)	228(10)	-65(9)	25(9)	-24(11)
C(16)	437(15)	472(14)	288(11)	-123(10)	-26(11)	-158(13)
C(17)	538(16)	336(14)	281(12)	-126(10)	41(12)	-22(13)
C(18)	429(15)	325(12)	240(11)	-15(9)	117(10)	40(10)
C(19)	264(12)	272(11)	225(10)	21(8)	26(8)	-13(9)
C(20)	160(10)	262(11)	200(9)	52(8)	5(8)	22(9)
C(21)	452(14)	365(13)	217(10)	46(9)	41(10)	62(12)
C(22)	675(19)	526(17)	226(12)	194(12)	3(13)	76(16)
C(23)	571(17)	352(15)	438(15)	207(12)	18(13)	77(13)
C(24)	296(13)	271(13)	460(14)	84(10)	10(11)	39(11)
C(25)	244(11)	291(12)	262(11)	46(9)	-2(9)	-7(10)
C(26)	382(13)	135(11)	357(12)	-37(8)	-201(10)	4(9)
C(27)	346(14)	283(12)	458(13)	-14(10)	-271(11)	10(10)
C(28)	330(14)	1110(30)	170(10)	-62(16)	-2(9)	100(20)
C(29)	940(30)	1040(30)	670(20)	400(20)	-520(20)	-740(20)
C(30)	780(20)	520(20)	1260(30)	-380(20)	-720(20)	109(18)
C(31)	690(20)	1110(40)	630(20)	-470(20)	-158(17)	220(20)
C(32)	212(13)	1260(30)	493(15)	490(20)	-165(11)	-218(18)
C(33)	2060(50)	277(18)	2070(50)	0(20)	-1750(40)	170(30)
C(34)	160(10)	296(13)	295(11)	62(9)	1(8)	-25(8)
C(35)	273(11)	332(12)	307(11)	40(11)	-55(10)	-101(9)
C(36)	370(13)	312(12)	320(12)	19(11)	-7(11)	-125(10)

CALIFORNIA INSTITUTE OF TECHNOLOGY
BECKMAN INSTITUTE
X-RAY CRYSTALLOGRAPHY LABORATORY



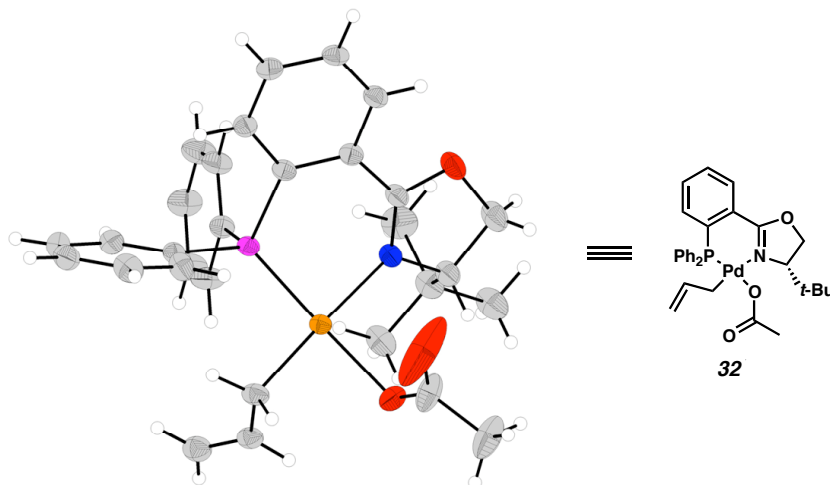
Date 09 September 2008

Crystal Structure Analysis of:
Palladium Allyl Acetate 32
(NHS22, 701671)

Contents

Table A2.11. Crystal Data 124
Figures Minimum Overlap
Table A2.12. Atomic Coordinates 126
Table A2.13. Selected Bond Distances and Angles 127
Table A2.14. Full Bond Distances and Angles 128
Table A2.15. Anisotropic Displacement Parameters 130
Observed and calculated structure factors are available upon request.

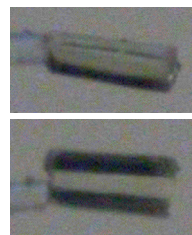
Figure A2.3. Representation of Palladium Allyl Acetate 32



Note: Crystallographic data have been deposited at the CCDC, 12 Union Road, Cambridge CB2 1EZ, UK, and copies can be obtained on request, free of charge, by quoting the publication citation and the deposition number 701671.

Table A2.11. Crystal Data and Structure Refinement for NHS22 (CCDC 701671).

Empirical formula	C ₂₉ H ₃₂ N ₅ O ₅ P Pd, C ₆ H ₆
Formula weight	690.03
Crystallization solvent	Dichloromethane/ether
Crystal habit	Rod
Crystal size	0.33 x 0.14 x 0.10 mm ³
Crystal color	Pale yellow



Data Collection

Type of diffractometer	Bruker KAPPA APEX II
Wavelength	0.71073 Å MoK α
Data collection temperature	100(2) K
θ range for 9097 reflections used in lattice determination	2.50 to 34.73°
Unit cell dimensions	a = 28.2427(10) Å b = 28.2427(10) Å c = 10.4684(4) Å
Volume	7231.4(5) Å ³
Z	9
Crystal system	Rhombohedral
Space group	R3
Density (calculated)	1.426 Mg/m ³
F(000)	3204
θ range for data collection	2.12 to 34.96°
Completeness to $\theta = 34.96^\circ$	95.1 %
Index ranges	-44 \leq h \leq 44, -44 \leq k \leq 44, -16 \leq l \leq 16
Data collection scan type	ω scans; 20 settings
Reflections collected	117262
Independent reflections	13097 [R _{int} = 0.0305]
Absorption coefficient	0.669 mm ⁻¹
Absorption correction	Semi-empirical from equivalents
Max. and min. transmission	0.7469 and 0.6754

Table A2.11. (cont.)**Structure Solution and Refinement**

Structure solution program	SHELXS-97 (Sheldrick, 2008)
Primary solution method	Direct methods
Secondary solution method	Difference Fourier map
Hydrogen placement	Geometric positions
Structure refinement program	SHELXL-97 (Sheldrick, 2008)
Refinement method	Full matrix least-squares on F^2
Data / restraints / parameters	13097 / 1 / 353
Treatment of hydrogen atoms	Riding
Goodness-of-fit on F^2	3.223
Final R indices [$I > 2\sigma(I)$, 12405 reflections]	$R_1 = 0.0283$, $wR_2 = 0.0620$
R indices (all data)	$R_1 = 0.0321$, $wR_2 = 0.0623$
Type of weighting scheme used	Sigma
Weighting scheme used	$w = 1/\sigma^2(F_o^2)$
Max shift/error	0.003
Average shift/error	0.000
Absolute structure parameter	-0.014(11)
Largest diff. peak and hole	0.926 and -0.561 e.Å ⁻³

Special Refinement Details

Crystals were mounted on a glass fiber using Paratone oil then placed on the diffractometer under a nitrogen stream at 100K.

A disordered benzene sits near the threefold rotation axis. Both components were constrained to ideal geometry with isotropic temperature factors; the minor component (44%) was assigned one overall temperature factor.

Refinement of F^2 against ALL reflections. The weighted R-factor (wR) and goodness of fit (S) are based on F^2 , conventional R-factors (R) are based on F , with F set to zero for negative F^2 . The threshold expression of $F^2 > 2\sigma(F^2)$ is used only for calculating R-factors(gt), etc., and is not relevant to the choice of reflections for refinement. R-factors based on F^2 are statistically about twice as large as those based on F , and R-factors based on ALL data will be even larger.

All esds (except the esd in the dihedral angle between two l.s. planes) are estimated using the full covariance matrix. The cell esds are taken into account individually in the estimation of esds in distances, angles, and torsion angles; correlations between esds in cell parameters are only used when they are defined by crystal symmetry. An approximate (isotropic) treatment of cell esds is used for estimating esds involving l.s. planes.

Table A2.12. Atomic Coordinates ($\times 10^4$) and Equivalent Isotropic Displacement Parameters ($\text{\AA}^2 \times 10^3$) for NHS22 (CCDC 701671). $U(\text{eq})$ is defined as the trace of the orthogonalized U^{ij} tensor.

	x	y	z	U_{eq}	Occ
Pd(1)	5618(1)	1009(1)	7615(1)	19(1)	1
P(1)	5171(1)	108(1)	7493(1)	18(1)	1
O(1)	5022(1)	689(1)	11364(1)	31(1)	1
O(2)	6063(1)	1851(1)	7815(2)	33(1)	1
O(3)	6590(1)	1744(1)	9230(2)	48(1)	1
O(4)	6005(1)	1107(1)	5946(1)	28(1)	1
O(5)	5242(1)	808(1)	4803(2)	41(1)	1
N(1)	5274(1)	943(1)	9349(1)	20(1)	1
C(1)	5242(1)	-151(1)	9029(2)	19(1)	1
C(2)	5276(1)	-626(1)	9092(2)	26(1)	1
C(3)	5274(1)	-864(1)	10250(2)	26(1)	1
C(4)	5240(1)	-634(1)	11370(2)	27(1)	1
C(5)	5214(1)	-154(1)	11345(2)	24(1)	1
C(6)	5212(1)	87(1)	10177(2)	20(1)	1
C(7)	5175(1)	589(1)	10230(2)	21(1)	1
C(8)	5111(1)	1243(1)	11280(2)	34(1)	1
C(9)	5146(1)	1360(1)	9848(2)	23(1)	1
C(10)	4629(1)	1321(1)	9247(2)	25(1)	1
C(11)	4129(1)	750(1)	9420(2)	31(1)	1
C(12)	4522(1)	1746(1)	9905(2)	35(1)	1
C(13)	4718(1)	1459(1)	7831(2)	29(1)	1
C(14)	4437(1)	-228(1)	7275(2)	19(1)	1
C(15)	4080(1)	-708(1)	7923(2)	24(1)	1
C(16)	3522(1)	-953(1)	7730(2)	27(1)	1
C(17)	3310(1)	-721(1)	6916(2)	25(1)	1
C(18)	3660(1)	-244(1)	6269(2)	24(1)	1
C(19)	4223(1)	2(1)	6434(2)	21(1)	1
C(20)	5427(1)	-191(1)	6348(2)	21(1)	1
C(21)	5080(1)	-637(1)	5595(2)	26(1)	1
C(22)	5292(1)	-870(1)	4778(2)	30(1)	1
C(23)	5856(1)	-654(1)	4700(2)	34(1)	1
C(24)	6205(1)	-211(1)	5451(2)	33(1)	1
C(25)	5994(1)	26(1)	6272(2)	27(1)	1
C(26)	6461(1)	2026(1)	8589(3)	39(1)	1
C(27)	6782(1)	2647(1)	8709(5)	92(2)	1
C(28)	5727(1)	976(1)	4889(2)	27(1)	1
C(29)	6075(1)	1044(1)	3734(2)	43(1)	1
C(41)	7391(2)	2775(1)	5211(4)	81(2)	0.560(7)
C(42)	7219(2)	2450(1)	4122(5)	132(4)	0.560(7)
C(43)	7255(2)	2686(2)	2934(4)	135(4)	0.560(7)
C(44)	7464(2)	3246(2)	2835(3)	87(2)	0.560(7)
C(45)	7637(2)	3571(1)	3924(4)	96(2)	0.560(7)
C(46)	7600(2)	3335(1)	5112(3)	42(1)	0.560(7)
C(51)	7230(2)	2547(2)	3398(5)	375(10)	0.440(7)
C(52)	7098(2)	2415(1)	4677(5)	375(10)	0.440(7)

C(53)	7168(2)	2818(2)	5543(4)	375(10)	0.440(7)
C(54)	7371(2)	3353(2)	5129(3)	375(10)	0.440(7)
C(55)	7503(2)	3485(1)	3850(4)	375(10)	0.440(7)
C(56)	7433(2)	3081(2)	2984(3)	375(10)	0.440(7)

Table A2.13. Selected Bond Lengths [\AA] and Angles [$^\circ$] for NHS22 (CCDC 701671).

Pd(1)-O(4)	2.0051(13)	O(4)-Pd(1)-N(1)	176.38(7)
Pd(1)-N(1)	2.0227(15)	O(4)-Pd(1)-O(2)	87.35(6)
Pd(1)-O(2)	2.0704(14)	N(1)-Pd(1)-O(2)	90.16(6)
Pd(1)-P(1)	2.2072(5)	O(4)-Pd(1)-P(1)	93.81(5)
		N(1)-Pd(1)-P(1)	88.53(4)
		O(2)-Pd(1)-P(1)	176.68(5)

Table A2.14. Bond Lengths [\AA] and Angles [$^\circ$] for NHS22 (CCDC 701671).

Pd(1)-O(4)	2.0051(13)	C(53)-C(54)	1.3899
Pd(1)-N(1)	2.0227(15)	C(54)-C(55)	1.3899
Pd(1)-O(2)	2.0704(14)	C(55)-C(56)	1.3899
Pd(1)-P(1)	2.2072(5)		
P(1)-C(20)	1.8116(18)	O(4)-Pd(1)-N(1)	176.38(7)
P(1)-C(14)	1.8130(17)	O(4)-Pd(1)-O(2)	87.35(6)
P(1)-C(1)	1.8187(18)	N(1)-Pd(1)-O(2)	90.16(6)
O(1)-C(7)	1.340(2)	O(4)-Pd(1)-P(1)	93.81(5)
O(1)-C(8)	1.459(2)	N(1)-Pd(1)-P(1)	88.53(4)
O(2)-C(26)	1.267(3)	O(2)-Pd(1)-P(1)	176.68(5)
O(3)-C(26)	1.230(3)	C(20)-P(1)-C(14)	106.98(8)
O(4)-C(28)	1.298(2)	C(20)-P(1)-C(1)	104.36(8)
O(5)-C(28)	1.210(2)	C(14)-P(1)-C(1)	103.18(8)
N(1)-C(7)	1.285(2)	C(20)-P(1)-Pd(1)	116.35(6)
N(1)-C(9)	1.488(2)	C(14)-P(1)-Pd(1)	117.09(6)
C(1)-C(2)	1.393(2)	C(1)-P(1)-Pd(1)	107.33(6)
C(1)-C(6)	1.399(3)	C(7)-O(1)-C(8)	105.75(15)
C(2)-C(3)	1.386(3)	C(26)-O(2)-Pd(1)	115.15(13)
C(3)-C(4)	1.366(3)	C(28)-O(4)-Pd(1)	119.55(12)
C(4)-C(5)	1.396(3)	C(7)-N(1)-C(9)	108.64(14)
C(5)-C(6)	1.399(3)	C(7)-N(1)-Pd(1)	128.56(12)
C(6)-C(7)	1.474(2)	C(9)-N(1)-Pd(1)	122.52(11)
C(8)-C(9)	1.528(3)	C(2)-C(1)-C(6)	118.10(17)
C(9)-C(10)	1.543(3)	C(2)-C(1)-P(1)	120.19(14)
C(10)-C(13)	1.522(3)	C(6)-C(1)-P(1)	121.44(13)
C(10)-C(11)	1.534(3)	C(3)-C(2)-C(1)	121.58(18)
C(10)-C(12)	1.538(3)	C(4)-C(3)-C(2)	120.27(17)
C(14)-C(15)	1.396(2)	C(3)-C(4)-C(5)	119.74(18)
C(14)-C(19)	1.398(2)	C(4)-C(5)-C(6)	120.18(18)
C(15)-C(16)	1.381(3)	C(1)-C(6)-C(5)	120.13(16)
C(16)-C(17)	1.383(3)	C(1)-C(6)-C(7)	122.95(16)
C(17)-C(18)	1.386(3)	C(5)-C(6)-C(7)	116.91(16)
C(18)-C(19)	1.391(2)	N(1)-C(7)-O(1)	116.13(16)
C(20)-C(21)	1.391(3)	N(1)-C(7)-C(6)	129.02(16)
C(20)-C(25)	1.401(3)	O(1)-C(7)-C(6)	114.85(16)
C(21)-C(22)	1.386(3)	O(1)-C(8)-C(9)	104.44(15)
C(22)-C(23)	1.395(3)	N(1)-C(9)-C(8)	100.86(14)
C(23)-C(24)	1.386(3)	N(1)-C(9)-C(10)	113.31(15)
C(24)-C(25)	1.391(3)	C(8)-C(9)-C(10)	115.30(17)
C(26)-C(27)	1.523(3)	C(13)-C(10)-C(11)	109.38(17)
C(28)-C(29)	1.508(3)	C(13)-C(10)-C(12)	107.97(17)
C(41)-C(42)	1.3900	C(11)-C(10)-C(12)	109.33(16)
C(41)-C(46)	1.3900	C(13)-C(10)-C(9)	110.43(15)
C(42)-C(43)	1.3900	C(11)-C(10)-C(9)	111.60(16)
C(43)-C(44)	1.3900	C(12)-C(10)-C(9)	108.05(16)
C(44)-C(45)	1.3900	C(15)-C(14)-C(19)	119.16(16)
C(45)-C(46)	1.3900	C(15)-C(14)-P(1)	121.94(13)
C(51)-C(56)	1.3899	C(19)-C(14)-P(1)	118.89(13)
C(51)-C(52)	1.3899	C(16)-C(15)-C(14)	120.31(17)
C(52)-C(53)	1.3899	C(15)-C(16)-C(17)	120.60(18)

C(16)-C(17)-C(18)	119.57(17)
C(17)-C(18)-C(19)	120.50(17)
C(18)-C(19)-C(14)	119.84(17)
C(21)-C(20)-C(25)	119.83(17)
C(21)-C(20)-P(1)	122.08(14)
C(25)-C(20)-P(1)	118.03(14)
C(22)-C(21)-C(20)	120.22(18)
C(21)-C(22)-C(23)	119.9(2)
C(24)-C(23)-C(22)	120.15(18)
C(23)-C(24)-C(25)	120.20(19)
C(24)-C(25)-C(20)	119.67(19)
O(3)-C(26)-O(2)	126.0(2)
O(3)-C(26)-C(27)	120.2(2)
O(2)-C(26)-C(27)	113.8(2)
O(5)-C(28)-O(4)	125.49(19)
O(5)-C(28)-C(29)	121.8(2)
O(4)-C(28)-C(29)	112.67(17)
C(42)-C(41)-C(46)	120.0
C(43)-C(42)-C(41)	120.0
C(42)-C(43)-C(44)	120.0
C(45)-C(44)-C(43)	120.0
C(44)-C(45)-C(46)	120.0
C(45)-C(46)-C(41)	120.0
C(56)-C(51)-C(52)	120.0
C(53)-C(52)-C(51)	120.0
C(54)-C(53)-C(52)	120.0
C(53)-C(54)-C(55)	120.0
C(56)-C(55)-C(54)	120.0
C(55)-C(56)-C(51)	120.

Table A2.15. Anisotropic Displacement Parameters ($\text{\AA}^2 \times 10^4$) for NHS22 (CCDC 701671). The anisotropic displacement factor exponent takes the form: $-2\pi^2 [h^2 a^{*2} U^{11} + \dots + 2 h k a^* b^* U^{12}]$.

	U ¹¹	U ²²	U ³³	U ²³	U ¹³	U ¹²
Pd(1)	154(1)	215(1)	198(1)	33(1)	10(1)	91(1)
P(1)	168(2)	235(2)	155(2)	-12(2)	0(2)	111(2)
O(1)	503(9)	363(7)	169(7)	-31(6)	1(6)	297(7)
O(2)	215(6)	241(6)	497(9)	81(6)	-1(6)	95(5)
O(3)	408(9)	455(9)	642(12)	-188(9)	-222(8)	274(8)
O(4)	211(6)	421(8)	204(7)	87(6)	44(5)	163(6)
O(5)	254(7)	723(12)	275(9)	70(8)	19(6)	263(8)
N(1)	206(7)	203(7)	201(8)	-22(6)	-14(5)	111(6)
C(1)	186(7)	247(8)	167(9)	5(6)	11(6)	127(6)
C(2)	292(9)	274(9)	253(10)	-41(7)	-12(8)	182(8)
C(3)	288(9)	261(9)	296(11)	8(8)	-14(8)	192(8)
C(4)	287(9)	298(9)	251(10)	70(8)	1(8)	165(8)
C(5)	298(9)	293(9)	177(9)	4(7)	-1(7)	173(8)
C(6)	206(7)	227(8)	177(9)	0(6)	-10(6)	125(6)
C(7)	242(8)	261(8)	147(9)	-24(7)	-21(7)	150(7)
C(8)	549(13)	324(10)	262(11)	-94(8)	-68(10)	295(10)
C(9)	264(8)	200(8)	257(10)	-40(7)	-28(7)	131(7)
C(10)	241(8)	251(8)	288(11)	-29(7)	-5(8)	146(7)
C(11)	234(9)	298(9)	376(12)	-30(8)	56(8)	123(7)
C(12)	380(11)	326(10)	420(13)	-38(9)	22(9)	238(9)
C(13)	300(9)	350(10)	305(11)	53(8)	5(8)	217(8)
C(14)	171(7)	236(8)	176(9)	-42(6)	-9(6)	110(6)
C(15)	207(8)	272(8)	217(10)	28(7)	3(7)	114(7)
C(16)	216(8)	305(9)	247(10)	25(8)	24(7)	100(7)
C(17)	178(7)	315(9)	240(10)	-50(7)	-4(7)	118(7)
C(18)	216(8)	303(9)	219(10)	0(7)	-12(7)	137(7)
C(19)	202(8)	235(8)	192(9)	1(7)	-7(7)	100(7)
C(20)	247(8)	282(8)	148(9)	10(7)	14(6)	172(7)
C(21)	305(9)	327(9)	180(10)	-13(7)	-21(7)	190(8)
C(22)	466(12)	355(10)	154(9)	-16(8)	-4(8)	272(10)
C(23)	585(14)	459(12)	187(10)	107(9)	125(9)	412(11)
C(24)	338(10)	488(12)	306(11)	118(10)	124(9)	310(10)
C(25)	256(8)	346(10)	245(10)	32(8)	28(7)	186(8)
C(26)	203(9)	279(10)	714(17)	-139(10)	-51(10)	145(8)
C(27)	405(15)	366(15)	1990(50)	-300(20)	-360(20)	195(13)
C(28)	242(8)	367(10)	259(11)	99(8)	61(7)	190(8)
C(29)	355(11)	785(18)	247(12)	114(11)	89(9)	361(12)

Chapter 3

Solution Structure and Behavior of Palladium Allyl Carboxylates and Carbonates[†]

3.1 Introduction

By monitoring the palladium-catalyzed decarboxylative allylic alkylation of allyl β -ketoester **7**, palladium carboxylate **31** was discovered and subsequently isolated (Scheme 3.1 on page 132).¹ Carboxylate **31** was identified as a significant intermediate in this reaction and determined to be the resting state of the active catalyst.¹ Carboxylate **31** and its subsequently synthesized parent **32** represent a series of unusual palladium η^1 -allyl carboxylate complexes with previously unstudied properties (Figure 3.1 on page 132). Beyond the actual role of carboxylate **31** in the allylic alkylation reaction, carboxylates **31** and **32** are thought to represent the best isolable model systems currently available for the elusive and important intermediate, palladium enolate **27**.^{2,3} Carboxylates **31** and **32** may also represent potentially significant model systems for the study of other palladium-catalyzed reactions, such as allylic oxidation^{4,5} and 1,4-diacetoxylation.^{4,6} As a result, the nature of the solution structures and dynamic behavior

[†] This work was done in collaboration with Dr. David VanderVelde.

of palladium allyl carboxylates **31** and **32** are potentially relevant to the mechanistic understanding of a number of different palladium-catalyzed reactions. To this effect, a thorough study of the solution structure and chemical behavior of isolated samples of carboxylates **31** and **32** was undertaken.

Scheme 3.1. Initial Observation of Palladium Allyl Carboxylate **31**

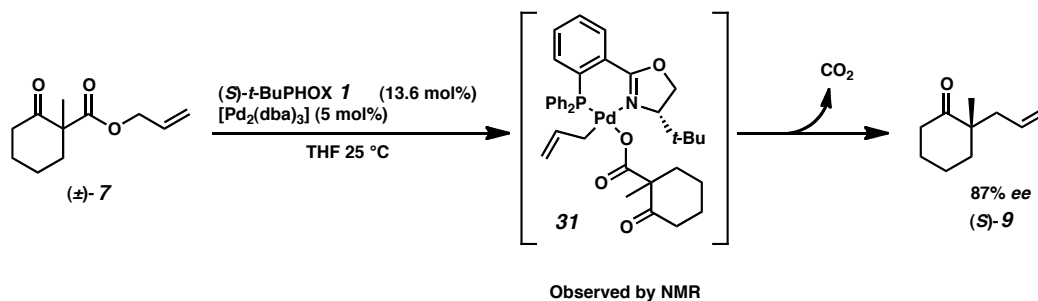
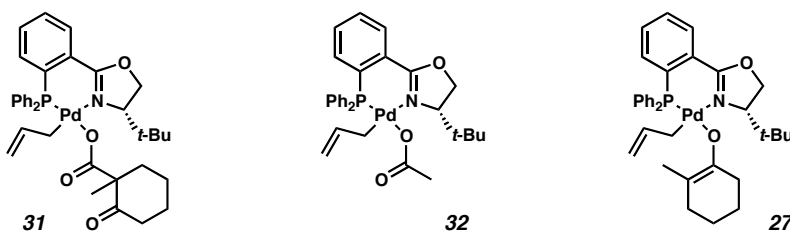


Figure 3.1. Palladium η^1 Allyl Species of Interest to the Study of Allylic Alkylation



3.2 Analyzing Solution Structure and Chemical Behavior via NMR

3.2.1 The Solution Structure of Carboxylates **31** and **32**

Examining complexes **31** and **32** by 1D and 2D NMR methods revealed that even at -20 °C these species possess a significant amount of dynamic chemical behavior when dissolved in THF_{d,8}. It is clear by NMR that the structures found in the solid state for complexes **31** and **32**, consisting of an η^1 -allyl ligand *cis* to an associated carboxylate ligand, is the dominant structure found for these species in solution as well. While 2D

^1H - ^1H NOESY and ROESY spectra helped confirm these solution structures,⁷ the strongest indication of the allyl ligand hapticity actually came from the 1D ^1H and ^{13}C NMR chemical shifts for the allyl ligands (Figure 3.2 on page 133 and Figure 3.3 on page 134). The resonances found for the allyl ligand in complexes **31** and **32** are consistent with those of other fully characterized and highly related palladium η^1 -allyl complexes reported in the literature.^{8,9}

The 1D ^{13}C NMR spectrum was the most sensitive tool for distinguishing between the η^1 and η^3 allyl ligands. While still noticeably shifted, the ^{13}C NMR chemical shifts for the allyl ligands of complexes **31** and **32** are closer to those found in free propene when dissolved in THF_{d-8} than they are to those found in the corresponding π -allyl cation **25** (Figure 3.2).¹⁰ The increased delocalization of the π -allyl ligand in **25** causes the chemical shifts for the protons and carbons found in the allyl ligand to shift inwards towards one another relative to the same resonances found in the complexes with η^1 -allyl ligands. This chemical shift averaging effect for the atoms in the allyl ligand of cation **25** is also manifested more strongly in the carbon spectrum than it is in the proton (Figure 3.2).

Figure 3.2. Characteristic η^1 and η^3 Allyl ^{13}C NMR Shifts (δ) Found for **31**, **32**, and **25** in THF_{d-8}

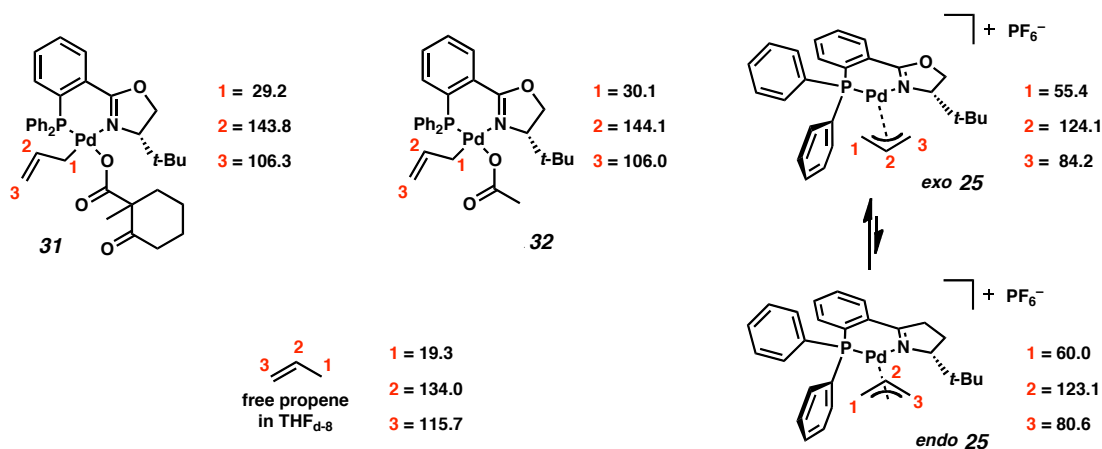
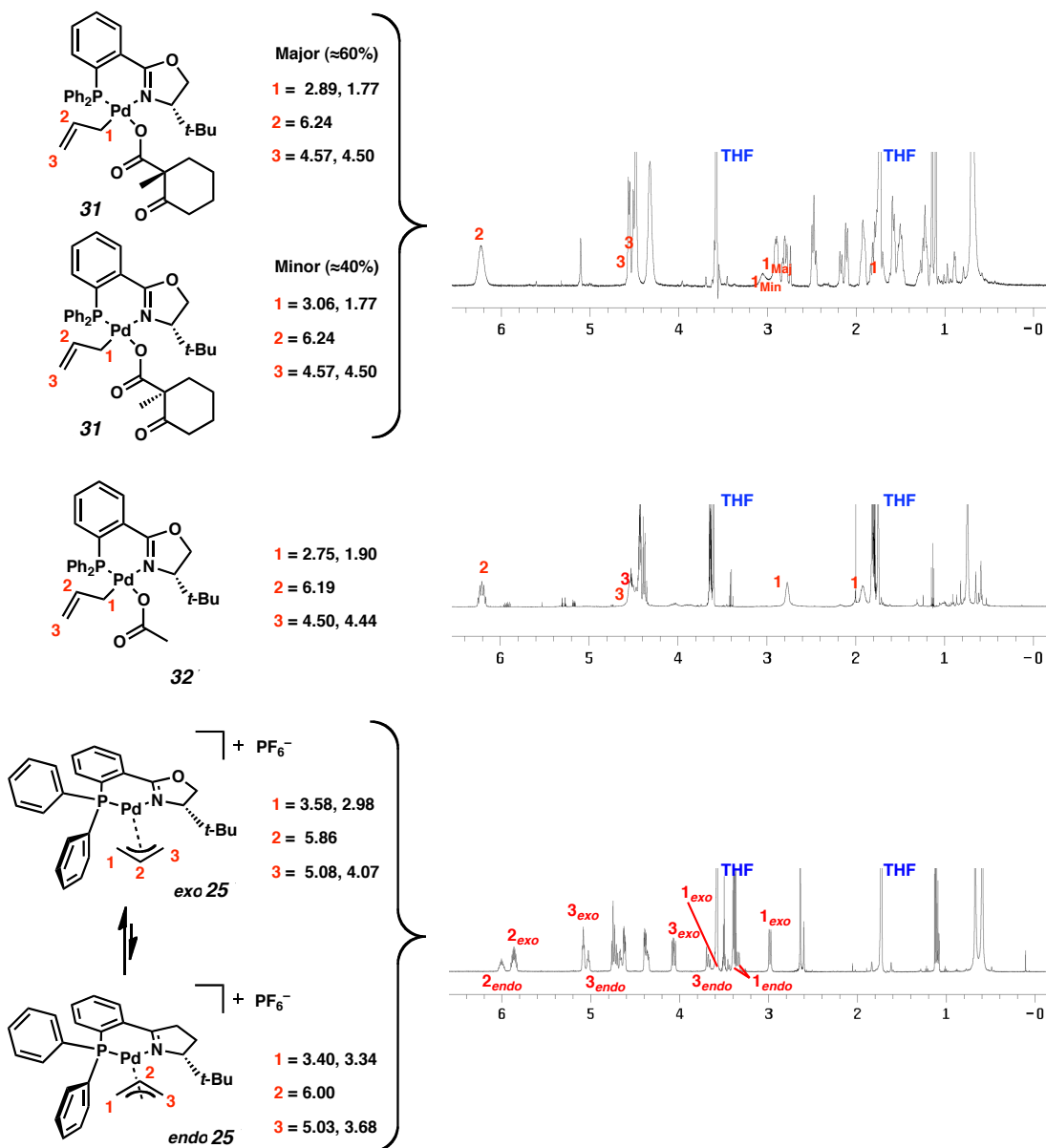


Figure 3.3. Characteristic η^1 and η^3 Allyl ^1H NMR Shifts (δ) Found for **31**, **32**, and **25** in THF_{d-8} 

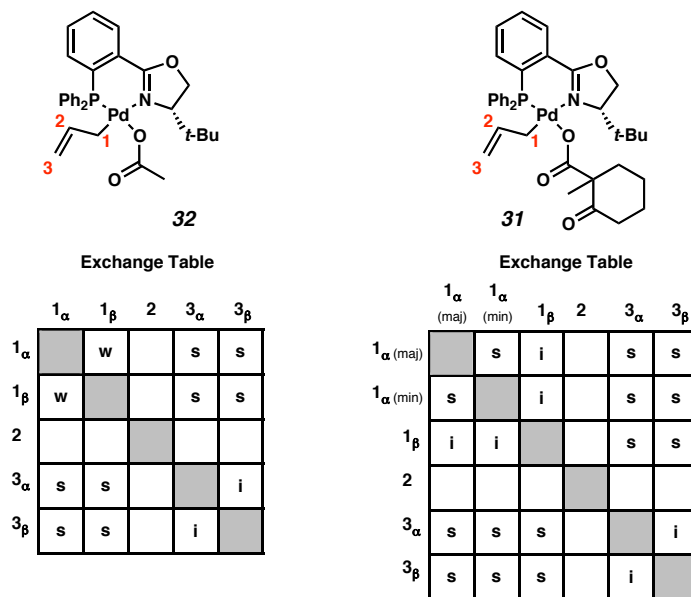
^1H NMR spectra of complexes **31**, **32**, and **25** in THF_{d-8} . The spectra were taken at -20°C for the stability of complex **31** which is prone to thermal decomposition near room temperature. Temperature was the same across all three spectra for the sake of comparison. The region highlighted, is $\delta = 6.8$ to -0.2 ppm.

3.2.2 The Chemical Behavior of Carboxylates **31** and **32** in Solution

Much of the dynamic chemical behavior of complexes **31** and **32** in THF solution occurring on the NMR time scale can be observed directly as chemical exchange in the

corresponding 2D EXSY NMR spectrum.¹¹ The exchange patterns found for both complexes **31** and **32** indicate complete allyl termini exchange (Figure 3.4 on page 135).¹² EXSY cross peaks show that the two vinyl termini protons ($3_\alpha \leftrightarrow 3_\beta$) and the two alkyl protons ($1_\alpha \leftrightarrow 1_\beta$) of the allyl ligands in carboxylates **31** and **32** rapidly interconvert with one another on the NMR timescale even at temperatures as low as -20°C in THF_{d-8} . While implied, the cross-peaks indicating interconversion of the two protons at each termini between one another (i.e., $1_\alpha \leftrightarrow 1_\beta$ and $3_\alpha \leftrightarrow 3_\beta$) for complexes **31** and **32** do not show up well in the EXSY spectra. This is because the corresponding EXSY cross-peaks are eclipsed by strong through space NOESY and ROESY cross-peaks of the opposite phase.¹³

Figure 3.4. Allyl Termini Exchange Patterns for **31** and **32**¹²

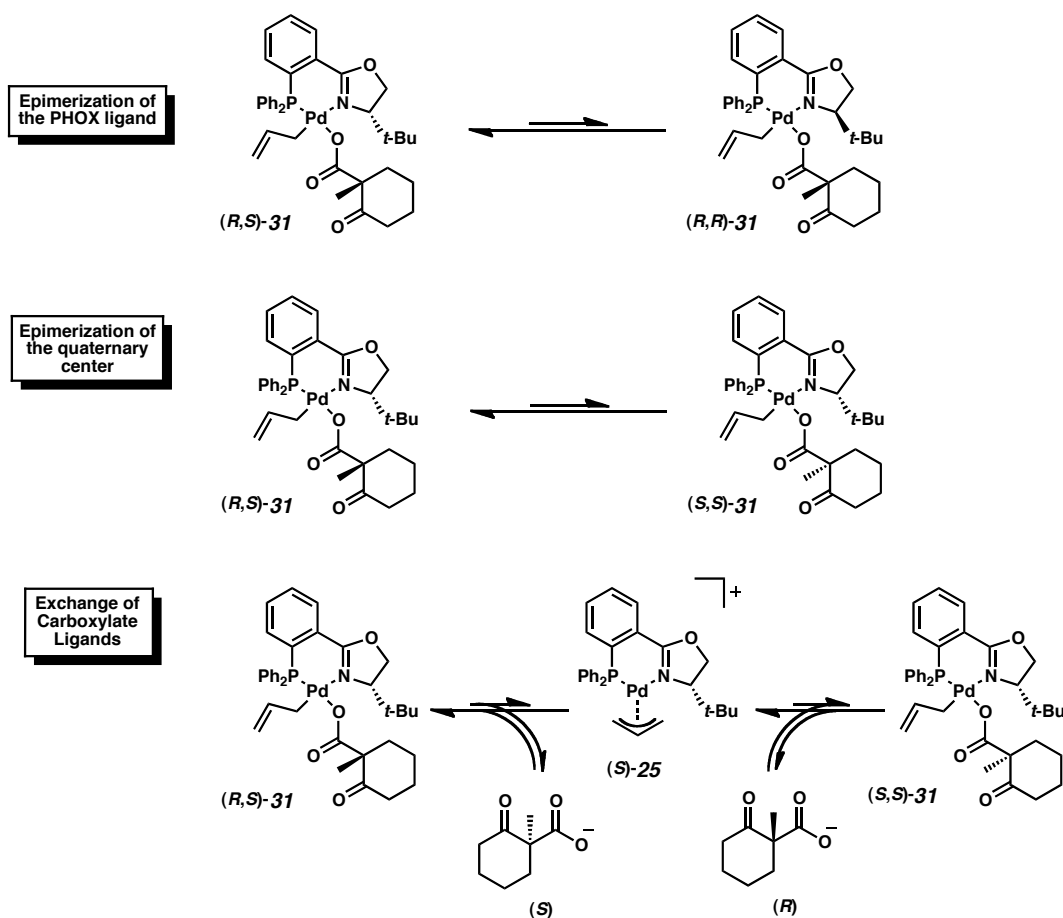
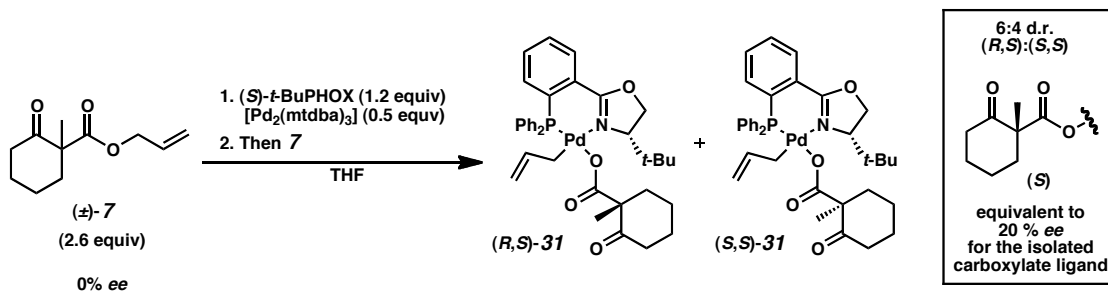


Exchange tables showing which protons exchange with each other on an NMR timescale in THF_{d-8} for **32** at 0°C and for **31** -20°C ¹²

The exchange patterns documented in Figure 3.4 indirectly imply a more elaborate pattern of chemical behavior for complexes **31** and **32**, as rapid allyl termini

exchange is generally not observed for stable palladium η^1 -allyl complexes directly.^{8c,14} Complete allyl termini exchange is, however, highly consistent with the reported solution behavior for a large number of palladium π -allyl complexes.¹⁵ Indeed evidence of significant, but transient, η^3 -allyl behavior is observed by NMR for both complexes **31** and **32** in solution. One of the most compelling indications of this is found in the EXSY NMR exchange between the diastereotopic alkyl methylene protons between the two diastereomers of palladium allyl carboxylate **31** (i.e., $1_{\alpha\text{-maj}} \leftrightarrow 1_{\alpha\text{-min}}$ in the exchange table for **31** in Figure 3.4 on page 135).

There are only three theoretical mechanisms that can explain chemical exchange between the two diastereomers of **31**: rapid racemization of the PHOX ligand, rapid racemization of the all-carbon quaternary stereocenter on the carboxylate ligand, or rapid exchange of the carboxylate ligands between palladium allyl species (Scheme 3.2 on page 137).¹⁶ Rapid racemization of the PHOX ligand in THF cannot be possible or else the enantioenriched allylic alkylation product, ketone **9** (Scheme 3.1 on page 132), produced by carboxylate **31** would be formed almost racemically under reaction conditions. Rapid racemization of the carboxylate all-carbon quaternary stereocenter is not possible as the stereochemical purity of this quaternary center is actually modestly amplified when synthesizing carboxylate **31** from racemic allyl β -ketoester **7** (Scheme 3.3 on page 137).¹⁷ Similarly, ^1H NMR shows that the d.r. for isolated samples of **31** does not change over time in solution, disproving the hypothetical epimerization processes of the quaternary center. However, the rapid exchange of potentially labile anionic ligands, such as a carboxylate, between palladium(II) allyl species, is both feasible and well preceded.¹⁸

Scheme 3.2. The Three Possible Mechanisms for Chemical Exchange Between (R,S) and (S,S) **31**Scheme 3.3. Stereochemical Enrichment of The Quaternary Center in the Synthesis of **31**

Thus, the observed diastereotopic chemical exchange cross-peak for carboxylate **31** is indicative of a particularly rapid exchange of carboxylate between individual molecules of **31**. Given the high degree of similarity between complexes **31** and **32**, it is expected that acetate ligands exchange rapidly between molecules of **32**

when in solution. However, the lack of diastereomers in carboxylate **32** eliminates the possibility of EXSY cross-peaks that could indicate this exchange.

In the absence of a carboxylate or other coordinating ligand, complexes **31** and **32** have a preferred η^3 -allyl structure as demonstrated by their corresponding π -allyl cation **25**. Complexes **31** and **32** should therefore be in equilibrium with π -allyl cation **25** at least transiently while carboxylate ligands are being exchanged between the molecules of these complexes.¹⁹ As π -allyl cation **25** is in equilibrium with carboxylates **31** and **32**, it would be reasonable to consider that **25** might be the source of the complete allyl termini scrambling observed for carboxylates **31** and **32**.

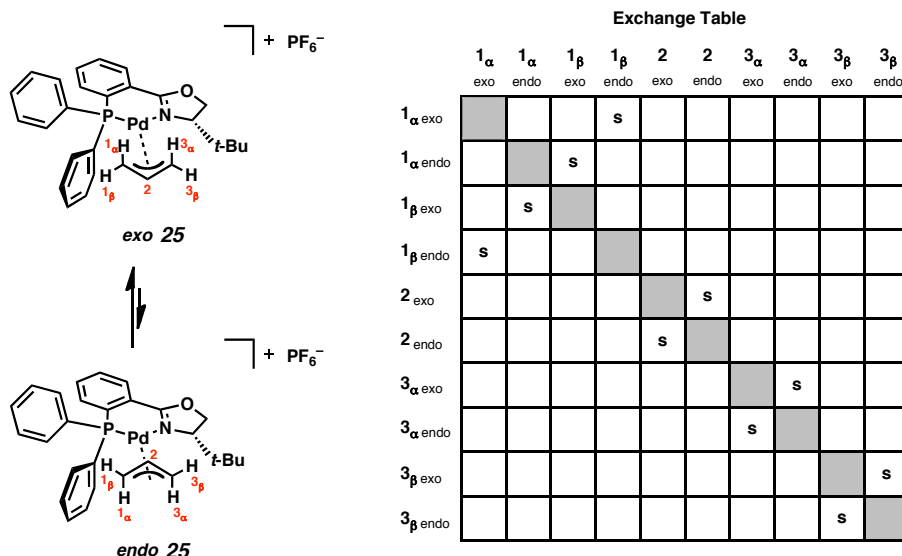
3.3 Analyzing the Solution Behavior of π -Allyl Cation **25** by NMR

3.3.1 EXSY Spectra for π -Allyl Cation **25**

Surprisingly, the 2D NMR EXSY spectrum of palladium π -allyl cation **25** exhibits a far simpler pattern of chemical exchange than either complex **31** or **32** (Figure 3.5 on page 139). The EXSY spectrum of palladium π -allyl cation **25** is consistent with only a single exchange pathway between its *endo* and *exo* isomers through a simple η^3 - η^1 - η^3 allyl isomerization. While two such isomerization paths are possible, only the η^3 - η^1 - η^3 allyl isomerization event where the η^1 -allyl intermediate is *trans* to the sp^2 nitrogen is observed for π -allyl cation **25** (Figure 3.6 on page 139).²⁰ Significantly this corresponds to the same regioselective *trans*-N η^1 -allyl isomer as seen in carboxylate complexes **31** and **32**. While most palladium π -allyl complexes exhibit a more intricate suite of allyl isomerization modes,²³ related palladium PHOX complexes,²⁰ as well as

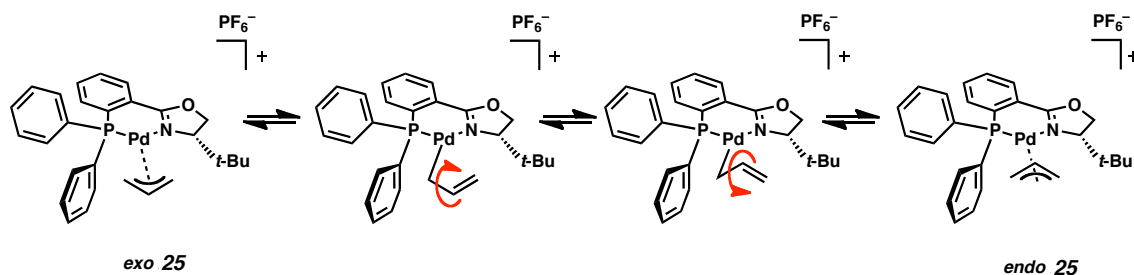
other more distant ligand frameworks,²¹ have also given rise to palladium π -allyl complexes that exhibit only a single regioselective η^3 - η^1 - η^3 allyl isomerization mode as is observed for complex **25**.

Figure 3.5. Allyl Exchange Pattern Between Endo and Exo **25**¹²



Exchange table showing which protons exchange on an NMR timescale in THF_{d-8} for **25**. The depicted exchange pattern is constant from -25 °C up to where complex **25** approaches coalescence at 60 °C.¹²

Figure 3.6. The Only Allyl Isomerization Mode Observable for **25**.

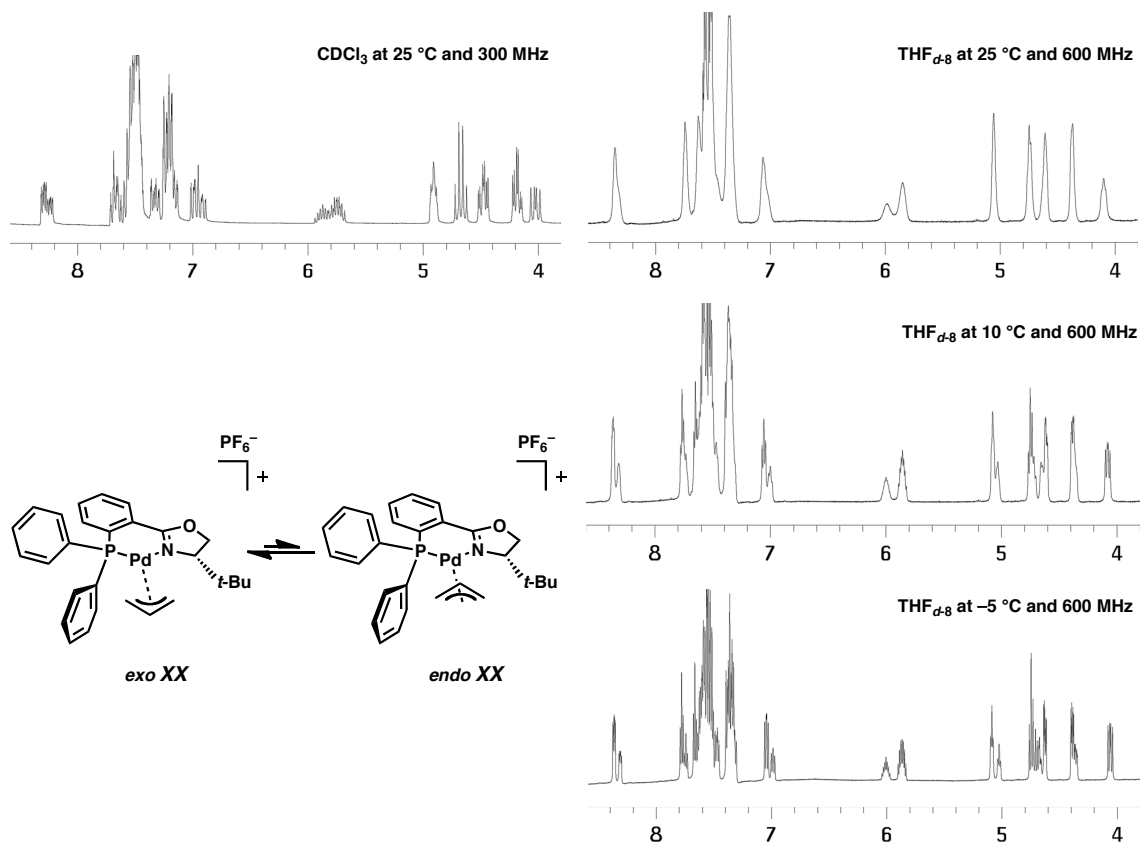


3.3.2 Analyzing the Exo/Endo Isomerization Mechanism of **25**

Saturation transfer NMR techniques were used to obtain the kinetics data for the allyl isomerization of **25** in THF_{d-8} and an Eyring plot was constructed. The activation

parameters thus determined show a negative entropy of activation (Figure 3.8 on page 141).¹² Similarly while the ^1H NMR spectra of **25** is sharp and well resolved at 25 °C in CDCl_3 , the same spectra in the less polar but more strongly coordinating solvent $\text{THF}_{d,8}$ is poorly resolved (Figure 3.7 on page 140). This is a result of allyl isomerization accelerating from slow exchange, observed in CDCl_3 at 25 °C, to a point approaching intermediate exchange, observed in $\text{THF}_{d,8}$ at 25 °C. Cooling solutions of **25** in $\text{THF}_{d,8}$ down to -5 °C or below produces sharp, well-resolved resonances like those seen in CDCl_3 at 25 °C. This is indicative of the allyl isomerization being accelerated by THF, and then approaching the slower rate of isomerization found in CDCl_3 when the THF solution is cooled.

Figure 3.7. ^1H NMR Broadening Indicating $\text{THF}_{d,8}$ Accelerated Allyl Isomerization Relative to CDCl_3



The addition of 4.4 equivalents of water, a modest but slightly superior nucleophile relative to THF, more than doubled the rate of the allyl isomerization as measured by saturation transfer (Figure 3.8 on page 141). Altogether, this data indicates that the $\eta^3\text{-}\eta^1\text{-}\eta^3$ allyl isomerization mode for palladium π -allyl cation **25** functions via an associative mechanism. By this mechanism, nucleophiles, such as THF, water, and carboxylate anions, can associate with π -allyl complex **25** and facilitate a *trans*-N regioselective $\eta^3\text{-}\eta^1\text{-}\eta^3$ allyl isomerization with bond rotation (Figure 3.9 on page 142 and Figure 3.10 on page 142).²² Similar associative $\eta^3\text{-}\eta^1\text{-}\eta^3$ allyl isomerization mechanisms have been reported for other palladium π -allyl complexes.^{18b} Ironically, this means that the mechanism for the only observed allyl isomerization mode active in π -allyl complex **25** between -25 and 60 °C requires species like carboxylates **31** and **32** as intermediates.

Figure 3.8. Activation Parameters for Exo/Endo Allyl Isomerization of **25**

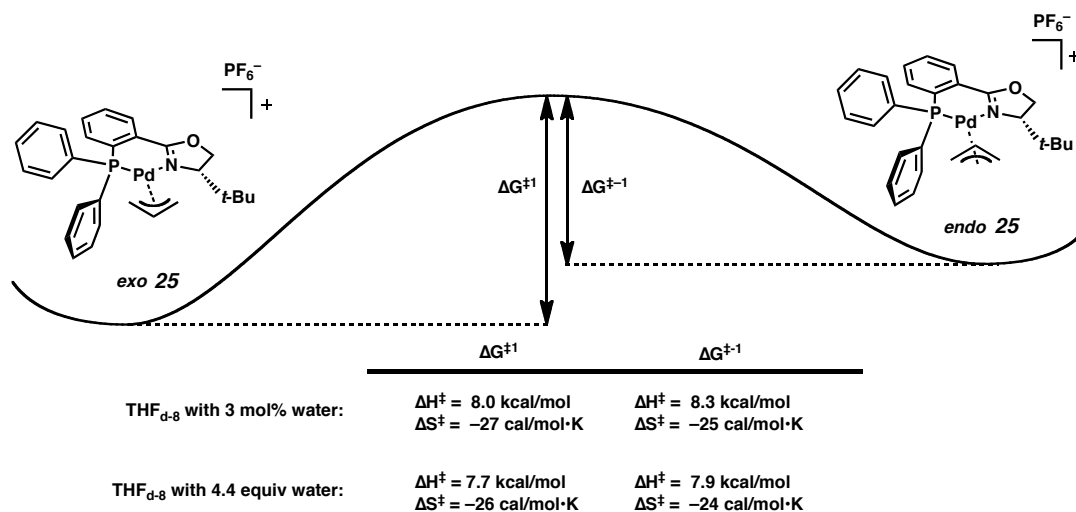
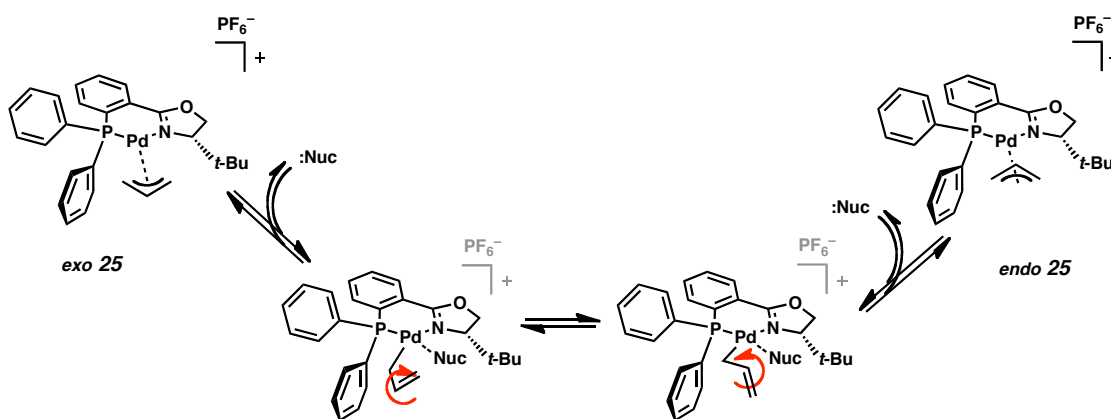
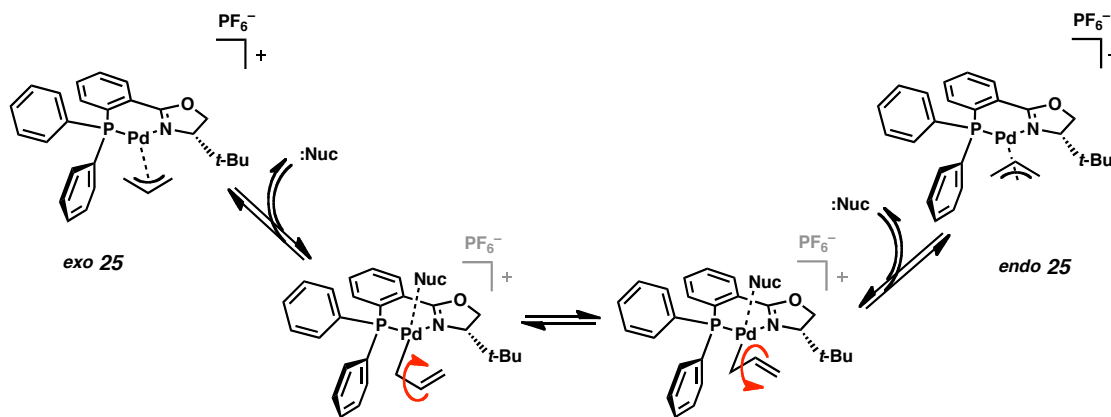


Table 3.1. Some Select Rates and the Effects of Water on the Exo/Endo Allyl Isomerization of **25**

	<i>exo</i> → <i>endo</i>	<i>endo</i> → <i>exo</i>
3.04 mol% water:	5°C = 4.49 s ⁻¹	5°C = 7.40 s ⁻¹
	-5°C = 2.36 s ⁻¹	-5°C = 3.88 s ⁻¹
	-10°C = 1.80 s ⁻¹	-10°C = 2.88 s ⁻¹
4.4 equiv water:	5°C = 9.56 s ⁻¹	5°C = 15.86 s ⁻¹
	-5°C = 5.83 s ⁻¹	-5°C = 13.53 s ⁻¹
	-10°C = 4.08 s ⁻¹	-10°C = 7.31 s ⁻¹

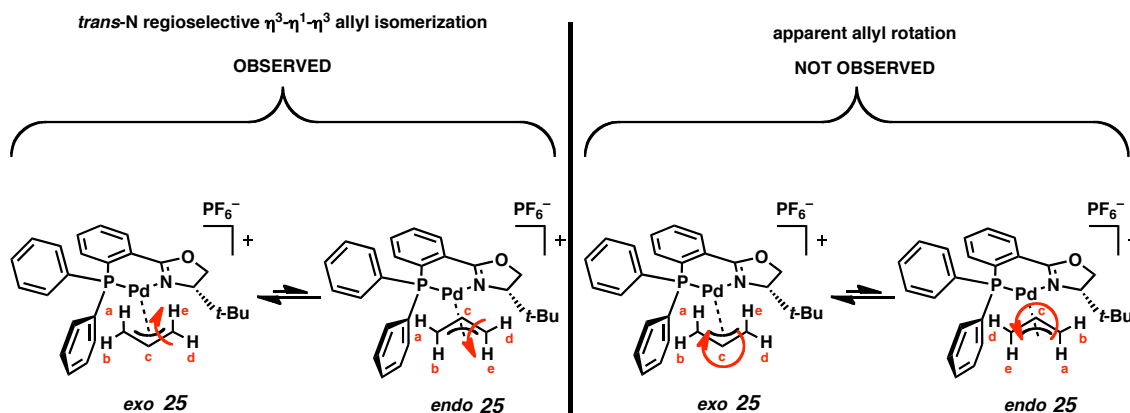
Figure 3.9. Equatorial Associative Exo/Endo Allyl Isomerization Mechanism of **25** as Demonstrated for Carboxylate Nucleophiles by Complexes **31** and **32**²²Figure 3.10. Possible Apical Associative Exo/Endo Allyl Isomerization Mechanism of **25**²²

3.3.3 No Allyl Termini Scrambling Caused by π -Allyl Cation **25**

The simple regioselective η^3 - η^1 - η^3 allyl isomerization pathway demonstrated by palladium π -allyl cation **25** cannot interchange all of the allyl termini protons. For the complete allyl termini exchange seen in carboxylate complexes **31** and **32** to be a result

of allyl isomerization from π -allyl cation **25**, other common allyl isomerization modes would be necessary. At a bare minimum, π -allyl cation **25** would need an apparent allyl rotation isomerization mode in addition to the observed regioselective *exo/endo* exchange path to be able to completely exchange all the protons in the allyl ligand termini (Figure 3.11 on page 143).²³

Figure 3.11. Minimum Isomerization Modes Necessary for **25** to Facilitate Complete Allyl Termini Exchange as Observed for Carboxylates **31** and **32**



To this effect, additional isomerization modes were sought for π -allyl cation **25** at higher temperatures. Examining both the ^1H and EXSY NMR spectra for π -allyl cation **25** in THF_{d-8} taken at $60\text{ }^\circ\text{C}$ showed the simple regioselective *trans-N* $\eta^3\text{-}\eta^1\text{-}\eta^3$ isomerization mode approaching complete coalescence. However, no new allyl isomerization pathways could be observed for π -allyl cation **25** in the EXSY spectrum. This eliminates the possibility that other allyl isomerization modes, possibly accelerated by the presence of carboxylate anions, could be active for π -allyl cation **25** at $-25\text{ }^\circ\text{C}$ but too slow to be observed by NMR at that temperature. As a result, the complete allyl termini exchange of carboxylate complexes **31** and **32** cannot be explained via the chemical behavior of the corresponding π -allyl cation **25** with which they are in

equilibrium. The allyl termini scrambling observed in carboxylates **31** and **32** must instead be the result of a mechanism that does not directly involve π -allyl cation **25**.

3.4 Allyl Termini Scrambling via Oxidative Addition and Reductive Elimination

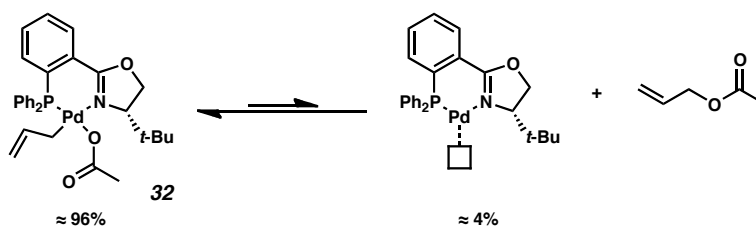
3.4.1 The Oxidative Addition and Reductive Elimination Equilibrium

The chemical process that gives a more satisfying explanation for the rapid and complete allyl termini exchange found in carboxylate complexes **31** and **32** is reductive elimination and oxidative addition. While little direct evidence of such an equilibrium can be observed for carboxylate complex **31**, the equivalent equilibrium is clearly visible in solution for the parent allyl acetate complex **32**. All samples of allyl acetate complex **32**, despite being verified as pure in the solid state by both elemental analysis and X-ray crystallography, show traces of other species in solution by NMR (Figure 3.12 on page 146). Of note, NMR integration shows that these minor species have a constant ratio of composition across different batches of **32**. This suggests that these species are part of an equilibrium involving carboxylate **32**.

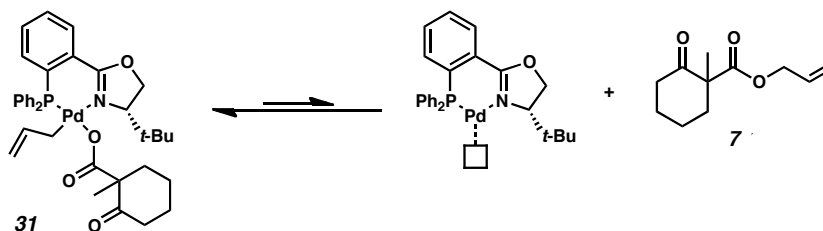
The majority of these minor complexes are too weak to be fully analyzed by most spectrographic means (approximately less than 1% composition in solution) making them difficult to analyze. However, there is a second complete set of resonances representing about 4% of the mass balance based on integration in both the ^1H and ^{31}P NMR (circled resonances in the middle and top spectra in Figure 3.12). This second set of 4% intensity resonances corresponds to free allyl acetate,¹⁰ and what is believed to be either [$\{(S)\text{-}t\text{-BuPHOX}\}\text{Pd}(0)$] or its corresponding solvento complex (allyl acetate resonances circled

in blue in the middle spectrum and compared to free allyl acetate in the bottom spectrum, $[\{(S)\text{-}t\text{-BuPHOX}\}\text{Pd}(0)]$ resonances circled in red in the top and middle spectra in Figure 3.12). This suggests that carboxylate complex **32** is part of a rapid equilibrium involving the reductive elimination and oxidative addition of allyl acetate (Scheme 3.4 on page 145). By analogy, carboxylate complex **31** is believed to be involved in a similar equilibrium (Scheme 3.5 on page 145). Related equilibria between palladium π -allyl cations with carboxylate counter ions and the corresponding allylic esters are well preceded in the literature (Scheme 3.6 on page 145).²⁴

Scheme 3.4. Allyl Acetate Reductive Elimination and Oxidative Addition Observed for **32** in $\text{THF}_{d,8}$



Scheme 3.5. Implied Equilibrium for Carboxylate **31** by Analogy to **32**



Scheme 3.6. Select Examples of Previously Reported Systems with Palladium Allyl Species in Equilibrium with Allyl Carboxylates^{24a,b}

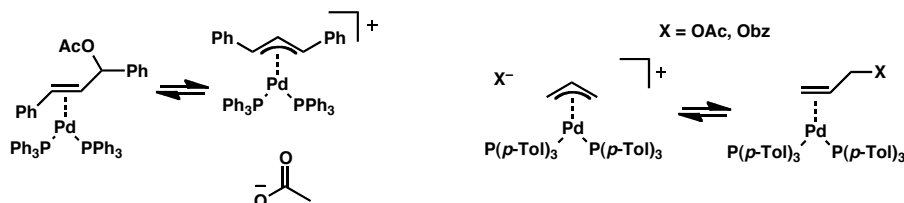
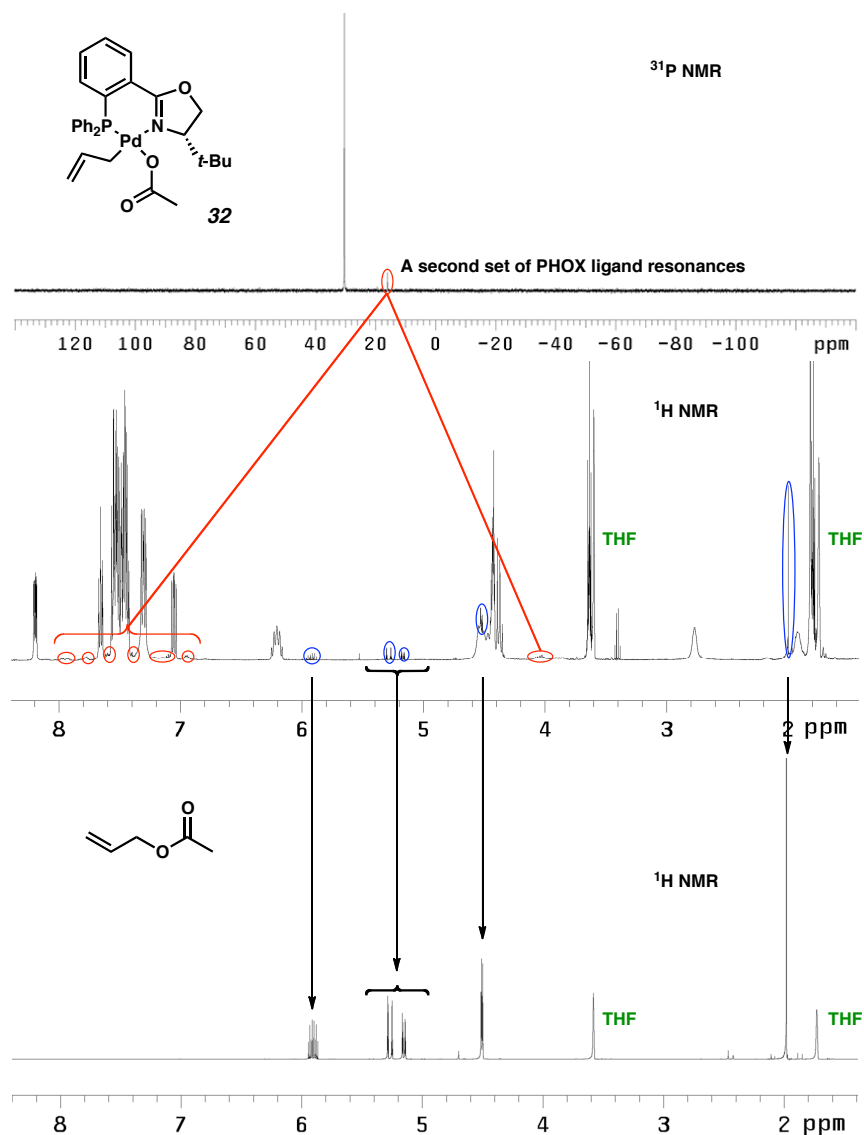


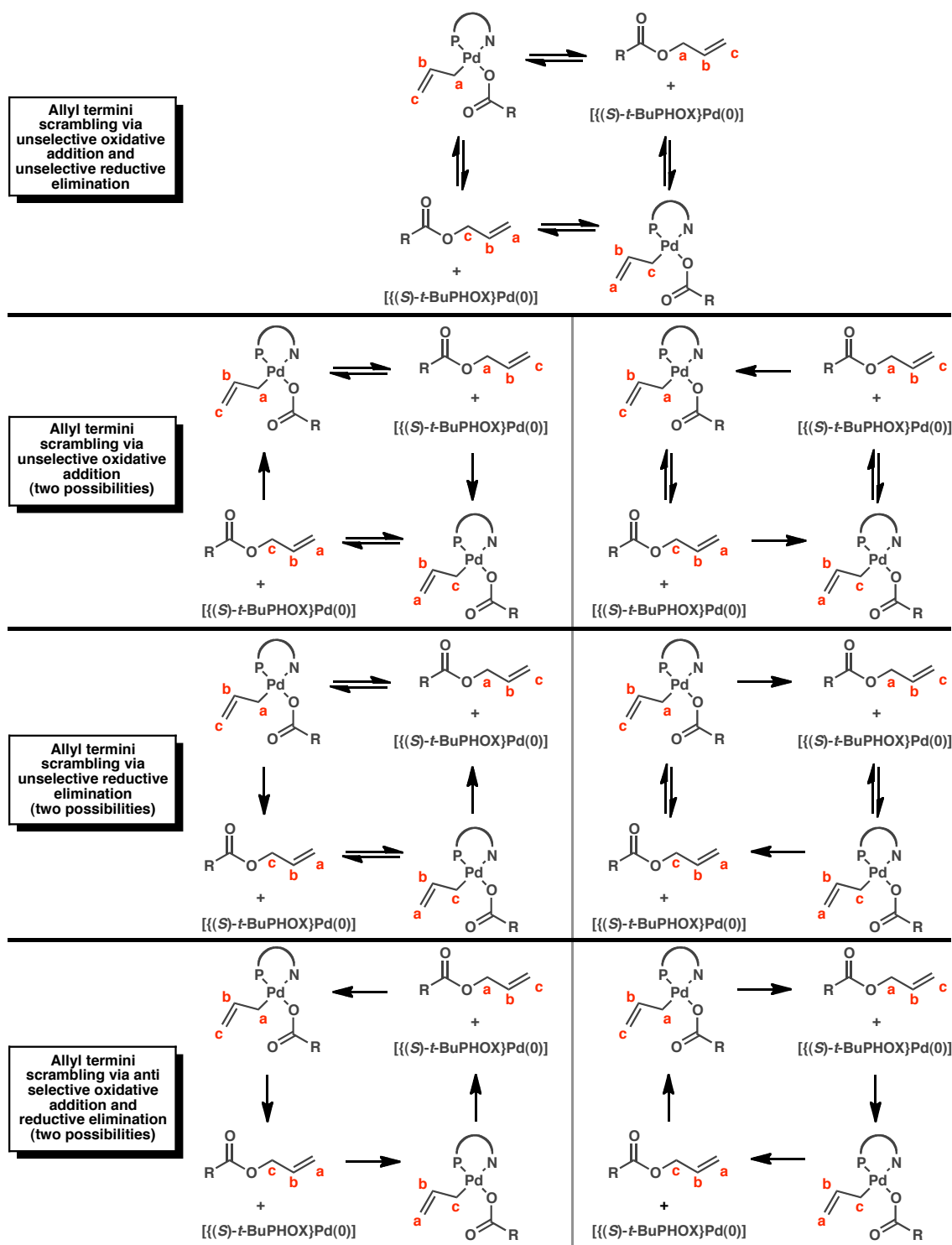
Figure 3.12. Apparent Free Allyl Acetate and Second Palladium Species in Equilibrium with **32**

Top spectrum: ^{31}P NMR in THF_{d-8} of a pure sample of complex **32** reveals a second minor phosphorous resonance upfield of the resonance associated with complex **32**. This minor resonance corresponds to about 4% of the total phosphorus integration. Middle spectrum: ^1H NMR in THF_{d-8} of the same sample of complex **32** shows a second set of PHOX ligand proton resonances. These resonances integrate 4:96 against the corresponding PHOX ligand resonances associated with **32**. The middle spectrum also shows a set of resonances that appear to correspond to free allyl acetate. Bottom spectrum: ^1H NMR in THF_{d-8} of free allyl acetate showing a perfect match to the allyl acetate resonances found in the middle spectrum.

3.4.2 Possible Mechanisms for Allyl Termini Scrambling

The equilibrium for complexes **31** and **32** consisting of facile reductive elimination and oxidative addition of allyl carboxylates, can easily account for the rapid and complete allyl termini scrambling observed for these complexes. There are four general mechanisms by which this scrambling could be possible via this equilibrium. Both reductive elimination and oxidative addition could be only weakly or even non-regioselective (top scenario pictured in Figure 3.13 on page 148). Either reductive elimination, or oxidative addition could be only weakly or even non-regioselective while its reverse is selective (middle four scenarios pictured in Figure 3.13). Oxidative addition and reductive elimination could both be regioselective but with strong preferences towards opposite termini of the allyl group from one another (bottom two scenarios pictured in Figure 3.13).

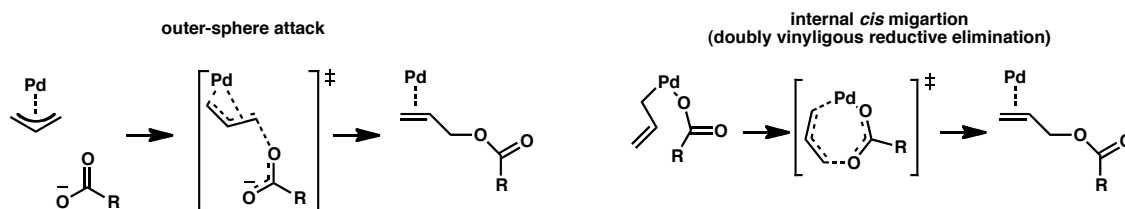
Figure 3.13. Possible Means of Allyl Termini Scrambling via the Allyl Carboxylate Equilibrium



3.5 Examining Selectivity in Reductive Elimination

3.5.1 Literature Precedent For the Reductive Elimination of Allyl Carboxylates

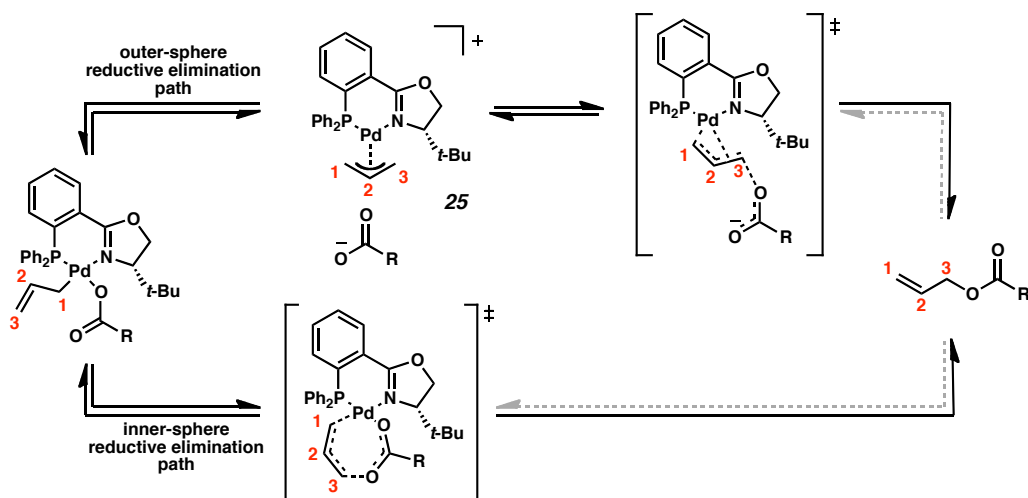
While the possibilities presented in Figure 3.13 (page 148) cannot be narrowed down farther with the current data alone, the literature on related studies recommends only two of the possibilities depicted in Figure 3.13. Much is already understood about the reductive elimination of allylic acetates from palladium(II) centers due to investigation of processes like palladium-catalyzed allylic oxidation and 1,4-diacetoxylation.^{4,5,6} Two competing paths have been reported for the reductive elimination of allylic acetates from palladium species. The first pathway is an outer-sphere attack of an acetate anion on an η^3 -allyl terminus (Figure 3.14 left, on page 150). This mechanism is simply an instance of palladium-catalyzed outer-sphere allylic alkylation of carbon nucleophiles.^{2,4,5,6} The second pathway is an internal *cis* migration of the carboxylate ligand (Figure 3.14 right). This mechanism is synonymous with palladium-catalyzed inner-sphere allylic alkylation via doubly vinylogous reductive elimination.^{2,3,4,5,6} Thus, the formation of allylic acetates via reductive elimination from palladium(II) allyl acetate species is effectively a specific subset of the well-studied general field of palladium-catalyzed allylic alkylation. Mechanistically this suggests that the reductive elimination of allylic carboxylates from palladium is heavily parallel to the mechanism of palladium-catalyzed allylic alkylation of α - β unsaturated carbon nucleophiles (e.g., ketone enolates).

Figure 3.14. Reported Mechanisms for Palladium Allyl Carboxylate Reductive Elimination^{4,5,6}

3.5.2 Mechanistic Possibilities with Selective Reductive Elimination

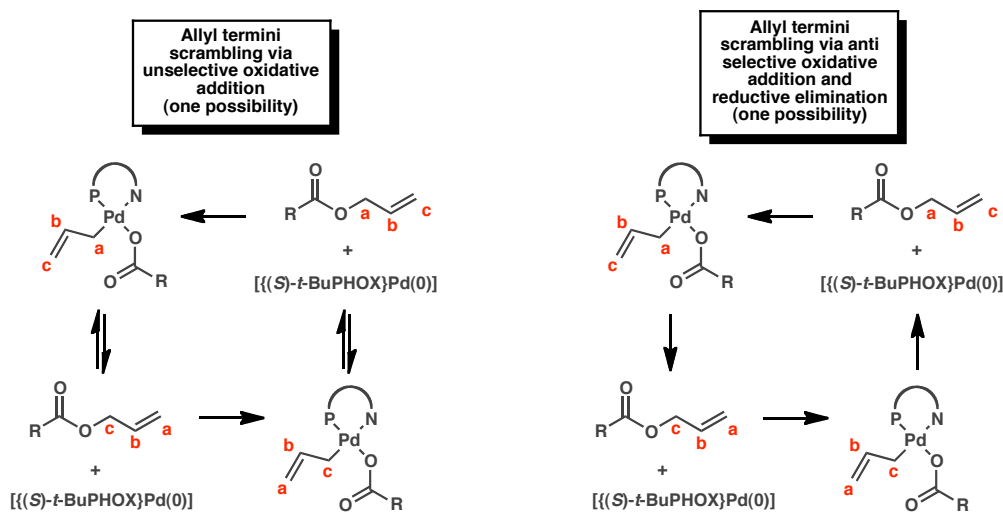
The studies of palladium-catalyzed allylic oxidation suggest that the reductive elimination of allyl acetates from palladium complexes possessing η^1 -allyl ligands *cis* to associated acetate ligands generally prefer to proceed via the inner-sphere doubly vinylogous reductive elimination pathway (Figure 3.14 left on page 150).^{4,5,6} However, the preference between the two mechanisms depicted in Figure 3.14 is expected to be irrelevant for allyl terminus selectivity in reductive elimination from carboxylates **31** and **32**. This is because the literature precedent for both outer-sphere and inner-sphere allylic alkylation with PHOX palladium allyl species universally states that both mechanisms are regioselective to the allyl terminus *trans* to phosphorous (Scheme 3.7 on page 151).^{2,3,25} As a result, regardless of which mechanistic path is preferred or what distribution of both paths may be taken, reductive elimination of allylic carboxylates from complexes **31** and **32** is postulated to have a very high allyl terminus regioselectivity (*trans*-P).

Scheme 3.7. The Same Allyl Terminus Selectivity is Expected for the Two Standard Mechanisms of Allyl Carboxylate Reductive Elimination in PHOX Palladium Allyl Carboxylates.



This would suggest that allyl termini scrambling in this system may actually be a result of oxidative addition. If correct, either oxidative addition of allylic carboxylates is non-selective, or it is anti-selective relative to the reductive elimination pathways (Figure 3.15 on page 151).²⁶ While farther experimentation is necessary to examine the possibility of this mechanistic hypothesis, the two mechanisms for allyl termini scrambling in Figure 3.15 are those most strongly consistent with both the acquired data and the accepted chemical behavior found in the literature.^{2,3,25}

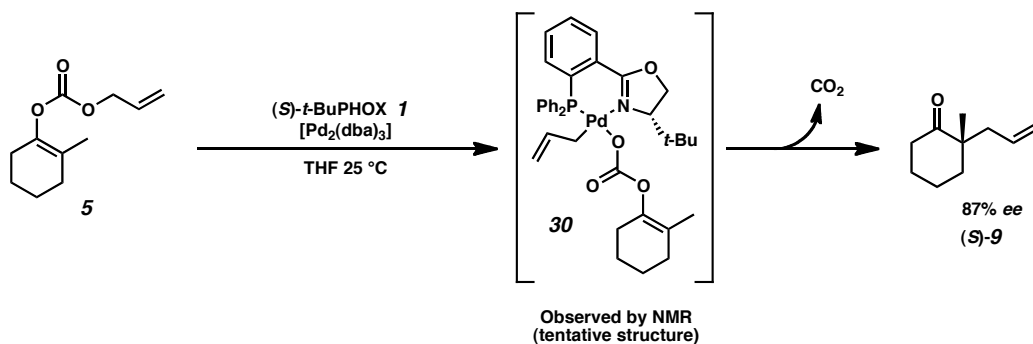
Figure 3.15. Allyl Termini Scrambling Mechanisms Most Consistent with the Literature



3.6 Effects on the Decarboxylative Allylic Alkylation of Ketone Enolates

As carboxylate **31** represents the resting state of the catalyst for decarboxylative asymmetric allylic alkylation of the allyl β -keto ester substrates,¹ by definition, the catalyst spends most of its time as carboxylate **31**. The similar reaction behavior observed for allyl enol carbonate substrates has suggested that there is likely an enol carbonate intermediate (such as **30**) which fills the same roll as carboxylate **31** (Figure 30).¹ Together the chemical behavior of carboxylate **31** and putative carbonate **30** are expected to have a significant impact on the behavior of the reaction as a whole due to their prominence in it. Indeed, it appears that much of the allyl scrambling and exchange behavior that has been observed for the allylic alkylation system can be attributed to **31** and **30**, respectively.

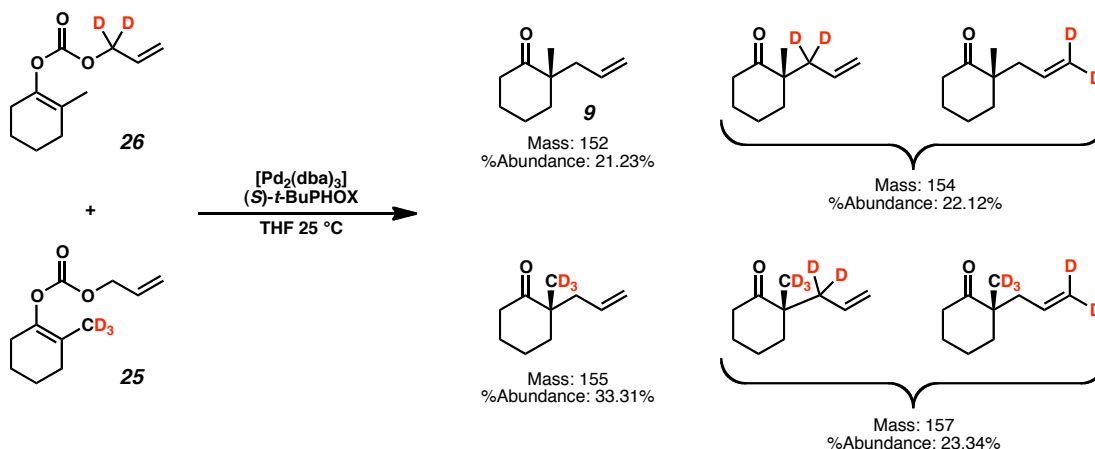
Figure 3.16. Carbonate **30**, the Putative Allyl Enol Carbonate Derived Analogue to Carboxylate **31**



Via a crossover experiment from a previous mechanistic investigation, the decarboxylative asymmetric allylic alkylation was shown to give a product distribution consistent with complete crossover in conjunction with complete allyl termini scrambling (Scheme 3.8 on page 153).^{2,27} Based on our originally proposed mechanism from a previous DFT study,^{2,3} there was no satisfying explanation for the net transfer of enolate fragments that would be necessary to produce crossover. Rationalization of crossover

was especially challenging given the inability of earlier mechanistic studies to demonstrate the presence of a free enolate in solution at any point of the reaction.² Similarly, of the intermediates ascribed to the mechanism from the previous DFT study,^{2,3} only π -allyl cation **25** was considered a possible candidate for producing the allyl termini scrambling seen in the crossover experiment.

Scheme 3.8. Crossover Experiment Shows Complete Crossover and Allyl Termini Scrambling²⁷

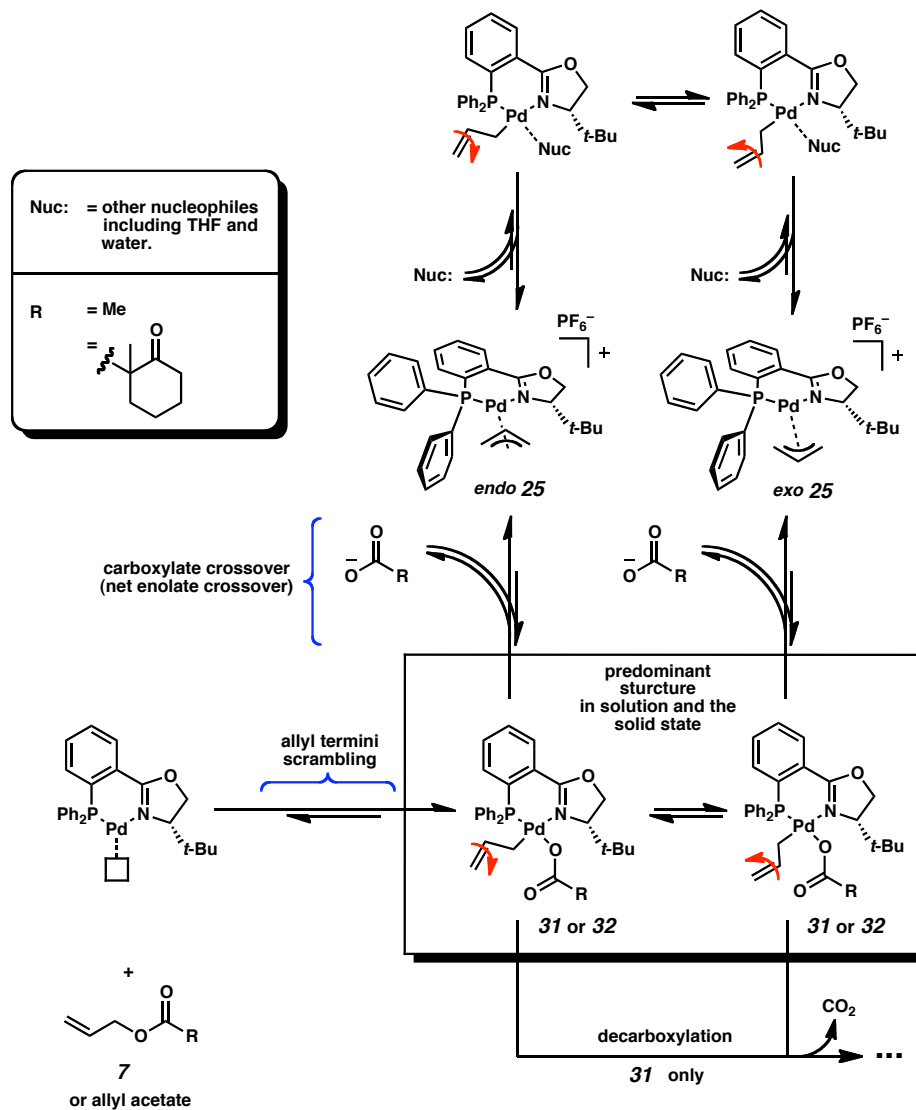


To the contrary, it appears that π -allyl cation **25** has little dynamic behavior in THF solution and is unable to exchange any of the termini for the allyl ligand. Instead, both allyl termini scrambling and crossover are caused by the long-lived intermediates **31** and **30**. Carboxylate **31** demonstrates extremely rapid exchange of carboxylate fragments and allyl termini scrambling even 55 °C below the temperature specified in the standard allylic alkylation conditions. Thus, the solution behavior of carboxylate **31**, and by analogy carbonate **30**, can fully account for the crossover and allyl termini scrambling observed in the products of the decarboxylative asymmetric allylic alkylation.

Specifically, it appears that allyl termini scrambling is the result of some combination of non-selective oxidative addition or reductive elimination of an allylic alkylation substrate to and from species such as **31** and **30**. If so, improving the

selectivity of these elementary steps should yield allylic alkylation conditions that have good regiocontrol over the allyl terminus where allylic alkylation occurs. Altogether a complete picture of the solution chemical behavior for complexes **31**, **32**, and **25** emerges (Figure 3.17 on page 154).

Figure 3.17. Complete Solution Behavior for Complexes **31**, **32**, and **25**



3.7 Experimental Procedures

3.7.1 Materials and Methods

Complexes **31**, **32**, and **25** • PF₆⁻ • 1/2EtOH have been previously characterized and were prepared as previously reported.¹ After synthesis, **25** • PF₆⁻ • 1/2EtOH was dried in vacuo for 24nh before being cycled into a nitrogen glovebox and recrystallized from anhydrous THF and then stored in the glove box. The NMR solvents CDCl₃ and THF_{d-8} were purchased from Cambridge Isotope Laboratories and used as received. THF_{d-8} was purchased as 1 or 0.75 mL ampoules, which were only used in a nitrogen glove box to exclude water. ¹H NMR spectra are reported relative to residual CHCl₃ (δ 7.26)²⁸ or to the downfield proton in residual THF_{d-7} (δ 3.58).²⁸ ¹³C NMR spectra are reported relative to CDCl₃ (δ 77.16)²⁸ or to the downfield carbon in THF_{d-8} (δ 67.21).²⁸ ³¹P NMR spectra are reported relative to H₃PO₄ (δ 0.00) as an external standard consisting of 85% neat phosphoric acid. All filtrations performed in a glove box or otherwise associated directly or indirectly with inorganic or organometallic complexes were performed exclusively with scintillated glass Buchner funnels or using 2.4 mm GF/A Whatman glass microfiber filter paper.

3.7.2 Measuring the Kinetics and Activation Parameters for Exo/Endo Allyl Isomerization in π -Allyl Cation **25** via Saturation Transfer

3.7.2.1 Kinetics Measurements Via Saturation Transfer for π -Allyl Cation **25**

Sample Preparation and Setup: In a nitrogen glove box, 10 mg of the half ethanol adduct of π -Allyl Cation **25** PF₆⁻ salt (14 μ mol, 1 equiv) was weighed into a 1 dram vial. A fresh ampule of THF_{d-8} was opened and added to the vial. The contents

were mixed manually by pipette until all the material had dissolved. This solution was filtered into an NMR tube, which was sealed with an appropriately fitted septum, and the tube was removed from the glove box. For the run with 4.4 equiv water, the intended amount of distilled water (1.1 μL , 1.1 mg, 63 μmol , 4.4 equiv) was added to the solution via a microliter syringe outside the glove box, and the tube was inverted once to mix the contents.²⁹ An initial ^1H NMR spectrum was obtained at 25 $^\circ\text{C}$, and the actual water content was measured by integrating the water resonance against resonances of the π -Allyl Cation **25**.³⁰ The solution was cooled in the NMR down to the highest temperature where the *exo* and *endo* *t*-Bu resonances did not show an appreciable amount of overlap due to the beginnings of coalescence (qualitatively determined to be 10 $^\circ\text{C}$ with 3.04 mol% water, and 5 $^\circ\text{C}$ for 4.4 equiv water). Then measurements (see procedure below) were taken every 5 $^\circ\text{C}$ down to -25 $^\circ\text{C}$ or -30 $^\circ\text{C}$ just into the temperature range that coincides with an apparent change in rate determining step (*vide infra*, see Section 3.7.2.2 on page 159)

Measurement Procedure: At each temperature, a T_1 measurement of both the *exo* and *endo* *t*-Bu group resonances was acquired using a standard inversion recovery method. Two arrays of presaturation experiments were taken which arrayed varying saturation delay times starting at zero. The d_1 for all the presaturation experiments was set to at least five times the measurement for the largest T_1 found between the *t*-Bu resonances at that temperature. The two arrays of presaturation experiments were used to obtain the peak height (h) of the *exo* *t*-Bu resonance when presaturating the *endo* *t*-Bu resonance, and vice versa, at both T_0 [$h(T_0)$ = peak high at zero saturation delay] and T_∞ .

[$h(T_\infty)$ = the height of the asymptote approached by the diminishing resonance across the array of increasing saturation delay times]. The rate constant k was calculated by:

$$k = \frac{h(T_0) - h(T_\infty)}{T_1 \cdot h(T_\infty)}$$

Raw Data and Calculations for 3.04 mol% Water:

T ₁ Measurements for 3.04 mol% Water				
temp (°C)	<i>endo</i> T ₁ (s)	<i>endo</i> T ₁ error	<i>exo</i> T ₁ (s)	<i>exo</i> T ₁ error
-25	0.2418	0.0007074	0.2463	0.0007295
-20	0.2524	0.0005425	0.2562	0.0006287
-15	0.2598	0.001489	0.2662	0.001066
-10	0.2773	0.0006935	0.2815	0.0008757
-5	0.292	0.001097	0.2965	0.001009
5	0.3289	0.0009827	0.3326	0.0007701
10	0.3461	0.001694	0.35	0.001214

Presaturation Measurements for 3.04 mol% Water				
temp (°C)	<i>endo</i> h(T ₀)	<i>endo</i> h(T _∞)	<i>exo</i> h(T ₀)	<i>exo</i> h(T _∞)
-25	360.721	272.416	634.514	493.685
-20	379.217	270.551	678.541	514.621
-15	381.904	246.14	710.52	517.925
-10	340.202	189.119	650.277	431.42
-5	328.49	153.946	649.126	381.766
5	253.17	73.7155	546.659	219.197
10	223.261	49.995	505.922	165.137

Calculated Rates for 3.04 mol% Water		
temp (°C)	k _{<i>exo</i> → <i>endo</i>} (s ⁻¹)	k _{<i>endo</i> → <i>exo</i>} (s ⁻¹)
-25	1.158184509	1.340591269
-20	1.243269603	1.591311447
-15	1.396915326	2.123064957
-10	1.802111957	2.880915814
-5	2.361970598	3.882877273
5	4.491630882	7.40170316
10	5.896143375	10.01348329

Raw Data and Calculations for 4.4 Equiv Water:

T ₁ Measurements for 4.4 Equiv Water				
temp (°C)	<i>endo</i> T ₁ (s)	<i>endo</i> T ₁ error	<i>exo</i> T ₁ (s)	<i>exo</i> T ₁ error
-30	-30	0.2254	0.0006561	0.2286
-25	-25	0.2361	0.0004719	0.2397

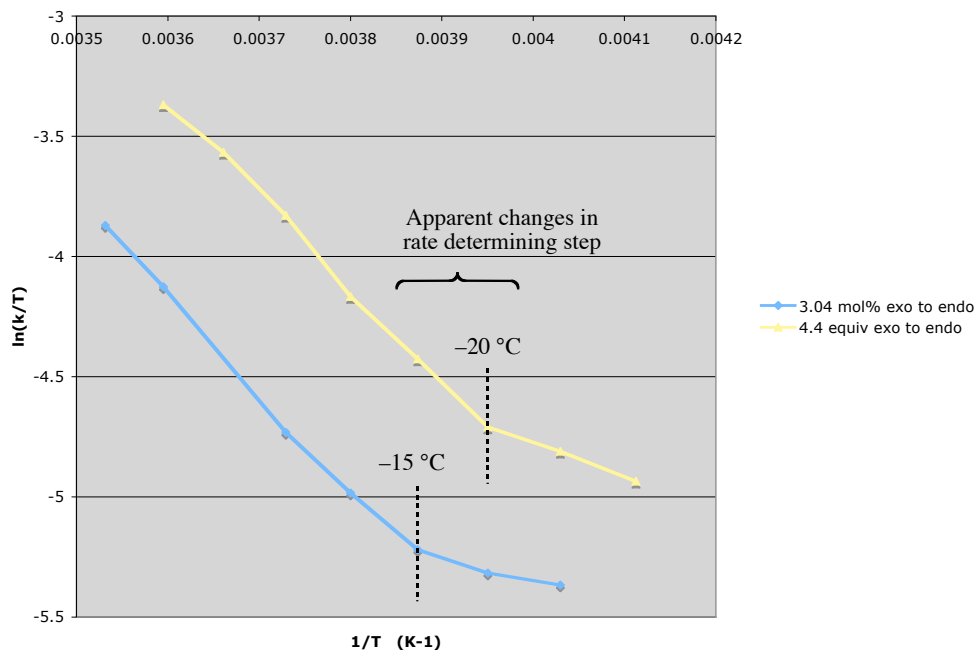
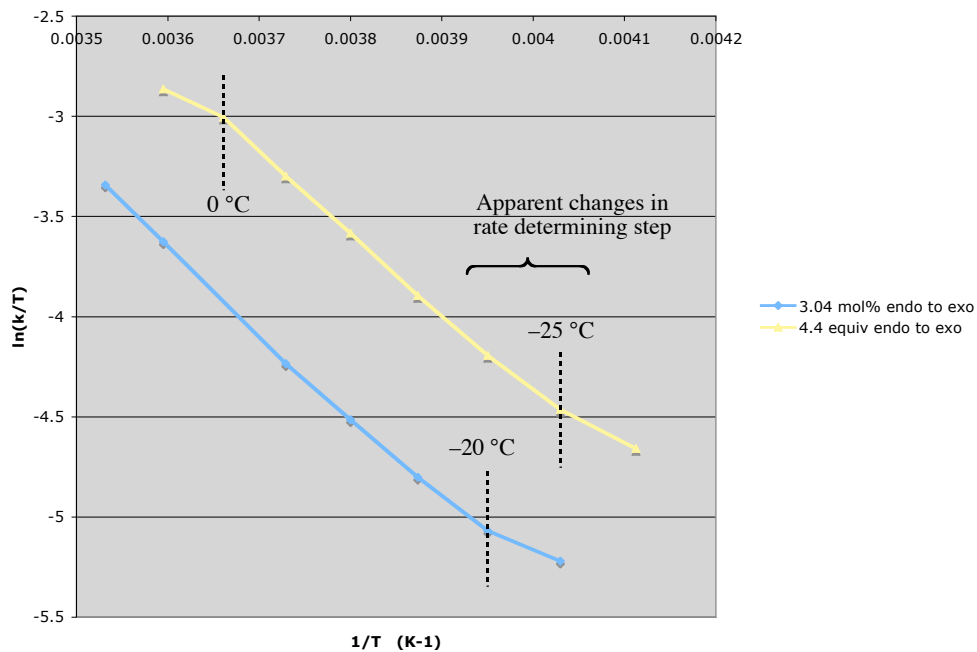
-20	-20	0.2502	0.0009163	0.2547
-15	-15	0.259	0.001098	0.2616
-10	-10	0.278	0.001051	0.2789
-5	-5	0.293	0.0007455	0.2947
0	0	0.311	0.001166	0.3117
5	0.3331	0.001309	0.3316	0.001599

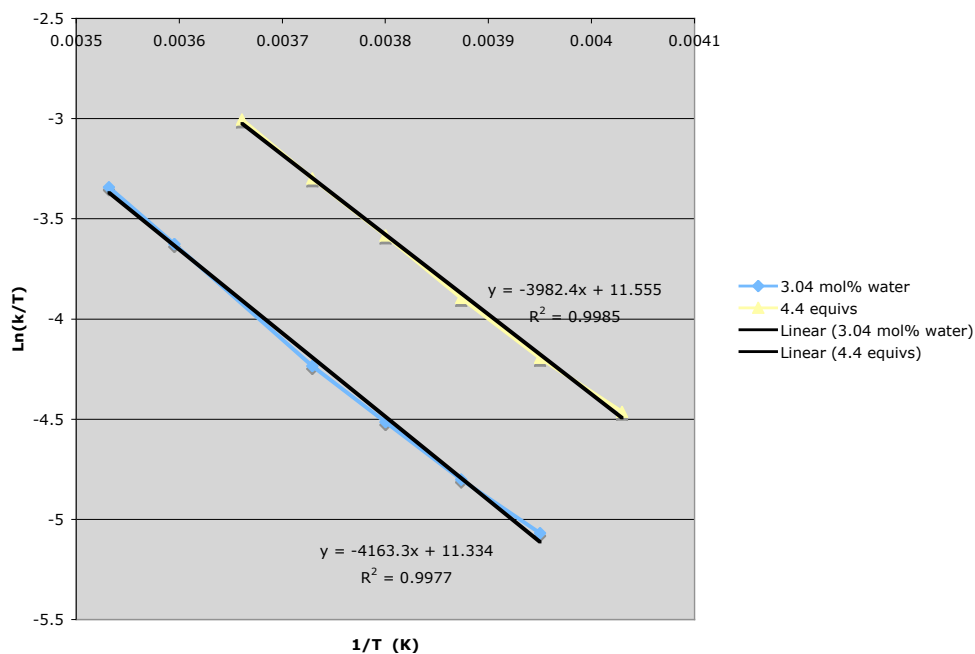
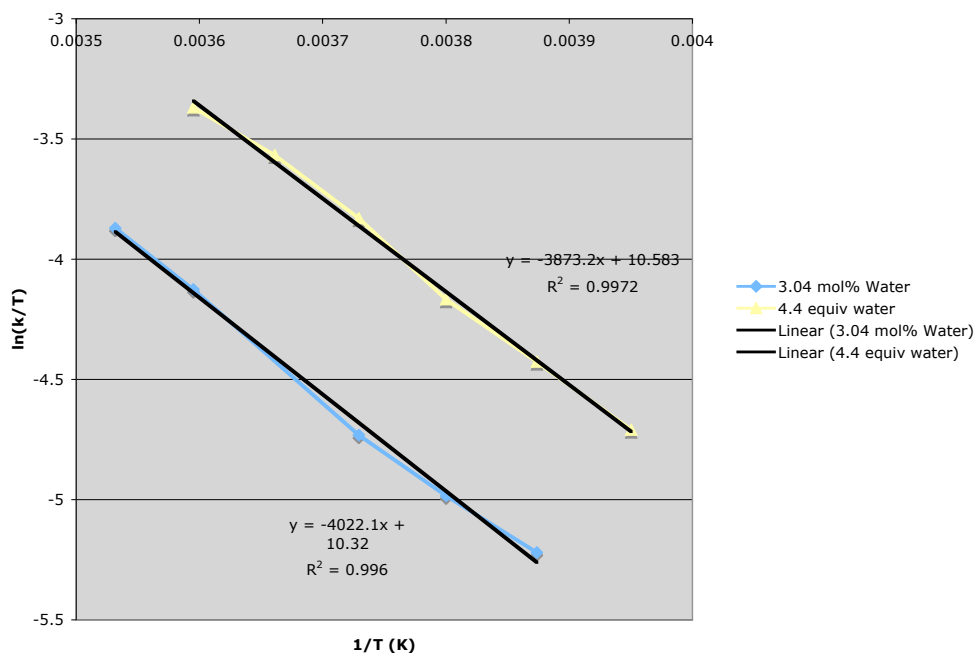
Presaturation Measurements for 4.4 Equiv Water

temp (°C)	<i>endo</i> h(T ₀)	<i>endo</i> h(T _∞)	<i>exo</i> h(T ₀)	<i>exo</i> h(T _∞)
-30	181.613	119.566	310.764	222.038
-25	192.922	115.159	349.838	235.673
-20	203.288	103.99	386.761	244.723
-15	199.622	84.6114	397.716	220.118
-10	155.716	51.3619	333.117	155.896
-5	142.439	36.5186	323.736	119.183
0	124.587	23.9298	294.784	86.6597
5	105.811	16.8408	261.461	62.6516

Calculated Rates for 4.4 Equiv Water

temp (°C)	$k_{exo \rightarrow endo}$ (s ⁻¹)	$k_{endo \rightarrow exo}$ (s ⁻¹)
-30	1.158184509	1.340591269
-25	1.243269603	1.591311447
-20	1.396915326	2.123064957
-15	1.802111957	2.880915814
-10	2.361970598	3.882877273
-5	4.491630882	7.40170316
0	5.896143375	10.01348329
5	1.158184509	1.340591269

3.7.2.2 Eyring Plot and Activation Parameters for π -Allyl Cation 25All Data Plotted for *Exo* to *Endo*All Data Plotted for *Endo* to *Exo*

Best Single Rate Data Plotted for *Exo* to *Endo*Best Single Rate Data Plotted for *Endo* to *Exo*

Raw Eyring Plot Parameters

Added Water	Slope <i>exo</i> → <i>endo</i> (K)	Slope <i>endo</i> → <i>exo</i> (K)	Intercept <i>exo</i> → <i>endo</i>	Intercept <i>endo</i> → <i>exo</i>
3.04 mol%	-4022.1	-4163.3	10.32	11.334
4.4 equiv	-3873.2	-3982.4	10.58	11.555

$$\Delta S^\ddagger (\text{J mol}^{-1} \text{K}^{-1}) = R \cdot [\text{Intercept} - \ln(k_b/h)]$$

$$\Delta H^\ddagger (\text{J mol}^{-1}) = -R \cdot \text{slope}$$

Activation Parameters

Added Water	ΔH^\ddagger (kcal/mol) <i>exo</i> → <i>endo</i>	ΔH^\ddagger (kcal/mol) <i>endo</i> → <i>exo</i>	ΔS^\ddagger (kcal/mol•K) <i>exo</i> → <i>endo</i>	ΔS^\ddagger (kcal/mol•K) <i>endo</i> → <i>exo</i>
3.04 mol%	8.0	8.3	-27	-25
4.4 equiv	7.7	7.9	-26	-24

- (1) See Chapter 2, or Sherden, N. H.; Behenna, D. C. Virgil, S. C. Stoltz, B. M. *Angew. Chem., Int. Ed.* **2009**, *48*, 6840–6843.
- (2) See Chapter 1.
- (3) (a) Keith, J. A. *Computational Insight into Homogeneous Organopalladium Catalysis*, Ph.D. Thesis, California Institute of Technology, Pasadena, CA, **2008**. (b) Keith, J. A.; Behenna, D. C.; Mohr, J. T.; Ma, S.; Marinescu, S. C. Oxgaard, J.; Stoltz, B. M. Goddard, W. A., III. *J. Am. Chem. Soc.* **2007**, *129*, 11876–11877.
- (4) (a) Grennber, H.; Langer, V.; Bäckvall, J.-E. *J. Chem. Soc. Chem. Commun.* **1991**, 1190–1192. (b) Bäckvall, J.-E.; Hopkins, R. B.; Grennberg, H.; Mader, M. M.; Awasthi, A. K. *J. Am. Chem. Soc.* **1990**, *112*, 5160–5166.
- (5) (a) Moiseev, I. I.; Vargaftik, M. N. *Coord. Chem. Rev.* **2004**, *248*, 2381–2391. (b) Hansson, S.; Heumann, A.; Rein, T.; Åkermark, B. *J. Org. Chem.* **1990**, *55*, 975–984. (c) Byström, S. E.; Larsson, E. M.; Åkermark, B. *J. Org. Chem.* **1990**, *55*, 5674–5675. (d) Åkermark, B.; Hansson, S.; Rein, T.; Vågberg, J.; Heumann, A.; Bäckvall, J.-E. *J. Organomet. Chem.* **1989**, *369*, 433–444.
- (6) Bäckvall, J.-E.; Byström, S. E.; Nordberg, R. E. *J. Org. Chem.* **1984**, *49*, 4619–4631.
- (7) For the 2D NMR spectra see the **XX** section of the experimentals section.
- (8) For the synthesis and discussion of some of the first and most highly related palladium η^1 -allyls, see: (a) Zhang, J.; Braunstein, P.; Welter, R. *Inorg. Chem.* **2004**, *43*, 4172–4177. (b) Braunstein, P.; Zhang, J.; Welter, R. *Dalton Trans.* **2003**, 507–509. (c) Kollmar, M.; Helmchen, G. *Organometallic*, **2002**, *21*, 4771–4775. (d) Braunstein, P.; Naud, F.; Dedieu, A.; Rohmer, M.-M.; DeCian, A.; Rettig, S. J. *Organometallics* **2001**, *20*, 2966–2981.

-
- (9) For a more recent publication of a highly related palladium η^1 -allyl complex, see: Canovese, L.; Visentin, F.; Santo, C.; Chessa, G.; Bertolasi, V. *Organometallics* **2010**, *29*, 3027–3038.
- (10) For the ^1H and ^{13}C NMR chemical shifts of simple organic compounds, such as free propene and allyl acetate, dissolved in various common NMR solvents, including THF_{d-8}, see: Fulmer, G. R.; Miller, A. J. M.; Sherden, N. H.; Gottlieb, H. E.; Nudelman, A.; Stoltz, B. M.; Bercaw, J. E.; Goldberg, K. I. *Organometallics* **2010**, *29*, 2176–2179.
- (11) The EXSY NMR spectra refers to the cross peaks that are in phase with the diagonal of either a ROESY or NOESY NMR spectra. While the cross peaks of phase opposite to the diagonal in these spectra represent through-space contacts, the in-phase cross peaks represent chemical exchange and are referred to as the EXSY spectra. The EXSY spectra for **32** and **25** is interpreted from NOESY spectra while the EXSY spectra for **31** is interpreted from the ROESY spectra of the complex. The latter is necessary as the mass of complex **31** in conjunction with the reduced temperatures necessary to preserve **31** in solution long enough to take 2D NMR ($-20\text{ }^\circ\text{C}$) makes for a more viscous solution and causes the product of the rotational correlation time and the Larmor frequency to approach the NOESY null. NOESY spectra taken on samples approaching the null can cause EXSY and nOe cross peaks to become indistinguishable from one another or even disappear into the background noise.
- (12) In the exchange diagrams in this chapter (Figure 3.4 and Figure 3.5), the diagonal is grayed as a reference point and to signify that there can be no meaningful data for these spaces. A square containing an “s” signifies a strong EXSY cross-peak, i.e. the two protons interconvert rapidly and the EXSY cross-peak is not diminished by an overlapping NOESY or ROESY signal. A square containing a “w” signifies a weak EXSY cross-peak. A weak EXSY cross-peak can signify a slower exchange of protons than a more strongly exchanging cross peak, or a strong EXSY cross-peak that is diminished in intensity due to an overlap with a NOESY or ROESY cross-peak. The later is expected to be the case for $1_\alpha \leftrightarrow 1_\beta$ as depicted in Figure 3.4 for complex **32**, as complex **31** shows a clear ROESY cross-peak between the equivalent 1_α and 1_β protons. A square containing an “i” means an implied exchange. In such cases there is reason to expect an EXSY cross-peak between the two indicated protons, but instead a weak NOESY or ROESY signal is present and is presumed to be eclipsing the expected EXSY cross-peak (see endnote 13). An empty square means these protons do not show any signs of exchange.
- (13) Both sets of terminal protons, $1_\alpha/1_\beta$ and $3_\alpha/3_\beta$, for complexes **31** and **32** have strong nOe interactions between one another (i.e., $1_\alpha \leftrightarrow 1_\beta$ and $3_\alpha \leftrightarrow 3_\beta$) that create nOe cross-peaks directly on top of and of the opposite phase of the EXSY cross-peaks generated by chemical exchange. This phenomena is responsible for

the weak EXSY signal between 1_α and 1_β shown in Figure 3.4 for complex **32**. This is borne out by the rOe instead of EXSY cross-peak between 1_α and 1_β demonstrated in the related complex **31** at a lower temperature (-20°C instead of 0°C). At lower temperatures chemical exchange would be expected to be slower, and thus EXSY cross-peaks would be weaker relative to eclipsing rOe or nOe cross-peaks. Thus, the reduced temperature explains the $1_\alpha \leftrightarrow 1_\beta$ exchange being completely obscured by a rOe cross-peak for complex **31** while only being weakened for complex **32** at a higher temperature. As a result it is assumed that both sets of protons, $1_\alpha/1_\beta$ and $3_\alpha/3_\beta$, for both **31** and **32** are in direct exchange (i.e., $1_\alpha \leftrightarrow 1_\beta$ and $3_\alpha \leftrightarrow 3_\beta$) even though most of these implied exchange cross-peaks cannot be directly observed in the EXSY spectrum. Even in the unlikely event where these protons do not undergo direct exchange, they can still exchange indirectly via EXSY observable paths such as: $1_\alpha \rightarrow 1_\beta$ via $1_\alpha \rightarrow 3_\beta$ then $3_\beta \rightarrow 1_\beta$. Given how rapid the direct exchange paths appear to be, even such an indirect exchange path should result in an EXSY cross-peak between the two protons (i.e., $1_\alpha \rightarrow 1_\beta$) under the given conditions. This suggests yet again that the EXSY cross-peaks for $1_\alpha \leftrightarrow 1_\beta$ and $3_\alpha \leftrightarrow 3_\beta$ exist, but are obscured by eclipsing NOESY or ROESY cross-peaks. As such, the exchange paths $1_\alpha \leftrightarrow 1_\beta$ and $3_\alpha \leftrightarrow 3_\beta$ are implicit.

- (14) There is little discussion in the literature about allyl termini scrambling for palladium η^1 -allyl species. It is occasionally noted, however, that the allyl ligands found in isolable palladium η^1 -allyl species are not fluxional, and do not seem to have any exchange paths at all let alone those that would allow for allyl termini scrambling. Also, published studies of the dynamic behavior of fluxional palladium η^1 -allyl species rarely results in a report of allyl termini exchange. Instead the reported fluxional behaviors are typically the result of other ligands on the complex changing conformation or binding. For select examples of fluxional palladium η^1 -allyl species see references 8a,b,d.
- (15) For some select examples and relevant discussion see: (a) Vázquez, J.; Goldfuss, B.; Helmchen, G.; *J. Organomet. Chem.* **2002**, *641*, 67–70. (b) Kollmar, M.; Steinhagen, H.; Janssen, J. P.; Goldfuss, B.; Malinovskaya, S. A.; Vázquez, Rominger, F.; Helmchen, G. *Chem.—Eur. J.* **2002**, *8*, 3103–3114. (c) Kollmar, M.; Goldfuss, B.; Reggelin, M.; Rominger, F.; Helmchen, G. *Chem.—Eur. J.* **2001**, *7*, 4913–4927. Also see reference 18b.
- (16) An extremely unlikely and unprecedented fourth mechanism could also theoretically explain this diastereotopic chemical exchange cross-peak: the allyl ligand 1_α protons could be physically transferred between the two diastereomers of **31**. Beyond being an unlikely proposition in its own right, such a process would result in deuteria migrating from the di-deuterated allyl ligand to other allyl ligands in the allyl enol carbonate cross-over experiment (see **XX**). Thus, if this hypothetical allyl ligand proton exchange pathway were operative, the cross-over

- experiment should have also produced ketone **9** with mono-, tri-, and tetra-deuterated allyl ligands. Such products were not observed.
- (17) The stereochemical enrichment found when synthesizing carboxylate **31** is expected to be a result of a kinetic resolution occurring somewhere in the course of the decarboxylative asymmetric allylic alkylation. Current results suggest that decarboxylation may actually be slightly faster for the (*S,S*)-diastereomer relative to the (*R,S*)-diastereomer of carboxylate **31**, thus resulting in a kinetic resolution that can stereochemically enrich this intermediate. Alternately it is possible that one diastereomer of **31** is more soluble than the other, and thus purification of carboxylate **31**, which is done via recrystallization, results in diastereomeric enrichment of **31** even though both diastereomers co-crystallize. However, the stereochemical enrichment of the quaternary stereocenter in **31** being the result of stereoselective deallylation of allyl β -ketoester **7** has been disproved.
- (18) (a) Johns, A. M.; Utsunomiya, M.; Incarvito, C. D.; Hartwig, J. F. *J Am. Chem. Soc.* **2006**, *128*, 1828–1839. (b) Hansson, S.; Norrby, P.-O.; Sjögren, M. P. T.; Åkermark, B.; Cucciolito, M. E.; Giordano, F.; Vitagliano, A. *Organometallics* **1993**, *12*, 4940–4948. (c) Åkermark, B.; Åkermark, G.; Hegedus, L. S.; Zetterberg, K. *J. Am. Chem. Soc.*, **1981**, *103*, 3037–3040.
- (19) In every literature report, when a ligand *cis* to an η^1 -allyl ligand on palladium is removed from the complex, the η^1 -allyl ligand isomerizes to η^3 and fills the newly vacated coordination site extremely rapidly. This results in the generation of the corresponding palladium π -allyl species, typically a π -allyl cation. For select examples, see reference 8. By analogy, a palladium η^1 -allyl complex with a *cis* labile ligand, such as carboxylate, should also result in the corresponding π -allyl species whenever the labile *cis* ligand disassociates from the palladium center.
- (20) The EXSY spectra for palladium π -allyl cation **25** in THF_{d,8} shows an identical means of η^3 - η^1 - η^3 (or π - σ - π) conversion between its *exo* and *endo* isomers as is shown in the EXSY spectra published for the highly related unsubstituted palladium π -allyl cation of the *i*-Pr PHOX ligand in CDCl₃, published by Helmchen. See: Sprinz, J.; Kiefer, M.; Helmchen, G. *Tetrahedron Lett.*, **1994**, *35*, 1523–1526.
- (21) (a) Pregosin, P. S.; Salzmann, R.; Togni, A. *Organometallics* **1995**, *14*, 842–847. (b) Abbenhuis, H. C. L.; Burckhardt, U.; Gramlich, V.; Köllner, C.; Pregosin, P. S.; Salzmann, R.; Togni, A. *Organometallics* **1995**, *14*, 759–766. (c) Breutel, C.; Pregosin, P. S.; Salzmann, R.; Togni, A. *J. Am. Chem. Soc.* **1994**, *116*, 4067–4068.
- (22) Different nucleophiles, especially those of different strengths, may have different preferences for how they bind to complex **25**. While carboxylate nucleophiles have demonstrated a distinct preference for binding in the square plane via

- carboxylates **31** and **32**, it is entirely possible that weaker nucleophiles, such as THF or water, might only associate at the apical position of π -allyl cation **25**. Beyond their association with the metal center, nothing more can be said about where isomerization catalyzing nucleophiles might prefer to bind to π -allyl cation **25** from the current data.
- (23) For an NMR study of the solution behavior for palladium π -allyl complexes possessing a larger set of allyl isomerization modes, including apparent allyl rotation, and an in-depth discussion thereof, see reference 18b.
- (24) (a) Evans, L.; A.; Fey, N.; Harvey, J. N.; Hose, D.; Lloyd-Jones, G. C.; Murray, P.; Orpen, A. G.; Osborne, R.; Owen-Smith, G. J. J.; Purdie, M. *J. Am. Chem. Soc.* **2008**, *130*, 14471–14473. (b) Amatore, C.; Bahsoun, A. A.; Jutand, A.; Mensah, L.; Meyer, G.; Ricard, L. *Organometallics* **2005**, *24*, 1569–1577. (c) Amatore, C.; Gamez, S.; Jutand, A. *Chem.—Eur. J.* **2001**, *7*, 1273–1280.
- (25) For a thorough mechanistic discussion about the allyl terminus regioselectivity of outer-sphere allylic alkylation on palladium using the PHOX ligand architecture, see: (a) Helmchen, G.; Steinhagen, H.; Reggelin, M.; Kudis, S. In *Selective Reactions of Metal-Activated Molecules*, (Eds. Werner, H.; Schreier, P.), Vieweg Verlag, Wiesbaden, **1998**, 205–215. (b) Helmchen, G. *J. Organomet. Chem.* **1999**, *576*, 203–214. (c) Steinhagen, H.; Reggelin, M.; Helmchen, G.; *Angew. Chem., Int. Ed.* **1997**, 2108–2110. (d) Helmchen, G.; Kudis, S.; Sennhenn, P.; Steinhagen, H. *Pure Appl. Chem.* **1997**, *69*, 513–518. (e) Sprintz, J.; Kiefer, M.; Helmchen, G.; Reggelin, M.; Huttner, G.; Walter, O.; Zsolnal, L. *Tetrahedron Lett.* **1994**, *35*, 1523–1526.
- (26) In turn, this implies that system redesigns that influence allyl termini selectivity of oxidative addition towards the same preference seen in reductive elimination might allow for kinetic instead of thermodynamic regiocontrol on the allyl fragment of terminally substituted allylic alkylation products. Among other possibilities such kinetic regiocontrol could allow for palladium-catalyzed allylic alkylation processes selective for the branched allyl product, which is in stark contrast to the high preference for linear allylic alkylation products generally exhibited by palladium species (for a very brief discussion and some examples of the allyl termini selectivity preference found in palladium-catalyzed allylic alkylation see Chapter 1).
- (27) Mohr, J. T.; Behenna, D. C.; Harned, A. M.; Stoltz, B. M. *Angew. Chem., Int. Ed.* **2005**, *44*, 6924–6927.
- (28) Fulmer, G. R.; Miller, A. J. M.; Sherden, N. H.; Gottlieb, H. E.; Nudelman, A.; Stoltz, B. M.; Bercaw, J. E.; Goldberg, K. I. *Organometallics* **2010**, *29*, 2176–2179.

-
- (29) For the run with 3.04 mol% water, no water was manually added. It is likely the 3.04 mol% water came from π -allyl cation **25**, which was prepared on the bench top and recrystallized from ethanol as previously published,¹ before being subjected to extended drying in vacuo giving ample opportunity for the sample of **25** to pick up a small amount of moisture. Alternatively, as THF solutions of **25** PF₆⁻ are fairly hygroscopic, the 3.04 mol% water may have leaked into the NMR tube after the sample was prepared.
- (30) When integrating against π -Allyl Cation **25**, the resonances from both the *endo* and *exo* isomers were integrated and the value was added together. Water was integrated against the smaller resonances of π -Allyl Cation **25** such as the oxazoline or π -Allyl proton resonances. For each run, a few such resonances in π -Allyl Cation **25** were selected at random and the concentration of water was reported as an average of integrating against these resonances. The chemical shift of water in THF_{d-8} is $\delta = 2.46$ ppm (see reference 28).

Appendix 3

Comprehensive Bibliography

- (1) Pfaltz, A.; Lautens, M. in *Comprehensive Asymmetric Catalysis* (Eds: Jacobsen, E. N.; Pfaltz, A.; Yamamoto, H.), Springer, Heidelberg, **1999**, 833–886.
- (2) Abbenhuis, H. C. L.; Burckhardt, U.; Gramlich, V.; Köllner, C.; Pregosin, P. S.; Salzmann, R.; Togni, A. *Organometallics* **1995**, *14*, 759–766.
- (3) Åkermark, B.; Åkermark, G.; Hegedus, L. S.; Zettergerg, K. *J. Am. Chem. Soc.* **1981**, *103*, 3037–3040.
- (4) Åkermark, B.; Hansson, S.; Rein, T.; Vågberg, J.; Heumann, A.; Bäckvall, J.-E. *J. Organomet. Chem.* **1989**, *369*, 433–444.
- (5) Åkermark, B.; Jutand, A. *J. Organomet. Chem.* **1981**, *217*, C41–C43.
- (6) Amatore, C.; Bahsoun, A. A.; Jutand, A.; Mensah, L.; Meyer, G.; Ricard, L. *Organometallics* **2005**, *24*, 1569–1577.
- (7) Amatore, C.; Gamez, S.; Jutand, A. *Chem.—Eur. J.* **2001**, *7*, 1273–1280.
- (8) Amatore, C.; Jutand, A.; Mensah, L.; Ricard, L. *J. Organomet. Chem.* **2007**, *692*, 1457–1464.
- (9) Bäckvall, J.-E.; Byström, S. E.; Nordberg, R. E. *J. Org. Chem.* **1984**, *49*, 4619–4631.
- (10) Bäckvall, J.-E.; Hopkins, R. B.; Grennberg, H.; Mader, M. M.; Awasthi, A. K. *J. Am. Chem. Soc.* **1990**, *112*, 5160–5166.

- (11) Behenna, D. C. ; B. M. Stoltz, B. M. *J. Am. Chem. Soc.* **2004**, *126*, 15044–15045.
- (12) Behenna, D. C. *Progress Toward the Synthesis of (+)-Zoaanthenol and The Development of an Asymmetric Tsuji Allylation Reaction*, Ph.D. Thesis, California Institute of Technology, Pasadena, CA, **2007**.
- (13) Bélanger, É.; Cantin, K.; Messe, O.; Tremblay, M.; Paquin, J.-F. *J. Am. Chem. Soc.* **2007**, *129*, 1034–1035.
- (14) Böttcher, L.; Scholz, A.; Walther, D.; Weisbach, N.; Görls, H. *Z. Anorg. Allg. Chem.* **2003**, *629*, 2103–2112.
- (15) Braun, M.; Meier, T. *Synlett* **2006**, 661–676.
- (16) Braun, M.; Thorsten, M. *Angew. Chem., Int. Ed.* **2006**, *45*, 6952–6955.
- (17) Braunstein, P.; Naud, F.; Dedieu, A.; Rohmer, M.-M.; DeCian, A.; Rettig, S. J. *Organometallics* **2001**, *20*, 2966–2981.
- (18) Braunstein, P.; Zhang, J.; Welter, R. *Dalton Trans.* **2003**, 507–509.
- (19) Breutel, C.; Pregosin, P. S.; Salzmann, R.; Togni, A. *J. Am. Chem. Soc.* **1994**, *116*, 4067–4068.
- (20) Burger, E. C.; Barron, B. R.; Tunge, J. A. *Synlett* **2006**, 2824–2826.
- (21) Byström, S. E.; Larsson, E. M.; Åkermark, B. *J. Org. Chem.* **1990**, *55*, 5674–5675.
- (22) Canovese, L.; Visentin, F.; Santo, C.; Chessa, G.; Bertolasi, V. *Organometallics* **2010**, *29*, 3027–3038.
- (23) Cardenas, D. J.; Echavarren, A. M. *New J. Chem.* **2004**, *28*, 338–347.
- (24) Chattopadhyay, K.; Jana, R.; Day, V. W.; Douglas, J. T.; Tunge, J. A. *Org. Lett.* **2010**, *12*, 3042–3045.
- (25) Christoffers, J.; Mann, A. *Angew. Chem., Int. Ed.* **2001**, *40*, 4591–4597.
- (26) Corey, E. J.; Guzman-Perez, A. *Angew. Chem, Int. Ed.* **1998**, *37*, 388–401.
- (27) Dawson, G. J.; Frost, C. G.; Williams, J. M. J.; Coote, S. J.; *Tetrahedron Lett.* **1993**, *34*, 3149–3150.

- (28) Dervisi, A.; Edwards, P. G.; Newman, P. D.; Tooze, R. P.; Coles, S. J.; Hursthouse, M. B.; *J. Chem. Soc. Dalton Trans.* **1999**, 1113–1120.
- (29) Douglas, C. J.; Overman, L. E. *Proc. Natl. Acad. Sci. U.S.A.* **2004**, *101*, 5363–5367.
- (30) Du, C.; Li, L.; Li, Y.; Xie, Z. *Angew. Chem., Int. Ed.* **2009**, *48*, 7853–7856.
- (31) Enquist, J. A.; Stoltz, B. M. *Nature* **2008**, *453*, 1228–1231.
- (32) Evans, L.; A.; Fey, N.; Harvey, J. N.; Hose, D.; Lloyd-Jones, G. C.; Murray, P.; Orpen, A. G.; Osborne, R.; Owen-Smith, G. J. J.; Purdie, M. *J. Am. Chem. Soc.* **2008**, *130*, 14471–14473.
- (33) Evans, P. A.; Nelson, J. D. *J. Am. Chem. Soc.* **1998**, *120*, 5581–5582.
- (34) Fiaud, J.-C.; Legros, J.-Y. *J. Org. Chem.* **1990**, *55*, 4840–4849.
- (35) Flegeau, E. F.; Schneider, W.; Kobayashi S. *Chem.—Eur. J.* **2009**, 12247–12254.
- (36) Fristrup, P.; Ahlquist, M.; Tanner, D.; Norrby, P.-O. *J. Phys. Chem. A* **2008**, *112*, 12862–12867.
- (37) Fulmer, G. R.; Miller, A. J. M.; Sherden, N. H.; Gottlieb, H. E.; Nudelman, A.; Stoltz, B. M.; Bercaw, J. E.; Goldberg, K. I. *Organometallics* **2010**, *29*, 2176–2179.
- (38) Glorius, F.; Pfaltz, A. *Org. Lett.* **1999**, *1*, 141–144.
- (39) Graening, T.; Hartwig, J. F. *J. Am. Chem. Soc.* **2005**, *127*, 17192–17193.
- (40) Grennber, H.; Langer, V.; Bäckvall, J.-E. *J. Chem. Soc. Chem. Commun.* **1991**, 1190–1192.
- (41) Hagelin, H.; Svensson, M.; Åkermark, B.; Norrby, P.-O. *Organometallics*, **1999**, *18*, 4574–4583.
- (42) Hansson, S.; Norrby, P.-O.; Sjögren, M. P. T.; Åkermark, B.; Cucciolito, M. E.; Giordano, F.; Vitagliano, A. *Organometallics* **1993**, *12*, 4940–4948.
- (43) Hayashi, T.; Kanehira, K.; Hagihara, T.; Kumada, M. *J. Org. Chem.* **1988**, *53*, 113–120.
- (44) Helmchen, G. *J. Organomet. Chem.* **1999**, *576*, 203–214.
- (45) Helmchen, G.; Ernst, M.; Paradies, G. *Pure Appl. Chem.* **2004**, *76*, 494–506.

- (46) Helmchen, G.; Kudis, S.; Sennhenn, P. Steinhagen, H. *Pure Appl. Chem.* **1997**, *69*, 513–518.
- (47) Helmchen, G.; Pfaltz, A. *Acc. Chem. Res.* **2000**, *33*, 336–345.
- (48) Helmchen, G.; Steinhagen, H.; Reggelin, M.; Kudis, S. in *Selective Reactions of Metal-Activated Molecules*, (Eds: Werner, H.; Schreier, P.) Vieweg Verlag: Wiesbaden, **1998**, 205–215.
- (49) Hong, A. Y.; Krout, M. R.; Jensen, T.; Bennet, N. B.; Harned, A. M.; Stoltz, B. M. *Angew. Chem., Int. Ed.* **2011**, *in press*.
- (50) I. J. S. Fairlamb, A. R. Kapdi, A. F. Lee, *Org. Lett.* **2004**, *6*, 4435–4438.
- (51) Jacob, V.; Weakley, T. J. R.; Haley, M. M. *Organometallics* **2002**, *21*, 5394–5400.
- (52) Jensen, T.; Fristrup, P. *Dansk Kemi* **2009**, *90*, 32–34.
- (53) John Blacker, A.; Clark, M. L.; Loft, M. S.; Williams, J. M. J. *Chem. Commun.* **1999**, 913–914.
- (54) Johns, A. M.; Utsunomiya, M.; Incarvito, C. D.; Hartwig, J. F. *J Am. Chem. Soc.* **2006**, *128*, 1828–1839.
- (55) Tani, K.; Behenna, D. C.; McFadden, R. M.; Stoltz, B. M. *Org. Lett.* **2007**, *9*, 2529–2531.
- (56) Kagan, H. B.; Girard, C. *Angew. Chem., Int. Ed.* **1998**, *37*, 2922–2959.
- (57) Keith, J. A. *Computational Insight into Homogeneous Organopalladium Catalysis*, Ph.D. Thesis, California Institute of Technology, Pasadena, CA, **2008**.
- (58) Keith, J. A.; Behenna, D. C.; Mohr, J. T.; Ma, S.; Marinescu, S. C. Oxgaard, J.; Stoltz, B. M. Goddard, W. A., III. *J. Am. Chem. Soc.* **2007**, *129*, 11876–11877.
- (59) Kollmar, M.; Goldfuss, B.; Reggelin, M.; Rominger, F.; Helmchen, G. *Chem.—Eur. J.* **2001**, *7*, 4913–4927.
- (60) Kollmar, M.; Helmchen, G. *Organometallic*, **2002**, *21*, 4771–4775.
- (61) Kollmar, M.; Steinhagen, H.; Janssen, J. P.; Goldfuss, B.; Malinovskaya, S. A.; Vázquez, Rominger, F.; Helmchen, G. *Chem.—Eur. J.* **2002**, *8*, 3103–3114.

- (62) Konnick, M. M.; Guzei, L. A.; Stahl, S. S. *J. Am. Chem. Soc.* **2004**, *126*, 10212–10213.
- (63) Krout, M. R.; Mohr, J. T.; Stoltz, B. M. *Org. Synth.* **2009**, *86*, 181–193.
- (64) Kuhn, O.; Mayr, H. *Angew. Chem., Int. Ed.* **1999**, *38*, 343–346.
- (65) Kuwano, R.; Ito, Y. *J. Am. Chem. Soc.* **1999**, *121*, 3236–3237.
- (66) Kuwano, R.; Uchida, K.; Ito, Y. *Org. Lett.* **2003**, *5*, 2177–2179.
- (67) Liu, S.; Müller, J. F. K.; Neuburger, M. Schaffner, S.; Zehnder, M. *J. Organomet. Chem.* **1997**, *549*, 283–293.
- (68) Lloyd-Jones, G. C.; Pfaltz, A. *Angew. Chem., Int. Ed.* **1995**, *34*, 462–464.
- (69) Low, J. J.; Goddard, W. A., III. *J. Am. Chem. Soc.* **1986**, *108*, 6115–6128.
- (70) Low, J. J.; Goddard, W. A., III. *Organometallics* **1986**, *5*, 609–622.
- (71) M. J. Payne, D. J. Cole-Hamilton, *J. Chem. Soc. Dalton Trans.* **1997**, 3167–3176.
- (72) M. Peer, J. C. de Jong, M. Kiefer, T. Langer, H. Rieck, H. Schell, P. Sennhenn, J. Sprinz, H. Steinhagen, B. Wiese, G. Helmchen, *Tetrahedron* **1996**, *52*, 7547–7583.
- (73) Méndez, M.; Cuerva, J. M.; Gómez-Bengoia, E., Cárdenas, D. J.; Echavarren, A. *M. Chem.—Eur. J.* **2002**, *8*, 3620–3628.
- (74) Mohr, J. T.; Behenna, D. C.; Harned, A. M.; Stoltz, B. M. *Angew. Chem., Int. Ed.* **2005**, *44*, 6924–6927.
- (75) Mohr, J. T.; Krout, M. R.; Stoltz, B. M. *Org. Synth.* **2009**, *86*, 194–211.
- (76) Mohr, J. T.; Stoltz, B. M. *Chem. Asian J.* **2007**, *2*, 1476–1491
- (77) Moiseev, I. I.; Vargaftik, M. N. *Coord. Chem. Rev.* **2004**, *248*, 2381–2391.
- (78) Nakamura, M.; Hajra, A.; Endo, K.; Nakamura, E. *Angew. Chem., Int. Ed.* **2005**, *44*, 7248–7251.
- (79) Ozawa, F.; Son, T.-i.; Ebina, S.; Osakada, K.; Yamamoto, A. *Organometallics*, **1992**, *11*, 171–176.
- (80) Pawlas, J.; Nakao, Y.; Kawatsura, M.; Hartwig, J. F. *J. Am. Chem. Soc.* **2002**, *124*, 3669–3679.

- (81) Pérez-Rodríguez, M.; Braga, A. A. C.; de Lera, A. R.; Maseras, F.; Álvarez R. *Organometallics*, **2010**, *29*, 4983–4991.
- (82) Planas, J. G.; Marumo, T.; Ichikawa, Y.; Hirano, M.; Komiya, S. *J. Mol. Catal. A* **1999**, *147*, 137–154.
- (83) Pregosin, P. S.; Salzmann, R.; Togni, A. *Organometallics* **1995**, *14*, 842–847.
- (84) Recio, A. III.; Tunge, J. A. *Org. Lett.* **2009**, *24*, 5630–5633.
- (85) Liu, S.; Müller, J. F. K.; Beuburger, M.; Schaffner, S.; Zehnder, M. *J. Organomet. Chem.* **1997**, *549*, 283–293.
- (86) Satyanarayana, T.; Abraham, S.; Kagan, H. B. *Angew. Chem., Int. Ed.* **2009**, *48*, 456–494.
- (87) Sawamura, M.; Nagata, H.; Sakamoto, H.; Ito, Y. *J. Am. Chem. Soc.* **1992**, *114*, 2586–2592.
- (88) Schulz, S. R.; Blechert, S. *Angew. Chem., Int. Ed.* **2007**, *46* 3966–3970.
- (89) Sherden, N. H.; Behenna, D. C. Virgil, S. C. Stoltz, B. M. *Angew. Chem., Int. Ed.* **2009**, *48*, 6840–6843.
- (90) Shimizu, I.; Yamada, T.; Tsuji, J. *Tetrahedron Lett.* **1980**, *21*, 3199–3202.
- (91) Sprintz, J.; Kiefer, M.; Helmchen, G.; Reggelin, M.; Huttner, G.; Walter, O.; Zsolnai, L. *Tetrahedron Lett.* **1994**, *35*, 1523–1526.
- (92) Sprinz, J.; Helmchen, G. *Tetrahedron Lett.* **1993**, *34*, 1769–1772.
- (93) Sprinz, J.; Kiefer, M.; Helmchen, G. *Tetrahedron Lett.* **1994**, *35*, 1523–1526.
- (94) Steinhagen, H.; Reggelin, M.; Helmchen, G. *Angew. Chem., Int. Ed.* **1997**, 2108–2110.
- (95) Suzuki, T.; Fujimoto, H. *Inorg. Chem. (Washington, DC, U. S.)* **1999**, *38*, 370–382.
- (96) Tang, D.; Luo, X.; Shen, W.; Li, M. *J. Mol. Struct.* **2005**, *716*, 79–87.
- (97) Trost, B. M. *J. Org. Chem.* **2004**, 532–539.
- (98) Trost, B. M.; Bream, R. N.; Xu, J. *Angew. Chem., Int. Ed.* **2006**, *45*, 3109–3112.

- (99) Trost, B. M.; Crawly, M. L. *Chem. Rev.* **2003**, *103*, 2921–2943. (h) Kazmaier, U. *Curr. Org. Chem.* **2003**, *7*, 317–328.
- (100) Trost, B. M.; Hachiya, I. *J. Am. Chem. Soc.* **1998**, *120*, 1104–1105.
- (101) Trost, B. M.; Jiang, C.; *Synthesis* **2006**, *3*, 369–396.
- (102) Trost, B. M.; Keinan, E. *J. Org. Chem.* **1979**, *44*, 3451–3457.
- (103) Trost, B. M.; Lee, C. in *Catalytic Asymmetric Synthesis*, 2nd ed. (Ed.: Ojima, I.), Wiley-VCH, New York, **2000**, pp. 593–649.
- (104) Trost, B. M.; Radinov, R.; Grenzer, E. M. *J. Am. Chem. Soc.* **1997**, *119*, 7879–7880.
- (105) Trost, B. M.; Schroeder, G. M. *J. Am. Chem. Soc.* **1999**, *121*, 6759–6760.
- (106) Trost, B. M.; Schroeder, G. M.; Kristensen, J. *Angew. Chem., Int. Ed.* **2002**, *41*, 3492–3495.
- (107) Trost, B. M.; Van Vranken, D. L. *Chem. Rev.* **1996**, *96*, 395–422 and references therein.
- (108) Trost, B. M.; Xu, J. *J. Am. Chem. Soc.* **2005**, *127*, 17180–17181.
- (109) Trost, B. M.; Xu, J. *J. Am. Chem. Soc.* **2005**, *127*, 2846–2847.
- (110) Trost, B. M.; Xu, J.; Reichle, M. *J. Am. Chem. Soc.* **2007**, *129*, 282–283.
- (111) Trost, B. M.; Xu, J.; Schmidt, T. *J. Am. Chem. Soc.* **2009**, *131*, 18343–18357.
- (112) Tsuji, J.; Minami, I.; Shimizu, I. *Chem. Lett.* **1983**, 1325–1326.
- (113) Tsuji, J.; Minami, I.; Shimizu, I. *Tetrahedron Lett.* **1983**, *24*, 1793–1796.
- (114) Vázquez, J.; Goldfuss, B.; Helmchen, G.; *J. Organomet. Chem.* **2002**, *641*, 67–70.
- (115) von Matt, P.; Pfaltz, A. *Angew. Chem., Int. Ed. Engl.* **1993**, *32*, 566–568.
- (116) Herrmann, W. A.; Thiel, W. R.; Broßmer, C.; Öfele, K.; Priermeier, T.; Scherer, W. *J. Organomet. Chem.* **1993**, *461*, 51–61.
- (117) Wencel, J.; Laurent, I.; Toupet, L.; Crévisy, C.; Mauduit, M. *Organometallics*, **2010**, *29*, 1530–1533.

- (118) Zalubovskis, R.; Bouet, A.; Fjellander, E.; Constant, S.; Linder, D.; Fischer, A.; Lacour, J.; Privalov, T.; Moberg, C. *J. Am. Chem. Soc.* **2008**, *130*, 1845–1855.
- (119) You, S.-L.; Dai, L.-X. *Angew. Chem. Int. Ed.* **2006**, *45*, 5246–5248.
- (120) Zhang, J.; Braunstein, P.; Welter, R. *Inorg. Chem.* 2004, *43*, 4172–4177.
- (121) Zhang, P.; Brozek, L. A.; Morken, J. P. *J. Am. Chem. Soc.* 2010, *132*, 10686–10688.

About the Author

Nathaniel Haynes Sherden was born in Boston, Massachusetts, on July 18th, 1982, to William A. and Molly H. Sherden. He spent his childhood and adolescent years growing up on Walnut St. in Boston with his younger brother Christian. At an early age, unchecked curiosity led him to be interested in all things science. Before he understood much about it or what field he preferred, he had already decided that it would be his life goal to try and make a career out of it. In eighth grade, he had a particularly engaging teacher, Mr. Pain, who taught a small amount of organic chemistry as part of his comprehensive science review class. As a result, chemistry instantly became Nathaniel's passion. He subsequently took all the chemistry classes that his high school offered, and then joined with a few other enthusiastic students to petition the school for more chemistry class offerings beyond the AP level.

In 2000, he began undergraduate studies at the University of Chicago. He joined the Hillhouse group and his ever more specific scientific enthusiasm quickly honed in on organometallic chemistry with its rich array of chemical properties and colors. In 2004, Nathaniel graduated with a B.S. in Chemistry, along with a B.S. in Computer Science (he figured the best way to get really serious and proficient with a hobby was to take it up as a second major). He graduated with general honors and subject honors in Chemistry.

In September 2005, Nathaniel moved to Pasadena, California, where he began doctoral research with Professor Brian Stoltz at the California Institute of Technology. In late spring 2011 he left for the Massachusetts Institute of Technology and then the John Innes Centre under the supervision of Professor Sarah O'Connor.